Technical Report Documentation Page

1. Report No.	2. Government Accession No.	3. Recipient's Catalog No.
FHWA/TX-05/0-4468-2		

4. Title and Subtitle	5. Report Date
COMPARISON OF FATIGUE ANALYSIS APPROACHES FOR TWO HOT MIX ASPHALT CONCRETE (HMAC) MIXTURES	December 2004 Resubmitted: August 2005
	6. Performing Organization Code

7. Author(s)	8. Performing Organization Report No.
Lubinda F. Walubita, Amy Epps Martin, Sung Hoon Jung, Charles J. Glover, Eun Sug Park, Arif Chowdhury, and Robert L. Lytton	Report 0-4468-2

9. Performing Organization Name and Address	10. Work Unit No. (TRAIS)
Texas Transportation Institute The Texas A&M University System College Station, Texas 77843-3135	11. Contract or Grant No. Project 0-4468

12. Sponsoring Agency Name and Address	13. Type of Report and Period Covered
Texas Department of Transportation Research and Technology Implementation Office P. O. Box 5080 Austin, Texas 78763-5080	Technical Report: September 2002-August 2004
	14. Sponsoring Agency Code

15. Supplementary Notes

Project performed in cooperation with the Texas Department of Transportation and the Federal Highway Administration.

Project Title: Evaluate the Fatigue Resistance of Rut Resistance Mixes

URL: http://tti.tamu.edu/documents/0-4468-2.pdf

16. Abstract

Over the past decade, the Texas Department of Transportation (TxDOT) focused research efforts on improving mixture design to preclude rutting in the early life of the pavement. However, these rut resistant stiff mixtures may be susceptible to long-term fatigue cracking in the pavement structure as the binder stiffens due to oxidative aging. To address this concern, TxDOT initiated a research study with the primary goal of evaluating and recommending a HMAC mixture fatigue design and analysis system to ensure adequate mixture fatigue performance in a particular pavement structure under specific environmental and traffic loading conditions. A secondary goal of the research was to compare the fatigue resistance of commonly used TxDOT HMAC mixtures including investigating the effects of binder aging on fatigue performance. Four fatigue analysis approaches, the mechanistic empirical (ME), the calibrated mechanistic with (CMSE) and without (CM) surface energy measurements, and the proposed NCHRP 1-37A Pavement Design Guide were investigated in this project to evaluate the fatigue resistance of two common TxDOT mixtures (Rut Resistant and Basic Type C) including the effects of aging.

Based on the value engineering assessment including test results, statistical analysis, costs, and relative comparison of each analysis procedure, the continuum micromechanics based CMSE fatigue analysis approach was recommended for predicting HMAC mixture fatigue life (N_f). While binder oxidative aging reduced the HMAC mixture resistance to fracture and its ability to heal, the Rut Resistant mixture exhibited better fatigue resistance in terms of N_f magnitude compared to the Basic Type C mixture possibly due to an increased polymer modified binder content. Test results also indicated that both binders and mixtures stiffen with oxidative aging, and that mixture aging correlated quantitatively with binder aging. From the binder shear properties and binder-mixture relationships, aging shift factors were developed and produced promising results. Nonetheless, more CMSE laboratory HMAC mixture fatigue characterization and field validation is recommended.

17. Key Words	18. Distribution Statement
Asphalt, Asphalt Concrete, Fatigue, Aging, Fracture, Microcracking, Healing, Mechanistic Empirical, Calibrated Mechanistic, Surface Energy, Anisotropy	No restrictions. This document is available to the public through NTIS: National Technical Information Service Springfield, Virginia 22161 http://www.ntis.gov

19. Security Classif.(of this report)	20. Security Classif.(of this page)	21. No. of Pages	22. Price
Unclassified	Unclassified	312	

COMPARISON OF FATIGUE ANALYSIS APPROACHES FOR TWO HOT MIX ASPHALT CONCRETE (HMAC) MIXTURES

by

Lubinda F. Walubita
Graduate Research Assistant, Texas Transportation Institute

Amy Epps Martin
Associate Research Engineer, Texas Transportation Institute

Sung Hoon Jung
Graduate Research Assistant, Texas Transportation Institute

Charles J. Glover
Research Engineer, Texas Transportation Institute

Eun Sug Park
Assistant Research Scientist, Texas Transportation Institute

Arif Chowdhury
Associate Transportation Researcher, Texas Transportation Institute

and

Robert L. Lytton
Research Engineer, Texas Transportation Institute

Report 0-4468-2
Project 0-4468
Project Title: Evaluate the Fatigue Resistance of Rut Resistance Mixes

Performed in cooperation with the
Texas Department of Transportation
and the
Federal Highway Administration

December 2004
Resubmitted: August 2005

TEXAS TRANSPORTATION INSTITUTE
The Texas A&M University System
College Station, Texas 77843-3135

DISCLAIMER

The contents of this report reflect the views of the authors, who are responsible for the facts and the accuracy of the data presented herein. The contents do not necessarily reflect the official view or policies of the Federal Highway Administration (FHWA) or the Texas Department of Transportation (TxDOT). This report does not constitute a standard, specification, or regulation, nor it is intended for construction, bidding, or permit purposes. Trade names were used solely for information and not for product endorsement. The engineers in charge were Amy Epps Martin, P.E. (Texas No. 91053) and Charles J. Glover, P.E. (Texas No. 48732).

ACKNOWLEDGMENTS

This project was conducted for TxDOT, and the authors thank TxDOT and FHWA for their support in funding this research project. In particular, the guidance and technical assistance provided by the project director (PD) Gregory Cleveland of TxDOT, the project coordinator (PC) James Travis of FHWA, and German Claros of the Research and Technology Implementation (RTI) office is greatly appreciated. Special thanks are also due to Lee Gustavus, Rick Canatella, Scott Hubley, Sharath Krishnamurthy, Amit Bhasin, Jeffrey Perry, and Andrew Fawcett from the Texas Transportation Institute (TTI) and Texas Engineering Experiment Station (TEES) for their help in specimen/sample preparation, laboratory testing, and data analysis. The various TxDOT district offices that provided the material mix-designs and assistance in material procurement are also thanked.

TABLE OF CONTENTS

TABLE OF CONTENTS (continued)

TABLE OF CONTENTS (continued)

TABLE OF CONTENTS (continued)

TABLE OF CONTENTS (continued)

TABLE OF CONTENTS (continued)

TABLE OF CONTENTS (continued)

LIST OF FIGURES

Figure **Page**

LIST OF FIGURES (continued)

LIST OF FIGURES (continued)

LIST OF FIGURES (continued)

LIST OF FIGURES (continued)

LIST OF TABLES

Table **Page**

LIST OF TABLES (Continued)

CHAPTER 1
INTRODUCTION

Hot mix asphalt concrete (HMAC) mixtures are designed to resist aging and distress induced by traffic loading and changing environmental conditions. Common HMAC distresses include rutting, fatigue, and thermal cracking. Over the past decade, the Texas Department of Transportation (TxDOT) focused research efforts on improving mixture design to preclude rutting in the early life of the pavement. Improvements in rutting resistance also offered increased resistance to moisture damage. However, a concern arose that these stiff mixtures may be susceptible to fatigue cracking in the long term in the pavement structure, particularly if the binder stiffens excessively due to oxidative aging. Therefore, in 2002 TxDOT initiated a research study with the following two primary objectives:

(1) To evaluate and recommend a fatigue HMAC mixture design and analysis system for TxDOT to ensure adequate mixture performance in a particular pavement structure under specific environmental and traffic loading conditions that incorporates the effects of binder oxidative aging.
(2) To comparatively evaluate and establish a database of fatigue resistance of commonly used TxDOT HMAC mixtures.

WORK PLAN

To accomplish these goals, researchers utilized four fatigue analysis approaches to predict fatigue lives of one common TxDOT mixture and another TxDOT mixture frequently used for rutting resistance under representative environmental conditions and typical loading conditions in standard pavement structures.

The selected approaches included the following:

- the mechanistic empirical (ME) approach developed during the Strategic Highway Research Program (SHRP) using the bending beam fatigue test (*1,2*);
- the proposed National Cooperative Highway Research Program (NCHRP) 1-37A 2002 Pavement Design Guide using the dynamic modulus test (*3, 4*);
- a calibrated mechanistic (CM) approach developed at Texas A&M University that requires strength and repeated loading tests in uniaxial tension and relaxation tests in uniaxial tension and compression for material characterization and monitoring dissipated pseudo strain energy (*5*); and
- an updated calibrated mechanistic (CMSE) approach developed at Texas A&M University that also requires measuring surface energies of component materials in addition to the material characterization tests from the original calibrated mechanistic approach (*6*).

At the conclusion of the original project in August 2004, the research team recommended the best approach for fatigue design and analysis based on a value engineering assessment. This comparison of the four fatigue analysis approaches considered variability; required resources; implementation issues; the ability to incorporate the important effects of aging, fracture, and healing; practicality; and the capability to interface with pavement design. A key element of this two-year research effort was progress made in the investigation of the relationship between the change in mixture fatigue resistance due to aging and aged binder properties. With a better understanding of this relationship, the effects of aging on fatigue life may be quantified.

In a modified third year of the project, fatigue lives of additional mixtures will be predicted using the recommended CMSE design and analysis system. These additional mixtures will explore the effects on fatigue life of mixture parameters, including binder content and binder or modifier type. Further investigation of the effects of aging on mixture fatigue resistance is also being pursued.

SCOPE OF WORK

This interim report documents the following:

(1) detailed descriptions of the four fatigue analysis approaches used to predict fatigue life,
(2) a comparison of fatigue lives of two TxDOT HMAC mixtures,
(3) the effect of binder oxidative aging on binder and mixture properties and fatigue resistance,
(4) binder-mixture relationships with respect to binder oxidative aging, and
(5) development of shift factors due to aging based on binder visco-elastic properties.

The report describes fatigue analysis results for the two selected mixtures in five specific pavement structures designed over a range of typical traffic loading conditions and under two representative Texas environmental conditions.

DESCRIPTION OF CONTENTS

The interim report is divided into 13 chapters including this chapter (Chapter 1) that provides the motivation for the project, the overall objectives and work plan, and the scope of this report. The subsequent chapters describe the information search (Chapter 2) and experimental design (Chapter 3) that includes selection of fatigue analysis approaches, materials, specimen fabrication protocols, aging conditions, and typical pavement structures. Next, the four fatigue analysis approaches are described in detail in Chapters 4 through 7. Chapter 8 describes binder testing followed by the testing and analysis utilized to explore the relationship between binder and HMAC mixture aging in Chapter 9. Then, the results, including the resulting fatigue lives from all the approaches and the aging evaluation, are described and discussed in Chapters 10, 11, and 12. This report concludes in Chapter 13 with a summary of findings, recommendations, and a work plan to complete the project in a modified third year. Appendices of detailed laboratory test results and other important data are also included.

SUMMARY

The following bullets summarize the project objectives, the work plan, scope of work, and the contents of this interim report:

- The primary objectives of this project were twofold:
  (1) to evaluate and recommend a fatigue HMAC mixture design and analysis system for TxDOT to ensure adequate mixture performance in a particular pavement structure under specific environmental and traffic loading conditions that incorporates the effects of binder oxidative aging, and
  (2) to comparatively evaluate and establish a database of fatigue resistance of commonly used TxDOT HMAC mixtures.
- The work plan entailed utilization of four fatigue analysis approaches (mechanistic empirical and calibrated mechanistic) to predict fatigue lives of one common TxDOT mixture and another TxDOT mixture frequently used for rutting resistance under representative environmental conditions and typical loading conditions in standard pavement structures. Thereafter, the best approach for fatigue design and analysis was recommended based on a value engineering assessment including the ability to incorporate practicality and the important effects of aging, fracture, and healing.
- The scope of the research work was limited to: a) two TxDOT HMAC mixtures, b) four fatigue analysis approaches, c) three binder oxidative aging conditions, d) five standard pavement structures, and e) two Texas environmental conditions.
- The report consists of 13 chapters. Chapter 1 is the introduction, and Chapters 2 and 3 are the information search and experimental design, respectively. Chapters 4 through 7 describe the four fatigue analysis approaches, followed by binder testing in Chapter 8. Chapter 9 describes the binder-mixture characterization with respect to aging. Mixture results are presented in Chapter 10, followed by a discussion, conclusions, recommendations, and future work plans in Chapters 11, 12, and 13. Other data including detailed laboratory test results are included in the appendices.

CHAPTER 2
INFORMATION SEARCH

An information search utilizing a field survey questionnaire, electronic databases, and resulting publications was conducted to gather data on current fatigue design and analysis approaches; related laboratory tests, materials, pavement structures and design; corresponding standards or references; and resources or methodologies used to obtain fatigue resistant HMAC mixtures. Effects of aging, healing, and fracture on fatigue HMAC mixture performance were also reviewed; and the literature found was summarized and documented. Researchers also reviewed and documented commonly used TxDOT mixtures, material characteristics, and other general input parameters including pavement structures, traffic loading, environmental conditions, mix designs, aging conditions, and reliability levels.

Data gathered from the information search aided the research team in selecting the appropriate fatigue analysis approaches for a comparative evaluation and subsequent recommendation to TxDOT. These data also served as the basis for formulating the experimental design including materials selection for this project.

FIELD SURVEY QUESTIONNAIRES

A field survey of government agencies and the industry addressed some of the key aspects of fatigue analysis approaches, laboratory tests, material characteristics, pavement structures and design, corresponding standards or references, and resources used for fatigue resistant HMAC mixtures. Appendix A shows an example of the field survey questionnaire.

Thirty-nine surveys were emailed to a list of contacts familiar to the research team in the industry, academia, and relevant personnel at state Departments of Transportation (DOTs). Approximately half (10) of the 23 responses received do not consider fatigue in their HMAC mixture design and analysis. Some of the responses referred the survey to other contacts, and seven responses, primarily from research agencies, provided valuable references and information that were reviewed and provided an input into the research methodology and experimental design for the project. The results from these field survey questionnaires are summarized in Appendix A from six respondents.

Of the positive responses received, a majority of the DOTs and private industry use the Superpave, mechanistic empirical, association of American State Highway and Transportation Officials (AASHTO), Asphalt Institute, and visco-elastic continuum-damage analysis either for mixture design and analysis or just to check for fatigue resistance in the final pavement structural design (Appendix A). Laboratory tests include bending beam, dynamic modulus, indirect tension, uniaxial fatigue, moisture sensitivity, and retained indirect tensile strength. Some of these approaches and associated laboratory tests have been included in the experimental design and are discussed subsequently.

LITERATURE REVIEW

From a detailed review of the information search, the research team summarized information on the prediction of HMAC mixture fatigue resistance and binder aging and its effects on HMAC mixture fatigue resistance.

Prediction of HMAC Mixture Fatigue Resistance

An approach that predicts HMAC mixture resistance to fatigue requires an understanding and description of material behavior under repeated loads that simulate field conditions (*1*). This broad description is valid for approaches that are mechanistic empirical to varying degrees. A more empirically based approach requires that the laboratory test simulate field conditions, but a constitutive law for material behavior in a more mechanics-based approach requires only material properties determined from laboratory test(s) measured using a simple stress state if possible.

In a review of flexure, supported flexure, direct uniaxial, diametral or indirect tension, triaxial, fracture mechanics, and wheel-tracking test methods conducted a decade ago, continued research in the use of dissipated energy and fracture mechanics approaches with flexure or direct or indirect tension testing were recommended (*1*). This recommendation highlighted the shift from more empirically based approaches to those able to incorporate a more fundamental mechanistic understanding of fatigue crack initiation, crack propagation, and failure.

This shift over the last decade toward the use of more applicable material behavior models and numerical analysis methods to simulate the fatigue mechanism and failure was possible due to the rapid increase in computing power. This section provides a brief review of previous and current approaches that are more empirical in nature, those that provided a bridge toward mechanistic analysis methods, and current mechanistic analysis approaches.

Mechanistic Empirical Approaches

Most previous approaches for predicting fatigue resistance of HMAC involve either controlled stress or controlled strain laboratory testing at a single representative temperature over a series of stress or strain levels, respectively, and determination of fatigue life at a stress or strain level assumed to be critical and caused by a single type of vehicle load. These approaches predict the number of stress or strain cycles to crack initiation in flexure, direct or indirect tension, or semi-circular bending tests. A method to determine a single representative temperature for laboratory testing and a temperature conversion factor to account for the fact that loading occurs over a range in temperatures is required. A shift factor is also required to account for other differences between field and laboratory conditions, including the effects of wander, healing, and crack propagation. A lengthy testing program is required with replicate tests (to account for relatively large variability) at different stress or strain levels to define an empirical fatigue relationship for a specific HMAC mixture. The determination of the critical stress or strain constitutes the mechanistic part of this type of approach, and this calculated value varies depending on the assumed model of material behavior (where layered elastic is most commonly used). The location of the critical stress or strain also limits the analysis to either bottom-up or top-down fatigue cracking without consideration of both.

Even with the limitations of mechanistic-empirical approaches, validation has been illustrated through comparisons with fatigue life measured in the field, particularly at accelerated pavement testing (APT) facilities. The mechanistic empirical approach developed at the University of California at Berkeley during the Strategic Highway Research Program as part of Project A-003A provides a widely used example with results validated with full-scale Heavy Vehicle Simulator (HVS) tests (*2*, *7*, *8*).

Another mechanistic empirical approach explored at the University of Nottingham in conjunction with the SHRP A-003A project was validated using a laboratory scale APT device. Indirect tensile fatigue testing was also utilized at the University of Nottingham, and this testing method was included in a comprehensive APT project that included scaled testing with the Model Mobile Load Simulator (MMLS3). These approaches are described in brief detail in subsequent subsections, followed by a subsection on improvements in mechanistic-empirical approaches to account for changing environmental and loading conditions.

SHRP A-003A (University of California at Berkeley). The SHRP A-003A approach utilizes the flexural beam fatigue test (third-point loading); incorporates reliability concepts that account for uncertainty in laboratory testing, construction, and traffic prediction; and considers environmental factors, traffic loading, and pavement design (*2*). Specimen preparation by rolling wheel compaction is strongly recommended as part of this approach to simulate the engineering properties of extracted pavement cores. Conditioning prior to testing to a representative or worst-case aging state is also suggested. This approach was selected for this project as the mechanistic empirical approach discussed in more detail in Chapter 4.

University of Nottingham. Fatigue research at the University of Nottingham provided validation of the SHRP A-003A analysis system through wheel tracking tests and trapezoidal fatigue testing (*2*, *9*). Validation of flexural beam fatigue tests for one aggregate type was successful for the thick wheel tracking slabs that approximated a controlled stress mode of loading. Mixture rankings by the laboratory scale APT device were also approximately equivalent to those based on indirect tensile stiffness and fatigue life determined by an indicator of the ability to dissipate energy. Large variability in the wheel tracking results was highlighted.

Fatigue analysis continued at the University of Nottingham with the inclusion of a visco-elastic model for material behavior that utilizes improvements in the conversion of dynamic shear test results to dynamic flexural results first developed as part of the SHRP A-003A system (*2*, *10*).

A visco-elastic material model was used in a mechanistic-empirical fatigue relationship to predict crack initiation based on dissipated energy to account for nonsymmetrical stress/strain response measured under full-scale loads and remove the effect of mode of loading during laboratory testing. This model provides dissipated energy contour maps where the maximum value can be located throughout the HMAC layer.

Indirect Tension Testing. Indirect tension offers a simple mode for dynamic frequency sweep, fatigue, or strength testing, although a biaxial stress state and the inability to test with stress reversal have been cited as disadvantages (*11*). The University of Nottingham has utilized this testing mode in measuring stiffness and evaluating the fatigue resistance of HMAC mixtures for overlay design (*10*).

More extensive indirect tensile fatigue testing for a range of materials in a complex layered pavement structure was included in a comprehensive evaluation of two rehabilitation strategies by TxDOT (*12*, *13*). Relative fatigue lives were defined as the ratio of fatigue resistance of untrafficked materials in these structures compared with those of the same materials trafficked with a scaled APT device (MMLS3). These ratios provided an indication of the detrimental effect of moisture damage and the improvement in fatigue resistance due to increased temperatures and subsequent compaction. A series of time-consuming tests with an average duration of 20 hours was completed at a single representative temperature (20 °C [68 °F]) and frequency (10 Hz) with no rest periods in a controlled stress mode at a stress level equal to 20 percent of the indirect tensile strength of the same HMAC material.

Tensile strength tests were also conducted in a semi-circular bending mode that induces a direct tensile load to the center zone of a semi-circular shaped specimen to supplement the indirect tensile test results. This test was considered as a possible candidate for fatigue testing in this project due to reduced load requirements for the same stress level as compared to indirect tensile testing, but it was not selected for evaluation because the associated analysis system is still under development (*14*).

Improvements to Mechanistic Empirical Approaches

The approach first developed during SHRP A-003A has been expanded further using the full-scale APT WesTrack project to develop fatigue models and associated pay factors based on construction quality (*15*, *16*). The models developed were used to predict fatigue crack initiation in the 26 original WesTrack sections.

Hourly changes in both environmental and traffic conditions (wander) were incorporated in this mechanistic empirical analysis that assumed: (1) a critical binormal strain distribution beneath dual tires at the base of the HMAC surface layer, (2) layered elastic behavior, and (3) valid extrapolation of fatigue life for temperatures greater than 30 °C (86 °F). No shift factor was applied to the fatigue life relationship that must be defined through laboratory testing for each HMAC mixture type that is different from the Superpave WesTrack HMAC mixtures.

Empirical fatigue relationships developed by the Asphalt Institute and Shell have also been improved through the definition of a continuous function of cumulative fatigue damage using Miner's Law to replace prediction of a specific level of fatigue cracking (*17, 18*). This function assumes bottom-up cracking and utilizes a layered elastic material behavior model but accounts for changing environmental and loading conditions in the accumulation of fatigue damage. Further refinement with an expanded Long Term Pavement Performance (LTPP) dataset that contains pavements exhibiting fatigue failure was recommended.

Tsai et al. have also adopted the Recursive Miner's Law for cumulative fatigue damage analysis of HMAC mixtures (*18*, *19*). This Recursive Miner's Law approach attempts to directly incorporate the significant effects of traffic, environment, material properties, and pavement structure in HMAC mixture fatigue modeling using mechanistic empirical relationships and a Weibull-type fatigue life deterioration function. In their findings, Tsai et al. observed that mixture properties played the most significant role in the fatigue damage accumulation of HMAC pavement structures under traffic loading, while the randomness of vehicle speed and traffic wander had the least effect (*18*).

Other research to further improve mechanistic empirical fatigue analysis has accounted for the effects of dynamic loads (*20*). This approach considers a moving and fluctuating concentrated load and utilizes Miner's Law (*19*) with the assumption of bottom-up cracking to predict fatigue crack initiation and cumulative fatigue damage.

The Proposed NCHRP 1-37A 2002 Pavement Design Guide Methodology for Fatigue Resistance

The NCHRP 1-37A 2002 Pavement Design Guide adopts a mechanistic empirical approach for the structural design of HMAC pavements (*3*). The basic inputs for pavement design include environmental, materials, and traffic data. There are two major aspects of ME-based material characterization: pavement response properties and major distress/transfer functions (*4*).

Pavement response properties are required to predict states of stress, strain, and displacement within the pavement structure when subjected to external wheel loads. These properties for assumed elastic material behavior are the elastic modulus and Poisson's ratio. The major distress/transfer functions for asphalt pavements are load related fatigue fracture, permanent deformation, and thermal cracking.

The current version of the NCHRP 1-37A 2002 Pavement Design Guide (and its software), which is discussed in greater detail in Chapter 7, utilizes the Asphalt Institute damage predictive equation (*21*). Unlike most ME-based approaches, this procedure incorporates two types of fatigue damage criteria. Bottom-up fatigue cracking assumes crack initiation at the bottom of the asphalt layer and propagation through the HMAC layer thickness to the surface. Top-down fatigue cracking assumes crack initiation at the pavement surface and propagation downward through the HMAC layer. In both failure criteria, tensile strain is the primary mechanistic failure load-response parameter associated with crack growth. As discussed in Chapter 7, this new design guide characterizes pavement materials in a hierarchical system comprised of three input levels. Level 1 represents a design philosophy of the highest practically achievable reliability, and Levels 2 and 3 have successively lower reliability.

For the 2002 Pavement Design Guide approach, NCHRP Project 9-19 researchers suggested constructing a dynamic modulus master-curve for all HMAC mixtures. This master-curve is developed by conducting frequency sweeps at five different temperatures and six frequencies. The same master-curve can be used as an input for predicting rutting damage. Preliminary efforts in NCHRP Project 9-19 did not show a strong correlation between dynamic modulus and fatigue cracking at full-scale APT facilities (*22*). This finding provided increased motivation to explore other approaches in this project.

Toward Mechanistic Analysis

The shift toward mechanistic analysis of fatigue cracking was recognized and encouraged through a review of the use of fracture mechanics in both HMAC and Portland cement concrete (PCC) pavements (*23*). This history highlighted early efforts utilizing linear elastic fracture mechanics and a single material property (K_{1c}) providing the driving force for crack propagation characterized by Paris' Law.

Further efforts to consider a process zone ahead of the crack tip were also reviewed, and the concept of similitude to provide a dimensionless parameter equivalent for both field and laboratory conditions was described. A warning considering the specimen-size effect and its implications for scaling cracking behavior was also issued.

The application of fracture mechanics to composite materials to advance the understanding of the mechanism of fatigue cracking was recognized as a slow process but one worth pursuing. This pursuit has continued to address the limitations of previous ME approaches and expand the knowledge base and application of HMAC fatigue analysis.

Laboratory Test Programs. To address the limitation of a lengthy testing program, researchers suggested characterizing the stiffness of HMAC using a master-curve from simple dynamic direct or indirect tensile tests that reflects the dependence on time of loading and temperature (*24*). Parameters from the master-curve were successfully used to predict the coefficients in empirical fatigue relationships. The range of HMAC mixture variables, including modified binders utilized in developing the regression relationships, were also provided.

Linear Visco-Elastic Models. To address the limitation of assumed layered elastic material behavior, other researchers produced an integrated HMAC mixture and pavement design that allows for more realistic linear visco-elastic behavior (*25*). This type of material model accounts for asymmetrical stress-strain distributions under moving wheel loads and the effect of time of loading history. In a multi-tiered analysis, the approach separately utilized two conventional empirical fatigue relationships (based on strain and dissipated energy) for crack initiation and Paris' Law for crack propagation as described by Schapery (*26*).

Laboratory testing requirements include frequency sweep, creep, and strength testing in direct tension or compression at relevant temperatures. A nonlinear finite element simulation of a multi-layer pavement structure that selects an appropriate HMAC stiffness as a function of a more realistic asymmetrical stress state was also utilized in conjunction with mechanistic empirical fatigue relationships (*27*). Numerical techniques were also used to model the behavior of three specific materials using elastic-plastic fracture mechanics (*28*). Both crack initiation and propagation were modeled, but the viscous behavior of HMAC was not taken into account.

Fracture Mechanics Approach. Further research toward improving the linear elastic fracture mechanics approach with Paris' Law as described by Schapery related the fracture coefficients A and n and described the use of uniaxial dynamic and strength tests to determine both parameters from a master stiffness curve and mixture correction factors (*29*). Crack propagation using Paris' Law was also incorporated successfully in two- and three-dimensional finite element simulations (*30*). This approach spread complex simulation computations over the material lifetime, incorporating damage and resulting stress redistribution. Crack propagation was extrapolated between simulations to determine fatigue life from propagation of an initial crack size assumed related to maximum aggregate size. This approach that assumes elastic material response to a single type of load was validated using flexural beam fatigue tests. Nonlinear fracture mechanics were applied to compare crack propagation parameters of different materials at low temperatures and highlight the need to include effects of inelastic dissipated energy in fatigue analysis (*31*).

Continuum Mechanics Approach. Research in fatigue analysis over the past decade has expanded to include investigation of both damage due to repeated loading and healing due to repeated rest periods (*32*, *33*). Recovery of a loss in stiffness monitored during fatigue testing was noted for short rest periods in direct uniaxial testing in a review of laboratory fatigue tests, and the lack of fatigue cracking in thick HMAC pavements was attributed to a healing effect in an evaluation toward revising design procedures (*11*, *34*).

A continuum mechanics approach developed through research efforts at North Carolina State University and Texas A&M University successfully accounted for damage growth through crack initiation and propagation and healing for any load history or mode of loading (*32*, *33*).

This approach utilizes the visco-elastic correspondence principle and work potential theory described by Schapery (*26*) to remove viscous effects in monitoring changes in pseudo-stiffness in repeated uniaxial tensile tests. Coefficients in the visco-elastic constitutive model describe differences in damage and healing behavior of different materials. This model was validated with both laboratory and field results and behavior predicted from the micromechanical approach also developed at Texas A&M University and described in a subsequent subsection (*33*).

The continuum approach has also led to the development of two simplified fatigue analysis systems (*35*, *36*). One system predicts fatigue behavior for temperatures less than 20 °C (68 °F) from a characteristic damage curve generated based on frequency sweep and strength tests in uniaxial tension at multiple temperatures (*35*). Improvements to this system to consider aging and healing and application to other HMAC mixture types were recommended. The other system utilizes indirect tensile creep and strength testing with a longer gauge length than the standard Superpave mixture test and visco-elastic analysis of material response (*36*, *37*). The use of fracture energy based on tests at 20 °C (68 °F) to predict fatigue cracking was validated using data from the full-scale APT WesTrack project.

With a shift toward more mechanics-based approaches, fatigue analysis is expected to become independent of many factors and variables that limit the application of ME approaches that were the only available analysis tools prior to the rapid increase in computing power. These factors and variables include mode of loading (controlled stress or controlled strain), laboratory test type, time of loading, temperature, type and location of loading, rest periods, and HMAC mixture variables.

Empirical to ME to Calibrated Mechanistic

A major reason for the gradual change of mixture fatigue analysis from empirical or phenomenological to ME to calibrated mechanistic is the greatly increased capabilities of computers to model material behavior realistically, using mechanics and user friendly computational packages such as finite element programs. As computers become faster with larger memories in the future, these approaches will be the simplest, most direct, and probably most practical way to design HMAC mixtures and pavements.

These computational packages can only utilize material properties as input, instead of empirical constants or ME regression coefficients used in previous approaches. This development brings with it an added bonus that laboratory or non-destructive field measurement of material properties is much simpler than determination of these constants and coefficients through extensive laboratory testing.

Calibrated Mechanistic Approaches. The calibrated mechanistic approaches are based on the theory that HMAC is a complex composite material that behaves in a nonlinear visco-elastic manner, ages, heals, and requires that energy be stored on fracture surfaces as load-induced damage in the form of fatigue cracking progresses. Energy is also released from fracture surfaces during the healing process. HMAC mixture resistance to fatigue cracking thus consists of two components, resistance to fracture (both crack initiation and propagation) and the ability to heal, that both change over time.

Several approaches that predict fatigue life require material characterization and account for both the fracture and healing processes in HMAC that have been developed over the past decade. In the SHRP A-005 project, a complete model of fatigue fracture and healing was developed (*38*). Other researchers showed the importance of the use of fracture and dissipated energy in measuring the fracture resistance of a HMAC mixture (*39*). This same concept of dissipated energy per load cycle provides the driving force for fatigue crack initiation and propagation, and researchers demonstrated that the fracture energy approach was able to accurately predict the fatigue life of a wide variety of HMAC mixture designs as compared to other approaches (*40*, *41*). SHRP A-005 results and a finite element computer program have been used to illustrate substantial agreement with these results in predicting the two phases of crack growth, initiation, and propagation (*42*).

The Texas A&M Calibrated Mechanistic Approach. A micromechanical approach developed at Texas A&M University based on the SHRP A-005 results requires only creep or relaxation, strength, and repeated load tests in uniaxial tension and compression and a catalog of fracture and healing surface energy components of asphalt binders and aggregates measured separately (*43, 44*, *45*).

Surface energy components of various common aggregates and binders have been measured at Texas Transportation Institute (TTI) in various studies (*43*, *44, 46, 47*). The results have been cataloged and are also proving useful in other ongoing TTI studies including moisture damage prediction in HMAC pavements. In this approach selected for evaluation in this project, HMAC behavior in fatigue is governed by the energy stored on or released from crack faces that drive the fracture and healing processes, respectively, through these two different mechanisms. Chapter 5 discusses this approach in greater detail.

Computational models that incorporate more realistic material behavior for HMAC are expected to be increasingly faster and user-friendly in the near future. Convenient and efficient methods of characterizing the fracture and healing properties of HMAC mixtures will be useful to take advantage of these continued advances that promise improved mixture and pavement design.

Binder Aging and HMAC Mixture Fatigue Resistance

TTI's Center for Asphalt and Materials Chemistry (CMAC) has studied the effect of oxidative aging on asphalt binders over the last 15 years. During this time, CMAC researchers have conducted a comprehensive study of the oxidation kinetics of binders under varying conditions of temperature and oxygen pressure and of the effect of this oxidation on the physical properties of binders. Both of these issues are crucial to understanding the rate at which asphalt binders age in service in the field and the results of these changes on performance. This section briefly summarizes CMAC's relevant results.

Fundamentally, the oxidation of binder results in compounds that are more polar and therefore form strong associations with each other. These associations result in both a greater resistance to flow (higher viscosity) and larger elastic modulus. Together these effects result in higher stresses in HMAC under load. This greater resistance to flow can be beneficial at high temperatures by reducing permanent deformation. A problem emerges, however, when aging is excessive, leading to excessively large stresses that result in binder failure at lower temperatures (thermal cracking).

This effect of oxidative aging must also contribute to failure by repeated load (fatigue cracking) through its effect on HMAC stiffness that governs material response to load. It also explains why producing binders that have higher high-temperature Superpave grades (and thus provide stiffer mixtures at rutting temperatures) may be more prone to premature fatigue cracking. Starting out stiffer puts these HMAC mixtures at a disadvantage as stiffness age-hardening proceeds throughout the lifetime of the HMAC pavement.

The following subsections provide more detail on these effects of oxidation on binders and thus on HMAC mixture fatigue resistance.

Effect of Aging on Binder Viscosity

Binder viscosity increases dramatically due to oxidation, in fact, by orders of magnitude over the life of a pavement. Figure 2-1 shows typical changes in the dynamic viscosity master-curve for a binder at a reference temperature of 4 °C (39.2 °F). The effect is most significant at high temperatures (low frequency) but plays a role in pavement performance at all practical temperatures. The increase in log viscosity with oxidation is linear and has no bound within the practical limits encountered by binder during a normal pavement life.

Figure 2-2 shows the increase in low shear-rate dynamic viscosity (η_0^*) measured at 60 °C (140 °F) versus aging time at 60 °C (140 °F) and atmospheric air pressure for two binders. These data were obtained in thin films, and thus the hardening rates reflected by the slope of these lines are higher than those that occur in the field, but the effect and ultimate result that is dependent on binder type is clear nonetheless.

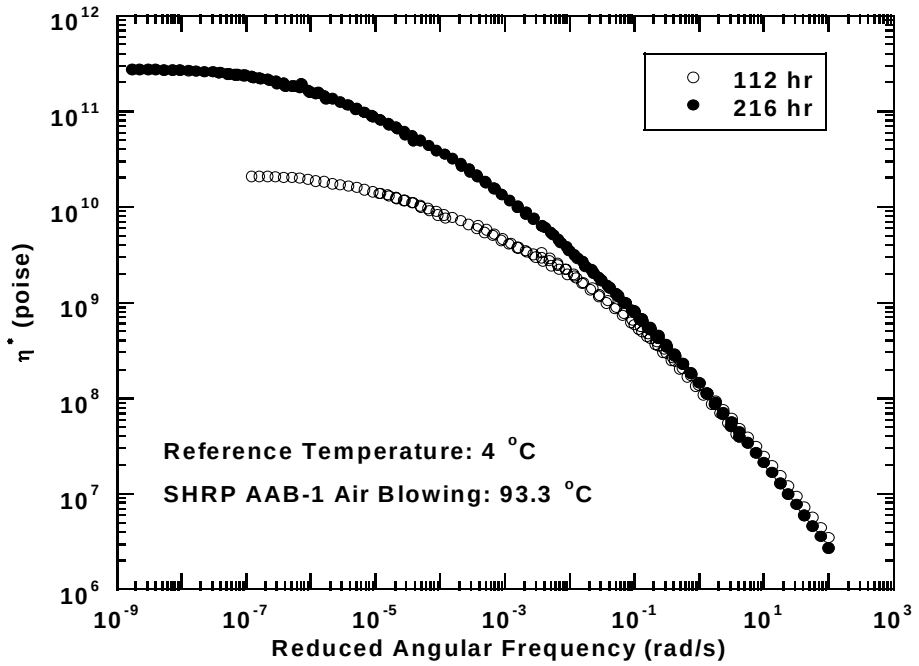

Figure 2-1. Master-Curve for SHRP AAB-1 at Two Aging Times (°F = 32 + 1.8(°C)).

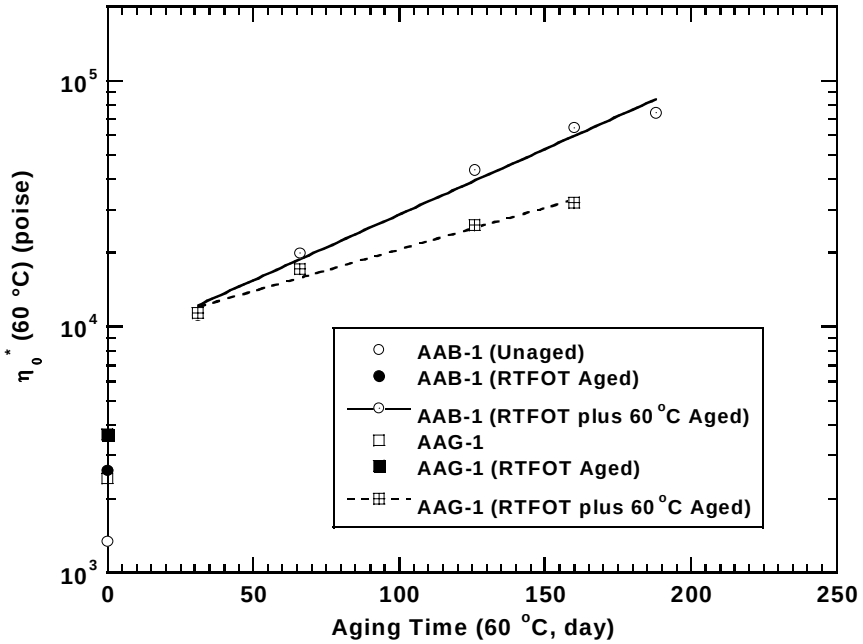

Figure 2-2. Effect of Aging on Low Shear-Rate Limiting Viscosity (°F = 32 + 1.8(°C)).

Effect of Aging on Low-Temperature Superpave Performance Grade

Viscosity is inversely related to the *m*-value in the Superpave low-temperature performance grade for binders and elastic modulus is related to stiffness. Thus as binders age, *m* decreases and stiffness increases. This increase in stiffness (and decrease in *m*) results in a deterioration of the low-temperature grade as a binder oxidizes (*48*). Figure 2-3 shows this deterioration that results from extended exposure to long-term aging in the Pressure Aging Vessel (PAV). Similar effects occur due to aging at pavement field conditions.

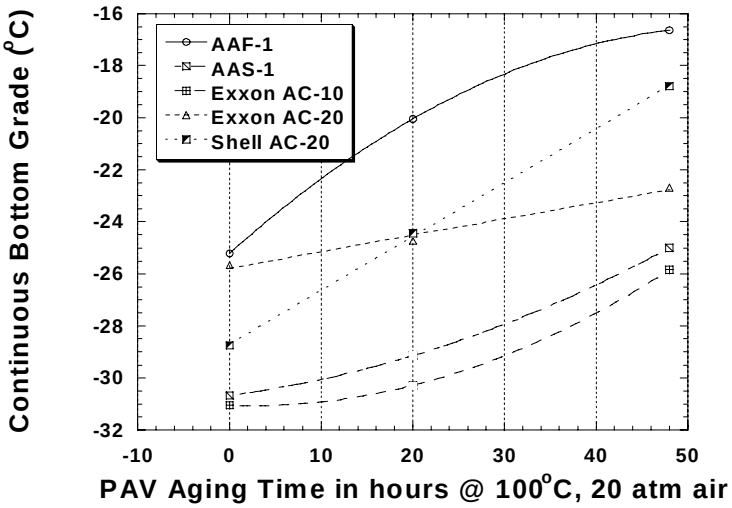

Figure 2-3. Continuous Bottom Grade as a Function of PAV Aging Time (°F = 32 + 1.8(°C)).

Effect of Aging on Ductility and Shear Properties

One of the significant results from the literature is that ductility at 15 °C (59 °F) relates well to pavement performance (*49*, *50*). According to these studies, when the ductility of a binder decreases to a minimum value in the range of about of 3 to 5 cm (1.18 to 1.98 inches) (at an extension rate of 1 cm/min (0.39 inches/min)), the pavement condition tends to suffer from fatigue cracks. CMAC researchers have related this ductility to the dynamic shear rheometer (DSR) loss (*G''*) and storage moduli (*G'*). As these moduli increase, the binder breaks at smaller values of strain (loss of ductility) due to higher values of stress.

This correlation between ductility and the DSR function $G''(\eta''/G')$ is shown in Figure 2-4 for some 20 conventional binders in the low ductility region thought to be near HMAC pavement failure (*51*). The DSR function increases and the ductility decreases with oxidative aging. TxDOT Project 0-1872 evaluated the correlation between this DSR function and field performance (*52*).

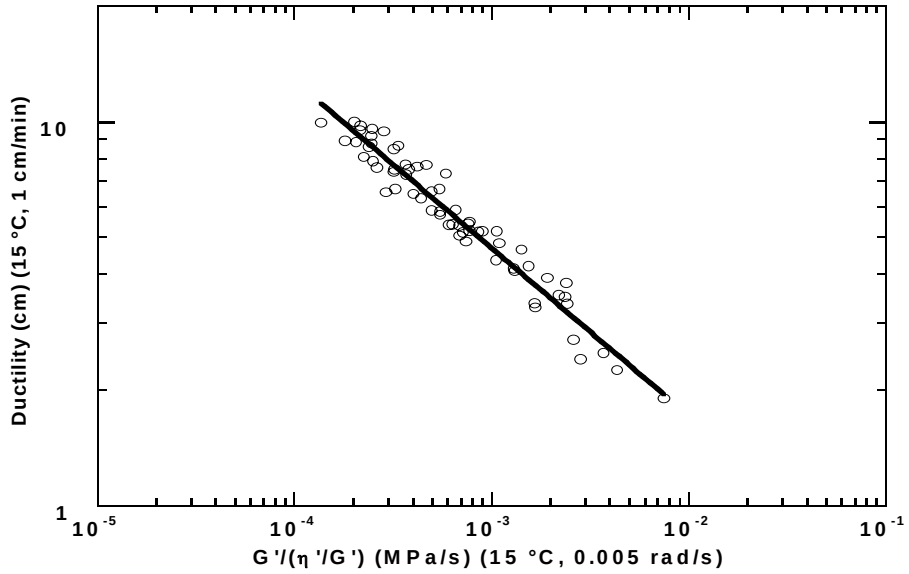

Figure 2-4. Ductility versus DSR Function G'/(η' /G') (°F = 32 + 1.8(°C)).

Hypothetical Mechanisms

Based on the results described, CMAC researchers hypothesize a correlation between oxidative aging and pavement failure by two mechanisms:

- Increased stresses under load (compared to new pavements) result from a decreased ability to flow and an increased elastic stiffness, both leading to cracking.
- A decreased ability to self heal results in a decrease in fatigue life.

Data described in this section lead to the following conclusion: oxidative aging produces a material that is more susceptible to fatigue cracking or other distress that occurs later in the life of the pavement. Consequently, an approach that predicts mixture fatigue resistance must be sensitive to changes in binder properties that occur due to oxidative aging. These changes vary for binder types that are different chemically and will thus exhibit different physical properties over time depending on the effects of oxidation. Assessment of the impact of aging on HMAC mixture fatigue resistance and the ability of different approaches to incorporate this effect in predicting fatigue life is therefore important and thus selected as part of this project. Binder tests and results are discussed in Chapters 8 through 11.

SELECTED FATIGUE ANALYSIS APPROACHES

Based on this extensive literature review and subsequent consultation with TxDOT project personnel, the research team selected the following fatigue analysis approaches for comparative evaluation in this project:

(1) The mechanistic empirical with flexural bending beam fatigue testing.
(2) The calibrated mechanistic with Surface Energy measurements.
(3) The calibrated mechanistic without surface energy measurements.
(4) The proposed NCHRP 1-37A 2002 Pavement Design Guide with dynamic modulus testing.

These approaches together with binder aging effects are discussed in more detail in Chapters 4, 5, 6, 7, and 8, respectively. Binder-mixture characterization that relates binder oxidative aging to HMAC mixture fatigue properties is presented in Chapter 9.

SUMMARY

The following bullets summarize the key points from the information search:

- Of the positive responses received, the field survey questionnaire indicated that the majority of the DOTs use Superpave, mechanistic empirical, AASHTO, Asphalt Institute, and visco-elastic continuum-damage analysis for their fatigue mixture design, analysis, and/or structural design check with laboratory tests including the bending beam, dynamic modulus, indirect tension, uniaxial fatigue, moisture sensitivity, and retained indirect tensile strength.
- A detailed literature review indicated that the major disadvantage of most ME approaches are the lengthy test programs and the fact that these approaches are phenomenologically or empirically based and often assume HMAC linear elastic behavior.
- With advances in computer technology, there has been a drive towards more simple and realistic calibrated mechanistic approaches that utilize continuum micro-mechanics with fracturing and healing as the two primary mechanisms governing HMAC fatigue damage. Utilization of finite element analysis provides HMAC modeling the potential to include visco-elastic behavior while calibration constants are used to realistically simulate field conditions.
- Binder oxidative aging has a significant impact on HMAC pavement fatigue performance primarily in terms of the HMAC mixture's resistance to fracture under traffic loading and ability to heal. The inclusion of aging in HMAC fatigue mixture designs is profoundly significant.
- Four fatigue analysis approaches: ME, CMSE, CM, and the proposed NCHRP 1-37A 2002 Pavement Design Guide, were selected for comparative evaluation and subsequent recommendation to TxDOT. This evaluation and recommendation are discussed in this interim report.

CHAPTER 3
EXPERIMENTAL DESIGN

The research methodology for this project involved an information search (discussed in Chapter 2) and subsequent selection of fatigue analysis approaches, drafting an experimental design program, laboratory testing, and subsequent data analysis. This chapter discusses the experimental design including materials selection and the corresponding specimen fabrication protocols and aging conditions. Field conditions in terms of the selected pavement structures, traffic, and environmental conditions are also presented. Laboratory testing including the appropriate fatigue analysis approaches and binder-mixture characterization are discussed in Chapters 4 through 9, respectively.

HMAC MIXTURES AND MIX-DESIGN

HMAC mixtures commonly used by TxDOT include Type C, Coarse Matrix High Binder (CMHB)-Type C, CMHB-Type F, Type A, Type B, Type D, Type F, Superpave, Stone Mastic Asphalt (SMA), Stone Filled Mixture, and Porous Friction Course (PFC) (*53*). Type C and CMHB-Type C are the most common. More specialized mixtures include the SMA and stone filled designs developed to provide superior rutting performance.

Aggregates generally include limestone, igneous, and gravel characterized and blended to typical TxDOT or Superpave standards. Among the Performance-Graded (PG) binders used by TxDOT, notable ones include PG 58-22, PG 64-22, PG 70-22, and PG 76-22 for the environmental conditions in Texas.

For this project, the research team selected two commonly used TxDOT HMAC mixtures for comparative fatigue performance evaluation. These were basic TxDOT Type C and rut resistant Superpave HMAC mixtures, defined as the Bryan (BRY) and Yoakum (YKM) mixtures, respectively, to represent the districts where the mix designs were obtained. Note that development of mix designs was not part of this project.

The Bryan Mixture – Basic TxDOT Type C (PG 64-22 + Limestone)

The Bryan HMAC mixture was designed using standard TxDOT gyratory design protocols from the Bryan District (*54*). This mixture consists of a performance-graded PG 64-22 binder mixed with limestone aggregates to produce a dense-graded TxDOT Type C mixture. The aggregate gradation curve for this mixture is shown in Figure 3-1. This mixture was used on highways US 290 and SH 47 in the Bryan District (*54*).

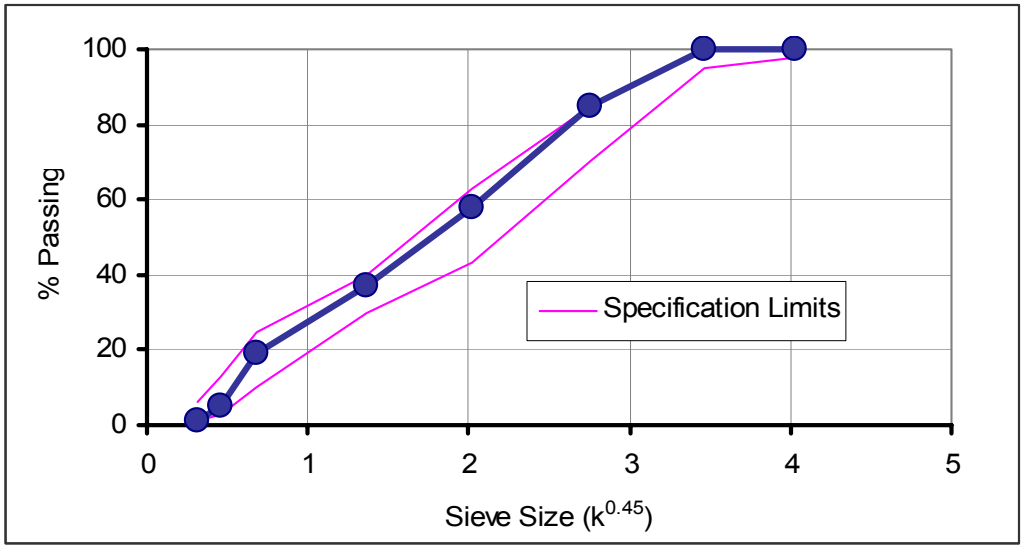

Figure 3-1. Limestone Aggregate Gradation Curve for TxDOT Type C Mixture.

The PG 64-22 binder was supplied by Eagle Asphalt, and the limestone aggregate was supplied by Colorado Materials, Inc. from its Caldwell plant. The mix design was 4.6 percent binder content by weight of aggregate (4.4 percent by weight of total mix) with a HMAC mixture theoretical maximum specific gravity of 2.419 (*54*). The target specimen fabrication air void (AV) content was 7±0.5 percent to simulate after in situ field construction and trafficking when fatigue resistance is critical.

The Yoakum Mixture – Rut Resistant 12.5 mm Superpave (PG 76-22 + Gravel)

The Yoakum HMAC mixture from the Yoakum District was a 12.5 mm Superpave mixture designed with a PG 76-22 binder and crushed river gravel. This mixture was used on US Highway 59 near the City of Victoria in Jackson County and is considered a rut resistant mixture. This type of HMAC mixture was selected to examine its fatigue properties consistent with the title and motivation of this project.

The binder and aggregates were sourced from Eagle Asphalt (Marlin Asphalt), Inc. and Fordyce Materials, respectively. Unlike PG 64-22, PG 76-22 is a modified binder with about 5 percent styrene-butadiene-styrene (SBS) polymer.

In addition to the crushed river gravel, the Yoakum mixture used 14 percent limestone screenings and 1 percent hydrated lime. Figure 3-2 shows the combined dense gradation of the Yoakum river gravel.

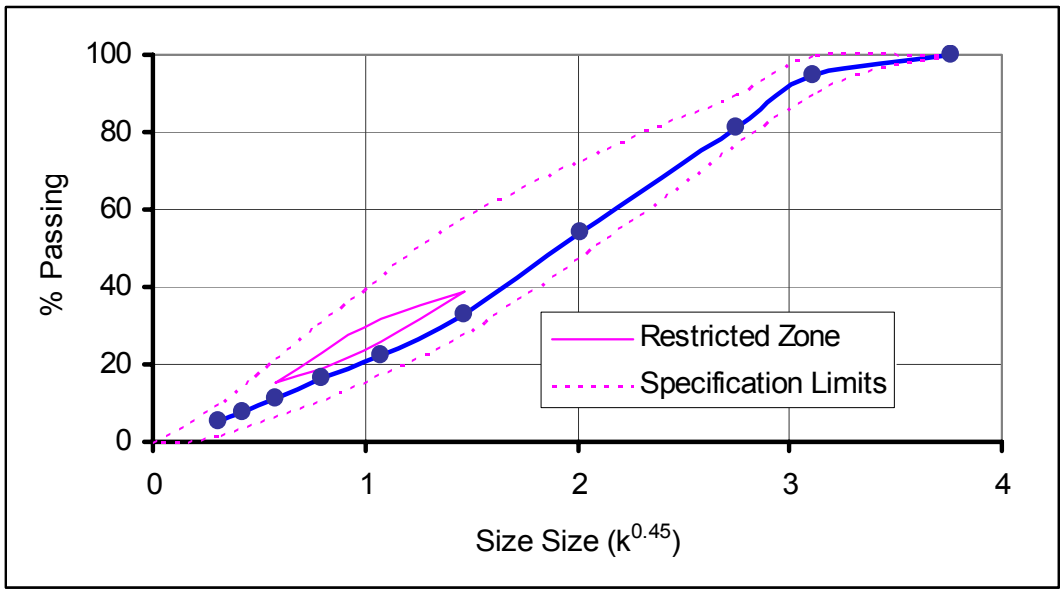

Figure 3-2. Gravel Aggregate Gradation Curve for Rut Resistant 12.5 mm Superpave Mixture.

The mix design was 5.6 percent binder content by weight of aggregate (5.3 percent by weight of total mix) with a HMAC mixture theoretical maximum specific gravity of 2.410. Like the Bryan mixture, the target specimen fabrication AV for the Yoakum HMAC mixture was 7±0.5 percent.

Material Properties for the Binders

Laboratory characterization of the binder materials based on the AASHTO PP1, PP6, T313, and T315 test protocols produced the results shown in Figures 3-3 through 3-5 (*55, 56*). These results represent mean values of at least two binder test samples.

Note that for most of the binder test results, metric units are used consistent with the PG specifications used by TxDOT for binders (*55*, *56*). English (U.S.) units or unit conversions are provided in parentheses to meet TxDOT requirements for other units including length and temperature.

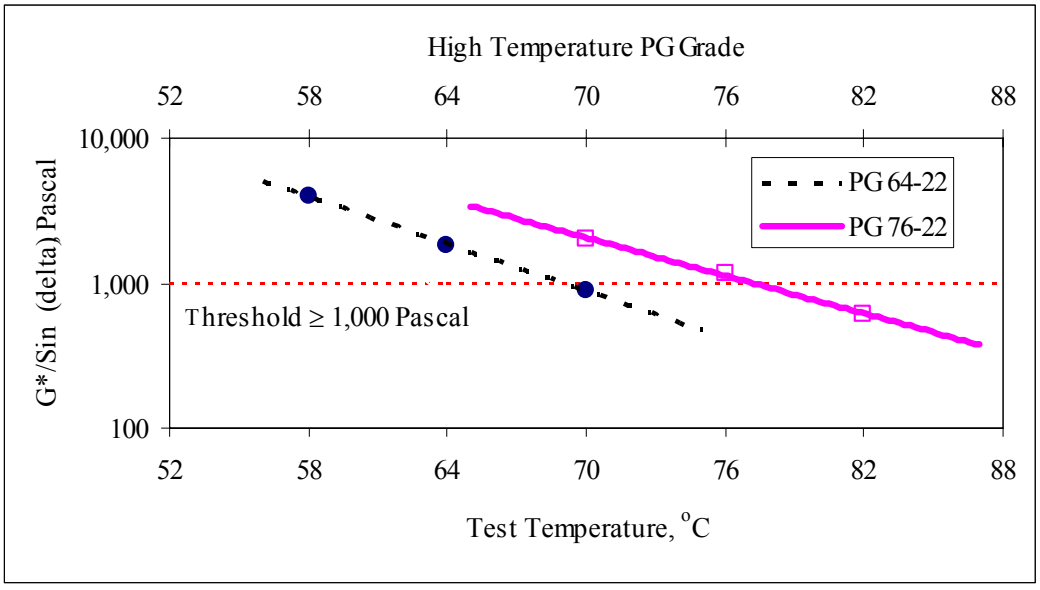

Figure 3-3. Binder High Temperature Properties – G*/Sin (delta) (Pascal) (°F = 32 + 1.8(°C)), (delta ≅ δ).

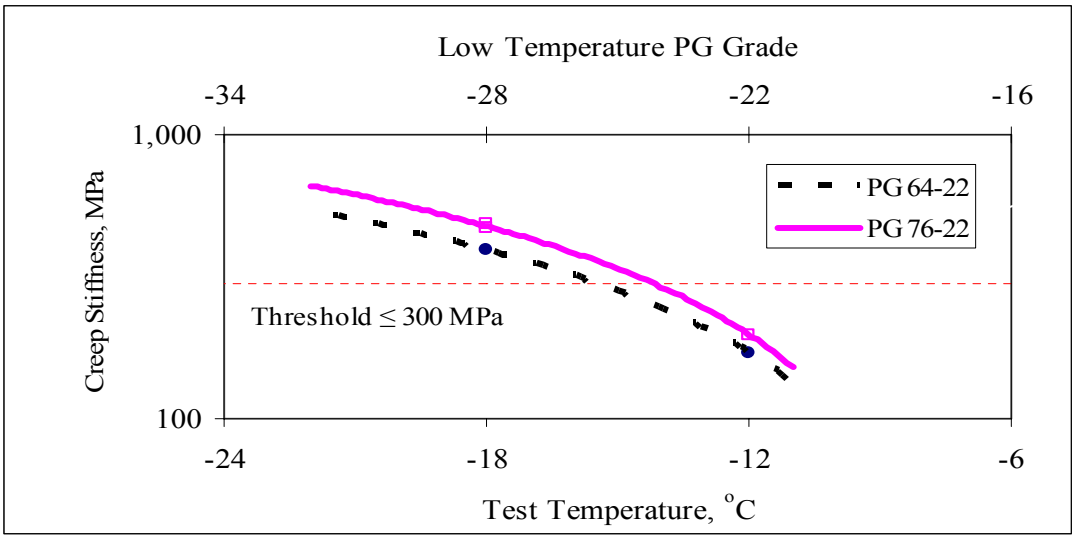

Figure 3-4. Binder Low Temperature Properties – Flexural Creep Stiffness (MPa)

(°F = 32 + 1.8(°C)).

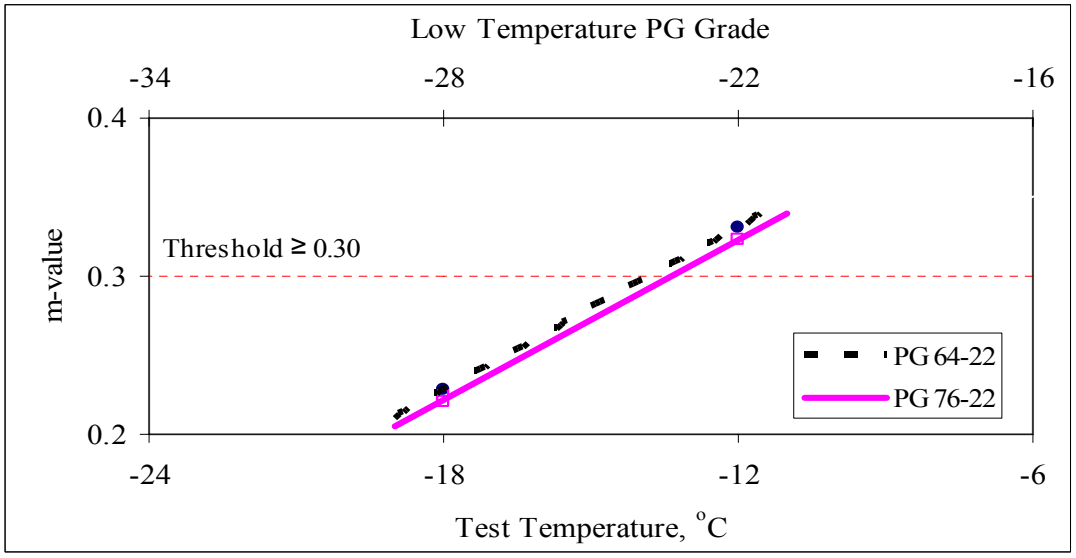

Figure 3-5. Binder Low Temperature Properties (m-value)

(°F = 32 + 1.8(°C)).

These verification results shown in Figures 3-3 through 3-5 indicate that the binders meet the PG specification consistent with the material properties for PG 64-22 and PG 76-22 binders (*55, 56*).

Table 3-1 shows the measured intermediate temperature properties of the binders at 25 °C (77 °F) in terms of the complex shear modulus (G^*) and the phase angle (δ). The results represent average values of three replicate binder-sample tests. These properties quantify the binders' resistance to fatigue associated cracking. As shown in Table 3-1, both the PG 64-22 and PG 76-22 met the required maximum specified threshold value of a $G^* \, Sin \, \delta$ of 5,000 kPa (*55, 56*).

Table 3-1. Intermediate Temperature Properties of the Binders at 25 °C (77 °F).

Binder	Average Value		Standard Deviation of G*Sin δ (kPa)	*CV* (G*Sin δ) (%)	PG Specification (kPa)
	δ (°)	G*Sin δ (kPa)			
PG 64-22	65	600	10.91	1.82	≤ 5000
PG 76-22	62	1019	70	6.90	≤ 5000

Note that these measured binder properties also constitute input parameters for the proposed NCHRP 1-37A Pavement Design Guide Level 1 analysis discussed in subsequent chapters. These material property results also indicate that, as expected, the complex shear modulus and flexural stiffness of the modified PG 76-22 binder at any test temperature is relatively higher than that of the PG 64-22.

Material Properties for the Aggregates

Material properties for the aggregates listed in Table 3-2 indicate that the aggregate meets the specification consistent with the respective test methods shown in the table (*57*). The bulk specific gravity for the combined aggregates was 2.591 and 2.603 for limestone and gravel, respectively.

Table 3-2. Aggregate Properties.

Test Parameter	Limestone	Gravel	Specification	Test Method
Soundness	18%	20%	≤ 30%	Tex-411-A
Crushed faces count	100%	100%	≥ 85%	Tex-460-A
Los Angeles (LA) abrasion	28%	25%	≤ 40%	Tex-410-A
Sand equivalent	74%	77%	≥ 45%	Tex-203-F

HMAC SPECIMEN FABRICATION

The basic HMAC specimen fabrication procedure involved the following steps: aggregate batching, binder-aggregate mixing, short-term oven aging (STOA), compaction, sawing and coring, and finally volumetric analysis to determine the AV. These steps are briefly discussed in this section.

Aggregate Batching

Aggregates were batched consistent with the gradations shown in Tables 3-3 and 3-4, which correspond to those shown in Figures 3-1 and 3-2, respectively.

Table 3-3. Limestone Aggregate Gradation for TxDOT Type C Mixture.

Sieve Size		TxDOT Specification (*53*)		% Passing
	mm	Upper Limit (%)	Lower Limit (%)	
5/8″	15.9	100	98	100.0
1/2″	12.5	100	95	100.0
3/8″	9.5	85	70	84.8
#4	4.75	63	43	57.9
#10	2.0	40	30	36.9
#40	0.425	25	10	19.0
#80	0.175	13	3	5.0
#200	0.075	6	1	1.0

Table 3-4. Gravel Aggregate Gradation for 12.5 mm Superpave Mixture.

Sieve Size		TxDOT Specification (*53*)		% Passing
	mm	Upper Limit (%)	Lower Limit (%)	
3/4″	19.00	100	--	100.0
1/2″	12.50	100	90	94.6
3/8″	9.50	90		81.0
#4	4.75			54.4
#8	2.36	58	28	32.9
#16	1.18			22.4
#30	0.60			16.2
#50	0.30			11.0
#100	0.150			7.6
#200	0.075	10	2	5.5

Mixing, Short Term Oven-Aging, Compaction, and Air Voids

The HMAC mixture mixing and compaction temperatures shown in Table 3-5 are consistent with the TxDOT Tex-205-F and Tex-241-F test specifications for PG 64-22 and PG 76-22 binders (*57*). Prior to binder-aggregate mixing, the limestone and gravel aggregates were pre-heated to a temperature of 144 °C (291 °F) and 163 °C (325 °F), respectively, for at least 4 hrs to remove any moisture. The binder was also heated at the mixing temperature for at most 30 minutes before mixing to liquefy it.

Table 3-5. HMAC Mixture Mixing and Compaction Temperatures.

Process	**HMAC Mixture Temperature (°C)**	
	Bryan Mixture	**Yoakum Mixture**
Aggregate pre-heating	144 (291 °F)	163 (325 °F)
Binder-aggregate mixing	144 (291 °F)	163 (325 °F)
4 hrs short-term oven aging	135 (275 °F)	135 (275 °F)
Compaction	127 (261 °F)	149 (300 °F)

HMAC mixture STOA lasted for 4 hrs at a temperature of 135 °C (275 °F), consistent with the AASHTO PP2 standard aging procedure for Superpave mixture performance testing (*58*). STOA simulates the time between HMAC mixing, transportation, and placement up to the time of in situ compaction in the field (*58*). Note that the acronym AASHTO PP2 is also used synonymously with the acronym STOA in this interim report.

Gyratory Compaction

All the cylindrical specimens for the Dynamic Modulus and CMSE/CM tests were gyratory compacted using the standard Superpave Gyratory Compactor (SGC) shown in Figure 3-6. Compaction parameters were 1.25° compaction angle and 600 kPa (87 psi) vertical pressure at rate of 30 gyrations per minute.

Figure 3-6. Superpave Gyratory Compactor.

Kneading Beam Compaction

Researchers compacted beam specimens for the flexural bending beam fatigue tests using the linear kneading compactor shown in Figure 3-7 up to the target AV content consistent with the specified beam thickness at a maximum compaction pressure of 6900 kPa (1000 psi) (*11, 12*).

Figure 3-7. Linear Kneading Compactor.

All HMAC specimens were compacted to a target AV content of 7±0.5 percent, as stated previously, to simulate after in situ field construction and trafficking when fatigue resistance is critical.

Sawing, Coring, Handling, and Storage

Cylindrical specimens were gyratory compacted to a size of 165 mm (6.5 inches) height by 150 mm (6 inches) diameter, while actual test specimens were sawn and cored to a 150 mm (6 inches) height and 100 mm (4 inches) diameter. Beam specimens were kneading compacted to a size of 457 mm (18 inches) length by 150 mm (6 inches) width by 63 mm (2.5 inches) thickness, and test specimens were sawn to a 380 mm (15 inches) length by 63 mm (2.5 inches) width by a 50 mm (2 inches) thickness (*11*). Figure 3-8 shows the dimensions of the final test specimens (where 1 mm ≅ 0.039 inches).

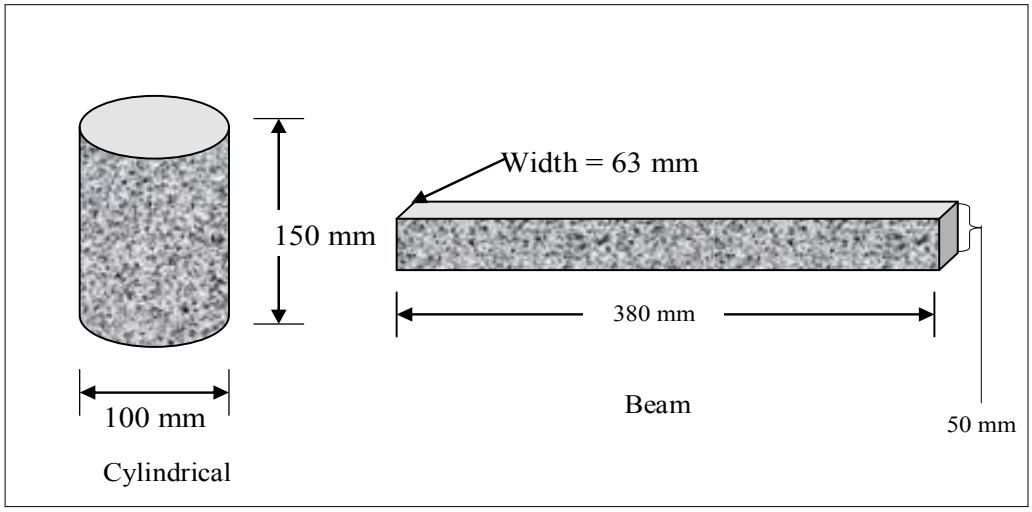

Figure 3-8. Laboratory Test Specimens (Drawing not to Scale) (1 mm ≅ 0.039 inches).

After the specimens were sawn and cored, volumetric analysis based on the fundamental principle of water displacement was completed to determine the actual specimen AV. HMAC specimens that did not meet the target AV content were discarded or used as dummies in trial tests. In total, a cylindrical specimen took approximately 40 hrs to fabricate while a beam specimen, because of the difficulty in sawing, took an additional 5 hrs. While beam specimens require delicate handling, the cylindrical specimens are not as sensitive to handling. Prior to laboratory testing, specimens were generally stored on flat surfaces in a temperature-controlled room at approximately 20±2 °C (68±36 °F).

BINDER AND HMAC MIXTURE AGING CONDITIONS

Researchers selected three aging conditions listed in Table 3-6 for this project for both the binder and HMAC compacted specimens. Consistent with the Superpave procedure, all HMAC mixtures were subjected to 4 hrs STOA, as discussed previously, prior to the simulated aging period for the three selected aging conditions.

Table 3-6. Aging Conditions for Binders and HMAC Compacted Specimens.

Aging Condition @ 60 °C (140 °F)	Description	Comment
0 months	Simulates time period just after in situ field construction at the end of compaction (*58*)	All HMAC mixtures (prior to compaction) were subjected to 4 hrs STOA (AASHTO PP2).
3 months	Simulates 3 to 6 years of Texas environmental exposure (*52*)	
6 months	Simulates 6 to 12 years of Texas environmental exposure (*52*)	

The aging process for HMAC specimens involved keeping the compacted specimens in a temperature-controlled room at 60 °C (140 °F) and at the same time allowing the heated air to circulate freely around the specimens. This allowed for accelerated oxidative aging of the binder within the HMAC specimens. An aging temperature of 60 °C (140 °F) was selected to accelerate aging because this temperature realistically simulates the critical pavement service temperature in Texas for HMAC aging. Based on previous research, the process also simulates the field HMAC aging rate (*52*). Chapter 8 discusses the aging process for the binder in detail.

Figure 3-9 is a schematic illustration of the HMAC specimen aging conditions considered in each respective fatigue analysis approach. The NCHRP 1-37A 2002 Pavement Design Guide software encompasses a Global Aging Model that takes into account the aging effects, which are discussed in Chapter 7. Therefore, it was deemed unnecessary to test aged specimens for the proposed NCHRP 1-37A 2002 Pavement Design Guide fatigue analysis.

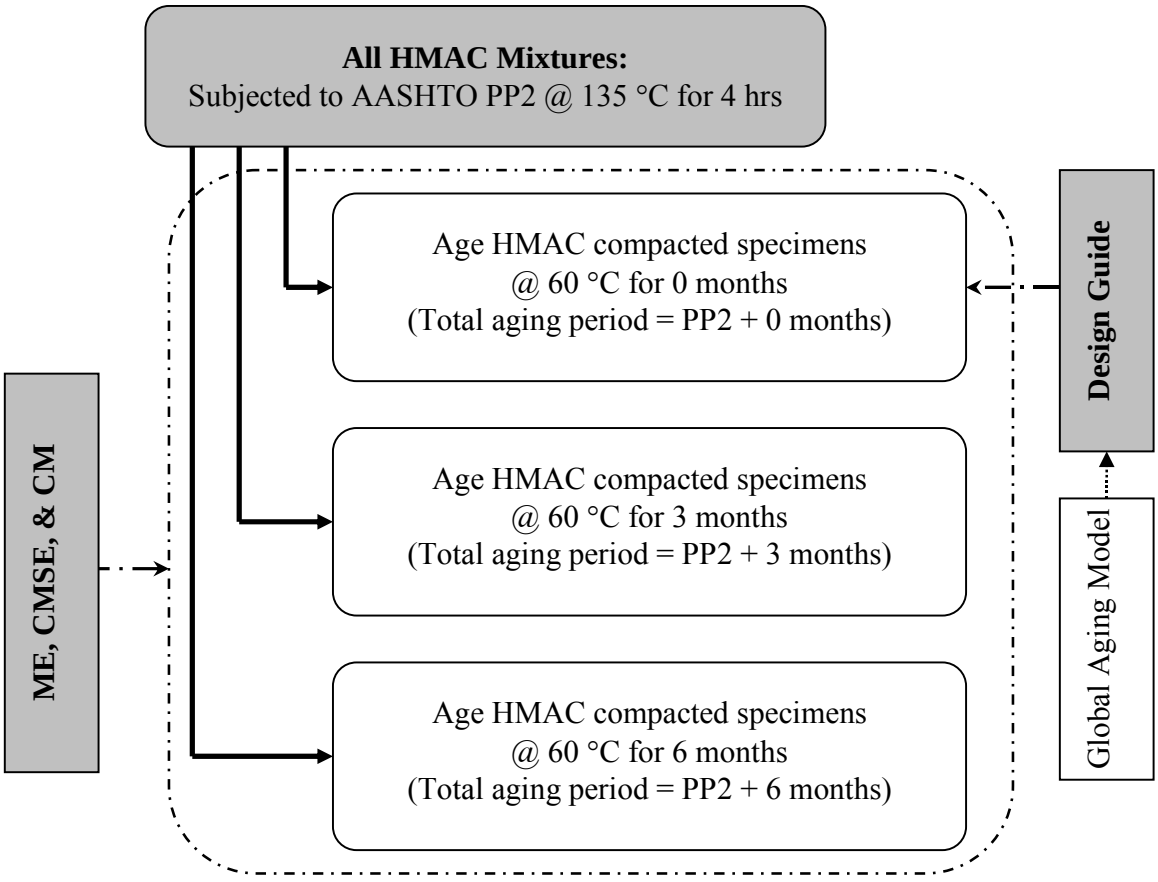

Figure 3-9. Fatigue Analysis Approaches and HMAC Mixture Aging Conditions (°F = 32 + 1.8(°C)).

HYPOTHETICAL FIELD PAVEMENT STRUCTURES AND TRAFFIC

Table 3-7 displays a list of the five selected TxDOT pavement structures (PS) and five associated traffic levels ranging between 0.25 to 11.00 × 10^6 equivalent single axle loads (ESALs) that were considered in this project. These pavement structures represent actual material properties and layer thicknesses that are commonly used on TxDOT highways (*60*). Typical traffic conditions consisted of an 80 kN (18 kip) axle load, 690 kPa (100 psi) tire pressure, 97 km/hr (60 mph) speed, and about 10 to 25 percent truck traffic over a design life of 20 years (*60*). In Table 3-7, PS# 5 represents the actual pavement structure where the Bryan mixture was used.

Table 3-7. Selected Pavement Structures and Traffic.

PS #	Material Type, Layer Thickness, and Elastic Modulus				Traffic ESALs	% Trucks
	Surfacing	Base	Subbase	Subgrade		
1	HMAC, 6 inches, 500,000 psi	Flex, 14 inches*, 28,000 psi**	-	9000 psi	5,000,000	25
2	HMAC, 2 inches, 500,000 psi	Flex, 10 inches, 60,000 psi	Lime stabilized, 6 inches, 35,000 psi	12,400 psi	1,399,000	23.7
3	HMAC, 2 inches, 500,000 psi	Asphalt stabilized, 7 inches, 500,000 psi	Flex, 8 inches, 24,000 psi	Silt-clay, 9600 psi	7,220,000	13
4	HMAC, 2 inches, 500,000 psi	Flex, 6 inches, 50,000 psi	Stabilized subgrade, 5 inches, 30,000 psi	10,000 psi	390,000	10.7
5	US 290 HMAC, 4 inches, 500,000 psi	Cemented, 14 inches, 150,000 psi	-	15,000 psi	10,750,000	15.2

*1 inch ≅ 25.4 mm. ** 1 psi ≅ 0.0069 MPa

ENVIRONMENTAL CONDITIONS

Figure 3-10 shows five Texas environmental zones based on annual precipitation, annual freezing index, and the number of wet days and freeze/thaw days (*60*). As shown in Figure 3-10, the TxDOT districts have been grouped into five environmental zones namely; Dry-Cold (DC), Wet-Cold (WC), Dry-Warm (DW), Wet-Warm (WW), and Moderate.

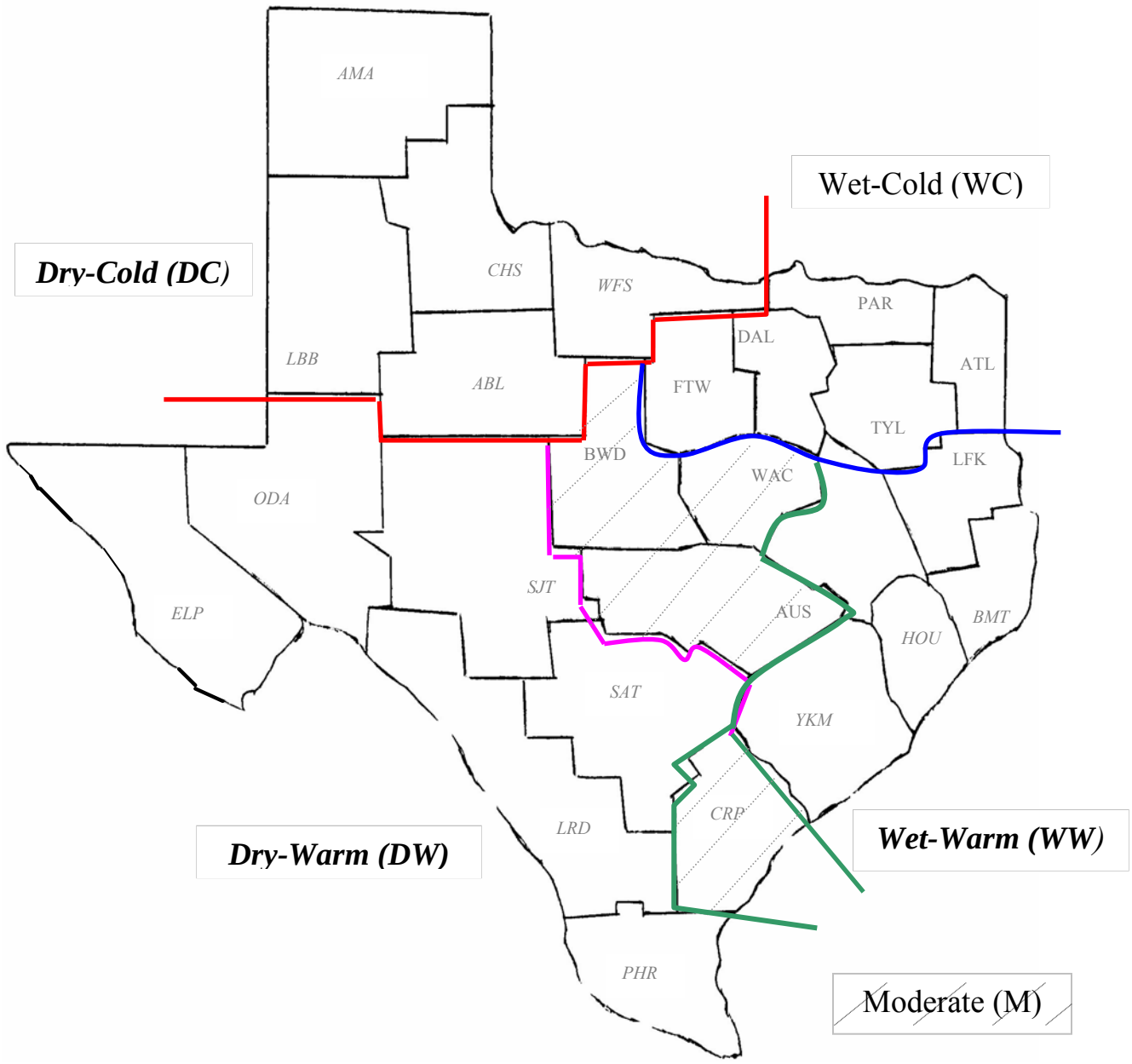

Figure 3-10. Texas Environmental Zoning (*60*).

The italicized environmental zones (*DC*, *WW*, and *DW*) in Figure 3-10 indicate zones that are critical to alligator (fatigue) cracking according to the TxDOT Pavement Management Information System (PMIS) report (*61*). Based on this PMIS report, 20 to 100 percent of the PMIS pavement sections in these locations exhibited alligator (fatigue) cracking.

Pavement material performance depends on both traffic and environment. It is therefore not uncommon that for a given design traffic level, a material that performs well in a particular environment may perform poorly in a different environmental location. Material properties for pavement design and performance evaluation are thus generally characterized as a function of environmental conditions.

HMAC, for instance, is very sensitive to temperature changes, while unbound materials in the base, subbase, or subgrade are generally more sensitive to moisture variations. Most often, the HMAC elastic modulus is characterized as a function of seasonal or monthly temperature variations, with the critical pavement temperature being at the mid-depth or two-thirds depth point in the HMAC layer. This pavement temperature generally exhibits a decreasing trend with depth. The subgrade elastic modulus is normally characterized as a function of the seasonal moisture conditions, with the wettest period of the year as the worst-case scenario assuming a conservative design approach. Note also that water seepage through cracks and/or accumulation in AV can accelerate damage, including fatigue cracking in HMAC materials.

In this project, two environmental conditions, WW and DC were considered (Figure 3-10). WW and DC are the two extreme Texas weather conditions the research team considered to have a significant impact on HMAC mixture fatigue performance. In fact, the 2003 TxDOT "Condition of Texas Pavements PMIS Annual Report" indicates that highway pavements in these environmental locations (WW and DC) are comparatively more susceptible to fatigue-associated cracking (*61*).

RELIABILITY LEVEL

For this project, the research team selected and utilized a reliability level of 95 percent. This is a typical value used for most practical HMAC pavement designs and analyses. In statistical terms, this means that for a given test or assessment criteria, there is 95 percent pass expectance or data accuracy, and that up to 5 percent failure or result inaccuracy is anticipated and tolerable. In simpler terms, for a 95 percent reliability level, it means that the acceptable risk level is 5 percent.

ELSYM5 STRESS-STRAIN ANALYSIS

For the five selected hypothetical PSs and environmental conditions (WW and DC) considered, elastic ELSYM5 stress-strain computations were adjusted based on FEM simulations to account for the HMAC visco-elastic behavior (*62, 63*).

ELSYM5 Input and Output Data

The bullets below summarize the typical input data requirement for ELSYM5 analysis:

- pavement structure (i.e., number of layers and layer thicknesses),
- material properties (i.e., elastic modulus and Poisson's ratio), and
- Traffic loading (i.e., axle load and tire pressure).

Table 3-7 displayed the PSs and the respective elastic moduli used for ELSYM5 analysis in this project. The axle load and tire pressure used were as discussed previously, 80 kN and 690 kPa. Typical Poisson's ratios used by the researchers in the analysis were 0.33, 0.40, and 0.45 for the HMAC layer, the base, and subgrade, respectively (*64*).

The basic output response parameters from the ELSYM5 computational analysis include the stresses, strains, and deformations. The strain response parameters were, however, adjusted according to FEM simulations discussed in the subsequent text to account for HMAC visco-elastic behavior.

These tensile (ε_t) and shear (γ) strains constitute input parameters for the ME, CMSE, and CM fatigue analysis, respectively, discussed in Chapters 4 through 6. Stress-strain computations for the proposed NCHRP 1-37A 2002 Pavement Design Guide (Chapter 7) is built into the analysis software.

FEM Strain-Adjustment

The FEM strain-adjustment factor for elastic strain analysis to account for HMAC visco-elastic behavior was determined as follows:

$$S_{adj\,(VE)i} = \frac{Strain_{FEM}}{Strain_{ELSYM5}} \qquad \text{(Equation 3-1)}$$

where:

$S_{adj(VE)}$	=	FEM strain-adjustment factor for HMAC visco-elastic behavior
$Strain_{FEM}$	=	Strain (ε_t or γ) computed via FEM analysis (mm/mm)
$Strain_{ELSYM5}$	=	Strain (ε_t or γ) computed via ELSYM5 analysis (mm/mm)
Subscript i	=	Stands for ε_t or γ

For this project, $S_{adj(VE)}$ values of 1.25 and 1.175 were used for ε_t and γ, respectively, based on the previous FEM work by Park (*63*, *65*). Note that while it is possible that these visco-elastic adjustments may vary for different mixtures, the adjustment from layered elastic to elasto-viscoplastic was assumed to be constant across both mixtures in this project. In addition, the elastic moduli values at 0 months aging for these two mixtures did not vary significantly. Thus for each computed ELSYM5 strain (ε_t and γ) for the PSs shown in Table 3-7, the $S_{adj(VE)i}$ was applied as follows:

$$\varepsilon_t = S_{adj(VE)e_t} \times \varepsilon_{t(ELSYM5)} = 1.25\varepsilon_{t(ELSYM5)} \qquad \text{(Equation 3-2)}$$

$$\gamma = S_{adj(VE)\gamma} \times \gamma_{(ELSYM5)} = 1.175\gamma_{(ELSYM5)} \qquad \text{(Equation 3-2)}$$

An example of the resulting strains (ε_t and γ) for the PSs shown in Table 3-7 for both WW and DC environments is shown in Table 3-8.

Table 3-8. Computed Critical Design Strains.

PS#	WW Environment		DC Environment	
	Tensile strain (ε_t)	Shear strain (γ)	Tensile strain (ε_t)	Shear strain (γ)
1	1.57×10^{-4}	1.56×10^{-2}	1.51×10^{-4}	1.51×10^{-2}
2	2.79×10^{-4}	1.98×10^{-2}	2.71×10^{-4}	1.89×10^{-2}
3	2.73×10^{-4}	1.91×10^{-2}	2.66×10^{-4}	1.86×10^{-2}
4	2.89×10^{-4}	2.06×10^{-2}	2.78×10^{-4}	1.96×10^{-2}
5	0.98×10^{-4}	1.41×10^{-2}	0.91×10^{-4}	1.46×10^{-2}

SUMMARY

Salient points from this chapter are summarized as follows:

- Two commonly used TxDOT HMAC mixtures, Bryan (PG 64-22 + limestone) and Yoakum (PG 76-22 + gravel) mixtures were selected for fatigue analysis in this project. Bryan is a normal basic TxDOT Type C HMAC mixture, while Yoakum is a Rut Resistant 12.5 mm Superpave HMAC mixture. Both the binder and aggregate material properties were consistent with the Superpave PG and TxDOT standards.
- Two laboratory compactors, the standard SGC and kneading beam, were utilized for compacting cylindrical and beam HMAC specimens, respectively. The target specimen fabrication AV content was 7±0.5 percent to simulate the in situ AV field compaction after construction and trafficking when fatigue resistance is critical.
- Three aging conditions for both binders and HMAC mixtures at a critical temperature of 60 °C (140 °F) were selected to investigate the effects of oxidative aging on binder and HMAC mixture fatigue properties, including fatigue life. These aging conditions were 0, 3, and 6 months that simulate up to 12 years of Texas environmental-field HMAC aging.

- Five commonly used TxDOT HMAC pavement structures with corresponding traffic levels of 0.25 to 11.00 million ESALs and 10 to 25 percent truck traffic were selected for analysis. Using layered elastic analyses (ELSYM5) and adjusting based on FEM simulations, tensile and shear strains within the pavement HMAC layer were determined and utilized as the failure load-response parameters associated with fatigue cracking when predicting the HMAC mixture fatigue resistance.
- Two Texas environmental conditions (Wet-Warm and Dry-Cold) critical to fatigue associated (alligator) cracking in HMAC pavements were selected for the analysis.

CHAPTER 4
THE MECHANISTIC EMPIRICAL APPROACH

This chapter discusses the mechanistic empirical approach for HMAC pavement fatigue analysis including the fundamental theory, input/output data, required flexural bending beam laboratory testing, failure criteria, analysis procedure, and variability.

FUNDAMENTAL THEORY

The selected SHRP A-003A ME approach in this project utilizes the flexural bending beam fatigue test (third-point loading) and considers bottom-up cracking to determine an empirical fatigue relationship of the simple power form shown in Equation 4-1 (*25*).

$$N = k_1 \varepsilon^{-k_2} \qquad \text{(Equation 4-1)}$$

where:

N = Number of load cycles to fatigue failure

ε = Applied tensile strain (mm/mm)

k_i = Laboratory determined material constants

The SHRP A-003A fatigue analysis approach incorporates reliability concepts that account for uncertainty in laboratory testing, construction, and traffic prediction; and considers environmental factors, traffic loading, and pavement design. The SHRP A-003A is the ME fatigue analysis approach utilized in this project, and the BB testing to determine the HMAC mixture fatigue empirical relationship shown in Equation 4-1 was based on the AASHTO TP8-94 test protocol (*59, 66*). The AASHTO TP8-94 test protocol is discussed later in this chapter.

HMAC specimen preparation by rolling or kneading wheel compaction is strongly recommended as part of this ME approach to simulate the engineering properties of extracted field pavement cores. Conditioning prior to testing to a representative or worst-case aging state is also suggested.

The AASHTO TP8-94 test protocol requires testing conditioned specimens at two different controlled strain levels under sinusoidal repeated loading to generate an empirical fatigue relationship, as shown in Equation 4-1 (*59*).

Determination of the experimental fatigue relationship, as expressed by Equation 4-1, constitutes the empirical part of the ME approach of fatigue modeling of HMAC mixtures. This empirical fatigue relationship (Equation 4-1) is then used in the design and analysis system illustrated schematically in Figure 4-1.

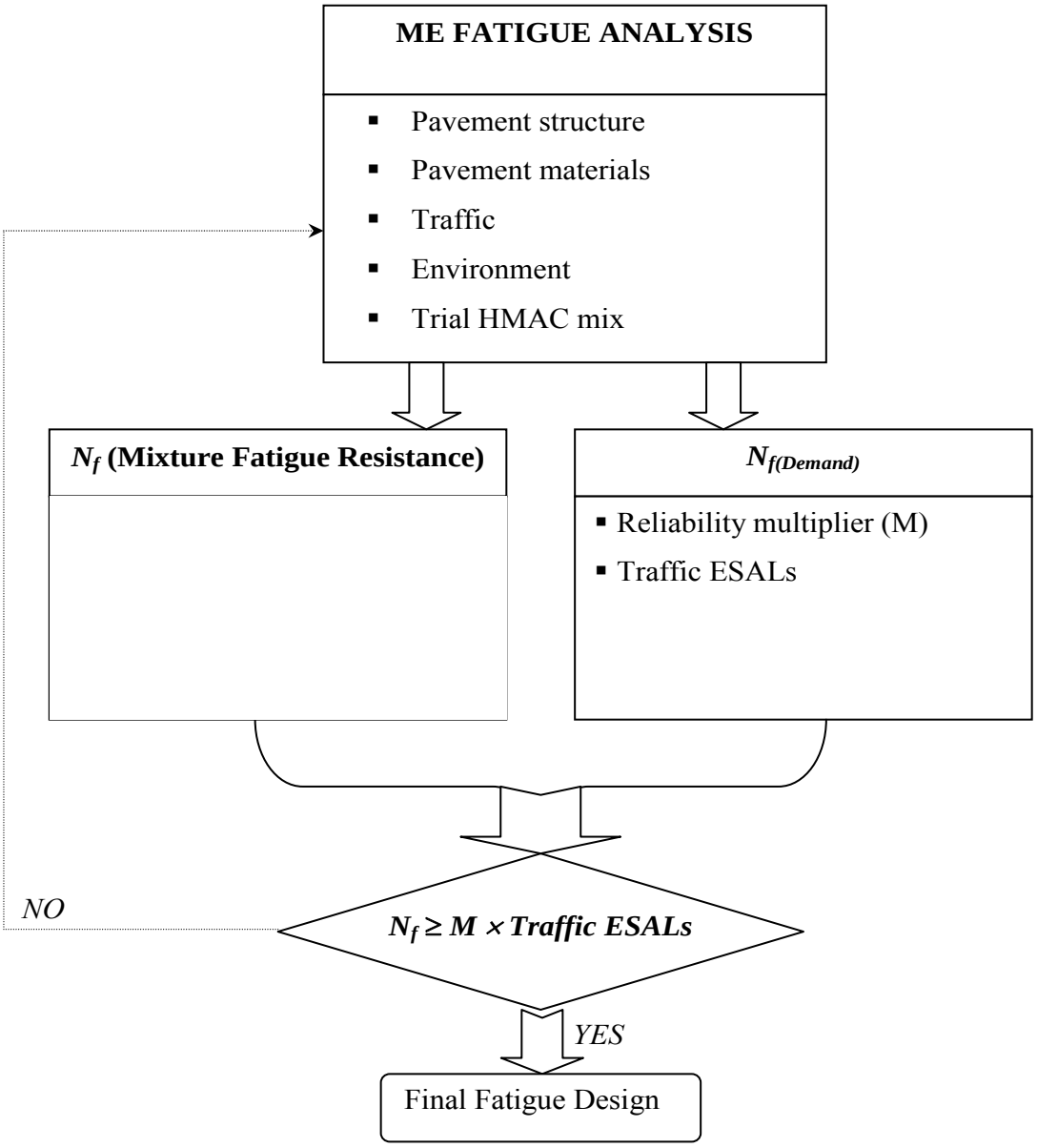

Figure 4-1. The ME Fatigue Design and Analysis System.

The fatigue analysis system shown in Figure 4-1 evaluates the likelihood that the selected design HMAC mixture will adequately resist fatigue cracking in a specific pavement structure under anticipated in situ conditions including traffic and environment. The designer must, however, select a specific level of reliability commensurate with the pavement site for which the mixture will be utilized as well as the required level of service of the pavement structure.

A HMAC mixture is expected to perform adequately if the number of load repetitions sustainable in laboratory testing after correcting for field conditions exceeds the number of load repetitions anticipated in service. The design strain at which the pavement fatigue life must be estimated using the empirical fatigue relationship developed based on laboratory test results is often computed using a simple multilayer elastic theory. For this computation, the design strain of interest is the maximum principal tensile strain at the bottom of the HMAC layer in the specific pavement structure, assuming the bottom-up mode of fatigue cracking. The determination of this field critical design tensile strain within a representative field pavement structure at the bottom of the HMAC layer constitutes the mechanistic part of the ME approach.

INPUT/OUTPUT DATA

Table 4-1 summarizes the general ME fatigue analysis input and the expected output data based on the SHRP A-003A approach and the AASHTO TP8-94 BB test protocol (*59*). These parameters and their respective components are discussed in more detail in subsequent sections.

Table 4-1. Summary of ME Fatigue Analysis Input and Output Data.

Source	Parameter
Laboratory test data (HMAC mixture testing of beam specimens)	- Strain (ε_t) & stress - # of fatigue load cycles (N)
Analysis of laboratory test data	- Flexural stiffness or dissipated energy - Empirical fatigue relationship ($N = f(\varepsilon_t)$)
Field conditions (design data)	- Pavement structure (layer thickness) - Pavement materials (elastic modulus & Poisson's ratio) - Traffic (ESALs, axle load, & tire pressure) - Environment (temperature & moisture conditions) - Field correction/shift factors (i.e., temperature)
Computer stress-strain analysis	- Design tensile strain (ε_t) @ bottom of the top HMAC layer
Other	- Reliability level (i.e., 95%) - Reliability multiplier (M)
OUTPUT	- HMAC mixture fatigue resistance ($N_{f(Supply)}$) - Pavement fatigue life ($N_{f(Demand)}$) - Assessment of adequate or inadequate performance

LABORATORY TESTING

The BB fatigue test, including the test equipment, specimen setup, and data acquisition, was conducted consistent with the AASHTO TP8-94 test procedure (*11, 12*). This section summarizes the BB fatigue test protocol.

The BB Fatigue Test Protocol

The BB fatigue test consists of applying a repeated constant vertical strain to a beam specimen in flexural tension mode until failure or up to a specified number of load cycles. In this project, the test was strain controlled, and the input strain waveform was sinusoidal shaped, applied at a frequency of 10 Hz. The BB device and the loading configuration are shown in Figures 4-2 and 4-3, respectively.

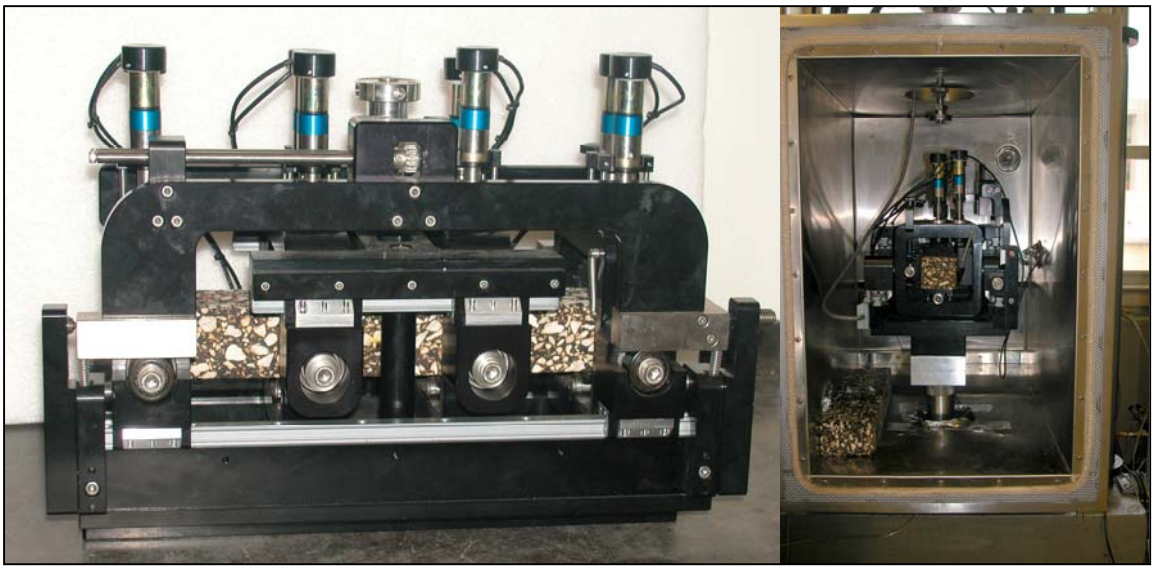

Figure 4-2. The Bending Beam (BB) Device.

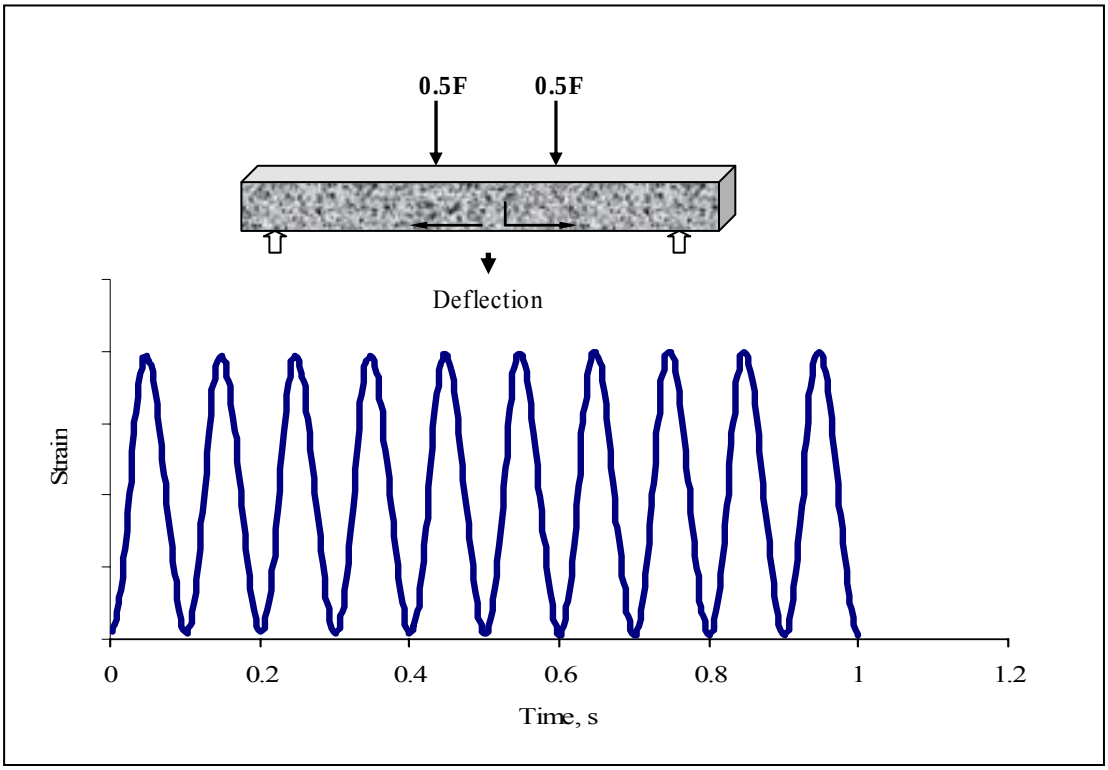

Figure 4-3. Loading Configuration for the BB Fatigue Test.

As evident in Figure 4-3, repeated vertical loading causes tension in the bottom zone of the specimen, from which cracking will subsequently initiate and propagate, thus simulating pavement fatigue failure under traffic loading. The test was conducted at two strain levels of approximately 374 and 468 microstrains (i.e., an equivalence of 0.20 and 0.25 mm deflections, respectively), consistent with the AASHTO TP8-94 test protocol to generate the required material N-ε_t empirical relationship shown in Equation 4-1 (*59*). These test strain levels are within the recommended AASHTO TP8-94 test protocol range to reduce test time while at the same time capturing sufficient data for analysis.

A 10 Hz frequency (Figure 4-3) without any rest period was used for the test. The average duration of each test was approximately 5 hrs. Note that the BB test time is inversely proportional to the magnitude of the input strain wave. Testing can, however, be terminated either when the initial application load response (stress) recorded at the 50^{th} load cycle decreases to 50 percent in magnitude or when a preset number of load cycles such as 100,000 is reached. The former approach was used in this project.

Test Conditions and Specimens

HMAC is temperature sensitive, so the test was conducted in an environmentally controlled chamber at a test temperature of 20±0.5 °C (68 ±32.9 °F), consistent with the AASHTO TP8-94 test procedure (*59*). The minimum specimen conditioning time was 2 hrs. However, specimens were actually preconditioned at 20 °C (68 °F) on a more convenient 12 hrs overnight-time period. The test temperature was monitored and recorded every 600 s via a thermocouple probe attached inside a dummy specimen also placed in the environmental chamber. Figure 4-4 is an example of a temperature plot captured during the BB test at 20 °C (68 °F).

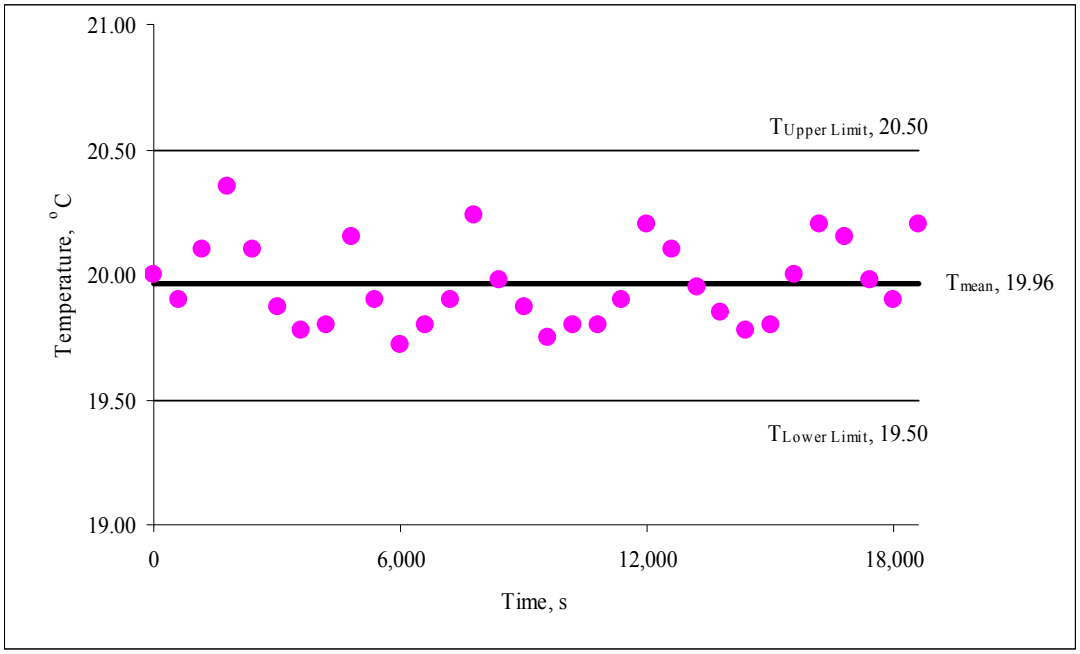

Figure 4-4. Example of Temperature Plot for the BB Test.

As evident in Figure 4-4, the average temperature for this particular test was 19.96 °C (67.93 °F) with a coefficient of variation of 0.84 percent. Three replicate beam specimens were tested for each strain level, so a complete BB test cycle for low and high strain level tests required a minimum of six beam specimens per aging condition per mixture type.

Test Equipment and Data Measurement

A servo electric-hydraulic controlled material testing system (MTS) equipped with an automatic data measuring system applied the sinusoidal input strain waveform. Actual loading of the specimen was transmitted by the BB device shown in Figure 4-2, to which the beam specimen is securely clamped.

Loading data were measured via the MTS load cell, and flexural deflections were recorded via a single linear differential variable transducer (LVDT) attached to the center of the specimen. During the test, load and flexural deformation data were captured electronically every 0.002 s. Figure 4-5 is an example of the output stress response from the BB test at 20 °C (68 °F) based on a 374 test microstrain level.

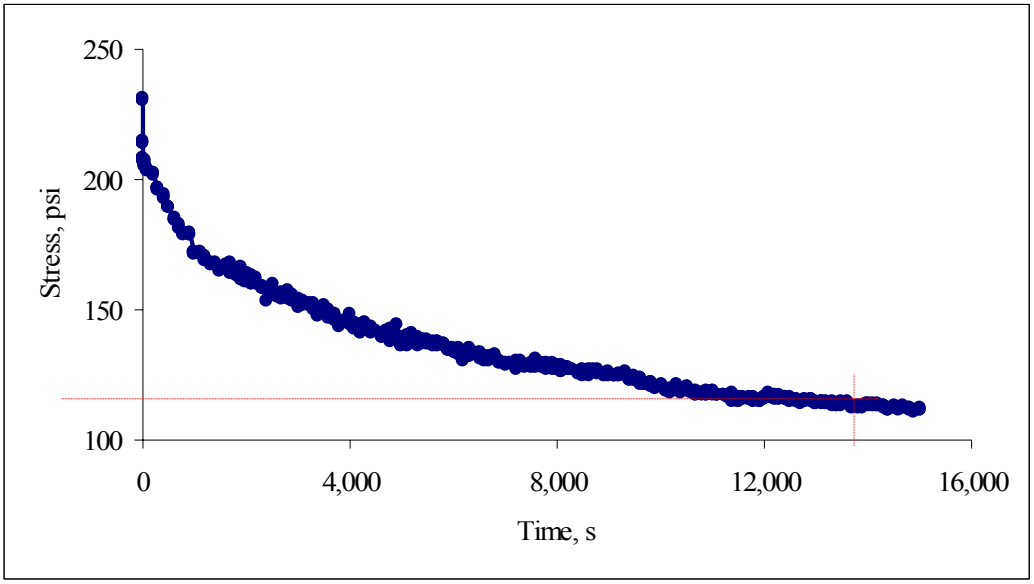

Figure 4-5. Example of Stress Response from BB Testing at 20 °C (68 °F) (374 microstrain level).

FAILURE CRITERIA

For HMAC compacted specimens subjected to repeated flexural bending, failure is defined as the point at which the specimen flexural stiffness is reduced to 50 percent of the initial flexural stiffness (*59, 66*). This initial stiffness is generally defined as the specimen flexural stiffness measured at the 50th load cycle. With this criterion, fatigue cracking was considered to follow the bottom-up failure mode assuming a service temperature of 20 °C (68 °F).

ANALYSIS PROCEDURE

The ME fatigue analysis utilized in this project was a five-step procedure involving laboratory test data analysis to determine the HMAC N_f-ε_t empirical relationship expressed by Equation 4-1, computer stress-strain analysis to determine the design maximum ε_t within a selected and representative pavement structure at the bottom of the HMAC layer, statistical analysis to predict the design HMAC mixture fatigue resistance, determination of the required pavement life, and finally, a design check for adequate performance. These analyses, which are illustrated schematically in Figure 4-1, are discussed in this section.

Step 1: Laboratory Test Data Analysis (N-ε_t Empirical Relationship)

Laboratory test data from the BB fatigue test, which is discussed subsequently, was analyzed using the AASHTO TP8-94 calculation procedure. Equations 4-2 to 4-4 are the fundamental basis for BB test data analysis (*59*).

$$S = \frac{\sigma_t}{\varepsilon_t} \qquad \text{(Equation 4-2)}$$

$$N_{50\%} = \frac{\ln\left(\frac{S_{50\%}}{A}\right)}{b} = -0.69315b^{-1} \qquad \text{(Equation 4-3)}$$

where:

S	=	Flexural stiffness (MPa)
σ_t	=	Maximum measured tensile stress per load cycle (kPa)
ε_t	=	Maximum measured tensile strain per load cycle (mm/mm)
$N_{50\%}$	=	Number of load cycles to failure during BB testing
$S_{50\%}$	=	Flexural stiffness at failure during BB testing (MPa)
A	=	Initial peak flexural stiffness measured at the 50th load cycle (MPa)
b	=	Exponent constant from log S versus log load cycles (N) plot

The solution of Equation 4-3 for two different input strain levels (i.e., low and high), and a plot of the resultant $N_{50\%}$ versus the respective applied ε_t on a log-log scale will generate the required empirical fatigue relationship of the simple power form shown in Equation 4-1.

Step 2: Stress-Strain Analysis, $\varepsilon_{t\,(Design)}$

Following establishment of the HMAC N_f-ε_t empirical relationship through laboratory test data analysis, computer stress-strain analysis was executed to determine the actual maximum design ε_t of a given pavement structure at the bottom of the HMAC layer. Input parameters for this analysis include traffic loading, pavement structure (layer thicknesses), material properties, and the desired response location, which in this project was (t – 0.01), where t is the thickness of the top HMAC layer in inches (or mm, where 1 inch ≅ 25.4 mm). Traffic loading data include the standard axle load (e.g., 80 kN [18 kip]), ESALs, and axle and tire configurations. Material properties including the elastic modulus and Poisson's ratio should be defined as a function of the environment in terms of temperature and subgrade moisture conditions.

In this project, a user-friendly and simple multi-layer linear-elastic software, ELSYM5, was used for ε_t computations at the bottom of the HMAC layer (*62*). Ideally, a FEM software that takes into account the visco-elastic nature of the HMAC material is desired for this kind of analysis. Consequently, adjustments were applied to the ELSYM5 linear-elastic analysis results, consistent with the FEM adjustment criteria discussed in Chapter 3.

Step 3: Statistical Prediction of HMAC Mixture Fatigue Resistance, $N_{f(Supply)}$

$N_{f(Supply)}$ is the laboratory design HMAC mixture fatigue resistance that was statistically determined as a function of the design ε_t (ELSYM5 analysis) and the laboratory determined empirical fatigue N-ε_t (Equation 4-1) relationship at a given reliability level. This is discussed in great detail in the subsequent section.

While $N_{f(Supply)}$ represents laboratory fatigue life, the final field fatigue life for this ME approach in this project was obtained as expressed by Equation 4-4.

$$N_f = \frac{SF\left(k_i\left[\varepsilon_t\right]^{-k_2}\right)}{TCF} = \frac{SF \times N_{f\,(Supply)}}{TCF} \qquad \text{(Equation 4-4)}$$

where:

TCF = Temperature conversion factor to laboratory test temperature

SF = Shift factor that accounts for traffic wander, construction variability, loading frequency, crack propagation, and healing

For simplicity, *TCF* and *SF* values of 1.0 and 19, respectively, were used in this project (*1*, *2*). Determination of these parameters generally requires local calibration to field conditions, which was beyond the scope of this project.

Step 4: Determination of the Required Pavement Fatigue Life, $N_{f(Demand)}$

$N_{f(Demand)}$ is the expected pavement fatigue life, which is representative of the actual applied traffic loading. It is a function of the total traffic ESALs summed over the entire pavement design life determined as expressed by Equation 4-5.

$$N_{f(Demand)} = M \times Traffic\ ESALs_{(Design)} \quad \text{(Equation 4-5)}$$

where:

M = Reliability multiplier

In the ME fatigue analysis approach, the safety factor associated with a specified level of reliability is often defined in terms of reliability multiplier (*M*) and applied to traffic demand (i.e., ESALs) as shown in Equation 4-5 (*1*, *2*). This factor accounts for mixture variability and the anticipated uncertainties in traffic estimate (demand) and mixture fatigue resistance (supply) and performance during service. For a reliability level of 95 percent, some studies have used an *M* value of 3.57, and this was the value used in this study (*1*, *2*).

Step 5: Fatigue Design Check for Adequate Performance

A fatigue design check for adequate performance requires that the HMAC mixture fatigue resistance be greater than or equal to the required pavement fatigue life as expressed by Equation 4-6.

$$N_f \geq N_{f(Demand)} \qquad \text{(Equation 4-6)}$$

If N_f is less than $N_{f(Demand)}$, a wide range of options including the following are available:

- redesigning the HMAC mixture by changing the binder content and/or type, AV, aggregate type or gradation;
- redesigning the pavement structure by changing the layer thicknesses, for example;
- redesigning the underlying pavement materials including the subbase, base, and/or subgrade,
- reducing the pavement design life; and/or
- allowing an increased risk of premature failure.

VARIABILITY, STATISTICAL ANALYSIS, AND N_f PREDICTION

Precision is inversely proportional to uncertainty/variability in a testing method. If N is the measured fatigue life and $N_{f(supply)}$ is the predicted fatigue life at a given design strain level, then the precision of the method (on a log scale) can be represented by the estimated variance of $Ln\left[N_{f(supply)}\right]$ as follows:

$$s_{y^*}^2 = s^2\left(1+\frac{1}{n}+\frac{(X-\bar{x})^2}{q\sum(x_p-\bar{x})^2}\right) \qquad \text{(Equation 4-7)}$$

where:

y^* = $Ln\lfloor N_{f(supply)} \rfloor$

$s^2_{y^*}$ = Estimated variance of $Ln\lfloor N_{f(supply)} \rfloor$

s^2 = $Var[Ln(N)]$

n = Number of test specimens

X = Ln[in situ strain] at which $Ln\lfloor N_{f(supply)} \rfloor$ must be predicted

$\bar{x}$ = Average Ln[test strain]

q = Number of replicate specimens at each test strain level

x_p = Ln[strain] at the pth test strain level

A prediction interval for $Ln\lfloor N_{f(supply)} \rfloor$ is another way of assessing the precision of the prediction. If the resulting interval is narrow, there is little uncertainty in $Ln\lfloor N_{f(supply)} \rfloor$, and the prediction is quite precise. An explicit formula for a 1-α prediction interval for the linear regression exists as follows:

$$a + bX \pm t_{1-\alpha/2,n-2} s_{y^*} \qquad \text{(Equation 4-8)}$$

where:

a, b = The estimated intercept and the estimated slope of the least squares line fitted on the $(Ln(strain), Ln(N_f))$ data

$t_{1-\alpha/2,n-2}$ = The t-critical value corresponding to the right tail probability of $\alpha/2$ of the t distribution with n-2 degrees of freedom

$s^2_{y^*}$ = The estimated variance of $Ln\lfloor N_{f(supply)} \rfloor$ as given in Equation 4-7

The estimated intercept and the estimated slope, *a* and *b*, respectively, can also be given explicitly as follows:

$$a = \bar{y} + b\bar{x} \qquad \text{(Equation 4-9)}$$

and

$$b = \frac{q\sum\left(x_p - \bar{x}\right)\left(y_p - \bar{y}\right)}{q\sum\left(x_p - \bar{x}\right)^2} \qquad \text{(Equation 4-10)}$$

where:

y_p = $Ln(N)$ at the *p*th test strain level

$\bar{y}$ = Average $Ln(N\ )$

Note that the predicted fatigue life $Ln\lfloor N_{\text{f(supply)}}\rfloor$ or the prediction interval estimate $\lfloor a + bX - t_{1-\alpha/2,n-2}s_{y^*}, a + bX + t_{1-\alpha/2,n-2}s_{y^*}\rfloor$ can be back-transformed by taking $\exp(\ )$ to provide the estimates in the original scale, but the variance estimate $s^2_{y^*}$ itself cannot be transformed in the same manner.

In summary, *Ln* $N_{f(supply)}$ values were predicted based on the least squares line regression analysis. Next, a 95 percent *Ln* N_f prediction interval was estimated based on the selected 95 percent reliability level. The predicted value and the prediction interval estimate estimates for $N_{f(supply)}$ were then obtained by back-transformation. As another measure of variability, a coefficient of variation (*COV*) of *Ln* N_f was computed based on the estimated standard deviation for the predicted Ln N_f value and the predicted mean Ln N_f value.

SUMMARY

This section summarizes the ME fatigue analysis approach as utilized in this project.

- The ME approach is mechanistic empirical and based on the fundamental concepts that fatigue cracking in HMAC pavements occurs due to critical tensile strains (ε_t) at the bottom of the HMAC layer and that the predominant mode of crack failure is bottom-up crack growth.
- Laboratory determination of the experimental N-ε_t fatigue relationship (i.e., the k_i constants) constitutes the empirical part of the ME approach, and determination of the field critical design ε_t within a representative field pavement structure at the bottom of the HMAC layer constitutes the mechanistic part.
- The flexural bending beam fatigue test conducted at 20 °C (68 °F) and 10 Hz in sinusoidal strain-controlled mode is the principal HMAC mixture fatigue characterization test for the ME approach. Under this BB testing, kneading or rolling compacted beam specimens are required.
- For HMAC compacted specimens subjected to repeated flexural bending, fatigue failure according to the ME approach is defined as the number of repetitive load cycles at which the specimen flexural stiffness is reduced to 50 percent of the initial flexural stiffness measured at the 50^{th} load cycle.

CHAPTER 5
THE CALIBRATED MECHANISTIC APPROACH WITH SURFACE ENERGY

In this chapter, the calibrated mechanistic approach with surface energy including the fundamental theory, input/output data, laboratory testing, failure criteria, analysis procedure, and variability is discussed.

FUNDAMENTAL THEORY AND DEVELOPMENT

HMAC is a complex composite material that behaves in a non-linear visco-elastic manner, ages, heals, and requires that energy be stored on fracture surfaces as load-induced damage in the form of fatigue cracking. Energy is also released from fracture surfaces during the healing process. HMAC mixture resistance to fatigue cracking thus consists of two components, resistance to fracture (both crack initiation and propagation) and the ability to heal, processes that both change over time. Healing, defined as the closure of fracture surfaces that occurs during rest periods between loading cycles, is one of the principal component of the laboratory-to-field shift factor used in traditional empirical fatigue analysis. Prediction of fatigue life or the number of cycles to failure (N_f) must account for this healing process that affects both the number of cycles for microcracks to coalesce to macrocrack initiation (N_i) and the number of cycles for macrocrack propagation through the HMAC layer (N_p) that add to N_f. Both components of mixture fatigue resistance or the ability to dissipate energy that causes primarily fracture at temperatures below 25 °C (77 °F), called dissipated pseudo strain energy (DPSE), can be directly measured in simple uniaxial tensile and compression tests (*5-6, 43-44,67*).

The CMSE approach is a micromechanical approach developed at Texas A&M University based on the SHRP A-005 results (*44-45*). The approach characterizes HMAC materials both in terms of fracture and healing processes, and requires only creep or relaxation tests in uniaxial tension and compression, strength and repeated load tests in uniaxial tension, and a catalog of fracture and healing surface energy components of binders and aggregates measured separately.

In this CMSE approach, HMAC behavior in fatigue is governed by the energy stored on or released from crack faces that drive the fracture and healing processes, respectively, through these two mechanisms of fracture and healing.

DPSE and pseudo strain are defined to quantify and monitor fracture and healing in HMAC mixtures. DPSE in an undamaged non-linear visco-elastic material is expected due to the viscous lag in material response. This pseudo strain energy is represented by the area in the pseudo hysteresis loop of a measured stress versus calculated PS after correcting for non-linearity, plotted as shown in Figure 5-1. Pseudo strain is determined by calculating the expected stress in a linear visco-elastic material under damaged conditions and dividing by a measured reference modulus (from the first stress cycle of a repeated load test), and a non-linearity correction factor ($\psi(t)$). This $\psi(t)$ is introduced to account for any non-linearity of the undamaged visco-elastic material (*68*).

Any departure from the initial pseudo hysteresis loop requires additional dissipated energy, indicating that fracture is occurring for temperatures less than 25 °C (77 °F). As fracture progresses with additional load cycles, DPSE will increase, while the HMAC mixture stiffness will decrease. The healing process, on the other hand, produces opposite results, with DPSE decreasing and the HMAC mixture stiffness increasing.

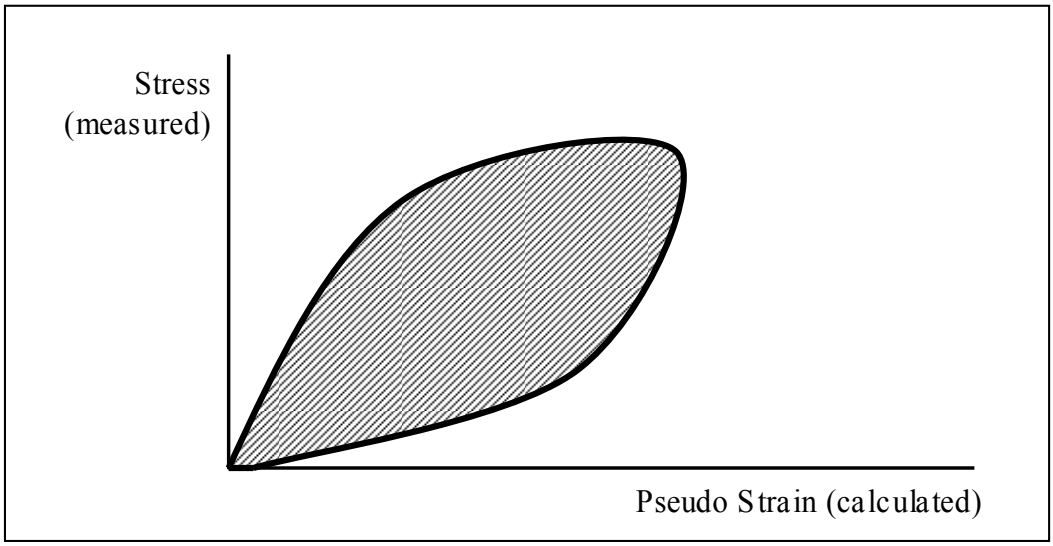

Figure 5-1. Example of Hysteresis Loop (Shaded Area is DPSE).

Monitoring of both DPSE and PS in repeated uniaxial tension tests is required in this micromechanical CMSE approach. The relationship between DPSE and N is modeled using either of two functional forms, linear logarithmic or simple power law, and calibrated using measured data. In this project, the research team used the former functional form, linear logarithmic.

These calibration coefficients and Paris' Law fracture coefficients determined by monitoring both DPSE and PS with microcrack growth are required to determine N_i for macrocrack initiation at an average microcrack size of 7.5 mm (0.30 inches) (*67, 69*). This calibration is required because the coefficients of the equation for microcrack growth are not widely known as compared to those for macrocrack growth. The size and shape of a microcrack is controlled by microscopic quantities such as mastic film thickness, aggregate particle size, and the degree of bonding of crack-arresting obstacles dispersed in the mastic. Nevertheless, microcrack growth is still controlled by the rate of change of DPSE and indicated by a reduction in HMAC mixture stiffness.

N_p for microcrack propagation is a function of the difference between fracture and healing speed. This N_p is primarily quantified in terms of Paris' Law fracture coefficients (A and n) and the shear strain. Fracture speed depends on material properties determined in uniaxial tensile creep or relaxation and strength tests at multiple temperatures and total fracture surface energy.

Healing occurs as a result of both short-term and long-term rates of rest periods, and depends on traffic rest periods, healing surface energy components, and the material properties measured in compression creep or relaxation modulus tests. Because the HMAC mixture healing properties are climatic dependent, fatigue healing calibration constants must be used to account for the climatic location of a given HMAC pavement structure (*67*). In determining the final field N_f, an anisotropic shift factor (discussed subsequently) is also introduced to account for the anisotropic nature of HMAC.

The surface energies of the binder and aggregate in HMAC are made up of contributions from nonpolar short-range Lifshitz-van der Waals forces and longer-range polar acid-base forces mainly associated with hydrogen bonding (*68, 70-71*).

The polar acid-base surface energy is itself also a combination of the acid surface energy and the base surface energy. These polar forces typical of hydrogen bonding take longer to form and act perpendicular to the crack faces to actively pull them together, while the nonpolar tensile short-range and short-lived Lifshitz-van der Waals forces act in the plane of the crack face to form a contractile skin that resists healing (*44-45, 68, 70-71*).

The difference between the total fracture and healing surface energies lies in the measurement of the individual surface energy components using carefully selected materials with known surface energy component values. Fracture components are found when dewetting, and healing components are determined when wetting (*44-45, 68, 70-71*).

Figure 5-2 is a schematic illustration of the CMSE design and analysis system. The figure shows that if the predicted N_f is less the design traffic ESALs, possible options include the following:

- modifying the pavement structure, materials, and reliability level; and/or
- changing the HMAC mix-design and/or material type;
- reducing the pavement design life; and/or
- allowing an increased risk of premature failure, i.e., reducing the reliability level.

In this CMSE approach, the design shear strain (Figure 5-2) computed within the HMAC layer of the pavement structure for N_p analysis constitutes the failure load-response parameter. This critical design shear strain is determined at the edge of a loaded wheel-tire using either a layered linear-elastic or visco-elastic model of material behavior characterization. The utilization of calibration constants in modeling SF_h, N_i, and N_p constitutes the calibration part of the CMSE approach. This calibration simulates the field mechanism of microcrack growth in the HMAC layer thickness with respect to traffic loading and environmental conditions.

INPUT/OUTPUT DATA

Table 5-1 summarizes the general CMSE fatigue analysis input and the expected output data. These parameters and their respective components are discussed in more detail in subsequent sections.

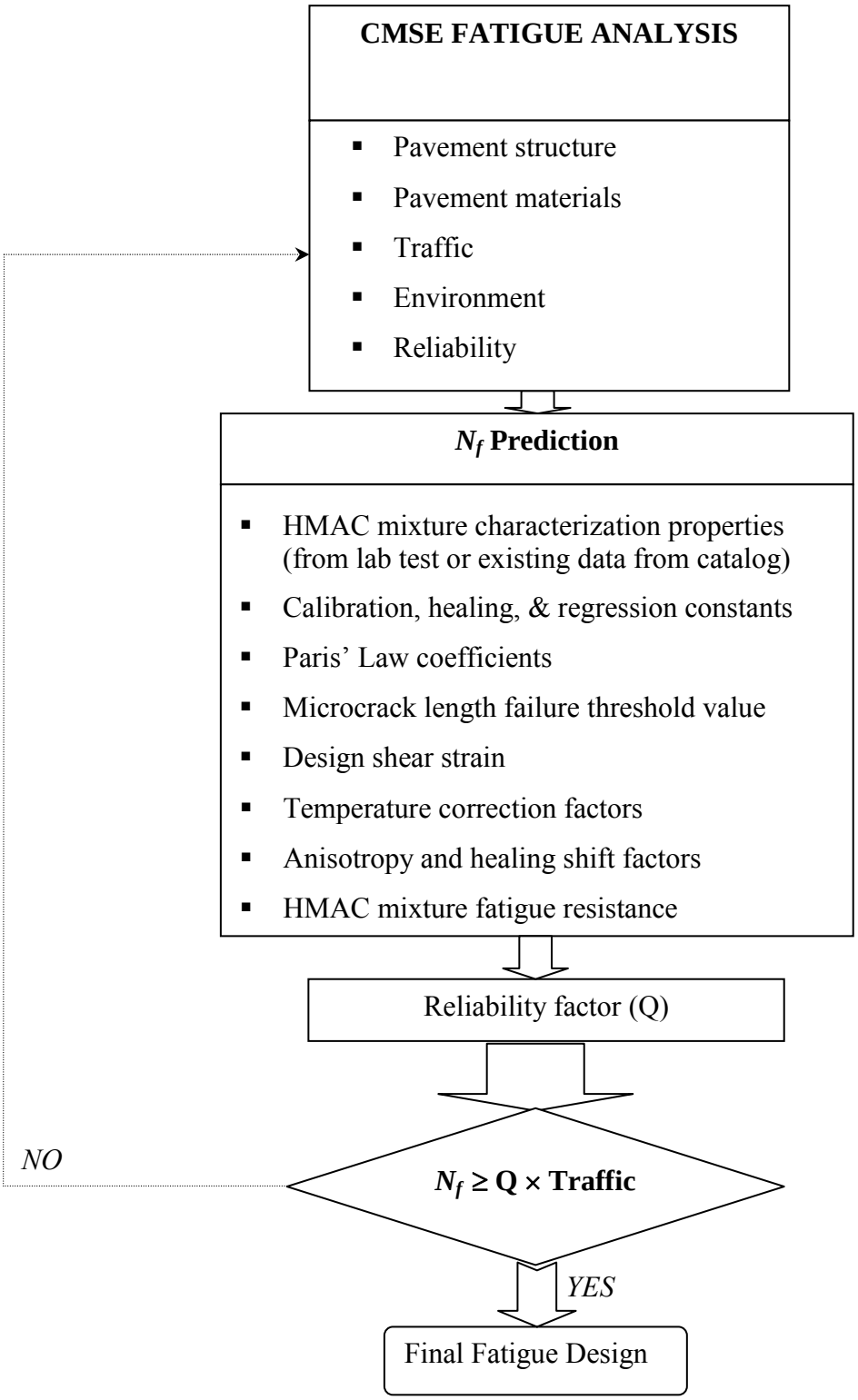

Figure 5-2. The CMSE Fatigue Design and Analysis System.

Table 5-1. Summary of CMSE Fatigue Analysis Input and Output Data.

Source	Parameter
Laboratory test data (HMAC mixture testing of cylindrical specimens)	- Tensile stress & strain - Relaxation modulus (tension & compression) - Uniaxial repeated direct-tension test data (strain, stress, time, & N) - Anisotropic data (vertical & lateral modulus) - Dynamic contact angle for binder surface energy (SE) - Vapor pressure and adsorbed gas mass for aggregate SE
Analysis of laboratory test data	- Tensile strength - Relaxation modulus master-curves (tension & compression) - Non-linearity correction factor - DPSE & slope of DPSE vs. Log N plot - SE (ΔG_f & ΔG_h) for binder & aggregates - Healing indices - Healing calibration constants - Creep compliance - Shear modulus - Load pulse shape factor
Field conditions (design data)	- Pavement structure (layer thickness) - Pavement materials (elastic modulus & Poisson's ratio) - Traffic (ESALs, axle load, & tire pressure) - Environment (temperature & moisture conditions.) - Field calibration coefficients - Temperature correction factor
Computer stress-strain analysis	- Design shear strain (γ) @ edge of a loaded tire
Other Parameters	- Reliability level (i.e., 95%) - Crack density - Microcrack length - HMAC brittle-ductile failure characterization - Stress intensity factors - Regression constants - Shear coefficient
OUTPUT	- Paris' Law fracture coefficients (A and n) - Shift factor due to anisotropy (SF_a) - Shift factor due to healing (SF_h) - Fatigue load cycles to crack initiation (N_i) - Fatigue load cycles to crack propagation (N_p) - HMAC mixture fatigue resistance (N_f)

LABORATORY TESTING

The required laboratory tests for the CMSE approach of HMAC mixture fatigue analysis include tensile strength, relaxation modulus in both tension and compression, uniaxial repeated direct-tension, and surface energy (*45, 68-69, 71*). These tests are described in this section. For each of these tests, at least two replicate cylindrical specimens were tested per aging condition per mixture type. The cylindrical HMAC specimen fabrication procedure, including the final dimensions consistent with the SGC compaction protocol, is described in Chapter 3.

Tensile Strength Test

The tensile strength test was conducted to determine the HMAC mixture tensile strength (σ_t), which is a required input parameter for CMSE N_f analysis.

Test Protocol

The tensile strength (TS) test protocol involves applying a continuous increasing tensile load to a cylindrical HMAC specimen at a constant elongation (deformation) rate of 1.27 mm/min (0.05 in/min) till failure (break point). This test is destructive and took at most 2 minutes to complete the test. Figure 5-3 shows the loading configuration for and typical results from the tensile strength test.

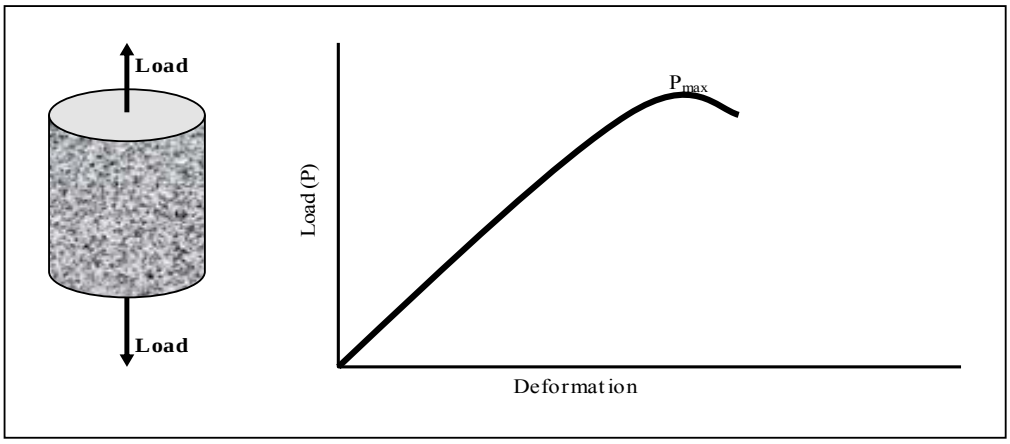

Figure 5-3. Loading Configuration for Tensile Strength Test.

Test Conditions and Data Acquisition

The tensile strength test was conducted in an environmentally controlled chamber at a test temperature of 20±0.5 °C (68±32.9 °F). Specimens were preconditioned to 20 °C (68 °F) for a minimum period of 2 hrs. The temperature was monitored and controlled through a thermocouple probe attached inside a dummy HMAC specimen also placed in the environmental chamber. An MTS equipped with an automatic data measuring system applied the loading. Loading data were measured via the MTS load cell, and deformations were recorded via three LVDTs attached vertically to the sides of the specimen. During the test, load and axial deformation data were captured electronically every 0.1 s. Two replicate specimens were tested per aging condition per mixture type.

Mixture tensile strength (σ_t) was calculated simply as the maximum tensile load at break divided by the specimen cross-sectional area as follows:

$$\sigma_t = \frac{P_{\max}}{\pi r^2} \qquad \text{(Equation 5-1)}$$

where:

σ_t = Tensile strength (MPa)

P_{max} = Maximum tensile load at break (MPa)

r = Radius of cylindrical specimen (mm)

Relaxation Modulus Test

The time-dependent elastic relaxation modulus (E_i), modulus relaxation rate (m_i), and temperature correction factor (a_T) constitute input parameters for the CMSE fatigue analysis. These material properties were determined from the relaxation modulus test (*30*).

Test Protocol

Relaxation modulus (RM) is a strain-controlled test. The test involves applying a constant axial strain to a cylindrical HMAC specimen either in tension or compression for a given time period and then releasing the strain for another given time period, thereby allowing the specimen to rest or relax (elastic recovery). The test loading configuration is shown in Figure 5-4.

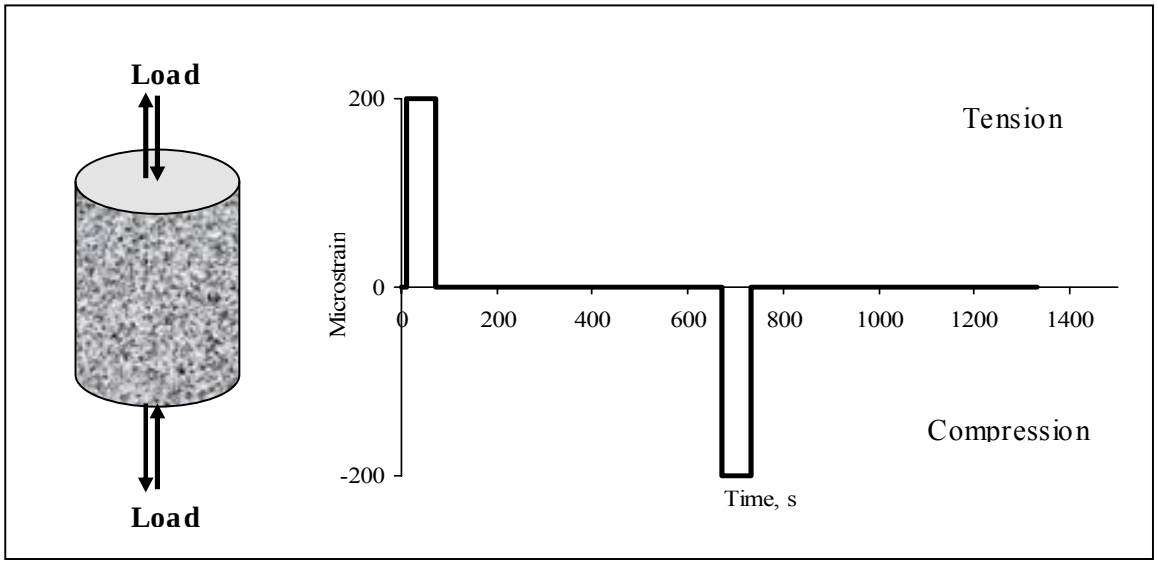

Figure 5-4 Loading Configuration for Relaxation Modulus Test.

As shown in Figure 5-4, the loading sequence consisted of a 200 tensile microstrain sitting for a period of 60 s followed by a 600 s rest period and application of a 200 compression microstrain for 60 s followed by another 600 s rest period (*30*). Researchers selected 200 microstrain because, for the HMAC mixtures considered in this project, prior trial testing with microstrains above 200 proved to be destructive, while those below 200 were too small to produce meaningful results. A 60 s strain loading time was considered adequate to prevent irrecoverable damage while a 600 s rest period was considered adequate to allow for elastic recovery. The time interval for the strain load application from 0 to +200 or -200 microstrain was 0.6 s, and the input strain waveform was actually a trapezoidal shape. Thus, the total test time for both the tensile and compressive loading cycle for a given test temperature, say 10 °C (50 °F), was approximately 25 minutes.

Test Conditions and Data Acquisition

The research team conducted RM testing in an environmentally controlled chamber at three temperatures, 10, 20, and 30 °C (50, 68, and 86 °F), to facilitate development of a time-dependent RM master-curve. This master-curve is a graphical representation of the HMAC mixture properties as a function of temperature and loading time. Note that HMAC is sensitive to temperature and time of loading.

The temperatures were monitored and controlled at a tolerance of ±0.5 °C (±32.9 °F) through a thermocouple probe attached inside a dummy HMAC specimen also placed in the environmental chamber. For each temperature-test sequence, the minimum specimen conditioning time was 2 hrs. The MTS provided the loading while an automated data measurement system captured the data (time, load, and deformation) electronically every 0.5 s. Loading data were measured via the MTS load cell, and deformations were recorded via three LVDTs attached vertically to the sides of the specimen. Three replicate specimens were tested per aging condition per mixture type.

Figure 5-5 is an example of the output stress response from the relaxation modulus test at a single test temperature of 10 °C (50 °F).

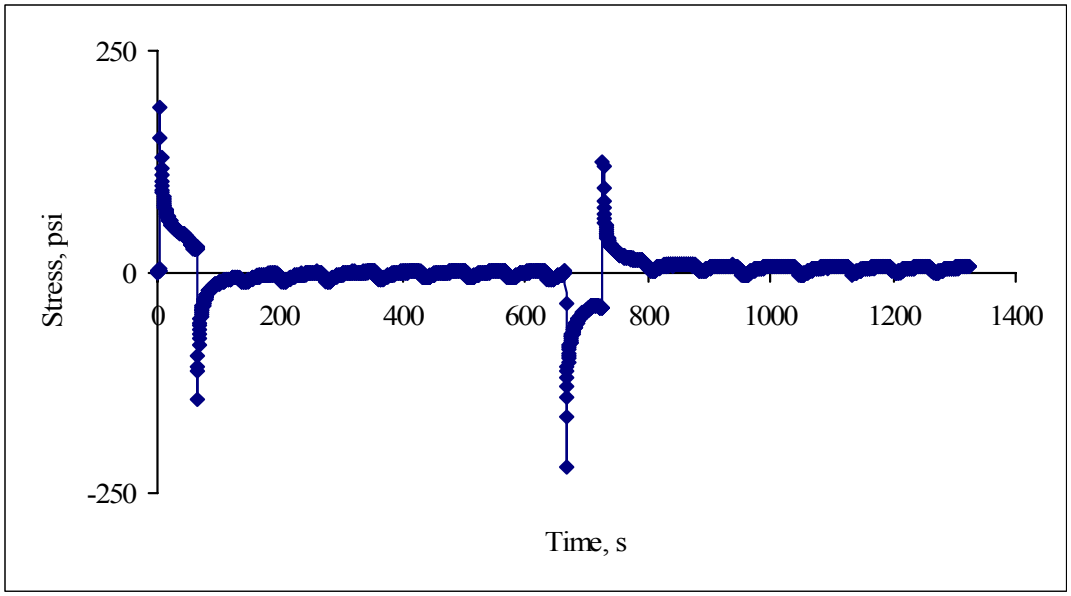

Figure 5-5. Example of Stress Response from RM Test at 10 °C (50 °F).

Equation 5-2 was used to calculate the elastic relaxation modulus as a function of the measured load (stress) and strain.

$$E = \frac{\sigma}{\varepsilon} = \frac{P}{\pi r^2 \varepsilon} \qquad \text{(Equation 5-2)}$$

where:

E = Elastic modulus (MPa)

P = Load (kN)

ε = Strain (mm/mm)

A time-reduced superposition logarithmic analysis of the elastic modulus data for each test temperature to a reference temperature of 20 °C (68 °F) generates the required time-dependent RM master-curve. This master-curve is represented in the form of a simple power law. By the same logarithmic analysis, temperature correction factors (a_T) are determined, where a_T has a value of 1.0 for the 20 °C (68 °F) reference temperature.

Uniaxial Repeated Direct-Tension Test

The time-dependent tensile stress ($\sigma(t)$) is an input parameter required to calculate the rate of dissipation of PS energy (b) that is necessary to calculate N_i. This material property was determined from the uniaxial repeated direct-tension test discussed subsequently.

Test Protocol

Like the RM test, the uniaxial repeated direct-tension (RDT) test was conducted in a strain controlled mode (*68*). An axial direct tensile microstrain of 350 was applied repeatedly to a cylindrical HMAC specimen at a frequency of 1 Hz for a total of 1000 load cycles. The input strain waveform was haversine shaped.

The actual loading time was 0.1 s with a 0.9 s rest period between load pulses. Thus, a complete load cycle including the rest period was 1.0 s. Figure 5-6 shows the loading configuration. The 0.9 s rest period allowed for HMAC relaxation between the load pulses and prevented the buildup of undesirable residual stresses discussed subsequently. This rest period can also promote a limited amount of healing.

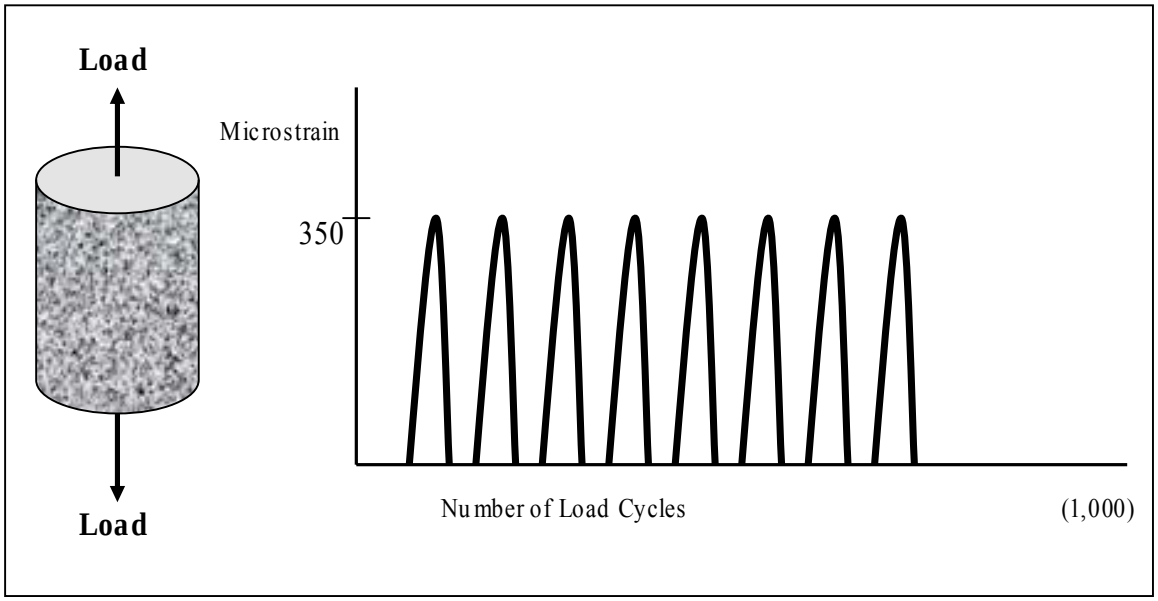

Figure 5-6. Loading Configuration for the RDT Test.

The haversine-shaped input strain waveform is representative of the field load pulse developed under moving wheel loads of commercial vehicles on interstate highways (*68*). A relatively high input strain magnitude of 350 microstrain was selected because this value (350 microstrain) was considered substantial enough to induce cumulative micro fatigue damage (microcracking) within the HMAC specimen during the test. In this test, while micro fatigue damage is desirable, an appropriate input strain level must be selected that will allow the test to continue to an appreciable number of load cycles to capture sufficient data that will allow for calculation of the *b* slope parameter needed in the CMSE analysis. For this project, testing was terminated at 1000 load cycles, during which time sufficient data had been captured for DPSE analysis and subsequent calculation of the constant *b*. A complete RDT test thus took about 20 minutes.

Test Conditions and Data Acquisition

The haversine input strain waveform was supplied by the MTS, and axial deformations were measured via three LVDTs. Data (time, load, and deformations) were captured electronically every 0.005 s. The research team conducted the RDT test in an environmentally controlled chamber at a test temperature of 30±0.5 °C (86±32.9 °F). The minimum conditioning period for the specimens was 2 hrs. The temperature was monitored and controlled through a thermocouple probe attached inside a dummy HMAC specimen also placed in the environmental chamber.

Three replicate cylindrical HMAC specimens that had previously been subjected to a series of RM tests at 10, 20, and 30 °C (50, 68, and 86 °F) were used for this test for each aging condition and each mixture type. It should be noted that the RM test was assumed to be non-destructive in this project. However, the RDT test is a destructive test since some microdamage occurs within the HMAC specimen even though damage may not be physically visible.

Figure 5-7 is an example of the stress response from the uniaxial repeated direct-tension test at 30 °C (86 °F). The measured stress ($\sigma(t)$), strain ($\varepsilon(t)$), and time (t) are the required input parameters for CMSE fatigue analysis to calculate DPSE.

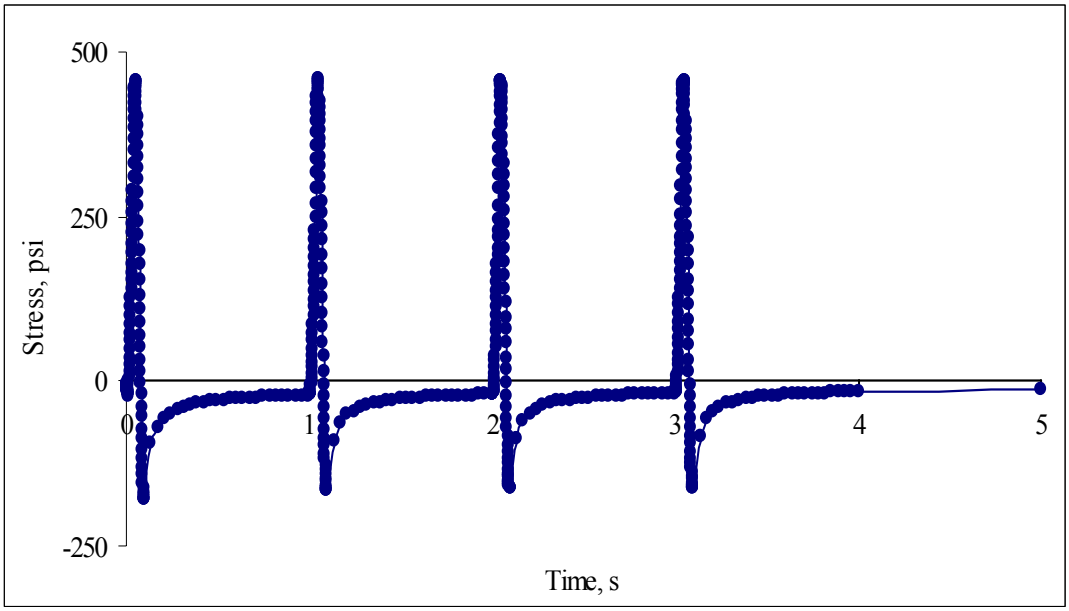

Figure 5-7. Stress Response from RDT Testing at 30 °C (86 °F).

Anisotropic Test

The modulus of HMAC is an important input parameter used in predicting HMAC mixture fatigue properties. HMAC is not an isotropic material, and therefore, its mechanical properties (i.e., elastic modulus) are directionally dependent (*72-73*). The objective of the anisotropic test was thus to measure the variation of HMAC modulus measured from different directions, vertical (E_z) and horizontal or lateral (E_x and E_y), which constitute input parameters for CMSE fatigue analysis. Primarily, the research team conducted the anisotropic (AN) test to determine the shift factor due to anisotropy (SF_a) discussed in the subsequent sections of this chapter.

Test Protocol

In this project, the research team conducted the AN test consistent with the HMAC elastic-resilient modulus test, but with both axial and radial deformation measurements for E_z and E_x determination, respectively (*64*). AN is a destructive stress-controlled test with a sinusoidal-shaped input stress waveform. The test involved repeated application of a sinusoidal-shaped stress magnitude of 690 kPa (100 psi) at a loading frequency of 1 Hz for a total of 200 load cycles without any rest period. Figure 5-8 shows the AN test loading configuration.

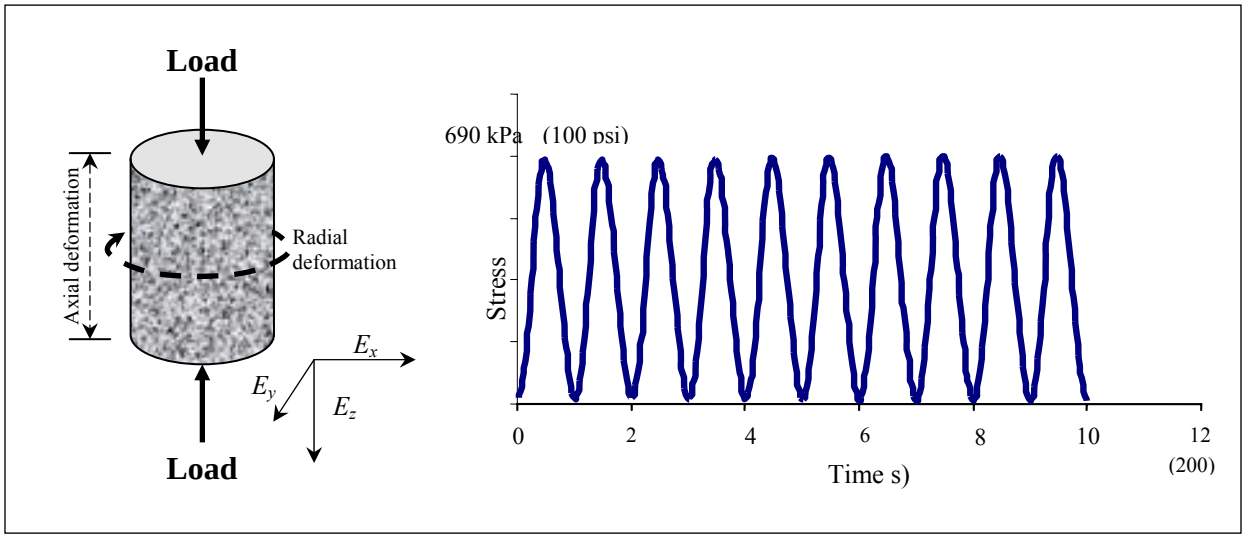

Figure 5-8. Loading Configuration for the AN Test

An input stress magnitude of 690 kPa is simulative of a truck tire pressure on an in situ field HMAC pavement structure. For this project, AN testing was terminated at 200 load cycles, during which time sufficient data had been captured for moduli analysis. With a loading frequency of 1 Hz, the total AN test time was at most 5 minutes. Although AN is a destructive test, the 200 load cycles was in most cases not sufficient enough to cause visible damage to some specimens.

For an AN test of this nature, it is always a normal practice to subject the test specimens to lateral pressure confinement to simulate field triaxial stress state, particularly when testing unbound granular materials (*74-75*). In this project, the AN test was conducted under unconfined lateral pressure conditions. However, the AN analysis models were adjusted to the lateral pressure confinement conditions to simulate the laboratory triaxial stress state. This adjustment was achieved through trial testing of several HMAC specimens under both unconfined and confined laboratory lateral (345 kPa) pressure conditions and then comparing the moduli results. The moduli results measured without pressure confinement were then adjusted/modified to match the moduli results under lateral pressure confinement conditions, thus accounting for triaxial stress state conditions. Note that it is much more convenient, easier, and practical to conduct the HMAC AN test under unconfined lateral pressure conditions.

Test Conditions and Data Acquisition

The sinusoidal input stress waveform was supplied by the MTS, while axial and radial deformations were measured via three LVDTs. Two LDVTs attached vertically to the sides of the specimen were used for axial measurements, and one LVDT attached radially around the center of the specimen was used for radial deformation measurements, as shown in Figure 5-8. Data (time, load, and deformations) were captured electronically every 0.02 s.

Like other HMAC mixture tests in this project, the research team conducted the AN test in an environmentally controlled chamber at a test temperature of 20±0.5 °C (68±32.9 °F). The minimum conditioning period for the specimens was 2 hrs. The temperature was monitored and controlled through a thermocouple probe attached inside a dummy HMAC specimen also placed in the environmental chamber. Three replicate specimens were tested per aging condition per mixture type.

Figure 5-9 is an example of the strain responses from the AN test at 20 °C (68 °F) recorded for a period of 60 s. While the AN test gives both the elastic and plastic strain responses as shown in Figure 5-9, the response component of interest that is critical to fatigue is the elastic strain. By contrast, the plastic strain is critical to permanent deformation, which was beyond the scope of this project.

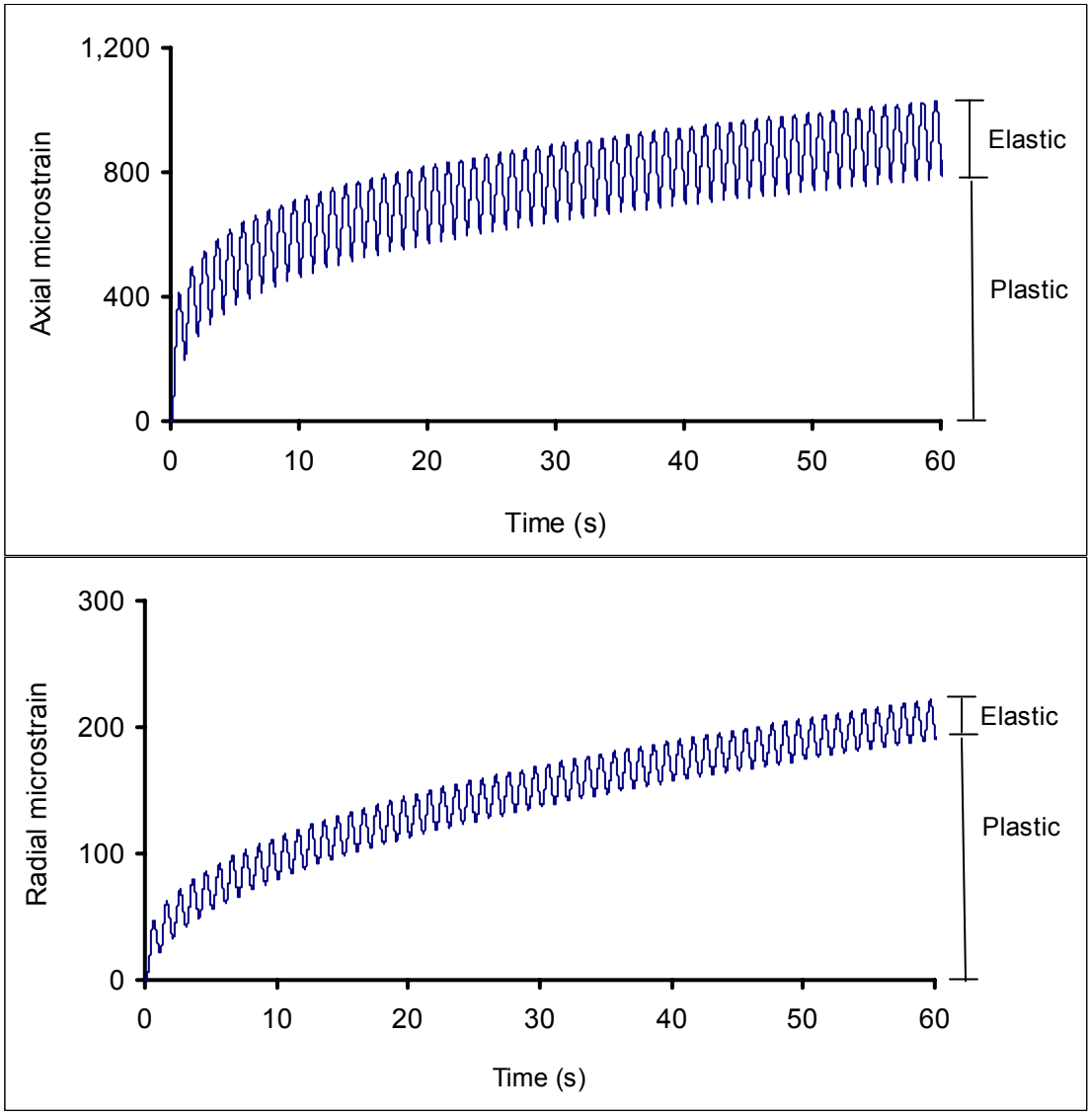

Figure 5-9. Example of Strain Responses from AN Testing @ 20 °C (68 °F).

From the measured AN test data, the elastic moduli were calculated as a function of the applied load (stress) and elastic strain response, as expressed by Equations 5-3 and 5-4 below (*64*, *74-75*). For simplicity, HMAC was assumed to be laterally isotropic, and therefore, E_x was considered equivalent to E_y in magnitude

$$E_z = \frac{\sigma_z}{a_z \varepsilon_z} \qquad \text{(Equation 5-3)}$$

$$E_x = E_y = a_x \frac{\nu \sigma_z}{\varepsilon_x} \qquad \text{(Equation 5-4)}$$

where:

E_z	=	Elastic modulus in the vertical direction (MPa)
E_x	=	Elastic modulus in the lateral direction (MPa)
σ_z	=	Applied compressive axial stress (MPa)
$\varepsilon_z, \varepsilon_x$	=	Axial and radial deformation, respectively (mm/mm)
ν	=	Poisson's ratio ($\nu \cong 0.33$)
a_x, a_z	=	Anisotropic adjustment factors that account for laboratory lateral pressure confinement conditions ($a_x \cong 1.15$, $a_z \cong 0.75$)

In this project, the mean a_x and a_z values were determined to be 1.15 and 0.75, respectively (for both mixtures), and these were the values used for moduli computations. The determination of these a_i adjustment factors is illustrated in Appendix B.

Surface Energy Measurements for the Binder – The Wilhelmy Plate Test

The surface energy measurements for the binders in this project were completed using the Wilhelmy plate method (*68*, *71*). Compared to other methods such as the drop weight, Du Nouy ring, pendant drop, Sessile drop, capillary rise, and maximum bubble pressure, the Wilhelmy plate method is relatively simple and does not require complex corrections factors to the measured data (*68*, *71*).

The contact angle between binder and any liquid solvent can be measured using the Wilhelmy plate method. This method is based on kinetic force equilibrium when a very thin plate is immersed or withdrawn from a liquid solvent at a very slow constant speed, as illustrated in Figure 5-10 (*76*).

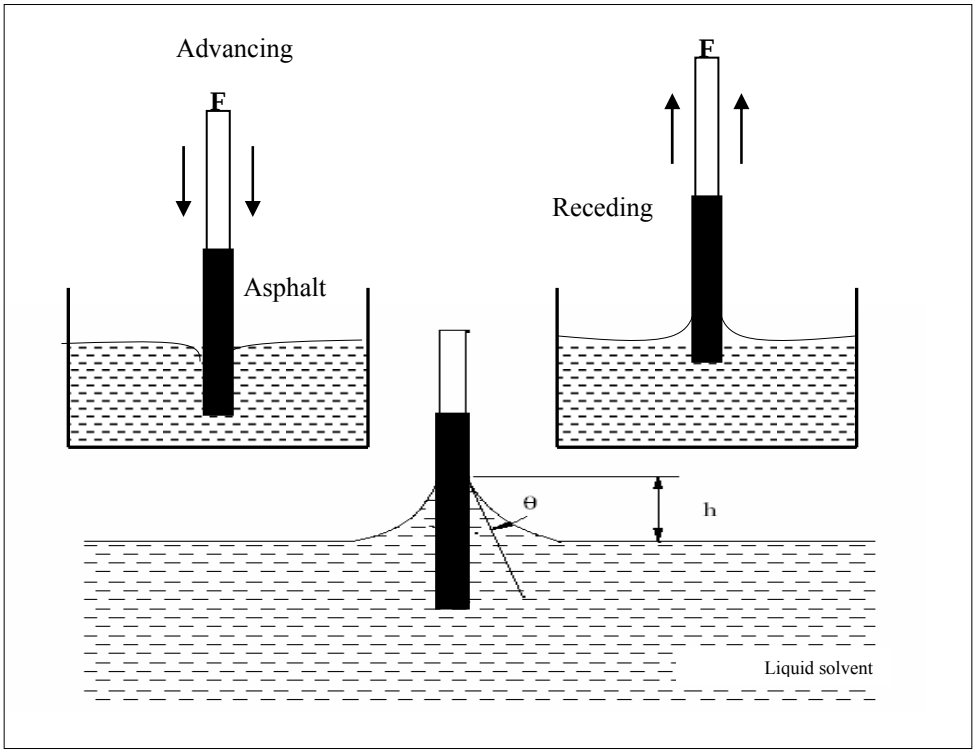

Figure 5-10. Loading Configuration for the Wilhelmy Plate Method.

The dynamic contact angle between binder and a liquid solvent measured during the immersing process is called the advancing contact angle, while the dynamic contact angle during the withdrawal process is called the receding contact angle.

The advancing contact angle, which is a wetting process, is associated with the healing process, while the receding angle is associated with the fracture mechanism. The total surface free energy and its components for binder are calculated from these advancing and receding contact angles. The surface free energy calculated from the advancing contact angles is called the surface free energy of wetting or healing, while the surface free energy computed from the receding contact angle is called the surface free energy of dewetting or fracturing.

Test Protocol and Data Acquisition

To complete the Wilhelmy plate test, approximately 0.65 g of hot-liquid binder heated to about 144 °C (291.2 °F) was coated onto glass plates 50 mm (≅2 inches) in length by 25 mm (≅1 inch) in width with a 0.15 mm (0.006 inches) thickness. By dipping the glass plate into a mass of hot-liquid binder to a depth of about 15 mm (0.6 inches), a thin binder film of approximately 1 mm (0.039 inches) thickness was created on the glass plate after allowing the excess binder to drain off (*68*, *71*).

As shown in Figure 5-7, the actual test protocol involves an automatically controlled cycle (s) of immersion and withdrawal (receding) processes of the binder coated glass plates into a liquid solvent to a depth of about 5 mm (0.2 inches) at an approximate uncontrolled ambient temperature of 20±2 °C (68±32.9 °F). The temperature is not tightly controlled in this test because previous research has indicated that the measurable contact angle, and consequently the surface free energy, are not very temperature sensitive (*68*, *71*). The total test time for both the immersion and withdrawal processes took approximately 15 minutes.

Prior to testing, the binder-coated glass plate must be vacuumed for about 12 hrs in a diseccator to de-air the binder. Three test binder samples are required per test per three liquid solvents, and thus a total of nine samples were used per aging condition (i.e., 0, 3, and 6 months).

Distilled water, formamide, and glycerol were the three selected liquid solvents used in this project because of their relatively large surface energies, immiscibility with binder, and wide range of surface energy components. Table 5-2 lists the surface energy components of these three liquid solvents (distilled water, formamide, and glycerol) (*68*, *71*).

Table 5-2. Surface Energy Components of Water, Formamide, and Glycerol.

Solvent	Surface Free Energy Components (ergs/cm^2) *(68, 71)*				
	Γ_{Li}	Γ_{Li}^{LW}	Γ_{Li}^{+}	Γ_{Li}^{-}	Γ_{Li}^{AB}
Distilled water	72.60	21.60	25.50	25.50	51.00
Formamide	58.00	39.00	2.28	39.60	19.00
Glycerol	64.00	34.00	3.60	57.40	30.00

During the test, the loading force for the immersion and receding processes was provided by an automatically controlled Dynamic Contact Analyzer (DCA) balance shown in Figure 5-11. Data (dynamic contact angle) were measured and captured electronically via the WinDCA software. Figure 5-12 is an example of the measured dynamic advancing and receding contact angles at 20±2 °C (68±35.6 °F).

Figure 5-11. The DCA Force Balance and Computer Setup - Wilhelmy Plate Test.

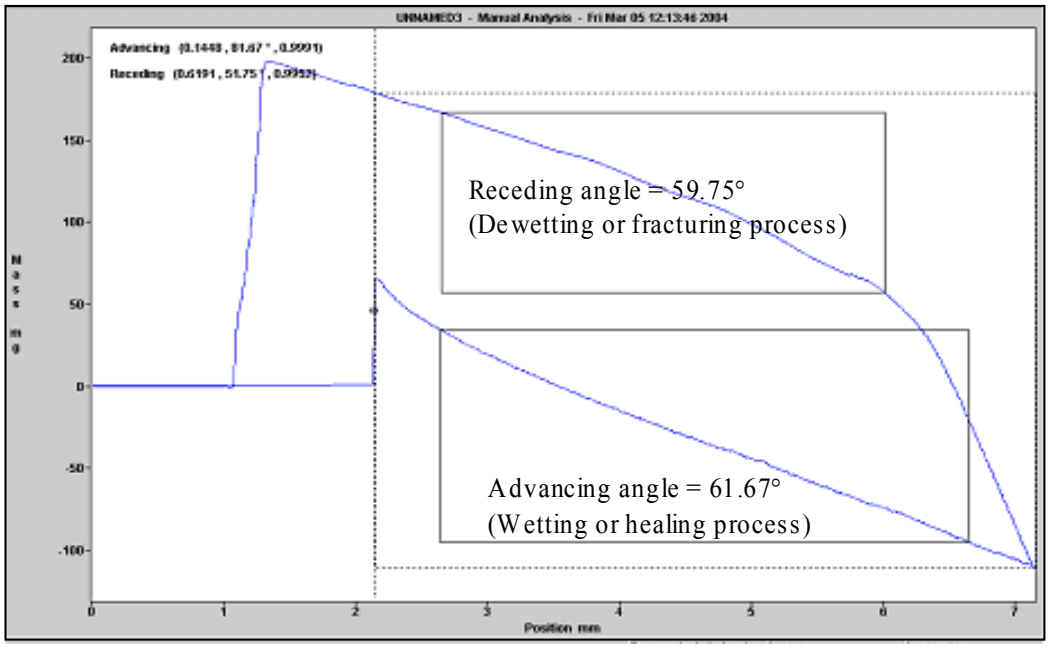

Figure 5-12. Example of the DCA Software Display (Advancing and Receding).

For clarity, the vertical axis title in Figure 5-10 is "mass" in mg with a scale of -100 to 200 mg, and the horizontal axis title is "position" in mm with a scale of 0 to 7 mm (0 to 0.28 inches).

Binder Surface Energy Calculations

Equation 5-3 is the force equilibrium equation resulting from the immersion (advancing) or the withdrawal (receding) processes during the Wilhelmy plate test. Based on the Young-Dupre theory and the assumption that binder equilibrium film pressure is zero, Equation 5-5 reduces to Equation 5-6 (*71*).

$$\Delta F = P_t \Gamma_L Cos\theta - V\rho_L g + V\rho_{Air} g \qquad \text{(Equation 5-5)}$$

$$\Gamma_{L_i}\left(1 + Cos\theta_i\right) = 2\sqrt{\Gamma_i^{LW}\Gamma_{L_i}^{LW}} + 2\sqrt{\Gamma_i^{-}\Gamma_{L_i}^{+}} + 2\sqrt{\Gamma_i^{+}\Gamma_{L_i}^{-}} \qquad \text{(Equation 5-6)}$$

where:

F	=	Applied force (kN)
P_t	=	Perimeter of the binder coated glass plate (m)
θ	=	Dynamic contact angle between binder and the liquid solvent, degrees (°)
V	=	Volume of immersed section of glass plate (m^3)
ρ	=	Density (subscript "L" for liquid solvent and "Air" for air) (g/cm^3)
g	=	Acceleration due to gravity (m/s^2)
Γ	=	Surface free energy ($ergs/cm^2$)

The dynamic contact angle θ (°) is the measurable parameter, advancing (wetting) or receding (dewetting). Γ_{Li}^{LW}, Γ_{Li}^{+}, and Γ_{Li}^{-} are known surface free energy components of the liquid solvent. Γ_i^{LW}, Γ_i^{+}, and Γ_i^{-} are the three unknown components of the binder surface free energy from Lifshtz-van der Waals forces, Lewis base, and Lewis acid, respectively, that need to be determined. Note that the advancing (wetting) and receding (dewetting) contact angles are used for determining the surface energy due to healing and fracturing, respectively.

Mathematically, three liquid solvents of known surface free energies must be used to solve Equation 5-6 for the three unknown parameters Γ_i^{LW}, Γ_i^{+}, and Γ_i^{-}. Algebraically, Equation 5-6 can easily be transformed into a familiar matrix form of simple linear simultaneous equations expressed by Equation 5-7 (*71*):

$$\begin{bmatrix} a_{11} & a_{12} & a_{13} \\ a_{21} & a_{22} & a_{23} \\ a_{31} & a_{32} & a_{33} \end{bmatrix} \begin{bmatrix} x_1 \\ x_2 \\ x_3 \end{bmatrix} = \begin{bmatrix} Y_1 \\ Y_2 \\ Y_3 \end{bmatrix} \qquad \text{(Equation 5-7)}$$

$$a_{1i} = 2\frac{\sqrt{\Gamma_{L_i}^{LW}}}{\Gamma_{L_i}},\ a_{2i} = 2\frac{\sqrt{\Gamma_{L_i}^{+}}}{\Gamma_{L_i}},\ a_{3i} = 2\frac{\sqrt{\Gamma_{L_i}^{-}}}{\Gamma_{L_i}} \qquad \text{(Equation 5-8)}$$

$$x_1 = \sqrt{\Gamma_i^{LW}},\ x_2 = \sqrt{\Gamma_i^{-}},\ x_3 = \sqrt{\Gamma_i^{+}} \qquad \text{(Equation 5-9)}$$

$$Y_i(x) = 1 + Cos\,\theta_i \qquad \text{(Equation 5-10)}$$

where:

a_{ki} = Known surface energy components of the three liquid solvents (distilled water, formamide, and glycerol) (ergs/cm^2) (Table 5-2)

x_i = The unknown surface energy components (Γ_i^{LW}, Γ_i^+, and Γ_i^-) of the binder that need to be determined (ergs/cm^2)

$Y_i(x)$ = Known function of the measured contact angles of the binder in the three liquid solvents (θ_{Water}, $\theta_{Formamide}$, and $\theta_{Glycerol}$)

The solution of Equation 5-10 provides the surface free energy components of the binder required for the CMSE fatigue analysis.

Surface Energy Measurements for the Aggregate – The Universal Sorption Device

In this project, the research team used the Universal Sorption Device (USD) for the surface energy measurements of aggregates. The USD method utilizes a vacuum gravimetric static sorption technique that identifies gas adsorption characteristics of selected solvents with known surface free energy to indirectly determine the surface energies of the aggregate. Sorption methods are particularly suitable for aggregate surface energy measurements because of their ability to accommodate the peculiarity of sample size, irregular shape, mineralogy, and surface texture associated with the aggregates *(71)*.

Test Protocol and Data Acquisition

The USD setup is comprised of a Rubotherm magnetic suspension balance system, a computer system (with Messpro software), a temperature control unit, a high quality vacuum unit, a vacuum regulator, pressure transducers, a solvent container, and a vacuum dissector. A schematic of the main components of the USD setup is illustrated in Figure 5-13.

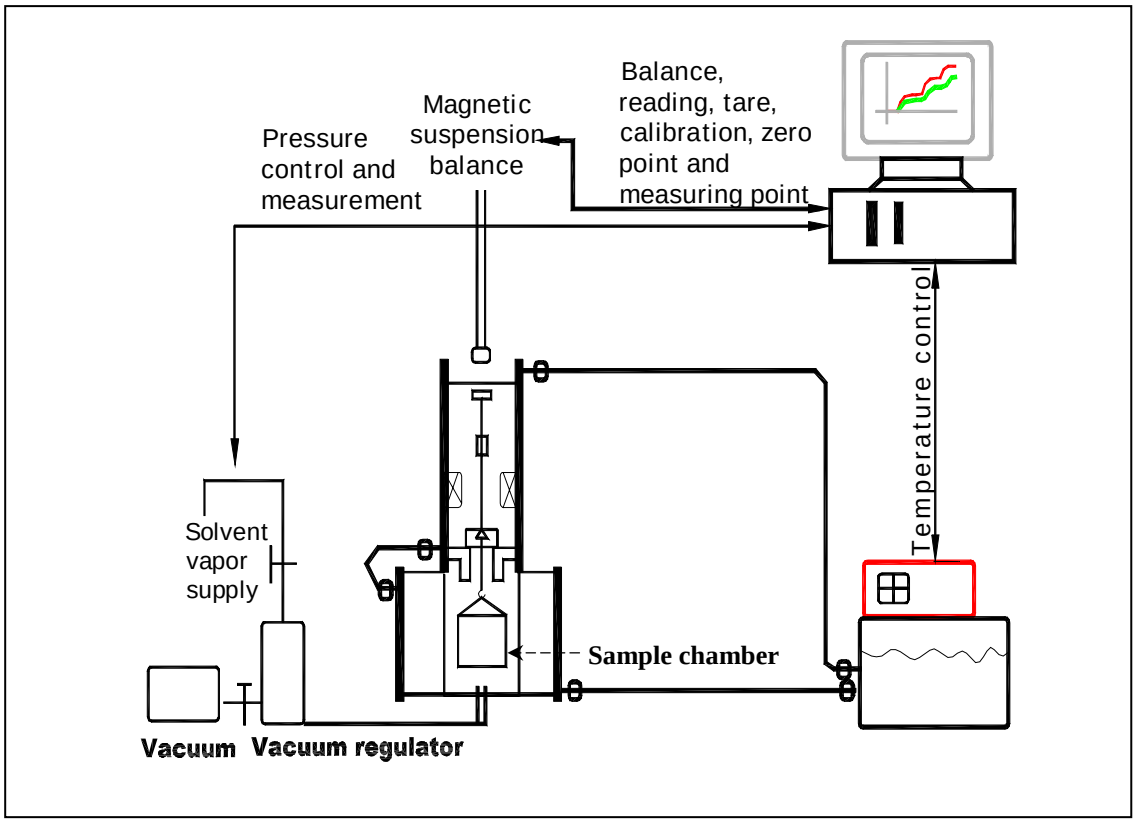

Figure 5-13. USD Setup.

A Mettler balance is securely established on a platform with the hang-down Rubotherm magnetic suspension balance and sample chamber beneath it. This magnetic suspension balance has the ability to measure a sample mass of up to 200 g to an accuracy of 10^{-5} g, which is sufficient for precise measurement of mass increase due to gas adsorbed onto the aggregate surface. The whole USD system is fully automated with about 8 to 10 predetermined pressure set-points that automatically trigger when the captured balance readings reach equilibrium.

With this USD sorption method, an aggregate fraction between the No.4 and No.8 sieve size is suspended in the sample chamber, in a special container. Essentially, the size of aggregate tested is that which passes the No.4 (4.75 mm [0.19 inches]) sieve but is retained on the No. 8 sieve (2.36 mm [0.09 inches]). Theoretically, the surface free energy of aggregate is not affected by the size of the aggregate because size is accounted for during the SE calculation process (*71*). However, this aggregate fraction size (No.4 < aggregate size < No. 8) used in the USD test is dictated by the limitation of the sample chamber size and the desired aggregate surface area for sufficient gas adsorption that is representative of all aggregate fractional sizes.

During the USD test process, once the chamber is vacuumed, a solvent vapor is injected into the aggregate system. A highly sensitive magnetic suspension balance is used to measure the amount of solvent adsorbed on the surface of the aggregate. The vapor pressure at the aggregate surface is measured at the same time. The surface energy of the aggregate is calculated after measuring the adsorption of three different solvents with known specific surface free energy components. In this project, three solvents: distilled water, *n*-Hexane, and Methyl Propyl Ketone 74 (MPK) with surface free energy components listed in Table 5-3, were used (*71*).

Table 5-3. Surface Energy Components of Water, n-hexane, and MPK.

Solvent	**Surface Free Energy Components (ergs/cm^2) (*68, 71*)**				
	Γ_{Li}	Γ_{Li}^{LW}	Γ_{Li}^{+}	Γ_{Li}^{-}	Γ_{Li}^{AB}
Distilled water	72.60	21.60	25.50	25.50	51.00
n-hexane	18.40	18.40	0.00	19.60	0.00
MPK	24.70	24.70	0.00	0.00	0.00

Like binder SE measurements, aggregate SE measurements are also insensitive to temperature, so the research team conducted the USD test at uncontrolled ambient temperature of approximately 25±2 °C (77±35.6 °F). The total test time for a complete test set with three solvents is about 60 to 70 hrs. For each solvent, 50 g sample of aggregates were tested for 0 months aging condition only. Note that aggregates are by nature insensitive to aging and thus 3 and 6 months aging at 60 °C (140 °F) were not considered for the aggregate SE measurements. Prior to testing, the aggregate sample must be thoroughly cleaned with distilled water and oven-dried (at about 120 °C (248 °F) for at least 8 hrs) to remove any dusty particles and moisture that might negatively impact the results.

Data (vapor pressure, adsorbed gas mass, and test time) were measured and captured electronically via the Messpro software. Figure 5-14 is an example of a typical output obtained from the USD adsorption test for n-hexane adsorption on limestone aggregate at 25 °C (77 °F).

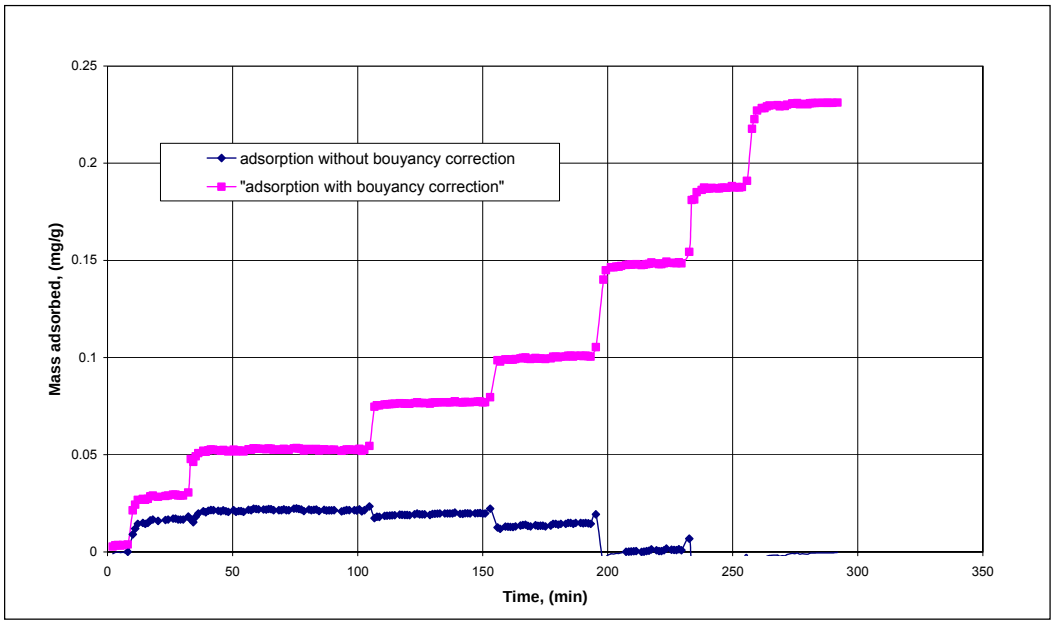

Figure 5-14. Example of Adsorption of n-Hexane onto Limestone under USD Testing.

Aggregate SE Calculations

Once the adsorbed solvent mass and vapor pressure on the aggregate surface have been measured and the adsorption data corrected for solvent vapor buoyancy using the generalized Pitzer correlation model, the specific surface area of the aggregate was then calculated using the BET (Brunauer, Emmett, and Teller) model shown by Equation 5-11 (*68*, *71*):

$$\frac{P}{n(P_0 - P)} = \left(\frac{c-1}{n_m c}\right)\frac{P}{P_0} + \frac{1}{n_m c} \qquad \text{(Equation 5-11)}$$

where:

P = Vapor pressure (MPa)

P_0 = Saturated vapor pressure of the solute (MPa)

n = Specific amount adsorbed on the surface of the absorbent (mg)

n_m = Monolayer capacity of the adsorbed solute on the absorbent (mg)

c = Parameter theoretically related to the net molar enthalpy of adsorption

For the type of isotherms associated with the pressure conditions in this USD test, n_m can be obtained from the slope and the intercept of the straight line that best fits the plot of *P/n(P-Po)* versus *P/Po*. The specific surface area (*A*) of the aggregate can then be calculated through the following equation:

$$A = \left(\frac{n_m N_o}{M} \right) \alpha \qquad \text{(Equation 5-12)}$$

And for a hexagonal close-packing model;

$$\alpha = 1.091 \left(\frac{M}{N_o \rho} \right)^{2/3} \qquad \text{(Equation 5-13)}$$

where:

α	=	Projected area of a single molecule (m^2)
N_o	=	Avogadros' number (6.02×10^{23})
M	=	Molecular weight (g)
ρ	=	Density of the adsorbed molecule in liquid at the adsorption conditions (g/cm^3)

The result from the BET equation is used to calculate the spreading pressure at saturation vapor pressure (π_e) for each solvent using Gibbs free energy Equation 5-14 (*71*):

$$\pi_e = \frac{RT}{A} \int_0^{P_0} \frac{n}{P} dP \qquad \text{(Equation 5-14)}$$

where:

π_e	=	Spreading pressure at saturation vapor pressure of the solvent ($ergs/cm^2$)
R	=	Universal gas constant (83.14 cm^3 bar/mol.*K*)
T	=	Absolute temperature (Kelvin, *K*) (*K = 273 + ℃*)

The work of adhesion of a liquid on a solid (W_A) can be expressed in terms of the surface energy of the liquid (Γ_l) and the equilibrium spreading pressure of adsorbed vapor on the solid surface (π_e) as shown in Equations 5-15 and 5-16:

$$W_a = \pi_e + 2\Gamma_l \qquad \text{(Equation 5-15)}$$

$$\pi_e + 2\Gamma = 2\sqrt{\Gamma_s^{LW}\Gamma_l^{LW}} + 2\sqrt{\Gamma_s^{+}\Gamma_l^{-}} + 2\sqrt{\Gamma_s^{-}\Gamma_l^{+}} \qquad \text{(Equation 5-16)}$$

where:

subscript s = Solid (aggregate)

subscript l = Liquid (solvent)

From Equations 5-15 and 5-16, the surface energy components and the total surface energy of the aggregate can be determined by employing Equations 5-17 through 5-20):

$$\Gamma_s^{LW} = \frac{\left(\pi_e + 2\Gamma_l\right)^2}{4\Gamma_l^{LW}} \qquad \text{(Equation 5-17)}$$

Equation 5-17 is used to calculate the Γ_s^{LW} of the surface for a non-polar solvent on the surface of the solid (aggregate). For a known mono-polar basic liquid vapor (subscript m) and a known bipolar liquid vapor (subscript b), the Γ_s^{+} and Γ_s^{-} values were calculated using Equations 5-18 and 5-19 as follows:

$$\Gamma_s^{+} = \frac{\left(\pi_e + 2\Gamma_{lm} - \sqrt{\Gamma_s^{LW}\Gamma_{lm}^{LW}}\right)^2}{4\Gamma_{lm}^{-}} \qquad \text{(Equation 5-18)}$$

$$\Gamma_s^{-} = \frac{\left(\pi_e + 2\Gamma_{lb} - \sqrt{\Gamma_s^{LW}\Gamma_{lb}^{LW}} - 2\sqrt{\Gamma_s^{+}\Gamma_{lb}^{-}}\right)^2}{4\Gamma_{lb}^{+}} \qquad \text{(Equation 5-19)}$$

Finally, the total surface energy of the aggregate (Γ_s) is calculated as expressed by Equation 5-20:

$$\Gamma_s = \Gamma_s^{LW} + 2\sqrt{\Gamma^+\Gamma^-} \quad \text{(Equation 5-20)}$$

Note, however that the current USD test protocol is still under development, in particular to improve its test time efficiency as well as a general review of the SE data analysis procedures (*77*). Appendix B provides a summary of the current USD test protocol and SE analysis procedure as utilized in this project.

FAILURE CRITERIA

For the CMSE approach, fatigue failure is defined as crack initiation and propagation through the HMAC layer thickness. In this project, researchers selected a maximum microcrack length of 7.5 mm (0.30 inches) as the failure threshold value for crack initiation. This 7.5 mm (0.30 inches) threshold value was selected based on Lytton et al.'s findings in their extensive fatigue tests that crack propagation in the HMAC layer begins when microcracks grow and coalesce to form a small crack of approximately 7.5 mm (0.30 inches) long (*45*).

ANALYSIS PROCEDURE

Equation 5-21, which relates field fatigue life (N_f) to the number of load cycles to crack initiation (N_i) and crack propagation (N_p) as a function of shift factors (SF_i), is the fundamental principle of the CMSE approach for fatigue modeling of HMAC mixtures (*45*).

$$N_f = SF_i\left(N_i + N_p\right) \quad \text{(Equation 5-21)}$$

where:

N_f = Fatigue life or number of load cycles to fatigue failure

SF_i = Product of the shift factors including HMAC anisotropy (SF_a), healing (SF_h), aging (SF_{ag}), residual stresses (SF_{rs}), stress state (SF_{ss}), resilient dilation (SF_d), and traffic wander (SF_{tw}).

N_i = Number of load cycles to crack initiation

N_p = Number of load cycles to crack propagation

Each of these terms in Equation 5-21 is discussed in the subsequent subsections. In Equation 5-21, the sum ($N_i + N_p$) constitutes the laboratory fatigue life and the product of the shift factors (SF_i) and the sum ($N_i + N_p$) constitute the field fatigue life.

Shift Factor due to Anisotropic Effect, SF_a

Anisotropy arises due to the fact that HMAC is not isotropic as often assumed. The mixture stiffness (modulus) in the lateral (horizontal) direction is not equal to that in the vertical direction due to the differences in the particle orientation during compaction/construction. During construction, there is always a high compactive effort in the vertical direction relative to other directions. So the HMAC behavior or response to loading and/or the environment is different in different directions. Consequently, the HMAC anisotropy must be considered in fatigue analysis. However, most laboratory test protocols measure only the vertical stiffness and assume isotropic behavior.

In the CMSE analysis, SF_a takes care of the anisotropic behavior of the HMAC mixture. Equation 5-22 shows the elastic modular relationship between the vertical (E_z) and horizontal (E_x) moduli used in this project. E_z and E_x are measurable parameters from the AN test (34).

$$SF_a = \left(\frac{E_z}{E_x}\right)^{1.75} \qquad \text{(Equation 5-22)}$$

where:

SF_a = Shift factor due to anisotropy, ranging between 1 and 5

E_z = Elastic modulus in vertical direction (MPa)

E_x = Elastic modulus in lateral or horizontal direction (MPa)

Generally, because of the vertical orientation of the compactive effort during field construction or laboratory compaction, E_z is always greater than E_x on the order of magnitude of about 1.5 times (*78*). For simplicity purposes, HMAC was assumed to be laterally isotropic, and therefore, E_x was considered as being equivalent to E_y in magnitude.

Shift Factor due to Healing Effect, SF_h

Due to traffic rest periods and temperature variations, the asphalt binder has a tendency to heal (closure of fracture surfaces), which often results in improvement in the overall HMAC mixture fatigue performance. The CMSE approach takes this into account and relates healing to traffic rest periods and temperature by the following equations (*45*, *71*):

$$SF_h = 1 + g_5\left(\frac{\Delta t_r}{a_{TSF}}\right)^{g_6} \quad \text{(Equation 5-23)}$$

$$\Delta t_r = \frac{31.536\times10^6\, P_{DL}}{80kN \text{ Traffic ESALs}} \quad \text{(Equation 5-24)}$$

$$g_5 = a(h_o)^{g_6} \quad \text{(Equation 5-25)}$$

$$h_o = \dot{h}_2 + \left(\frac{\dot{h}_1 - \dot{h}_2}{1+\left[\left(\frac{\dot{h}_1 - \dot{h}_2}{h_\beta}\right)\left(\frac{\Delta t C_{sr}}{a_{TSF}}\right)\right]}\right) \quad \text{(Equation 5-26)}$$

$$\dot{h}_1 = \left(\frac{C_1}{\left[\Delta G_h^{LW} E_c\right]^{\left(\frac{1}{m_c}\right)}}\right) \quad \text{(Equation 5-27)}$$

$$\dot{h}_2 = \left(\left[C_2\left(\frac{\Delta G_h^{AB}}{E_c}\right)\right]^{\left(\frac{1}{m_c}\right)} + C_3\right) \quad \text{(Equation 5-28)}$$

$$h_\beta = C_4\left(\frac{\Delta G_h^{AB}}{\Delta G_h^{LW}}\right)\left(\frac{C_5}{m_c}\right) \qquad \text{(Equation 5-29)}$$

where:

SF_h = Shift factor due to binder healing effects, ranging between 1 and 10

Δt_r = Rest period between major traffic loads (s)

Δt = Loading time (s)

a_{TSF} = Temperature shift factor for field conditions (~1.0)

C_{sr} = Square rest period factor (~1.0)

a, g_5, g_6 = Fatigue field calibration constants

h_0, $\dot{h}_{1-2}$, = Healing rates

h_β = Healing index, ranging between 0 and 1.0

P_{DL} = Pavement design life in years

80kN Traffic ESALs = Number of equivalent single axle loads over a given pavement design period (e.g., 5 million over a 20-year design period)

$C_{1\text{-}5}$ = Healing constants

E_c = Elastic relaxation modulus from compression RM master-curve (MPa)

m_c = Exponent from compression RM master-curve

ΔG_h^{AB}, ΔG_h^{LW} = Surface energies due to healing or dewetting (ergs/cm^2)

In Equation 5-23, Δt_r represents the field long-term rest period and depends on the pavement design life and traffic expressed in terms of traffic ESALs (*45*). The numerical value of 31.536×10^6 in Equation 5-24 represents the total time in seconds for a 365 day calendar year. The parameter a_{TSF} is a temperature shift factor used to correct for temperature differences between laboratory and field conditions. For simplicity, the research team used an a_{TSF} value of 1.0, but this value can vary depending on the laboratory and field temperature conditions under consideration. C_{sr} represents the shape of the input strain wave rest period during the RDT test.

As discussed previously, the periodic time interval between the input strain waveforms for the RDT test in this project simulated a square-shaped form, with a total duration of 0.9 s. This 0.9 s periodic time interval was considered as the square shaped rest period, so a C_{sr} value of 1.0 was used in the analysis (*79*). As stated previously, this rest period allowed for HMAC relaxation, healing, and prevented the buildup of undesirable residual stresses during RDT testing.

The parameters a, g_5, g_6 , h_0, and $\dot{h}_{1-2}$ are fatigue field calibration constants and healing rates quantifying the HMAC mixture healing properties as a function of climatic location of the pavement structure in question, *SE* due to healing, and HMAC mixture properties (E_c and m_c) obtained from compression relaxation modulus tests. These calibration constants and healing rates also represent the HMAC mixture short-term rest periods and asphalt binder healing rates, both short-term and long-term, respectively (*45*). The parameter h_β is a healing index ranging between 0 and 1.0 that represents the maximum degree of healing achievable by the asphalt binder (*71*).

The fatigue calibration coefficients g_5 and g_6 are climatic dependent. In this project, the research team used values shown in Table 5-4, assuming Wet-No-Freeze and Dry-No-Freeze climates. Table 5-5 provides an additional set of g_i values based on accelerated laboratory testing. These values in Tables 5-4 and 5-5 were established by Lytton et al. (*45*) in their extensive field calibration study of fatigue cracking through Falling Weight Deflectometer (FWD) tests in the field and accelerated laboratory tests. In their (Lytton et al.) findings, these calibration coefficients provided a good fit between measured and predicted fatigue cracking (*45*).

Table 5-4. Fatigue Calibration Constants Based on Backcalculation of Asphalt Moduli from FWD Tests (Lytton et al. [45]).

Coefficient	Climatic Zone			
	Wet-Freeze	Wet-No-Freeze	Dry-Freeze	Dry-No-Freeze
g_0	-2.090	-1.615	-2.121	-1.992
g_1	1.952	1.980	1.707	1.984
g_2	-6.108	-6.134	-5.907	-6.138
g_3	0.154	0.160	0.162	1.540
g_4	-2.111	-2.109	-2.048	-2.111
g_5	0.037	0.097	0.056	0.051
g_6	0.261	0.843	0.642	0.466

Table 5-5. Fatigue Calibration Constants Based on Laboratory Accelerated Tests (Lytton et al. [45]).

Coefficient	Climatic Zone			
	Wet-Freeze	Wet-No-Freeze	Dry-Freeze	Dry-No-Freeze
g_0	-2.090	-1.429	-2.121	-2.024
g_1	1.952	1.971	1.677	1.952
g_2	-6.108	-6.174	-5.937	-6.107
g_3	0.154	0.190	0.192	1.530
g_4	-2.111	-2.079	-2.048	-2.113
g_5	0.037	0.128	0.071	0.057
g_6	0.261	1.075	0.762	0.492

SE and RM tests were discussed in previous sections of this chapter. ΔG_h E_c, and m_c are material (binder, aggregate, and HMAC mixture) dependent but also vary with the aging condition of the binder and/or HMAC mixture, which has a net impact on SF_h and N_f. As discussed in Chapter 10, this preliminary study has shown that the variation of these parameters (ΔG_h, E_c, and m_c) with 3 and 6 months aging of the binder and HMAC mixture at 60 °C (140 °F) reduced the value of SF_h considerably, particularly the resultant N_f. Analysis procedures for ΔG_h, E_c, and m_c are discussed subsequently.

The healing constants C_1 through C_5 were backcalculated from regression analysis as a function of the measured E_c, ΔG_h due to healing, and the healing rates (h_i) using a spreadsheet sum of square error (SSE) minimization technique (*45*, *68*, *71*).

Other Shift Factors

The shift factor due to aging (SF_{ag}) is discussed in Chapters 10 and 11 of this report. In this current CMSE analysis, other shift factors including residual stress, stress state, dilation, and traffic wander were not considered or were simply assigned a numerical value of 1.0 based on the assumptions discussed in this section. In fact, the research team considered that some of these factors are already included in the SF_a and SF_h shift factors. Nonetheless, future CMSE studies should consider the possibility of exploring these shift factors in greater detail.

Residual Stresses, SF_{rs}

In the field, because of incomplete elastic relaxation/recovery and short time intervals between some traffic load applications (axles of the same vehicle), residual stresses can remain in the pavement after the passage of each load cycle and may thus prestress the HMAC layer so that the tensile stresses that occur with the next load cycle cause less, equivalent, or more damage. If present, these residual stresses occur either in tension or compression depending among other factors on the magnitude of the load and the pavement structure. On the same principle, residual stresses can also buildup in laboratory test fatigue specimens particularly if there is an insufficient rest period between load applications or if the specimens are not properly loaded during the test. Equations 5-30 and 5-31 show the estimation of SF_r according to Tseung et al. (*80*):

$$SF_r = \left(\frac{1}{1 \pm P_o t^{-m}}\right)^{k_{21}} = \left(1 \pm P_o t^{-m}\right)^{\left(\frac{-2}{m}\right)} \qquad \text{(Equation 5-30)}$$

$$P_o = \frac{\sigma_r(t)}{\varepsilon_t E(t)} \qquad \text{(Equation 5-31)}$$

where:

P_o	=	The percent of total strain remaining in the pavement as residual strain after passage of the traffic load (%)
t	=	Loading duration (s) (e.g., 0.1 s)
m	=	Stress relaxation rate (i.e., from tensile RM master-curve)
k_{21}	=	Laboratory determined constant as a function of m
$\sigma_r(t)$	=	Residual stresses (tensile or compressive) at time t (MPa)
ε_t	=	Total tensile strain (mm/mm)
$E(t)$	=	HMAC elastic modulus at time t (MPa)

Note that the expression $k_{21} = 2/m$ may be valid only for HMAC subjected to uniaxial strain-controlled loading tests. A different expression may be required for stress-controlled loading tests.

According to Lytton et al. (*45*), SF_r commonly ranges between 0.33 and 3.0 depending on whether the residual stresses are tensile or compressive. In the absence of sufficient field data to accurately predict the magnitude and/or determine whether these residual stresses (or strains) will be tensile or compressive, and the fact that there was insignificant residual stress build-up in the CMSE laboratory fatigue specimens under RDT testing (i.e., $\sigma_r(t) \approx P_o \approx 0.0$), a SF_r value of 1.0 was not an unreasonable assumption.

The RDT test in this project was conducted with a 0.9 s rest period between load pulses, while the actual loading time was 0.1 s. The RDT out put stress response indicated that this 0.9 s rest period sufficiently allowed for HMAC relaxation and subsequent prevention of residual stress buildup. In fact, Equations 5-30 and 5-31 also show that if there are no residual stresses ($\sigma_r(t) \approx 0.0$), as in the case of the RDT test in this project, P_o will be 0.0, and SF_r will have a numerical value of 1.0.

Note also that the CMSE fatigue analysis approach in this project assumes that there are no residual stresses due to construction compaction in the field or SGC compaction in the laboratory.

Stress State, SF_{ss}

In a pavement structure under traffic loading, a triaxial stress state exists. The continuum nature of the pavement material tends to transfer the applied stress in all three coordinate directions (x, y, and z) based on the Poisson's ratio and the interlayer bonding conditions. In the laboratory, the stress state can be uniaxial, biaxial, or triaxial depending on the test protocol. A shift factor is thus required to account for this difference in stress state between laboratory and field conditions.

In a linear elastic stress-strain analysis, Al-Qadi et al. found that a shift factor based on strain energy that accounts for the differences between laboratory and field pavement stress state can vary approximately between 1.0 and 6.0 (*81*). Among others, this stress state depends on materials, pavement structure, mode of loading (uniaxial, biaxial, or triaxial), and magnitude of loading. With sufficient laboratory and field data, Al-Qadi et al. proposed that SF_{ss} can be approximated by Equation 5-32 as follows (*81*):

$$SF_{ss} = \frac{W_{Lab}}{W_{Field}} = \frac{\sum_{i=x}^{y}(E_i \varepsilon_i) + \sigma_z^2 E_z}{\sum_{i=x}^{y}(E_i \varepsilon_i) + \sigma_z^2 E_z} \qquad \text{(Equation 5-32)}$$

where:

W_{Lab} = Total work done by laboratory loading ≅ strain energy (J/m^3)

W_{Field} = Total work done by traffic loading in the field ≅ strain energy (J/m^3)

σ, E, ε = stress (MPa), elastic modulus (MPa), and strain (mm/mm)

i = Subscript i, for x, y, and z coordinate directions

However, for the current CMSE analysis, the research team considered that the existence of stress state (uniaxial, biaxial or triaxial) under laboratory and/or field loading conditions is directly tied to the anisotropic response of HMAC. For example, the response behavior of HMAC in terms of the elastic modulus under loading is directionally dependent, which is a function of the stress state. Therefore, the effect of the stress state was considered to be indirectly incorporated in the SF_a factor.

Resilient Dilation, SF_d

Consistent with the theoretical definition of ν, resilient dilation will occur only for ν values greater than 0.5. For pavement material subjected to vertical loading, dilation occurs when the lateral deformation is greater than the vertical deformation, often as a result of inadequate lateral confinement or support. This tendency to dilate is generally caused by the motion of particles that tend to roll over one another (*45*).

Dilation is often very critical in unbound granular materials and the subgrade and can often have a very significant impact on the overall fatigue performance of the pavement structure in terms of stress-strain response. HMAC, on the other hand, is a bound material and is not very sensitive to dilation. However, its stress-strain response to traffic loading and overall performance can be greatly affected if the underlying pavement layers have potential to dilate.

SF_d often ranges between 1.0 and 5.0 depending upon how much larger the Poisson's ratio (ν) is greater than 0.5 (*45*). Since, in this project, all the values of ν used were less than 0.5 (Chapter 3), researchers assumed the minimum value of 1.0 for SF_d.

Traffic Wander, SF_{tw}

Controlled laboratory fatigue testing applies loading repetitively to the same exact location on the specimen. However, traffic loading in the field does not constrain itself to the same position in the wheelpath. Accordingly, SF_{tw} is needed to account for the traffic wander when modeling pavement response to loading.

Blab and Litzka (*82*) postulated that the vehicle positions within the wheelpaths follow a Laplace distribution function. Al-Qadi et al. (*81*) assumed a normal distribution around the wheelpath with a mean of zero and a standard deviation, σ. Based on transverse strain measurement in the wheelpath, Al-Qadi et al. derived SF_{tw} values ranging between 1.6 and 2.7 for a σ range of 0.5 to 1.0.

However, for a given infinitesimal point within the pavement structure (i.e., in the HMAC layer), the research team theorizes that the net engineering effect of traffic wander is to relax and/or rest that particular point, thus minimizing the effect of residual stresses (tensile or compressive) while simultaneously promoting elastic recovery and subsequent healing.

This stress relaxation or rest period occurs because of traffic wander, and subsequent loading follows a different path from the preceding one. Based on this theory, it can be assumed that the effect of traffic wander is indirectly tied to SF_{rs} and SF_h. Therefore, an independent SF_{tw} was not considered in the current CMSE approach.

Also, Al-Qadi et al.'s study seems to indicate that with the assumption of normal traffic distribution in the wheelpath and a relatively small value of σ (i.e., σ < 0.5), a SF_{tw} value of 1.0 can possibly be derived (*59*).

Number of Load Cycles to Crack Initiation, N_i

N_i is defined as the number of load cycles required to initiate and grow a microcrack to 7.5 mm (0.30 inches) in length in the HMAC layer. In the CMSE analysis, N_i is determined according to the following equation as a function of crack density, specimen cross-sectional area, Paris' Law fracture coefficients, and the rate that damage accumulates as indicated by DPSE (*29, 30, 34*):

$$N_i = \left(\frac{C_{\max}^{(1+2n)}}{A}\right)\left(\left[\frac{4\pi A_c}{b}\right]^n\right)(C_D)^n \qquad \text{(Equation 5-33)}$$

$$n = \left(\frac{1}{m_t}\right) \qquad \text{(Equation 5-34)}$$

$$A = \frac{k}{\sigma_t^2 I_i}\left(\left[\frac{D_1^{(1-m_t)} E_t}{\Delta G_f}\right]^{\left(\frac{1}{m_t}\left[\frac{1}{(n_{BD}+1)}\right]\right)}\right)\int_0^{\Delta t} w^n(t)dt \qquad \text{(Equation 5-35)}$$

$$D_1 = \left(\frac{1}{E_t}\right)\left(\frac{Sin[m_t\pi]}{m_t\pi}\right) \qquad \text{(Equation 5-36)}$$

$$I_i = \frac{2}{(1+n_{BD})} \qquad \text{(Equation 5-37)}$$

$$\int_0^{\Delta t} w^n(t).dt = \int_0^{\Delta t} \left(Sin^{2n}\left[\frac{\pi}{\Delta t} t\right]\right) dt = 0.5042 - 0.1744 \ln(n) \qquad \text{(Equation 5-38)}$$

where:

C_{max}	=	Maximum microcrack length (mm) (i.e., 7.5 mm (0.30 inches))
A, n	=	Paris' Law fracture coefficients
A_c	=	Specimen cross-sectional area (m^2)
b	=	Rate of accumulation of dissipation of pseudo strain energy
C_D	=	Crack density (m/m^2)
m_t	=	Exponent obtained from the tension RM master-curve (slope of the log relaxation modulus versus log time graph)
D_1	=	Time-dependent creep compliance (MPa^{-2})
E_t	=	Elastic modulus from tension RM master-curve (MPa)
k	=	Stress intensity factor (~0.33)
ΔG_f	=	Surface energy due to fracture or dewetting ($ergs/cm^2$)
σ_t	=	Maximum mixture tensile strength at break (kPa)
I_i	=	Dimensionless stress integral factor in crack failure zone, ranging between 1 and 2
n_{BD}	=	Dimensionless brittle-ductile factor, ranging between 0 and 1
Δt	=	Repeated loading time (s) (~0.01 s)
$\int_0^{\Delta t} w^n(t)dt$	=	Load pulse shape factor, ranging between 0 and 1
t	=	Time (s)

The parameter C_{max} defines the CMSE failure criterion and the subsequent failure threshold value discussed previously. The crack density (C_D) and rate of accumulation of dissipation of pseudo strain energy (b) are discussed in the subsequent subsections of this chapter.

The parameters A and n are Paris' Law fracture coefficients for material fracture properties, which quantifies the HMAC mixture's susceptibility to fracturing under loading. According to Paris' Law and Schapery's theory, the coefficient n can be defined simply as the inverse of the stress (tensile) relaxation rate (m_t) as expressed by Equation 5-34 (*26*, *68*, *71*). This assumption is valid for linear visco-elastic HMAC materials under a constant strain-controlled RDT test (*68, 71*). Paris' Law fracture coefficient A (Equation 5-35), on the other hand, is a function of many parameters including k, D_1, E_t, m_t, n_{BD}, ΔG_f, σ_t, I_i, and $w^n(t)$. Based on Equation 5-33, a small value of A is desirable in terms of HMAC mixture fatigue resistance. Numerical analysis, however, indicated that this coefficient A is very sensitive to n_{BD} and σ_t if other factors are held constant.

The parameter k is a material coefficient relating the length of the fracture process zone ($\propto$) to strain energy and mixture tensile strength. While this k is a measurable parameter, a value of 0.33 was used based on Lytton et al.'s work and the assumption that it ($k \cong 0.33$) does not vary significantly with microcrack length in the fracture process zone (*45*).

As expressed by Equation 5-36, the time-dependent creep compliance, D_1, was determined as a function of E_t and m_t. Although an exact value of D_1 can be measured from uniaxial creep tests, this less costly and simple approximation produces a reasonable value that is sufficient for use in HMAC mixture characterization analysis.

The numerical integration of $w^n(t)$ (Equation 5-38) with respect to time (t) describes the shape of the input load pulse as a function of material fracture coefficient n (Paris' Law). This integral exhibits a linear relationship with the Paris' Law fracture coefficient A, evident from Equation 5-26, and has a subsequent inverse relationship with N_i. For a haversine-shaped input strain waveform for the RDT test, as in this project, the integral reduces to a simple linear form shown in Equation 5-39 with n as the only variable. Note that material response to loading is not only magnitude dependent but also depends on the shape of the applied load form. As discussed previously, a haversine-shaped input load form is a close simulation of HMAC load-response under a moving wheel load (*45*, *68*). The parameters E_t, m_t, ΔG_f, and σ_t are discussed subsequently.

I_i is an elasticity factor due to the integration of the stresses near the microcrack tip over a small region in the microcrack failure zone (*45*, *68*, *71*). This factor, I_i, quantifies the materials' elasticity ranges between 1.0 and 2.0 for perfectly linear-elastic (brittle) and rigid-plastic (ductile) materials, respectively (*83*). Generally, a lower value (i.e., more linear-elastic) of I_i is indicative of high susceptibility to fatigue damage. As expressed by Equation 5-28, the research team quantified I_i simply as a function of n_{BD} in this project. This brittle-ductile factor n_{BD}, which ranges between 0.0 for perfectly plastic materials and 1.0 for brittle materials, is an age-related adjustment factor that accounts for the brittleness and ductility state of the HMAC mixture in terms of stress-strain response under loading. In this project, unaged HMAC specimens were assumed to exhibit plastic behavior and were subsequently assigned an n_{BD} value of 0.0. All the aged HMAC specimens were assumed to exhibit a brittle-ductile behavior lying somewhere between perfectly plastic and brittle behavior, and were thus assigned n_{BD} values of 0.5 and 0.75 for 3 and 6 months aging conditions, respectively.

Number of Load Cycles to Crack Propagation, *Np*

N_p refers to the number of load cycles required to propagate a 7.5 mm (0.30 inch) microcrack through the HMAC layer thickness. As expressed by Equation 5-39, N_p is determined as a function of the maximum microcrack length, HMAC layer thickness, shear modulus, Paris' Law fracture coefficients, and a design shear strain (*45*, *68*, *71*).

$$N_p = \left(\frac{d^{\left(1-\frac{n}{2}\right)}}{\left[A(2r)^n (SG)^n (1-nq)\right]} \right) \left(1 - \left[\frac{C_{\max}}{d} \right]^{(1-nq)} \right) \left(\frac{1}{\gamma} \right)^n \qquad \text{(Equation 5-39)}$$

$$S = \frac{(1-\nu)}{(1-2\nu)} \qquad \text{(Equation 5-40)}$$

$$G = E_t \left(\frac{G_{xz}}{E_z} \right) \qquad \text{(Equation 5-41)}$$

where:

A, n	=	Paris' Law fracture coefficients
r, q	=	Regression constants for stress intensity factor (~4.40, 1.18) (*45*)
S	=	Shear coefficient
G	=	Shear modulus (MPa)
C_{max}	=	Maximum microcrack length (mm) (i.e., 7.5 mm (0.30 inches))
d	=	HMAC layer thickness (mm)
γ	=	Maximum design shear strain at tire edge (mm/mm)
ν	=	Poisson's ratio
G_{xz}	=	Resilient shear modulus (MPa)
E_t	=	Elastic modulus from tensile RM master-curve (MPa)

If the elastic modular ratio G_{xz}/E_z in Equation 5-41 is unknown, Equation 5-42 below can be used to approximate G (*79*). Equation 5-42 is a simple shear-elastic modulus relationship based on elastic theory.

$$G = \frac{E_t}{2(1+\nu)} \qquad \text{(Equation 5-42)}$$

The parameters A, n, and C_{max} were discussed in the previous subsections, and γ is discussed in the subsequent text. Like N_i, an inverse relationship exists between A and N_p, indicating that a small value of A is desired in terms of HMAC mixture fatigue resistance. The failure load-response parameter γ also exhibits an inverse relationship with N_p.

Unlike for N_i, d is introduced in N_p because during the microcrack propagation process, for fatigue failure to occur, a microcrack length of a defined threshold value must actually propagate through the HMAC layer thickness. By contrast, the prediction relationship for N_i is a fatigue model for microcrack initiation and is independent of the parameter d.

Parameters r and q are regression constants that are a function of the stress intensity distribution in the vicinity of the microcrack tip. In this study, values of 4.40 and 1.18 were used, respectively, based on Lytton et al.'s work through FEM analysis (*45*). S is a shear coefficient, which as defined by Equation 5-40 is a function of the Poisson's ratio.

Surface Energies, ΔG_h^{AB}, ΔG_h^{LW}, and ΔG_f

To cause load-induced damage in the form of fatigue cracking, energy must be expended and equally energy must be expended to close the fracture surfaces. Surface energy data thus constitute input parameters for the healing, crack initiation, and propagation calculations in the CMSE fatigue analysis (Equations 5-43 through 5-49). The respective equations for the SE data analysis required for the CMSE approach based on adhesive mode of fracturing under dry conditions are described in this subsection.

$$\Delta G_h^{LW} = -\Gamma_{ij}^{LW} + \Gamma_i^{LW} + \Gamma_j^{LW} \quad \text{(Equation 5-43)}$$

$$\Delta G_h^{AB} = -\Gamma_{ij}^{AB} + \Gamma_i^{AB} + \Gamma_j^{AB} \quad \text{(Equation 5-44)}$$

$$\Delta G_f = \Delta G_f^{LW} + \Delta G_f^{AB} = -\Gamma_{ij}^{LW} + \Gamma_i^{LW} + \Gamma_j^{LW} - \Gamma_{ij}^{AB} + \Gamma_i^{AB} + \Gamma_j^{AB} \quad \text{(Equation 5-45)}$$

And;

$$\Gamma_{ij}^{LW} = \left(\sqrt{\Gamma_i^{LW}} - \sqrt{\Gamma_j^{LW}}\right)^2 \quad \text{(Equation 5-46)}$$

$$\Gamma_i^{AB} = 2\left(\sqrt{\Gamma_i^+ \Gamma_i^-}\right) \quad \text{(Equation 5-47)}$$

$$\Gamma_{ij}^{AB} = 2\left(\sqrt{\Gamma_i^+} - \sqrt{\Gamma_j^-}\right)\left(\sqrt{\Gamma_i^-} - \sqrt{\Gamma_j^-}\right) \quad \text{(Equation 5-48)}$$

$$\Gamma_j^{AB} = 2\left(\sqrt{\Gamma_j^+ \Gamma_j^-}\right) \quad \text{(Equation 5-49)}$$

where:

Γ = Surface free energy of binder or aggregate (ergs/cm^2)

i,j = Subscript “i” for binder (healing or fracture) and “j” for aggregate

h,f	=	Subscript "h" for healing and "f" for fracture
LW	=	Superscript "LW" for Lifshitz-van der Waals component
AB	=	Superscript "AB" for Acid-Base component
$+$	=	Superscript "+" for Lewis acid component of surface interaction
$-$	=	Superscript "–" for Lewis base component of surface interaction
Γ_{ij}	=	Interfacial surface energy between binder and aggregate due to "LW" or "AB" (superscripts) components (ergs/cm^2)
ΔG	=	Total surface free energy due to "h" or "f" (subscripts) for "LW" and/or "AB" (superscripts) components (ergs/cm^2)

Equations 5-43 through 5-47 are the nonpolar surface bond energy for healing, the polar surface bond energy for healing, the interactive term for the nonpolar LW surface bond energy component, and the polar surface energy component for binder, respectively. These equations quantify the bond strength within the binder mastic and the binder-aggregate adhesion.

Equation 5-45 is the total bond strength energy for fracture, which is made up of the Liftshitz-van der Waals nonpolar energy components and the acid-base polar energy components. Equation 5-45 is also commonly known as the total bond strength or Gibbs free energy of fracture for the binder (*83*).

According to Lytton et al., greater resistance to fracture, is provided by larger bond strength (cohesive or adhesive), and a greater healing capacity is promoted by the smallest LW bond strength and the largest AB bond strength (*45*). On this basis, the lower the value of ΔG_h, the greater the potential to heal; the higher the value of ΔG_f, the greater the resistance to fracture for HMAC.

In the simplest fundamental theory of energy, if a relatively higher amount of energy is required or must be expended to cause fracture damage (i.e., initiate and propagate a microcrack through the HMAC layer), then the HMAC mixture is substantially resistant to fracture. If, on the other hand, a higher amount of energy is required or must be expended to repair the fracture damage (i.e., healing which is defined as the closure of fracture surfaces) that occurred during the fracturing process, then the HMAC mixture has relatively less potential to self heal.

Relaxation Modulus, E_i, Exponent, m_i, and Temperature Correction Factor, a_T

The elastic relaxation modulus (E_i) and exponent (m_i) were determined from RM master-curves of log modulus (E_i) versus log time (t) obtained from tension and compression RM test data at a reference temperature of 20 °C (68 °F) (*68*). From the RM master-curve, a power function of relaxation modulus and loading time was generated as follows:

$$E(t) = E_i \xi^{-m_i} \qquad \text{(Equation 5-50)}$$

$$\xi = \frac{t}{a_T} \qquad \text{(Equation 5-51)}$$

where:

$E(t)$	=	Elastic relaxation modulus (MPa)
E_i	=	Initial elastic modulus (MPa) @ ξ = 1.0 s tension (E_t) or compression (E_c)
ξ, t	=	Reduced and actual test time, respectively (s)
m_i	=	Exponential stress relaxation rate ($0 \leq m_i < 1$)
i	=	Subscript "t" for tension and "c" for compression

Equation 5-50 is a simple power law relationship that is valid for most HMAC materials at intermediate and/or long times of loading (*68*). The exponent m_i refers to the rate of stress relaxation.

The temperature correction factors (a_T) were obtained through utilization of the SSE regression optimization technique using the spreadsheet "Solver" function and the Arrhenius time-temperature superposition model shown in Equation 5-52 (*84*). The reference temperature was 20 °C (68 °F), and thus, the a_T for 20 °C (68 °F) was 1.0.

$$Log(a_T) = A_a\left(\frac{1}{T} - \frac{1}{T_{ref}}\right) \qquad \text{(Equation 5-52)}$$

where:

A_a = Material constant that is a function of the activation energy (ΔH_a) and ideal gas constant (R_g) (i.e., $A_a = \Delta H_a / 2.303 R_g$)

T = Test temperature in degrees Kelvin ($K = 273 + ℃$)

T_{ref} = Reference temperature of interest (°K) ($K_{ref} = 273 + 20 = 293$)

A default C_a value of 13,631.28 for $\Delta H_a \cong 261{,}000$ J/mol and $R_g \cong 8.314$ J/(mol.°K) is often used. However, the constant A_a can also be obtained easily using the spreadsheet SSE regression optimization analysis.

DPSE and Constant, *b*

Researchers determined the constant b from a combination of the RM test data (E_t and m_t) in tension and the RDT test data. The constant b is defined as the rate of damage (energy dissipation) due to repeated loading that primarily causes fracture at intermediate temperatures (*68, 85*).

For any selected load cycle, the time-dependent linear visco-elastic stress (under damaged or undamaged conditions) was calculated using the Boltzmann superposition constitutive equation as a function of the RM and the RDT test data (*68*, 79, *85-86*). A temperature correction factor (a_T) was also introduced into the constitutive equation to normalize the calculated stress to a given reference temperature.

In this project, a_T was obtained from RM analysis, and the selected reference temperature was 20 °C (68 °F). This temperature is a realistic simulation of field service temperatures at which HMAC is susceptible to fracture damage under traffic loading. The RDT test was conducted at 30 °C (86 °F), and therefore, the calculated stress had to be normalized to 20 °C (68 °F).

Secondly, pseudo strain for damaged conditions was calculated as a function of the normalized calculated linear visco-elastic stress for damaged conditions, the reference modulus (E_R), and $\psi(t)$ (*68*). In the analysis, calculated PS rather than physically measured strain is used to characterize damage and healing to separate and eliminate the time-dependent visco-elastic behavior of the HMAC material from real damage during the strain controlled RDT test (*68*).

E_R is the modulus of the undamaged material determined from the first load cycle of the RDT test. Note that no significant fracture damage was considered to occur during the first RDT load cycle. The $\psi(t)$, which is a function of the calculated and measured stress at the first load cycle in an assumed undamaged condition, is introduced primarily to account for any non-linearity of the undamaged visco-elastic material.

Finally, DPSE was then calculated as a product of the measured stress and the calculated PS for damaged conditions using the double meridian distance method (DMD) for traverse area determination (*68, 87*). This DPSE is simply the area in the pseudo hysteresis loop of the measured tensile stress versus the calculated pseudo strain plotted as shown in Figure 5-1. The respective equations are:

$$DPSE = \sum \psi(t)\left(\varepsilon_R^d(t)\sigma_m^d(t)\right) \quad \text{(Equation 5-53)}$$

$$\varepsilon_R^d(t) = \frac{\sigma_c^d(t)}{E_R} \quad \text{(Equation 5-54)}$$

$$\Psi(t) = \frac{\sigma_{c(1)}^u(t)}{\sigma_{m(1)}^u(t)} \quad \text{(Equation 5-55)}$$

$$\sigma_c^u(t) \neq \sigma_m^u(t)\,,\ \sigma_c^d(t) \neq \sigma_m^d(t) \quad \text{(Equation 5-56)}$$

$$\sigma_{c(1)}^u(t) = \sigma_{c(1)}^d(t) \neq \sigma_{c(2\ldots N)}^d(t)\ ,\ \sigma_{m(1)}^u(t) = \sigma_{m(1)}^d(t) \neq \sigma_{m(2\ldots N)}^d(t) \quad \text{(Equation 5-57)}$$

$$\sigma_c(t) = \int_0^t E(t-\tau)\frac{\partial\varepsilon(\tau)}{d\tau}d\tau \quad \text{(Equation 5-58)}$$

Equation 5-58 is the general uniaxial stress-strain relationship applicable to most linear visco-elastic materials including HMAC (*68, 85*). For a haversine-shaped input strain waveform, Equation 5-58 can be written in the simple approximate numerical-integration form shown in Equation 5-59:

$$\sigma_c(t_{i+1}) = \sum_{k=0}^{k=i+1}\left(C_k \Delta\tau\left[E_\infty + E_1\left(t_{i+1} - t_k\right)^{-m}\right]\right) \qquad \text{(Equation 5-59)}$$

Assuming E_∞ is zero, and using E_t and m_t for undamaged conditions and a_T from RM analysis, Equation 5-59 reduces to Equation 5-60 shown below:

$$\sigma_c(t_{i+1}) = \sum_{k=0}^{k=i+1}\left(C_k \Delta\tau\left[E_t\left(\frac{(t_{i+1} - t_k)}{a_T}\right)^{-m_t}\right]\right) \qquad \text{(Equation 5-60[a])}$$

$$\sigma_c(t_{i+1}) = \Delta\tau E_t \sum_{k=0}^{k=i+1}\left(C_k\left(\frac{(t_{i+1} - t_k}{a_T}\right)^{-m_t}\right) \qquad \text{(Equation 5-60[b])}$$

where:

$\sigma^u_{c(1)}(t)$ = Calculated time-dependent linear visco-elastic tensile stress in an assumed undamaged condition at the first load cycle (kPa)

$\sigma^d_c(t)$ = Calculated time-dependent linear visco-elastic tensile stress under damaged conditions at any load cycle other than the first (kPa)

t_{i+1}, t_k = Present and previous time, respectively (s)

τ = Loading time history, e.g., 0.0 to 0.10 s at which strains were measured (s)

$\Delta\tau$ = Time increment (s) (e.g., 0.005 s)

$E(t-\tau)$ = Tensile relaxation modulus in assumed undamaged condition at time t-τ (MPa)

$\varepsilon(\tau)$ = Measured strain at previous time,τ (mm/mm)

C_k = Mean slope of any segment of the haversine input strain waveform

$\varepsilon^d_R(t)$ = Calculated pseudo strain for damaged conditions (mm/mm)

E_R = Reference modulus for assumed undamaged material calculated from the first load cycle (MPa)

$\psi(t)$ = Dimensionless non-linearity correction factor (NLCF)

$\sigma^{u}_{m(1)}(t)$ = Measured tensile stress for assumed undamaged condition at the first load cycle (MPa)

$\sigma^{d}_{m}(t)$ = Measured tensile stress for damaged conditions (kPa)

a_T = Temperature correction factor (from relaxation modulus analysis)

$DPSE$ = Dissipated pseudo strain energy (J/m^3)

g = Acceleration due to gravity (m/s^2)

For a haversine-shaped input strain waveform, both the measured and approximate (calculated) stress should exhibit a shape form of the format shown in Figure 5-15.

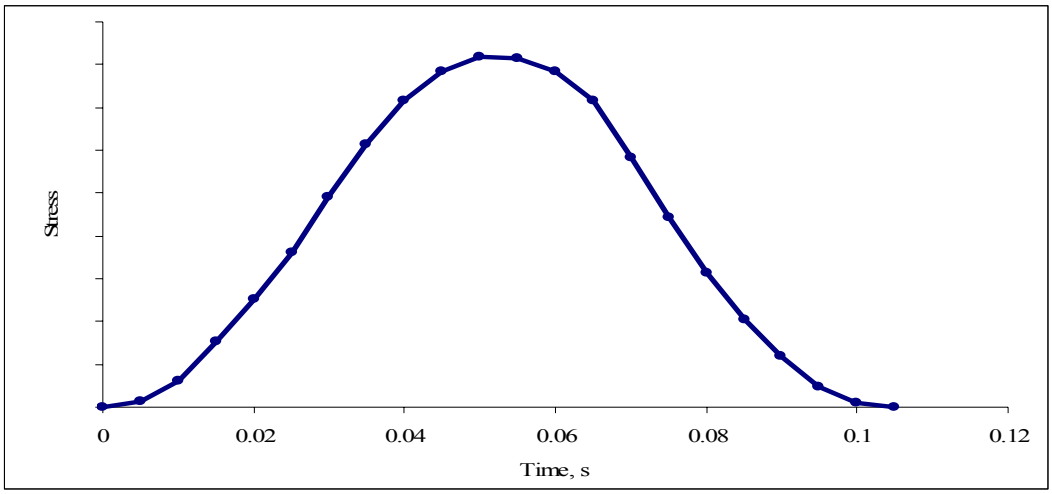

Figure 5-15. Output Stress Shape Form from RDT Test.

DPSE for selected laboratory test load cycles (N) was then plotted against log N to generate a linear function of the format shown in Equation 5-61. The constant b in Equation 5-61 also defined as the rate of change in DSPE during microcrack growth, is simply the slope of the DPSE versus log N plot, which is the required input parameter for the CMSE fatigue analysis (*68*).

$$W_R = a + bLog(N) \qquad \text{(Equation 5-61)}$$

where:

W_R	=	DPSE (J/m^3)
a	=	Constant or DPSE at the first load cycle
b	=	Slope of W_R-log N plot
N	=	Load cycle

A plot of DPSE versus log N should exhibit a simple linear graph of the format shown in Figure 5-16.

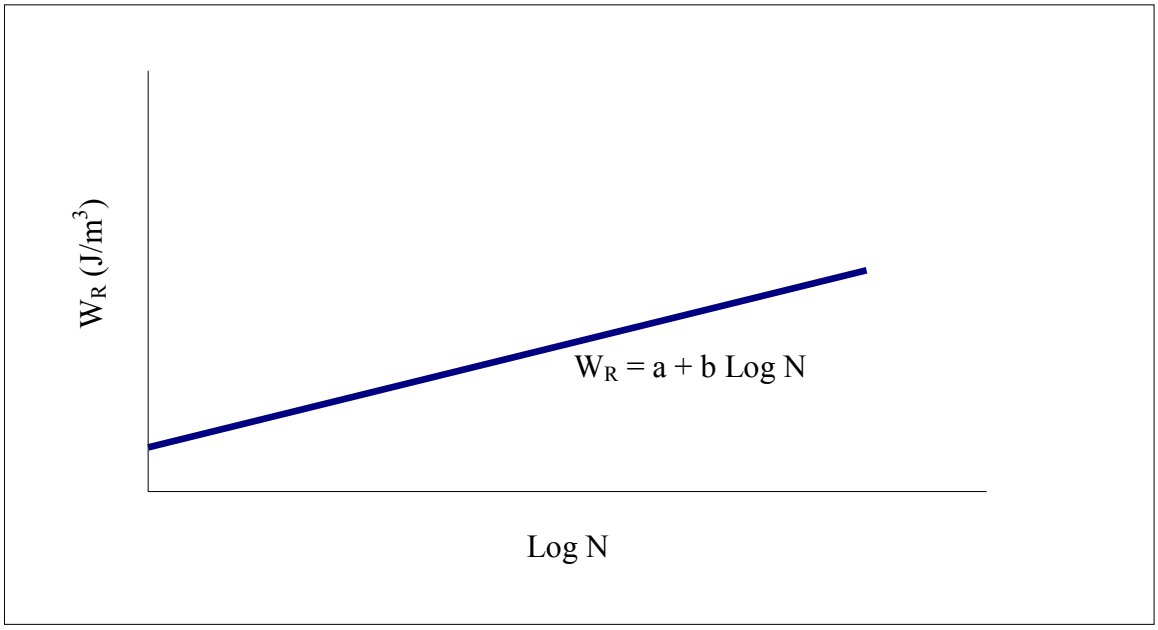

Figure 5-16. Example of W_R – Log N Plot.

The constant b is inversely related to the HMAC mixture fatigue resistance. Generally, a comparatively small value of b is indicative of a relatively low rate of accumulation of micro fatigue damage and consequently high HMAC mixture fatigue resistance.

Crack Density, C_D

Crack density calculations were based on the cavitation analysis by Marek and Herrin (*88*) assuming a brittle mode of crack failure for the HMAC specimen (Figure 5-17). In their analysis, Marek and Herrin used an average microcrack length of 0.381 mm (0.015 inches) based on 281 HMAC specimens (*88*). Using these data, the research team calculated microcrack density as a function of the number of cracks per specimen cross-sectional area to be 2.317 mm^{-2} (1495 in^{-2}). This is the crack density value (2.317 mm^{-2} (1495 in^{-2})) used for the CMSE fatigue analysis in this project.

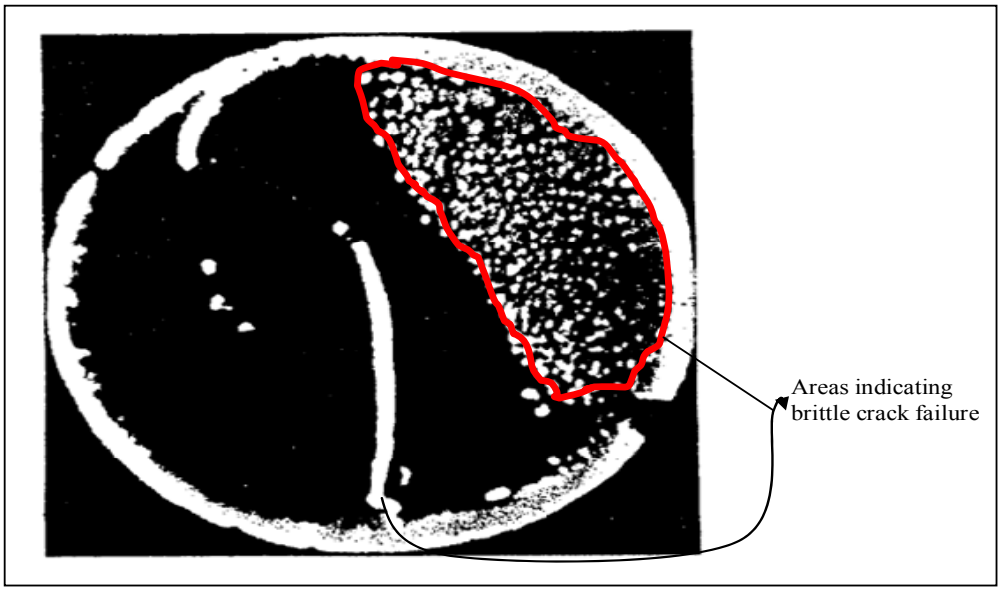

Figure 5-17. Brittle Crack Failure Mode (Marek and Herrin [*88*]).

Shear Strain, γ

FEM analysis software that takes into account the visco-elastic nature of HMAC is desirable for pavement stress-strain analysis to determine the maximum design shear strain γ at the edge of a loaded tire. If a linear elastic analysis software such as ELSYM5 (*62*) is used, an adjustment to the calculated γ must be done to account for the visco-elastic nature of HMAC. In this project, the research team adjusted the computed linear elastic γ consistent with the FEM adjustment criteria discussed in Chapter 3.

Input parameters for the stress-strain analysis include traffic loading (ESALs and the axle and tire configuration), pavement structure and material properties defined as a function of environment (temperature and subgrade moisture conditions), and desired response locations. If linear-elastic conditions are assumed, Equation 5-62 can be used to calculate γ (79).

$$\gamma = \frac{\sigma_p}{SG} \qquad \text{(Equation 5-62)}$$

where:

σ_p = Tire pressure (kPa) (~690 kPa ≅ 100 psi)
S = Shear coefficient
G = Shear modulus (MPa)

VARIABILITY, STATISTICAL ANALYSIS, AND N_f PREDICTION

A *COV* was utilized as an estimate of the variability of Ln N_f predicted by the CMSE approach. The *COV* expresses the standard deviation as a percent of the mean as follows:

$$COV = \frac{100s}{\bar{x}} \qquad \text{(Equation 5-63)}$$

where:

COV = Coefficient of variation
s = Sample standard deviation
$\bar{x}$ = Sample mean, calculated based on replicate measurements of N_f

The *COV* is basically a measure of relative variation, and it says that the measurements lie, on the average, within approximately *COV* percent of the mean (20). Replicate N_f predictions obtained by varying the material input parameters based on actual laboratory measured replicate values also provided a reasonable measure of variability and precision of the CMSE approach.

For this CMSE approach, mean Ln N_f values were predicted from laboratory measured material properties (i.e., tensile strength [σ_t]) on at least two replicate specimens. For this analysis, a typical spreadsheet descriptive statistics tool, supplemented by a one-sample t-test, was utilized. A 95 percent confidence/prediction interval (CI) for the mean Ln N_f was then computed as expressed by Equation 5-63 (with a one-sample t-test for an assumed t-value of zero) under the normality assumption on the distribution of Ln N_f .

$$95\%\ N_f\ \text{CI} = \bar{x} \pm t_{\frac{\alpha}{2},n-2}\left[\frac{s}{\sqrt{n}}\right] \qquad \text{(Equation 5-63)}$$

where:

CI	=	Confidence interval
$\bar{x}$	=	Mean *Ln* N_f value
s	=	Standard deviation of *Ln* N_f
α	=	Level of significance, i.e., 0.05 for 95% reliability level
n	=	Number of replicate specimens/measurements

SUMMARY

The following bullets summarize the CMSE fatigue analysis approach as utilized in this project:

- The CMSE approach was formulated on the fundamental concepts of continuum micromechanics and energy theory. This approach utilizes the fundamental HMAC mixture properties including tensile strength, fracture, healing, visco-elasticity, anisotropy, crack initiation, and crack propagation to estimate N_f. The energy theory in this CMSE approach is conceptualized on the basis that energy must be expended to cause load-induced damage in the form of cracking (fracture), and equally, energy must be expended to close up these fracture surfaces, a process called healing.

- The computation of the critical design shear strain at the edge of a loaded tire within a representative field HMAC pavement structure for N_p analysis constitutes the failure load-response parameter for this approach. The utilization of field calibration constants in modeling the healing process, N_i, and N_p constitute the calibration part.
- For this CMSE approach, the HMAC material is characterized in terms of fracture and healing processes and requires only relaxation tests in uniaxial tension and compression, tensile strength tests, repeated load tests in uniaxial tension, and a catalog of fracture and healing surface energy components of asphalt binders and aggregates measured separately.
- HMAC mixture characterization by CMSE laboratory testing utilizes gyratory compacted cylindrical specimens under strain and temperature controlled conditions.
- Fatigue failure according to the CMSE approach in this project was defined as the number of repetitive load cycles that are required to initiate and propagate a 7.5 mm (0.30 inches) microcrack through the HMAC layer thickness.

CHAPTER 6
THE CALIBRATED MECHANISTIC APPROACH WITHOUT SURFACE ENERGY

The calibrated mechanistic approach without surface energy measurements follows the same analysis concept and failure criteria as the CMSE approach except for a few differences. Laboratory testing differences include the absence of SE measurements and RM testing in compression. The analysis is slightly different to account for the fact that some of the input data (i.e., SE and RM in compression) are not measured. Figure 6-1 and Table 6-1 summarize the CM fatigue design and analysis system and input/output data.

The fundamental concepts, failure criteria, statistical analysis, and N_f prediction are similar to the CMSE approach (Chapter 5) and are therefore not discussed in detail again in this chapter.

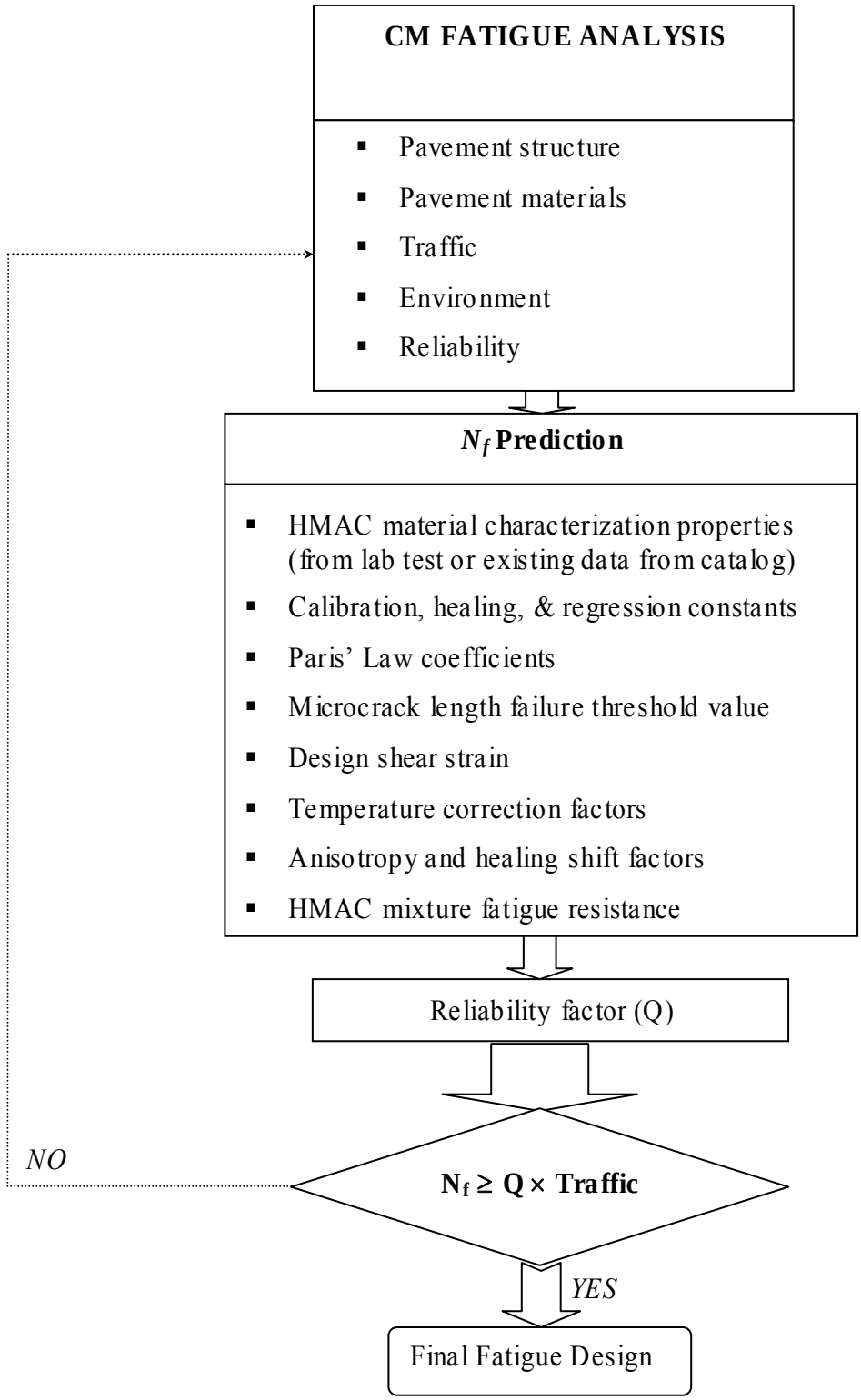

Figure 6-1. The CM Fatigue Design and Analysis System.

Table 6-1. Summary of CM Fatigue Analysis Input and Output Data.

Source	Parameter
Laboratory test data (HMAC mixture testing of cylindrical specimens)	- Tensile stress & strain - Relaxation modulus (tension) - Uniaxial repeated direct-tension test data (strain, stress, time, & N) - Anisotropic data (vertical & lateral modulus)
Analysis of laboratory test data	- Tensile strength - Relaxation modulus master-curves (tension & compression) - Non-linearity correction factor - DPSE & slope of DPSE vs. Log N plot - Healing indices - Healing calibration constants - Creep compliance - Shear modulus - Load pulse shape factor
Field conditions (design data)	- Pavement structure (i.e., layer thickness) - Pavement materials (i.e.,elastic modulus & Poisson's ratio) - Traffic (i.e., ESALs, axle load, & tire pressure) - Environment (i.e., temperature & moisture conditions) - Field calibration coefficients - Temperature correction factor
Computer stress-strain analysis	- Design shear strain (γ) @ edge of a loaded tire
Others	- Reliability level (i.e., 95%) - Crack density - Microcrack length - HMAC brittle-ductile failure characterization - Stress intensity factors - Regression constants - Shear coefficient
OUTPUT	- Paris' Law coefficients of fracture (A, n) - Shift factor due to anisotropy (SF_a) - Shift factor due to healing (SF_h) - Fatigue load cycles to crack initiation (N_i) - Fatigue load cycles to crack propagation (N_p) - HMAC mixture fatigue resistance (N_f)

LABORATORY TESTING

Unlike the CMSE approach, SE measurements (for both binders and aggregates) and mixture RM tests in compression are not required in the CM approach. However, all other test protocols are similar to that of the CMSE approach.

SE Measurements for Binders and Aggregates

The complete CMSE analysis procedure involves the determination of the surface energies of both binder and aggregate. The required SE input parameters for N_f prediction in the CMSE approach are used to calculate ΔG_f and ΔG_h. Determination of the SE components required for determining these inputs (ΔG_f and ΔG_h) is a time-consuming process, with the current SE test protocol (the Wilhelmy Plate and USD) requiring approximately 70 hrs to complete (Chapter 5).

Therefore, in order to improve the practicality of the CMSE approach, N_f were predicted using the CM procedure without using SE (ΔG_f and ΔG_h) as an input parameter. Consequently, no SE measurements are required in this CM approach.

RM Test in Compression

Mixture RM data in compression are required in the CMSE approach primarily to compute the SF_h. As discussed in the subsequent section, SF_h computation in the CM procedure does not require RM data in compression (i.e., E_{1c} and m_c) as input parameters.

ANALYSIS PROCEDURE

In terms of analysis, the major difference between the CMSE and CM approaches is in the computation of SF_h and Paris' Law fracture coefficients A and n. These differences are illustrated subsequently.

Shift Factor Due to Healing, SF_h

Equation 6-1 expresses the computation of SF_h in the CM approach.

$$SF_h = 1 + g_5\left(\frac{\Delta t_r}{a_{TSF}}\right)^{g_6} \quad \text{(Equation 6-1)}$$

$$\Delta t_r = \frac{31.536 \times 10^6 P_{DL}}{80kN \text{ Traffic ESALs}} \quad \text{(Equation 6-2)}$$

where:

Δt_r = Rest period between major traffic loads (s)

a_{TSF} = Temperature shift factor for field conditions (≅1.0)

g_i = Fatigue field calibration constants

P_{DL} = Pavement design life (i.e., 20 years)

It is clear that unlike the CMSE approach, ΔG_f, E_{1c}, and m_c are not required as input parameters for the computation of SF_h in this CM approach.

Paris' Law Fracture Coefficients, *A* and *n*

The modified and CMSE calibrated empirical Equations 6-3 and 6-4 based on Lytton et al.'s work show the computation of Paris' Law fracture coefficients A and n, respectively, according to the CM approach (*45*).

$$n = g_o + \left(\frac{g_1}{m_t}\right) \quad \text{(Equation 6-3)}$$

$$A = 10^{1+\left\{g_2 + \frac{g_3}{m_t}\log\left(\frac{Sin(m\pi)}{m\pi E_t}\right) + g_4\log(\sigma_t)\right\}} \quad \text{(Equation 6-4)}$$

where:

A, n	=	Paris' Law fracture coefficients
g_i	=	Fatigue field calibration constants
m_t	=	Stress relaxation rate from the tension RM master-curve
E_t	=	Elastic modulus from tension RM master-curve (MPa)
σ_t	=	Mixture maximum tensile strength at break (kPa)

Fracture coefficients A and n are required as inputs for the determination of N_i and N_p, and subsequently N_f. The fatigue calibration coefficients g_i are climatic dependent values that were established by Lytton et al. (45) and shown in Table 5-4 in Chapter 5.

Note that empirical Equations 6-1 through 6-4 in this project were calibrated to the CMSE approach by comparing the actual calculated numerical values to the corresponding values obtained via the CMSE approach. Equation 6-4, for instance, is the modification of Lytton et al.'s original Equation 6-5 (*45*).

$$A = 10^{\left\{g_2 + \frac{g_3}{m_t}\log\left(\frac{Sin(m\pi)}{m\pi E_t}\right) + g_4\log(\sigma_t)\right\}} \qquad \text{(Equation 6-5)}$$

The A values computed using this empirical Equation 6-5 differed from the CMSE A values by about 10 times (i.e., $A_{CMSE} \cong 10 \times A_{CM}$). Consequently, Equation 6-5 was modified as shown in Equation 6-4 to match the CMSE results. However, more HMAC fatigue characterization is required to further validate the simplified CM approach.

SUMMARY

The CM fatigue analysis approach, as utilized in this project, is summarized as follows:

- The CM approach follows the same concepts, failure criteria, and N_f prediction procedure as the CMSE approach. The major differences stem from a reduced laboratory testing program and resulting changes in the analysis procedure.

- The CM does not require SE measurements (both binder and aggregates) and RM tests in compression. Instead, these data inputs can be interpolated based on existing material empirical relationships or obtained from existing catalogued data if desired.
- The SF_h is computed primarily as a function of traffic rest periods, temperature shift factor, fatigue calibration constants, pavement design life, and the design traffic ESALs. In contrast to the CMSE approach, ΔG_f, E_{1c}, and m_c are not required as input parameters for the computation of SF_h in this CM approach.
- Paris' Law fracture coefficients A and n are computed as a function of the material tensile strength (σ_t), RM data in tension (E_{1t}, m_t), and fatigue field calibration constants (g_i) using empirically developed relationships that were calibrated to the CMSE approach.

CHAPTER 7
THE PROPOSED NCHRP 1-37A 2002 PAVEMENT DESIGN GUIDE

This chapter summarizes the relevant aspects of the proposed NCHRP 1-37A 2002 Pavement Design Guide as utilized in this project. Further details can be found elsewhere (*3*, *4, 89*).

FUNDAMENTAL THEORY

The proposed NCHRP 1-37A 2002 Pavement Design Guide (M-E Pavement Design Guide) adopts a ME approach for the structural design of HMAC pavements (*3*, *4, 89*). There are two major aspects of ME-based material characterization: pavement response properties and major distress/transfer functions. Pavement response properties are required to predict states of stress, strain, and displacement (deformation) within the pavement structure when subjected to external wheel loads. These properties for assumed elastic material behavior are the elastic modulus and Poisson's ratio.

The major distress/transfer functions for HMAC pavements are load-related fatigue fracture, permanent deformation, and thermal cracking. However, the focus of this project was on fatigue characterization of HMAC mixtures, and therefore, only the fatigue analysis component of the M-E Pavement Design Guide is discussed in this chapter. Figure 7-1 is a schematic illustration of the fatigue design and analysis system for the M-E Pavement Design Guide as utilized in this project.

Figure 7-1 shows that if the N_f prediction by the M-E Pavement Design Guide software in terms of traffic ESALs is less than the actual design traffic ESALs, the following options are feasible:

- reviewing/modifying the input data including the pavement structure, materials, traffic, environment, reliability level, pavement design life, and analysis parameters (distress failure limits);
- changing the HMAC mix-design and/or the material types; and
- changing the percentage crack failure criterion (i.e., 25 to 50 percent).

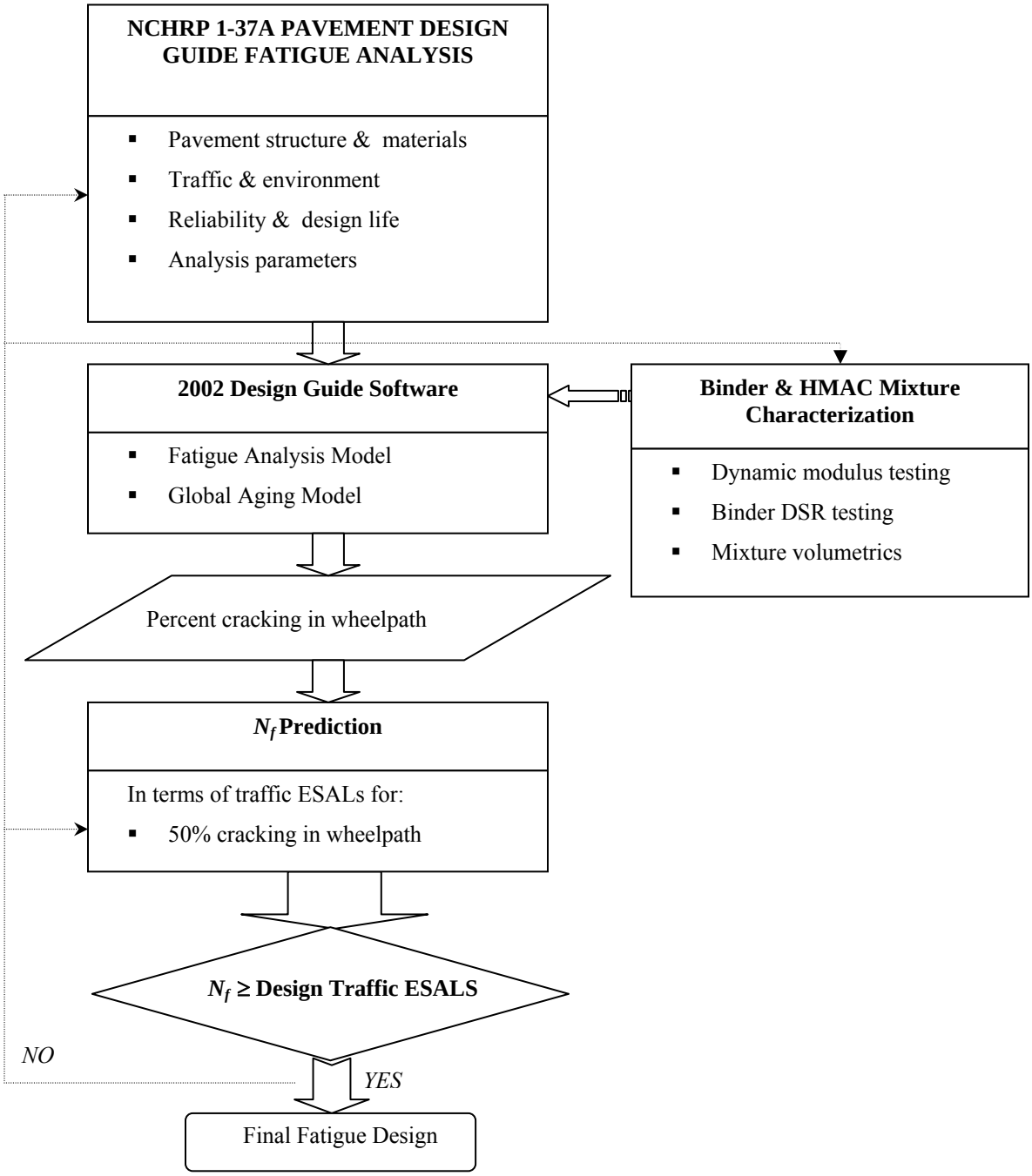

Figure 7-1. The Fatigue Design and Analysis System for the M-E Pavement Design Guide as Utilized in this Project.

INPUT/OUTPUT DATA

The M-E Pavement Design Guide suggests a hierarchical system for materials characterization. This system has three input levels. Level 1 represents a design philosophy of the highest practically achievable reliability, and Levels 2 and 3 have successively lower reliability. The Level 1 fatigue design procedure requires mixture volumetrics, dynamic modulus (DM) values for HMAC mixture and a complex shear modulus for unaged binder as input parameters. The binder data are used in the M-E Pavement Design Guide software to predict mixture aging using the Global Aging Model (*90*). Field input data include traffic, pavement structure, environment, and pavement design life. These input data requirements are summarized in Table 7-1.

Table 7-1. Input/Output Data for the M-E Pavement Design Guide Software.

Source	Parameter
Laboratory test data	- Dynamic modulus test data (i.e., temperature, frequency, & |E*| values) - Binder DSR test data (i.e., temperature, G*, & δ values) - Mixture volumetrics (i.e., binder content & AV)
Analysis of laboratory test data	- All calculations are software based
Field conditions (design data)	- Pavement structure (i.e., layer thickness) - Pavement materials (i.e., material type, elastic modulus, Poisson's ratio, gradations, and plasticity indices) - Traffic (i.e., AADT, axle load, & tire pressure) - Environment (i.e., climatic location) - Pavement design life (i.e., 20 years)
Computer stress-strain analysis	- All calculations are software based (utilized bottom-up crack failure mode in this project)
Other	- Reliability level (i.e., 95%) - Analysis parameters (i.e., distress failure limits)
OUTPUT	- Percentage cracking in wheelpath - N_f in terms of traffic ESALs for 50% cracking in the wheelpath - Assessment of adequate or inadequate performance

For the output data in terms of fatigue cracking (alligator cracking), the software predicts the percentage of fatigue cracking (along with other distresses) at any age of the pavement for a given structure and traffic level under a particular environmental location. The failure criteria can be set in two ways: setting the limit of percentage of cracks for a given number of traffic loads or determining the number of traffic loads in terms of ESALS to reach a certain percentage of cracks at a certain age of the pavement. In this project, the research team used the former criteria.

The output data in this project thus consisted of percentage cracking in the wheelpath for two input traffic levels of at least 2.5 and 5.0 million ESALs. Thereafter, N_f in terms of ESALs was statistically determined for 50 percent cracking in the wheelpath.

LABORATORY TESTING

Characterization of the HMAC mixture and binder properties for Level 1 fatigue analysis in the M-E Pavement Design Guide software requires the laboratory tests described in this section.

Dynamic Shear Rheometer Test

Binder dynamic shear complex modulus (G^*) and the phase angle (δ) required for Level 1 fatigue analysis were measured using the standard DSR consistent with the AASHTO test protocol designation TP5-98 (*56*). A minimum of two binder samples were tested, and test results are shown in Table 2-1 (Chapter 2).

Dynamic Modulus Test

For Level 1 fatigue analysis, the M-E Pavement Design Guide software require the dynamic modulus of the HMAC mixture measured over a range of temperatures and frequencies using the dynamic modulus test. A typical DM test is performed over a range of different temperatures by applying sinusoidal axial loading at different frequencies to an unconfined specimen.

Test Protocol

In this project, the DM test was conducted in accordance with the AASHTO designation: TP 62-03 Standard Method of Test for Determining Dynamic Modulus of Hot Mix Asphalt Concrete Mixtures at five test temperatures of -10, 4.4, 20, 38, and 54.4 °C (14, 40, 70, 100, and 130 °F) and six loading frequencies of 25, 10, 5, 1, 0.5, and 0.1 Hz (*91*).

DM is a stress-controlled test in compressive axial loading mode, and the test protocol in this project involved applying a sinusoidal dynamic compressive-loading (stress) to gyratory compacted cylindrical specimens of 150 mm (6 inches) in height by 100 mm (4 inches) in diameter. Figure 7-2 shows the DM loading configuration.

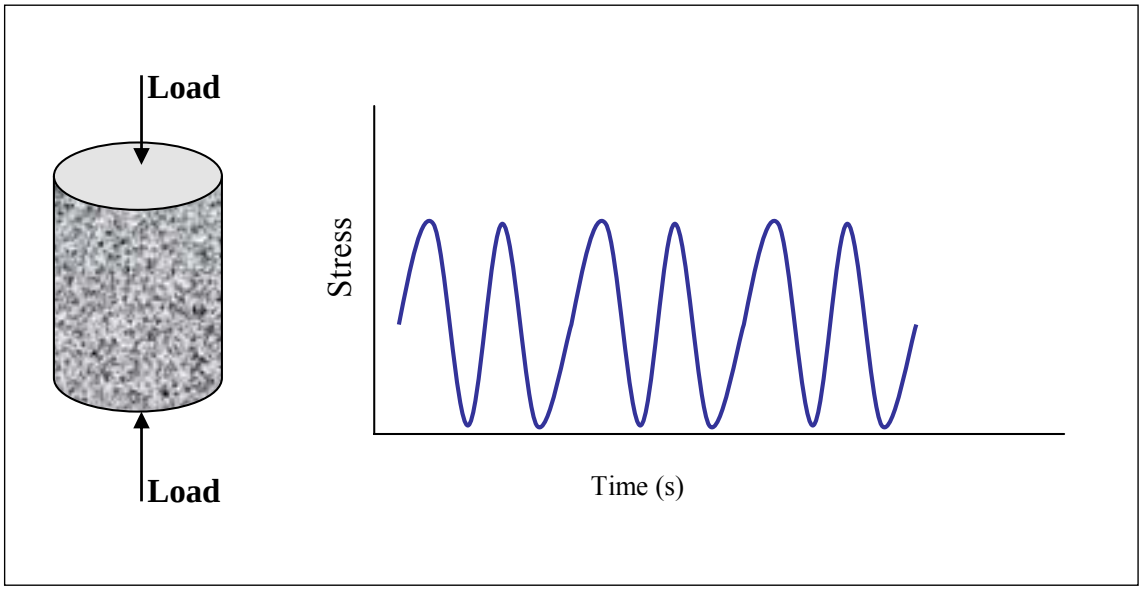

Figure 7-2. Loading Configuration for Dynamic Modulus Test.

The stress level for measuring the DM was chosen to maintain the measured resilient strain (recoverable) within 50 to 150 microstrains, consistent with the TP 62-03 test protocol (*91*). The order for conducting each test was from lowest to highest temperature and highest to lowest frequency of loading at each temperature to minimize specimen damage. For each temperature-frequency test sequence, the test terminates automatically when a preset number of load cycles have been reached (*91*).

Test Conditions and Data Acquisition

The sinusoidal axial stress waveform was supplied by the Universal Testing Machine (UTM-25) shown in Figure 7-3. Axial deformations were measured via three LVDTs. The research team conducted the DM test in an environmentally controlled chamber at test temperatures of -10, 4.4, 20, 38, and 54.4 °C (14, 40, 70, 100, and 130 °F) for each specimen. For each test temperature, the specimens were subjected to six consecutive loading frequencies of 25, 10, 5, 1, 0.5, and 0.1 Hz.

Figure 7-3. The Universal Testing Machine.

The minimum conditioning period for the specimens for each test temperature was 2 hrs. This temperature was monitored and controlled through a thermocouple probe attached inside a dummy HMAC specimen also placed in the environmental chamber. For each mixture type, three replicate HMAC specimens were tested, but only for 0 months aging condition. Note that the M-E Pavement Design Guide software encompasses a Global Aging Model that takes into account binder aging in the fatigue analysis (*90*).

During the DM tests, data (time, load, and deformations) were captured electronically every 0.001 s. Figure 7-4 is an example of the compressive axial strain response from DM testing at 4.4 °C (40 °F).

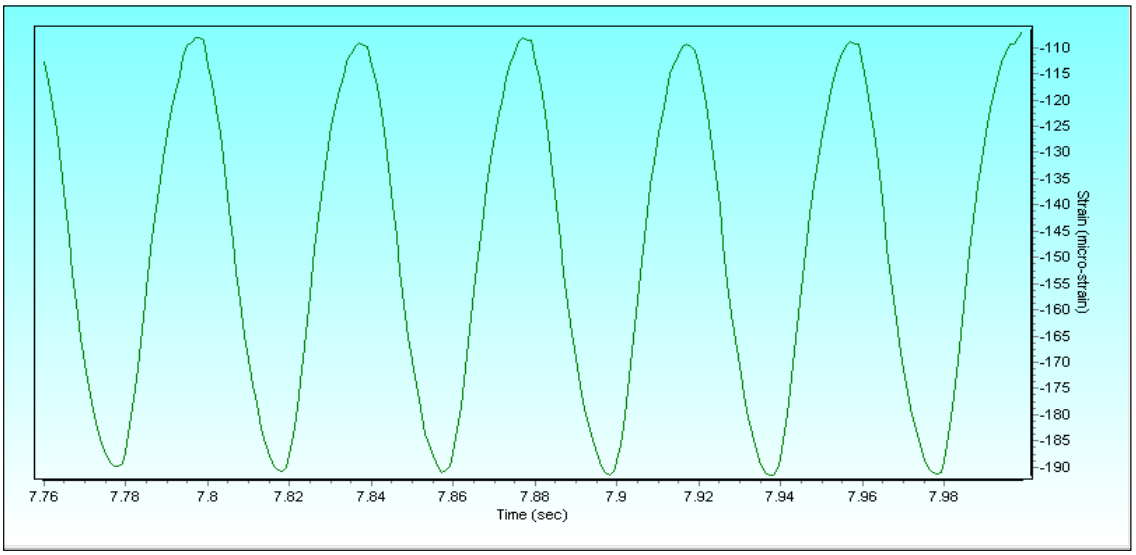

Figure 7-4. Compressive Axial Strain Response from DM Testing at 4.4 °C (40 °F).

The typical parameters, which result from DM testing, are the complex modulus (E^*) and the phase angle (δ). The E^* is a function of the storage modulus (E') and loss modulus (E''). The magnitude of the E^* is represented as shown in Equation 7-1.

$$E^* = \frac{\sigma_0}{\varepsilon_0} \qquad \text{(Equation 7-1)}$$

$$E' = E^* Cos\delta \qquad \text{(Equation 7-2)}$$

$$E'' = E^* Sin\delta \qquad \text{(Equation 7-3)}$$

where:

σ_0 = Axial stress (MPa)

ε_0 = Axial strain (mm/mm)

However, the *E** calculations were automatically done concurrently via the UTM-25 software during DM testing. Table 7-2 is an example of the output data from DM testing using the UTM test setup. The *E**, frequency, and temperature are actual input data to the M-E Pavement Design Guide software.

Table 7-2. Example of Output Data from DM Testing at 4. 4 °C (40 °F).

Parameter (summed average)	**Frequency (Hz)**					
	25	**10**	**5**	**1**	**0.5**	**0.1**
Dynamic modulus (|E*|)(MPa)	19,056	17,538	16,078	13,343	12,118	9,432
Phase angle (°)	5.24	8.31	9.84	13.15	14.95	18.99
Dynamic stress (kPa)	1567.7	1713.6	1653.9	1683.0	1607.7	1505.6
Recoverable axial microstrain	82.3	97.7	102.9	126.1	132.7	150.6
Permanent axial microstrain	106.6	152.1	160.9	173.7	175.4	271.1
Temperature (°C)	4.4	4.4	4.4	4.4	4.4	4.4

For generating the E* master-curve as a function of loading time or frequency, the following time-temperature superposition signomoidal model, as demonstrated by Pellinen et al., is often used and is in fact built in the M-E Pavement Design Guide software *(92)*:

$$Log(E^*) = \delta + \frac{\alpha}{1 + e^{\beta - \gamma \log(\xi)}} \qquad \text{(Equation 7-4)}$$

where:

E^* = Complex modulus (MPa)

ξ = Reduced frequency (Hz)

δ = Minimum modulus value (MPa)

α = Span of modulus values

β = Shape parameter

γ = Shape parameter

FAILURE CRITERIA

The fatigue failure criteria for the M-E Pavement Design Guide software in this project was defined as the number of traffic ESALs required to cause 50 percent alligator cracking (bottom-up) on a 152.4 m (500 ft) stretch of the wheelpath. This 50 percent threshold value is consistent with the TxDOT tolerable limit based on the 2003 TxDOT PMIS report (*61*).

ANALYSIS PROCEDURE

The fatigue analysis procedure for the M-E Pavement Design Guide is a step-by-step computerized process based on the modified Asphalt Institute predictive model incorporated in the software (*21, 89*).

$$N_f = \beta_{f1} k_1 (\varepsilon_t)^{-\beta_{f2} k_2} (E)^{-\beta_{f3} k_3} \qquad \text{(Equation 7-5)}$$

where:

N_f = Number of repetitions to fatigue cracking
ε_t = Tensile strain at the critical location of the HMAC layer
E = Stiffness of the HMAC mixture
β_{fi} = Calibration parameters
k_i = Laboratory regression coefficients

The β_{fi} calibration parameters incorporate state/regional/national calibration coefficients. In this project, default national calibration factors, which are inbuilt in the M-E Pavement Design Guide software, were used. Regression coefficients k_i are coefficients that relate to material properties. E is the stiffness of the HMAC mixture, which the M-E Pavement Design Guide software determines from the DM test data during that analysis. The horizontal tensile strain (ε_t) constitutes the mechanistic failure load-response parameter and was computed at the bottom of the HMAC layer in this project.

As pointed out previously, the M-E Pavement Design Guide incorporates a Global Aging Model that takes into account the effects of binder aging with time in the overall fatigue analysis process (*3*, *4*, *89*, *90*). The model is based on the change in binder viscosity as a function of pavement age, AV, environment, traffic loading, and pavement depth to account for both short-term aging that occurs during mixing and construction operations and long-term aging during service. The output of the Global Aging Model (GAM) is basically a prediction of the binder viscosity at any time and any depth in the pavement system, which is ultimately incorporated in the overall fatigue analysis process.

VARIABILITY, STATISTICAL ANALYSIS, AND N_f PREDICTION

For traffic input levels of 2.5 and 5.0 million ESALs and for each mixture type in each pavement structure and under each environmental condition, the research team predicted the percentage cracking in the wheelpath for at least two HMAC specimens using the M-E Pavement Design Guide software. Using these percentages, cracking output from the M-E Pavement Design Guide software for these specimens, mean N_f values in terms of ESALs were statistically predicted for 50 percent cracking. A 95 percent prediction interval was also determined using the least squares line regression analysis.

SUMMARY

The bullets below summarize the fatigue analysis component of the M-E Pavement Design Guide as utilized in this project:

- The M-E Pavement Design Guide adopts a ME approach for the structural design of HMAC pavements. In terms of fatigue analysis, the M-E Pavement Design Guide software utilizes the modified Shell Oil fatigue damage predictive equation with tensile strain as the primary mechanistic failure load-response parameter associated with crack growth.
- The M-E Pavement Design Guide software incorporates binder aging effects analysis using a Global Aging Model. It also incorporates comprehensive traffic and climatic analysis models.

- The Guide characterizes pavement materials in a three-level hierarchical system, with Level 1 representing the possible highest achievable reliability level.
- For Level 1 fatigue input analysis, HMAC mixture characterization through dynamic modulus testing at five different temperatures and six loading frequencies utilizes gyratory compacted cylindrical HMAC specimens. Other required material tests include mixture volumetrics and binder DSR data.
- Fatigue failure for the M-E Pavement Design Guide software analysis was defined as the number of applicable repetitive load cycles expressed in terms of traffic ESALs required to cause 50 percent cracking in the wheelpath.

CHAPTER 8
BINDER OXIDATIVE HARDENING BACKGROUND AND TESTING METHODOLOGY

Binder oxidation is a major contributor to age-related pavement failure (*93*). Through oxidation, the binder becomes stiffer and more brittle and thus less able to sustain, without damage, the deformations of flexible pavements. This project investigated the role that this binder embrittlement plays in the phenomenon of fatigue resistance.

This chapter includes further discussion of 1) binder oxidation and embrittlement in both laboratory and pavement aging, 2) the objectives of binder measurements in understanding pavement fatigue resistance, and 3) the experimental methodology used in this project to evaluate binder aging and to relate it to HMAC mixture properties.

BINDER OXIDATION AND EMBRITTLEMENT (*52, 93*)

As briefly introduced above, binders experience hardening and embrittlement over time that reduces the performance of flexible pavements. The process is relentless and thus, over time, can destroy the pavement. The constancy of the hardening rate over time and the depth to which oxidation occurs, based on recent pavement data, is surprising and at the same time critical to understanding pavement durability for both unmodified and modified binders.

As binders oxidize, carbonyl (– C=O) groups are formed that increase the polarity of their host compounds and make them much more likely to associate with other polar compounds. As they form these associations, they create less soluble asphaltene materials, which behave like solid particles. This composition change, taken far enough, results in orders-of-magnitude increases in both the binder's viscous and elastic stiffness properties. Thus the oxidized binder sustains sheared stress with deformation (high elastic stiffness) and simultaneously the material cannot relieve the stress by flow (high viscosity), resulting in a pavement that is very brittle and susceptible to fatigue and thermal cracking.

The Maxwell model is a very simple way of explaining, in a qualitative sense, the essence of the impact of this increase in both elastic stiffness and viscosity on elongational flow of a binder. The model is that of an elastic spring in series with a viscous dashpot element, as shown in Figure 8-1.

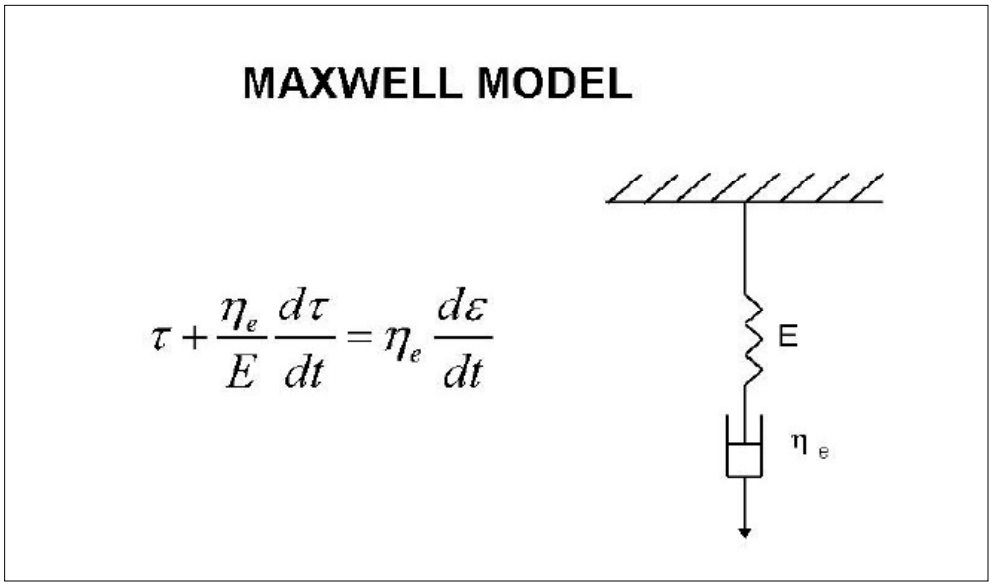

Figure 8-1. The Maxwell Model.

The stress that builds in the combined element is the result of the balance between the elastic modulus and the viscosity. Upon elongation at constant rate, the stress versus elongation response rises in response to the elastic spring but then goes through a maximum value before decaying over time in response to viscous flow. The value of the maximum stress depends upon the relative values of the elastic modulus and the viscosity. The higher their values, the higher the maximum stress; the lower the values, the lower the maximum stress. If the maximum stress exceeds the failure stress of the material, then failure occurs.

This Maxwell model is very simple and certainly is too simple to quantitatively characterize asphalt materials, but it still captures the basic elements that are important to understanding binder failure that occurs due to oxidation and embrittlement. As asphalts oxidize, they harden, a process that simultaneously increases its elastic stiffness and its viscosity. Consequently, in the context of the Maxwell model, with aging and consequent hardening, a binder cannot take as much deformation without building to a stress level that results in its failure stress being exceeded. So, as binders age and harden, their ductilities decrease dramatically. The binder ductility for a newly constructed pavement may be of the order of 30 cm (11.8 inches) (15 °C,1 cm/min) (59° F, 0.39 inches) where as the binder ductility of a heavily aged pavement will be much lower, down to 3 cm (1.18 inches) or less.

Literature reports emphasize the importance of a binder's ductility to pavement durability. Several studies report that a value of the 15 °C (59 °F) ductility at 1 cm/min (0.39 inches/min) in the range of 2 to 3 cm (0.79 to 1.18 inches) corresponds to a critical level for age-related cracking in pavements (*93, 94*).

This embrittlement of binders has been captured with the discovery of a correlation between binder ductility (measured at 15 °C, 1 cm/min) (59 °F, 0.39 inches/min) and binder DSR properties (dynamic elastic shear modulus, G' and dynamic viscosity, η', equal to G"/ω) shown in Figure 8-2. A very good correlation exists between binder ductility and G'/(η'/G') (or, equivalently G'/[G"/ωG']), demonstrating the interplay between elastic stiffness and ability to flow in determining binder brittleness, as discussed above in the context of the Maxwell model.

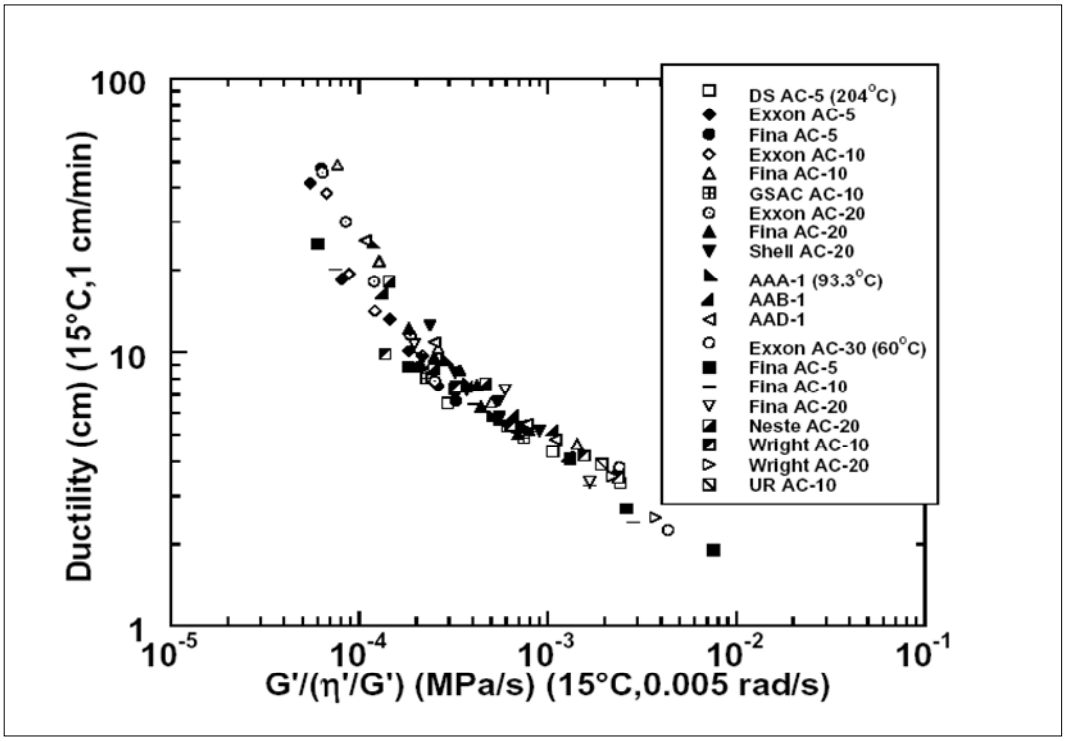

Figure 8-2. Correlation of Aged-Binder Ductility with the DSR Function G'/(η'/G') for Unmodified Binders (*52*) (°F = 32 + 1.8(°C)).

This correlation is depicted on a "map" of G' versus η'/G' (Figure 8-3), which tracks a pavement binder as it ages in service (*94-96*). This particular binder is from highway SH 21 between Bryan and Caldwell but represents the trends seen for all conventional binders.

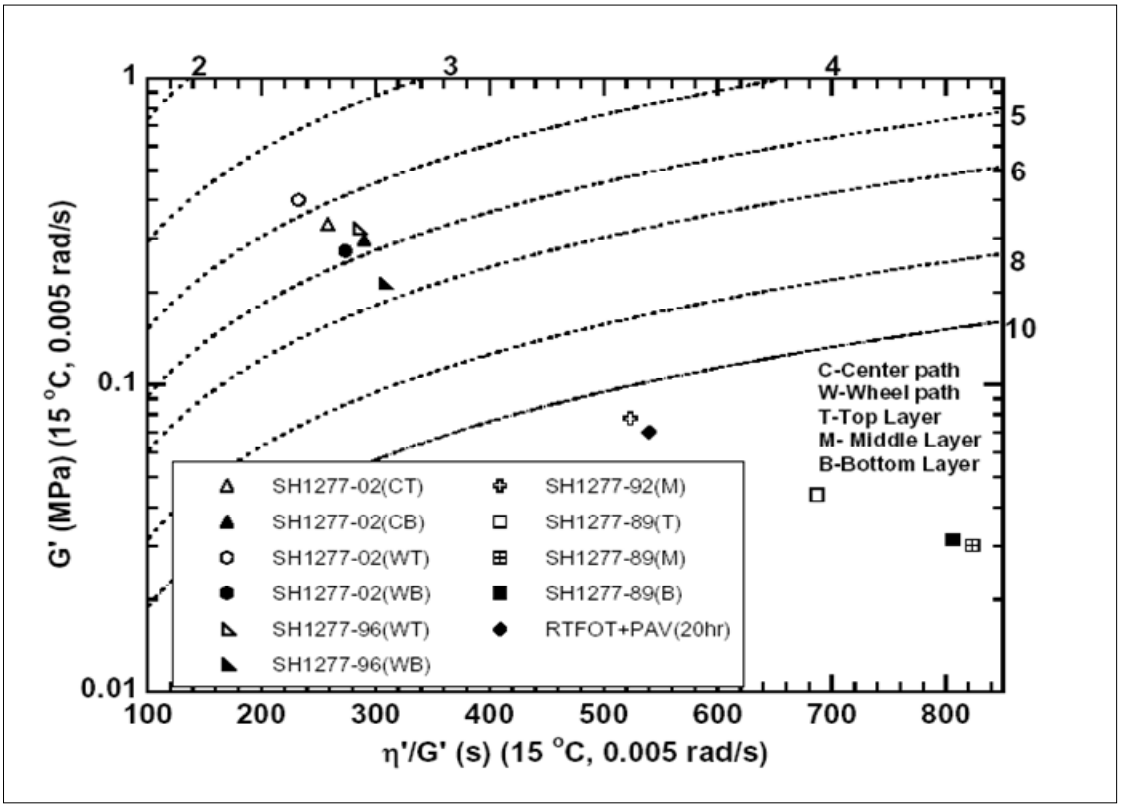

Figure 8-3. Binder Aging Path on a *G'* versus *η'/G'* Map (Pavement-aged Binders) (*52*) (°F = 32 + 1.8(°C)).

On this type of plot, with increased aging, a binder moves, over time, from the lower right toward the upper left as the result of increases in both the elastic stiffness and viscosity (but note that G' increases more than viscosity, i.e., G"/ω, because movement is toward the left with smaller values of η'/G'. Note also the dashed lines that represent lines of constant ductility, calculated from the correlation of Figure 8-2 below 10 cm (3.93 inches).

Recent evidence suggests that pavement binders age at surprisingly constant rates and to surprising depths. Figure 8-3 illustrates this conclusion from Glover et al. contained in Research Report 1872-2 (*52*), through measurements on highway SH 21 between Bryan and Caldwell; all data shown in this figure are from a single station, #1277. This highway was constructed from July 1986 to July1988 in three, 50 mm (2 inch) lifts. The solid symbols (with the exception of the solid diamond) are binder measurements from cores taken from the third lift down from the surface of the pavement, as originally constructed.

With each lift being 50 mm (2 inches) thick, this bottom lift had 100 mm (4 inches) of pavement material on top of it. (Note: In 2000, this pavement had a chip seal and overlay placed on top of it, burying the original lifts even more.) Yet, even buried this deeply, its binder moves across the DSR "map" in a relentless fashion and at about the same pace as the top lift (open symbols). Binder from the 1989 bottom lift has an estimated ductility of 20 cm (7.87 inches) at 15 °C (59 °F). By 1996, it was reduced by aging to 5.6 cm (2.2 inches), and by 2002, it was less than 5 cm (1.97 inches). Meanwhile, the top lift binder's ductility was estimated to be 16 cm (6.3 inches) in 1989, 4.5 cm (1.77 inches) in 1996, and about 4 cm (1.57 inches) in 2002. The march across the DSR map was not that different for the top lift compared to the bottom lift. Binder from the middle lift, taken in 1989 and 1992, is also shown and tracks well with the other lifts. Note that the rolling thin-film oven test (RTFOT) plus pressure aging vessel laboratory-aged binder matches the 1992 pavement-aged binder, suggesting that for this pavement, RTFOT plus PAV is approximately equivalent to hot-mix and construction aging plus four years of field pavement aging. These results are rather remarkable and strongly suggest, as noted above, that oxidative aging rates are remarkably constant over time and, beyond the very top portion of the pavement, proceed at remarkably uniform rates, at least to several inches below the surface of the pavement.

Note that the literature reports that ductility values in the range of 2 to 3 cm (0.79 to 1.18 inches) for 15 °C (59 °F) at 1 cm/min (0.39 inches/min) appear to correspond to a critical level for age-related cracking. Thus, the top-left corner of the pavement aging figure (Figure 8-3) is a suspect region for pavement performance. While this region has not yet been verified conclusively to be a critical zone, recent pavement data, including several long-term pavement performance pavements, are consistent with this preliminary conclusion.

Clearly, binder properties change drastically over the life of a pavement. These changes result in a dramatic decrease in flexibility and occur continuously throughout its service lifetime. It is the objective of this project to investigate how these changes impact the fatigue resistance of HMAC pavements. Ultimately, the objective is to predict reductions in pavement fatigue resistance from laboratory measurements of binder oxidation and embrittlement.

BINDERS STUDIED

Changes in binder properties with aging are to be related to changes in mixture properties with the objective of learning how to predict changes in mixture (and ultimately pavement) fatigue lives due to binder stiffening. To this end, a PG 64-22 unmodified binder was used in a basic mixture (denoted as the Bryan Mixture), and a PG76-22 modified binder was used in a rut resistant mixture (denoted as the Yoakum Mixture). These binders were tested in both aged and unaged conditions. Chapters 3 through 7 discussed the aging and testing of HMAC mixtures. The results from all of these tests are presented in Chapters 9 through 11.

Laboratory-Aged Binders

Two different methods of accelerated aging were used in this project. A stirred air flow test (SAFT), which stimulates the hot mix process, was used for short-term aging comparisons (*97*, *98*). An environmental room at 60 °C (140 °F) and atmospheric pressure and 50 percent relative humidity was used for long-term aging comparisons. Aging at 60 °C (140 °F) is used as an approximation to field aging.

Neat (original) binder was aged by both of these means and subsequently tested; binder in compacted mixes was aged in the 60 °C (140 °F) environmental temperature-controlled room and had to be extracted and recovered before testing.

Binders Recovered from HMAC Mixtures

An effective extraction and recovery process is necessary to compare the properties of mix-aged binder with those of the original binder. The process used in this project consisted of two parts: 1) the extraction process, and 2) the filtration and recovery process.

At a mixture binder content of about 5 percent of total mass, approximately 150 g of HMAC mixture were needed to obtain approximately 7 g of binder. The mixtures were broken into small pieces with a hammer before extracting the binder from the HMAC specimens.

Toluene and ethanol were used for the binder extraction process. A total of three successive washes were used in the extraction process. For the first wash, 100 mL of toluene was used to extract binder from the aggregate by contact for 20 minutes. The second and third washes, also for 20 minutes each, used a 15 percent weight ethanol-toluene solution. The washes were filtered two times using a new doubled coffee filter each time. The filtered solution was then distributed among six 15 mL conical type tubes (approximately 12 mL solution per tube) and centrifuged at about 3000 rpm for 10 minutes to remove aggregate from the solution.

The binder was recovered from the solvent with a Buchi, RE 111 rotovap. During removal of the solvent, the bath temperature was kept at 100 ^{o}C (212 °F) to avoid hardening or softening of the asphalt in dilute solution. When no more solvent could be detected visually dripping from the condenser, the temperature was increased to 173.9 ^{o}C (345 °F) to ensure sufficient solvent removal. The extraction and recovery procedure took from 3 to 4 hrs for each specimen. Two replicates were extracted and recovered for each mixture, and the properties of the recovered binders were compared to each other. When inconsistencies occurred in these recovered binder properties, additional replicates were extracted, up to four replicates total for a given mixture (*99*).

BINDER TESTS

Binder tests conducted included size exclusion chromatography, dynamic shear rheometry, ductility, and fourier transform infrared spectroscopy. These tests are discussed in the next sections, and results are presented and discussed in Chapters 9 and 11.

Size Exclusion Chromatography

After extraction and recovery, the binder was analyzed using Size Exclusion Chromatography (SEC) to ensure complete solvent removal. Test samples were prepared by dissolving 0.2 ± 0.005 g of binder in 10 mL of tetrahydrofuran (THF). The sample then was sonicated for 30 minutes to ensure complete dissolution and filtered through a 0.45µm polytetrafluoroethylene (PTFE) syringe filter. Samples of 100 µL were injected into 1000, 500, and 50 Å columns in series with THF carrier solvent flowing at 1.0 mL/min.

The chromatograms of binders obtained from the same replicate should overlay each other. If there was any solvent residue in the binder, there was a peak located at 38 minutes on the chromatogram (*100*).

Dynamic Shear Rheometer

A Carri-Med CSL 500 Controlled Stress DSR Rheometer measured the rheological properties of the binder.

The rheological properties of interest were the complex viscosity (η) measured at 60 ^{o}C (140 °F) and 0.1 rad/s (approximately equal to the low-shear rate limiting viscosity) and the storage modulus (G') and the dynamic viscosity (η'), both at 45 °C (113 °F) and 10 rad/s measured in a frequency sweep mode. A 2.5 cm (0.98 inches) composite parallel plate geometry was used with a 500 mm (19.5 inches) gap between the plates.

These rheological properties were used to understand how the physical properties of the binder changed with time. DSR measurements also were important for deciding whether the binder was changed in some way by the extraction and recovery process (*98-100*). If two extraction and recovery processes yielded binders with matching SEC chromatograms but significantly different complex viscosities, then at least one of the binders was suspected of having undergone solvent hardening or softening.

Ductility

Ductilities for long-term aged original binder, aged 3 and 6 months in a 60 ^{o}C (140 °F) room after SAFT for this report, were measured at 15 ^{o}C (59 °F) and an extensional speed of 1 cm (0.39 inches) per minute in accordance with ASTM D 113-86 (*101*). The ductility sample, which had been made in a mold, had a 3 cm (1.18 inches) initial gauge length and a tapered throat. The ductility was taken as the amount of extension in centimeters of the asphalt specimen when the binder fractured at the tapered throat.

Fourier Transform Infrared Spectroscopy

Carbonyl area (CA) was measured using a Galaxy 5000 fourier transform infrared spectroscopy **(**FTIR) spectrometer with an attenuated total reflectance (ATR) zinc selenide prism (*99*). CA is the area under the absorption band from 1650 to 1820 cm^{-1} (4231 to 4667 $inches^{-1}$) and relates directly to the oxygen content in the asphalt binder, and thus increases in CA are used to quantify oxidative aging (*102, 103*).

SUMMARY

The bullets below provide a summary of binder oxidative hardening in relation to HMAC mixture fatigue resistance and the testing methodology utilized in this project to characterize this phenomenon:

- Binder oxidative aging is a major contributor to age-related pavement failure. The prime objective of this chapter was to present a background of binder oxidative aging and analysis methodology as a context for understanding the effect of binder aging on HMAC mixture fatigue resistance, presented in Chapters 9 and 11.
- Over time, binders experience oxidative age-hardening that increases their elastic stiffness and simultaneously reduces their ability to flow or relieve stress, thus making the binders more brittle.
- The DSR function map of G' versus η'/G' is a useful method for tracking changes in a binder's rheology with aging in a way that relates at least for unmodified binders to binder ductility and, we hypothesize, to HMAC pavement durability.
- The DSR, ductility, SEC and FTIR were the tests utilized in this project to characterize the binder rheological and chemical properties of binders.

CHAPTER 9
BINDER-HMAC MIXTURE CHARACTERIZATION

Pavements deteriorate over time and eventually require maintenance or rehabilitation. While fatigue is considered to be a major factor leading to failure, binder embrittlement due to oxidative aging almost certainly plays a significant role as well. One objective of this project was to better understand the impact of oxidative aging on mixture fatigue resistance and on other mixture properties in general.

Mixture fatigue studies and the extent to which it is impacted by oxidative aging are documented elsewhere in this report. The effect of binder oxidative aging on fatigue was found to be significant.

The purpose of the work reported in this chapter was to address other binder-mixture relations besides fatigue. Of particular interest was the impact of binder aging on mixture stiffness, as characterized by the mixture's visco-elastic properties, and the relation of these mixture properties to changes in binder properties.

Loose mix, aged according to AASHTO PP2 4 hrs short-term aging, was compacted, tested in a nondestructive relaxation modulus procedure, aged further in a 60 °C (140 °F) environmental room for intervals of 3 months (from 0 to 6 months), and tested again after each of these aging intervals. In this way, the same physical specimen was tested at each aging level so that the effect of binder aging could be determined independent of other mixture variables. Replicate compacted mixture specimens were aged for the specified intervals and the binder recovered and tested for DSR properties that could be compared to the mixture properties.

The remainder of this chapter provides further details of binder and mixture experimental procedures, analysis procedures, and test results.

METHODOLOGY

Changes in binder properties with aging are to be associated with changes in mixture properties, with the objective of learning how to predict changes in mixture fatigue lives due to binder stiffening by aging. Two different binders were used: a PG 64-22 from a basic mixture design (denoted as the Bryan mixture) and a PG 76-22 from a rutting resistance mixture design (denoted as the Yoakum mixture). Binders in mixtures were conditioned and tested as shown in Figure 9-1.

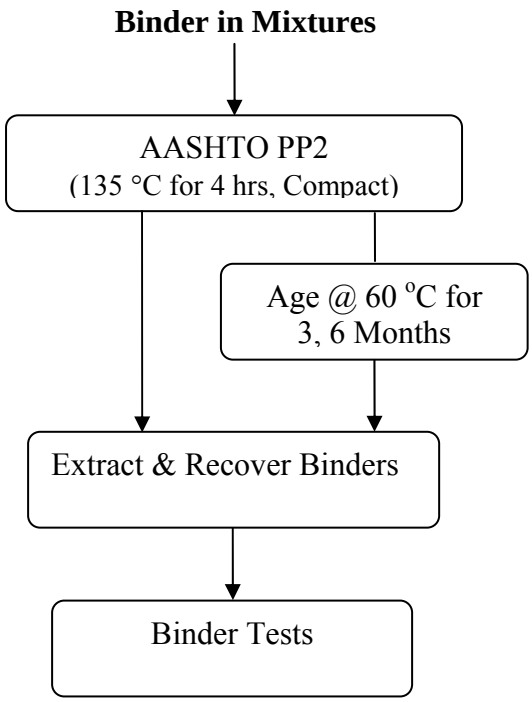

Figure 9-1. Binder Oxidative Aging and Testing

(°F = 32 + 1.8(°C)).

Binder aging and the extraction and recovery process were explained in Chapter 8. The binder tests included size exclusions chromatography and dynamic shear rheometry; details are also described in chapter 8.

Binder Data Analysis

G' and G'' values were measured at three different temperatures (20, 40, 60 °C) (68, 104, 140 °F), and master-curves for G', G'' were constructed using time-temperature superposition (TTSP) at 20 °C (68 °F). Shift factor data as a function of temperature were modeled as shown in Equation 9-1 (*104*):

$$\log a_T = \frac{-C_1(T - T_{ref})}{(C_2 + T - T_{ref})} \qquad \text{(Equation 9-1)}$$

where:

a_T = The shift factor at temperature T relative to the reference temperature T_{ref}

C_1, C_2 = Empirically determined coefficients

T = The selected temperature of interest, °C or K

T_{ref} = The reference temperature, °C or K

In addition to master-curves, the DSR function ($G'/(\eta'/G')$), measured at 44.7 °C (112.5 °F), 10 rad/sec but shifted to 15 °C (59 °F) 0.005 rad/sec by (TTSP), was used to track changes in binders with oxidative aging (*96*).

HMAC Mixture Tests

The binder-mixture (BM) test protocol was similar to the CMSE relaxation modulus test described in Chapter 6, except that the same HMAC specimen was repeatedly tested at different aging conditions. Thus, data were obtained at each test temperature for which the only variable mixture parameter was the aging condition of the binder; other mixture parameters (Void in Mineral Aggregates (VMA), Void Filled with Asphalt (VFA), aggregate size distribution, and configuration, etc.) were identical within the same specimen. The test was performed with both mixtures (Bryan and Yoakum) at 0, 3 and 6 months aging conditions with at least two replicate specimens for each mixture.

Figure 9-2 is a schematic illustration of the BM characterization test plan with RM testing.

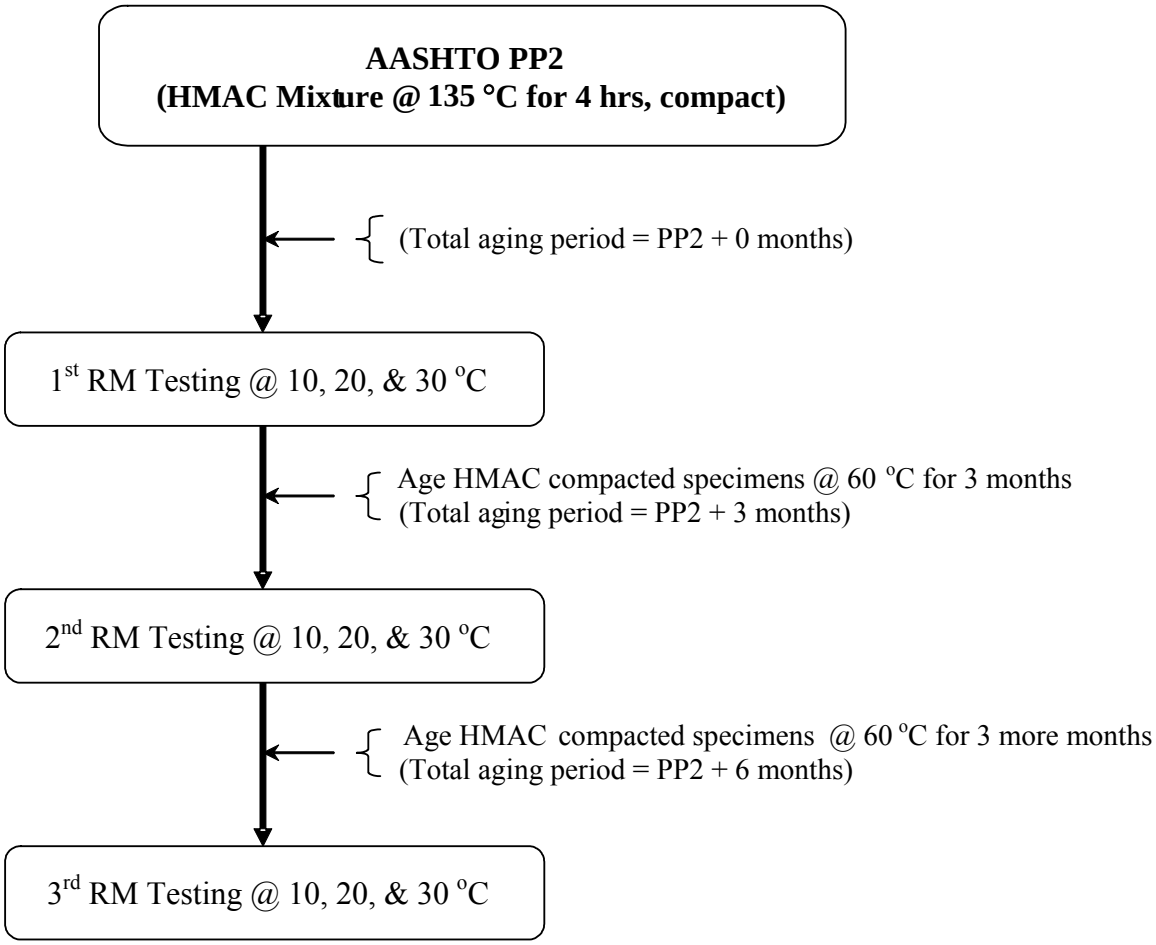

Figure 9-2. Binder-Mixture Characterization Test Procedure (°F = 32 + 1.8(°C)).

Chapter 5 describes the RM test conditions and loading configuration. Note that RM testing in this project was assumed non-destructive.

HMAC Mixture Visco-Elastic Characterization

The data obtained from the tensile RM test includes the time-dependent elastic relaxation modulus (E(t)), loading time (t), and test temperature (*T*). From these data, mixture visco-elastic properties were determined for comparison with the binder visco-elastic properties. The following procedure was used to estimate the mixture visco-elastic properties.

Elastic Modulus (E(t)) Master-Curve

A master-curve for *E(t)* was constructed at a reference temperature of 20 ^{o}C (68 °F) from the data obtained at three different temperatures (10, 20, and 30 ^{o}C) (50, 68, and 86 °F) by using the Williams-Landel-Ferry (WLF) TTSP procedures (*104*, *105*). As an example, the master-curve for *E(t)* in Figure 9-3 was constructed from data for a Yoakum mixture used for the CMSE procedure.

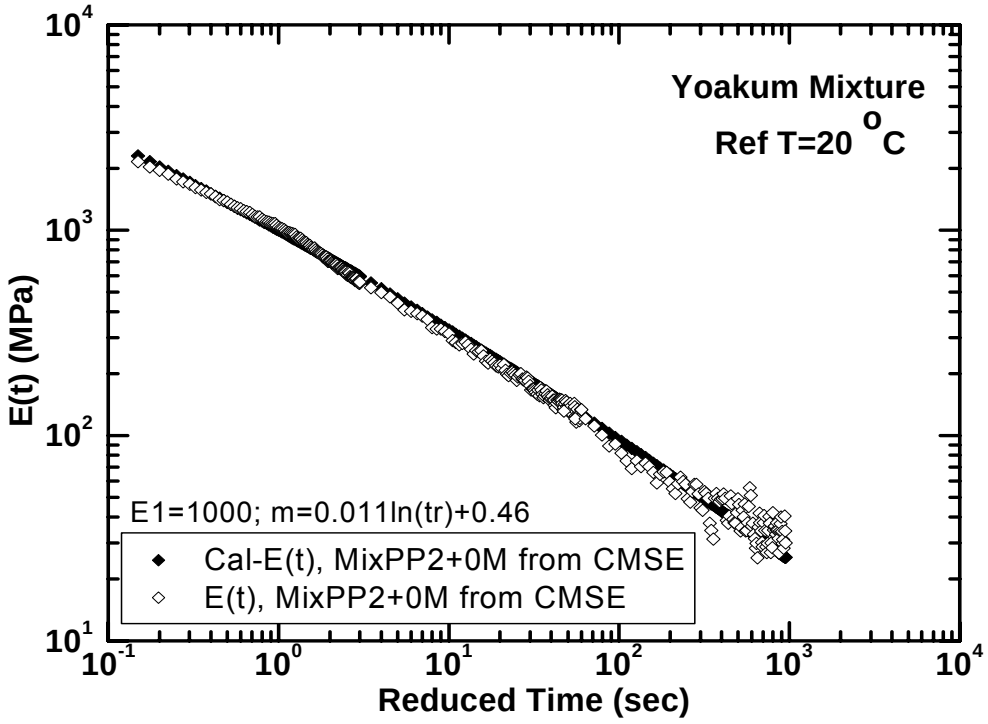

Figure 9-3. Relaxation Master-Curve for 0 Month Aged Yoakum Mixture Used for CMSE (°F = 32 + 1.8(°C)).

While there are some obvious inconsistencies in the data, $E(t_r)$ was found to be well represented by the model given by Equations 9-2 and 9-3:

$$E(t_r) = E_\infty + E_1 t_r^{-m} \cong E_1 t_r^{-m} = E_1 \left(\frac{t}{a_T(T)} \right)^{-m} \quad \text{(Equation 9-2)}$$

$$m = aLn(t_r) + b \quad \text{(Equation 9-3)}$$

$$t_r = \frac{t}{a_T(T)}$$

where:

$E(t)$, $E(t_r)$	=	Time-dependent elastic modulus at time t (MPa)
E_1	=	Initial (t_r = 1 sec) elastic modulus (MPa)
t	=	Time (s)
t_r	=	Reduced time (s)
T	=	Temperature (^oC)
a, b	=	Empirically determined coefficients
$a_T(T)$	=	The shift factor at temperature T relative to the reference temperature T_{ref}

The elastic modulus obtained by the RM test is a function of time because of the visco-elastic nature of the HMAC mixture. Under deformation, the stress builds because of the mixture's elastic nature but then relaxes at fixed strain because of its ability to undergo viscous flow. This relaxation is reflected in the decrease of $E(t_r)$ over time in the RM test. Therefore, storage (elastic) and loss (viscous) moduli can be calculated from the $E(t_r)$ master-curve.

The m value in Equation 9-2 was assumed to be a function of time and temperature according to Equation 9-3. Once the temperature shift factors are determined through TTSP alignment of the data, and the model parameters E_1, a, and b are estimated, $E(t_r)$ can be calculated. Figure 9-3 shows the result for this example.

Dynamic Mixture Storage and Loss Moduli

The elastic modulus is converted to a shear modulus according to Equation 9-4:

$$G(t_r) = \frac{E(t_r)}{2(1+\nu)},\ G_1 = \frac{E_1}{2(1+\nu)} \qquad \text{(Equation 9-4)}$$

Converting to frequency by Equation 9-5:

$$\omega \cong \frac{1}{2t_r} \qquad \text{(Equation 9-5)}$$

the dynamic shear storage (G') and loss (G'') moduli are calculated by *(45, 108)*:

$$G'(\omega) = G_1 \frac{\Gamma(1-m)}{\omega^{-m}} cos\left(\frac{m\pi}{2}\right) \qquad \text{(Equation 9-6)}$$

and

$$G''(\omega) = G_1 \frac{\Gamma(1-m)}{\omega^{-m}} sin\left(\frac{m\pi}{2}\right) \qquad \text{(Equation 9-7)}$$

and the magnitude of the complex dynamic shear modulus (G^*) is given by:

$$G^*(\omega) = \left((G')^2 + (G'')^2\right)^{\frac{1}{2}} \qquad \text{(Equation 9-8)}$$

where:

t_r	=	Reduced time (s)
t	=	Actual loading time (s)
$a_T(T)$	=	Temperature shift factor
m	=	Exponential stress relaxation rate ($0 \leq m < 1$)
ν	=	Poisson's ratio ($\cong 0.33$)

$G(t)$, $G(t_r)$	=	Time-dependent shear modulus at time t (MPa)
G_1	=	Initial shear modulus (MPa)
$G'(\omega)$	=	Elastic (storage) dynamic shear modulus (MPa)
$G''(\omega)$	=	Viscous (loss) dynamic shear modulus (MPa)
$G^*(\omega)$	=	Complex dynamic shear modulus (MPa)
Γ	=	Gamma function

For ν, the research team used a value of 0.33 for the HMAC mixture consistent with the work done by Huang and Lytton et al. (*45, 106*). Γ is the Lap lace (or Euler) Gamma transformation function that is widely used in many mathematical engineering applications.

The results of this procedure for the Yoakum mixture are shown in Figure 9-4. Note that at higher frequencies (lower temperatures) the storage modulus dominates the loss modulus, whereas at lower frequencies the reverse is true, typical of visco-elastic materials.

Mixture Visco-elastic (VE) Function

A visco-elastic function for mixtures can be calculated that is analogous to the DSR function for binders. As a first trial in this project, an angular frequency was arbitrarily selected where G''/G' is of the order of unity at 20 °C (68 °F), as it is for an aged binder at 15 °C (59 °F), 0.005 rad/sec. In this way, it was hoped that aging of the mixture would be readily observed from the visco-elastic properties. If the frequency is too high or the temperature too low, then the mixture would reflect elastic limit properties and not be sensitive to aging. So the VE function was calculated as follows:

VE function = $G'/(G''/(G'\omega))$ at 20 °C (68 °F), 0.002 rad/sec (Equation 9-9)

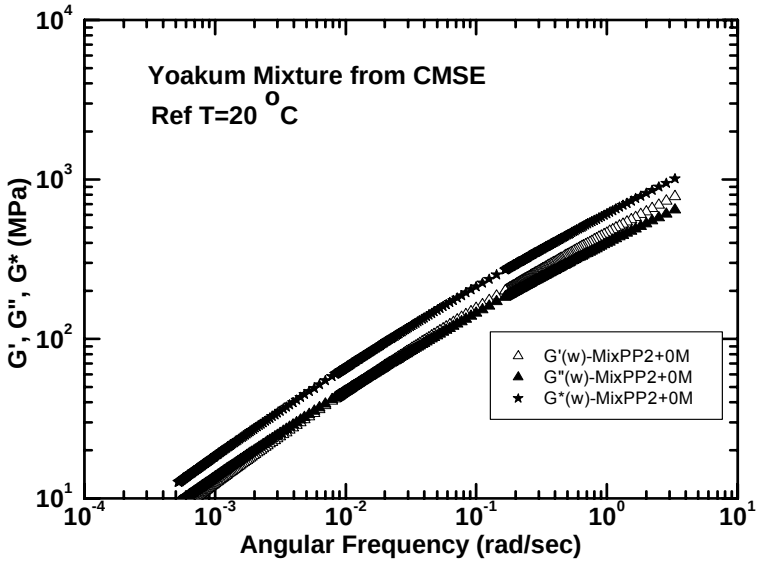

Figure 9-4. Shear Modulus Master-Curve for 0 Month Aged Yoakum Mixture used for CMSE (°F = 32 + 1.8(°C)).

RESULTS

The test results are presented in three sections: recovered binder properties, mixture visco-elastic properties, and binder-mixture relationships. As discussed at the beginning of this chapter, aged mixture samples were prepared using the PP2 4-hr short-term procedure. This aged mixture was then used to make replicate compacted mixtures. One of these replicates was tested as is (PP2 + 0 months), then aged for three months in the 60 °C (140 °F) environmental room (PP2 + 3 months) and tested again. The mixture test was the RM test conducted at 10, 20, and 30 °C (50, 68, and 86 °F). This same specimen has now been aged to a total of 6 months, but the testing was not complete in time for this report. Instead, a separate replicate sample was aged for 6 months (PP2 + 6 months), and the corresponding RM data are reported in this chapter. Binder was recovered from other replicate compacted and aged mixture samples and tested to provide binder properties to compare to the tested mixtures. From both binder properties and the corresponding mixture properties, the effect of binder hardening on mixtures was evaluated directly and without the variability created by mixture parameters other than binder rheology.

Recovered Binder Results

Binder master-curves for the dynamic shear storage $G'(\omega)$, loss $G''(\omega)$, and complex $G^*(\omega)$ moduli were used to track changes in binder properties with aging. Figures 9-5 to 9-8 show the results for binders recovered from Bryan and Yoakum mixtures at three levels of aging.

Figures 9-5 and 9-6 show that the complex moduli increase with aging for both unmodified (Bryan) and modified (Yoakum) binders. Figures 9-7 and 9-8 show that $G'(\omega)$ and $G''(\omega)$ increase with aging. Furthermore, $G'(\omega)$ is greater than $G''(\omega)$ at high frequency, and $G''(\omega)$ is greater than $G'(\omega)$ at low frequency at each aging level.

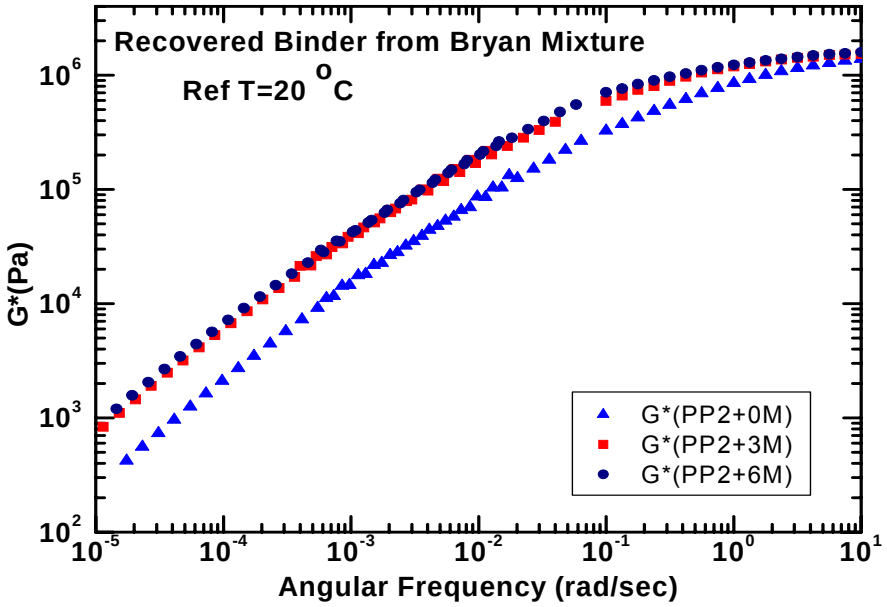

Figure 9-5. Master-Curves of Recovered Binders for *G*(ω)* from Bryan Mixture (°F = 32 + 1.8(°C)).

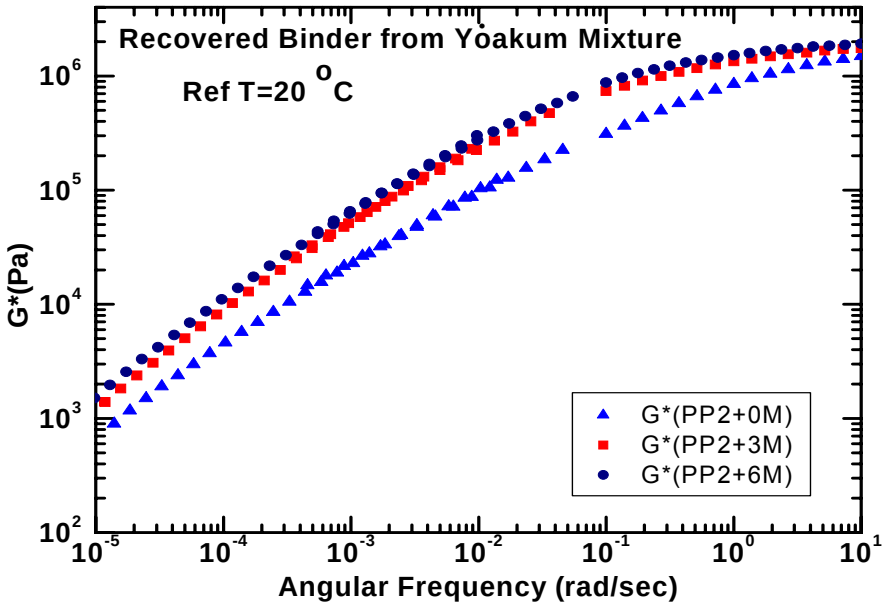

Figure 9-6. Master-Curves of Recovered Binders for *G*(ω)* from Yoakum Mixture (°F = 32 + 1.8(°C)).

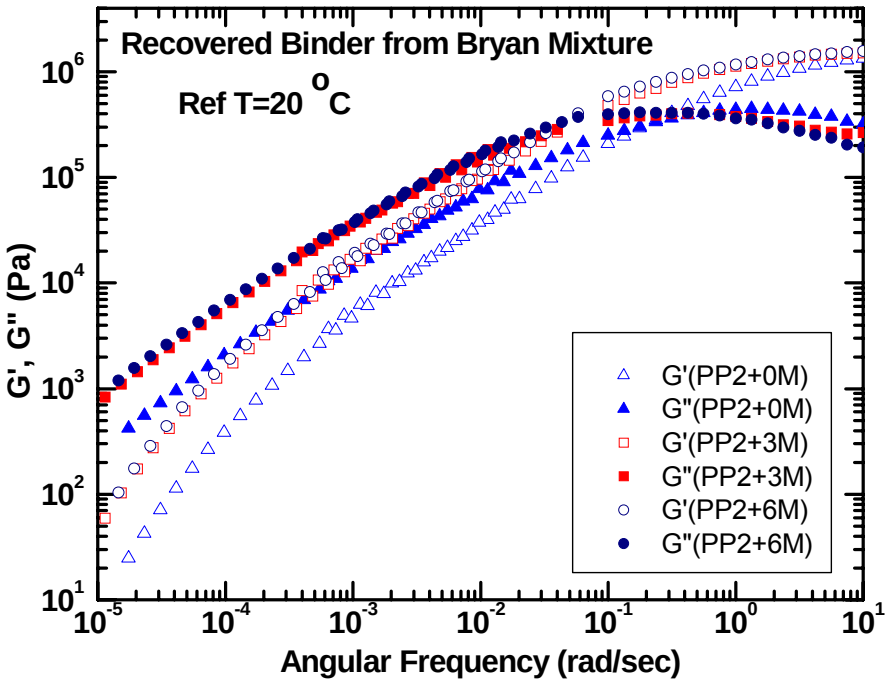

Figure 9-7. Master-Curves of Recovered Binders for $G'(\omega), G''(\omega)$ from Bryan Mixture (°F = 32 + 1.8(°C)).

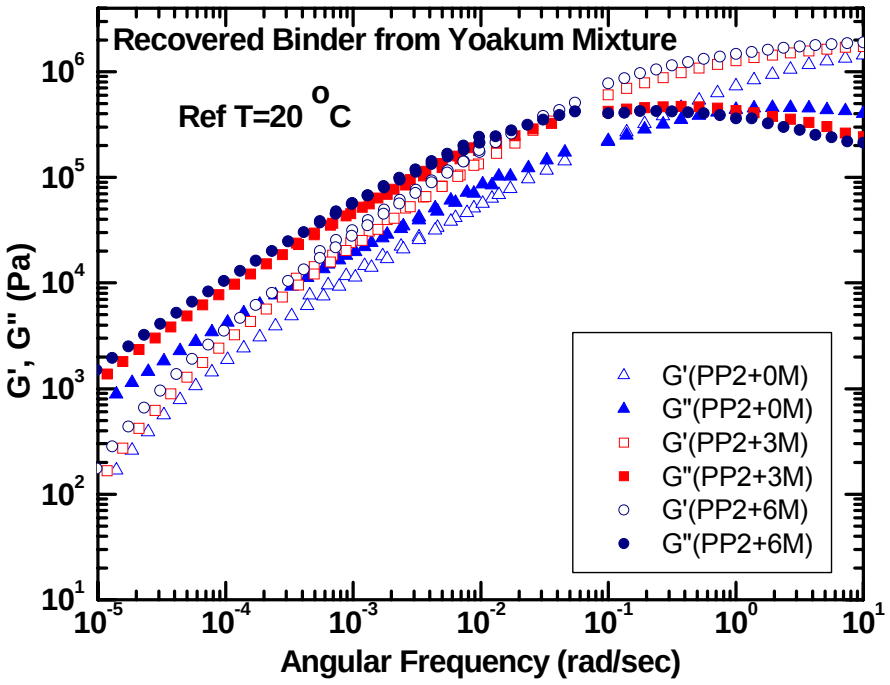

Figure 9-8. Master-Curves of Recovered Binders for $G'(\omega), G''(\omega)$ from Yoakum Mixture (°F = 32 + 1.8(°C)).

DSR map aging paths for the binder recovered from aged Bryan and Yoakum mixtures are shown in Figures 9-9 and 9-10, respectively.

In each case, the recovered binder moves upward and to the left with aging, as has been observed previously with neat binder aging (*52*, *96*). Interestingly, these two binder paths very nearly overlap each other, although the Yoakum binder is stiffer than the Bryan binder at each level of aging.

The curved, dashed lines shown are lines of constant ductility (cm at 15 °C, 1 cm/min) (59 °F, 0.39 inches/min) that were determined for unmodified binders by Ruan et al. (*52*, *96*); as a binder ages, its ductility decreases. Kandhal (*107*) concluded that a ductility of 3 cm (1.18 inches) at 15 °C (59 °F) is a value that corresponds well to age-related cracking failure in HMAC pavements.

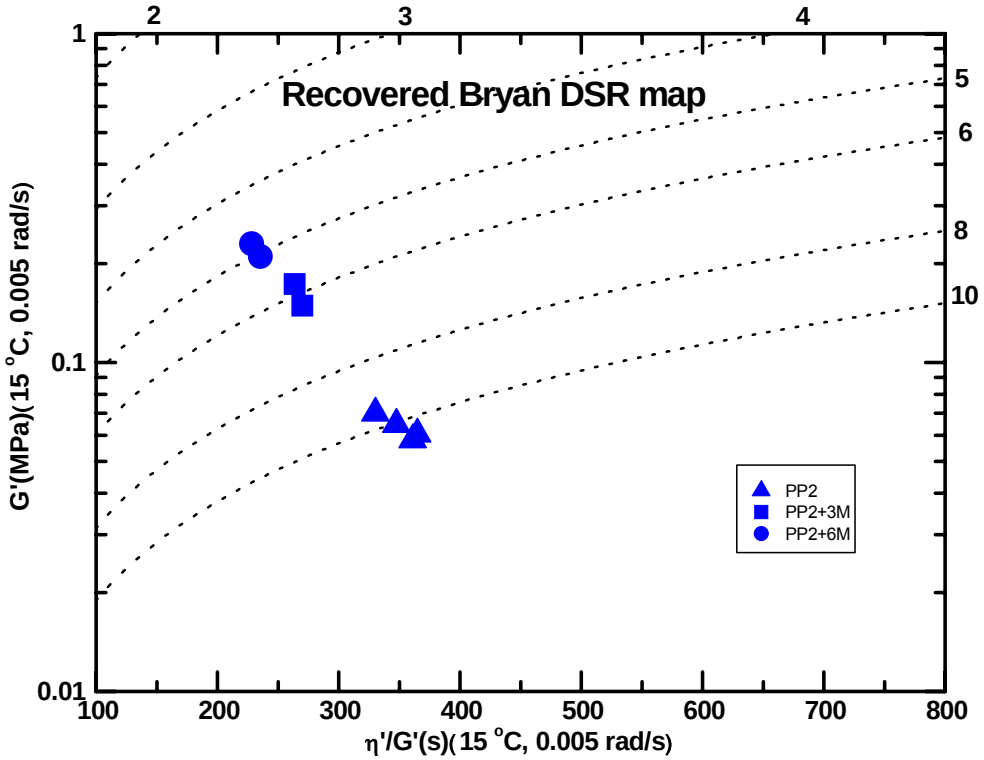

Figure 9-9. DSR Function of Recovered Binders from Bryan Mixture (°F = 32 + 1.8(°C)).

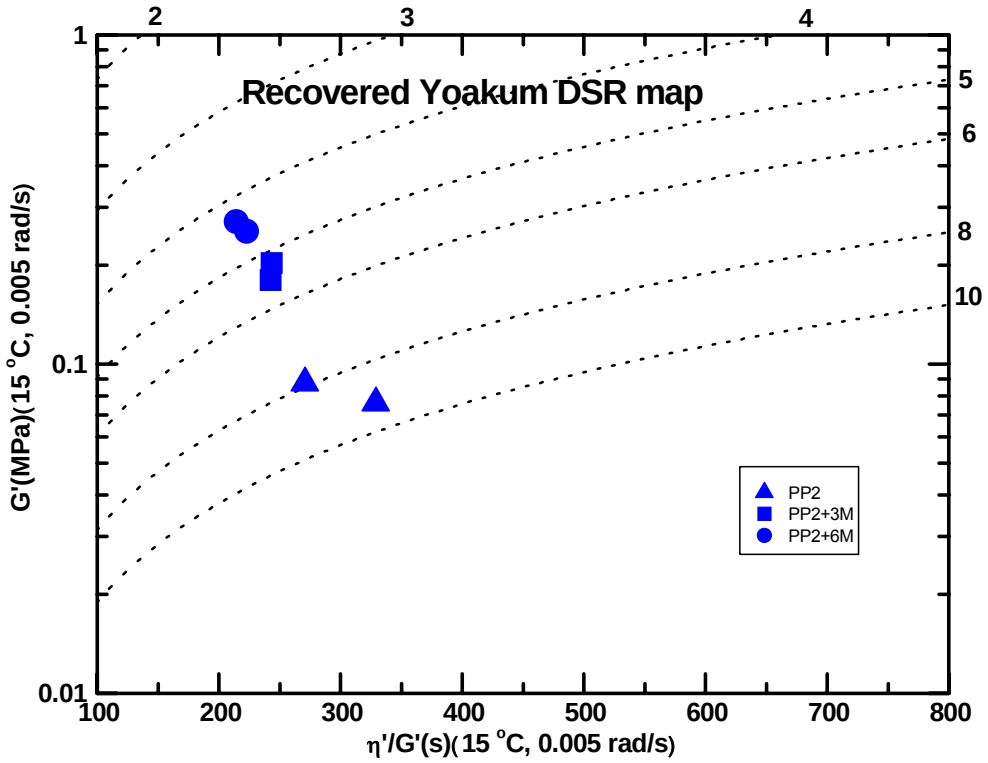

Figure 9-10. DSR Function of Recovered Binders from Yoakum Mixture (°F = 32 + 1.8(°C)).

HMAC Mixture Results

Following the procedure described in the previous section for mixture analysis, tensile RM master-curves were determined for both the Bryan and Yoakum mixtures. The results at a reference temperature of 20 °C (68 °F) are presented in Figures 9-11 and 9-12.

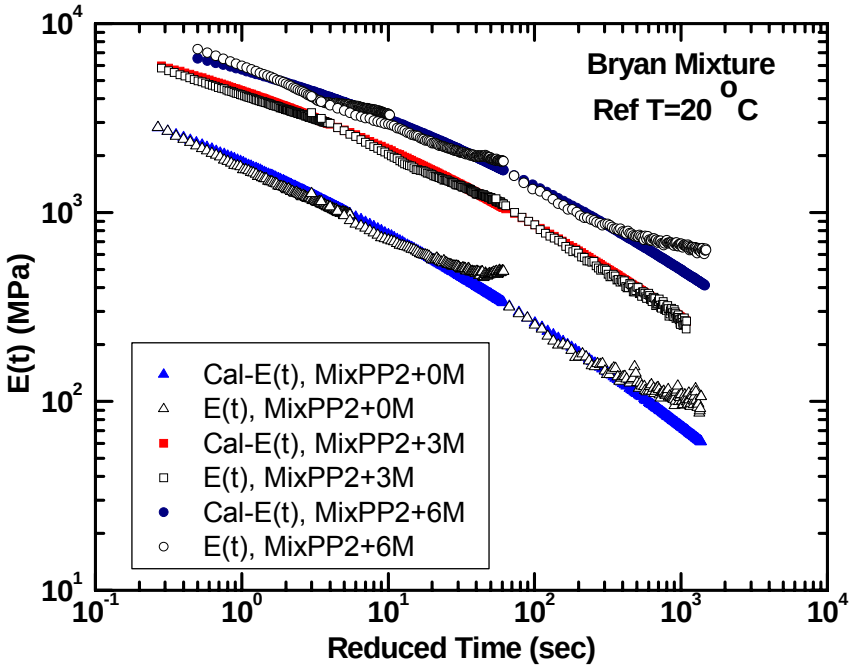

Figure 9-11. Master-Curves of Bryan Mixture for *E(t)* (°F = 32 + 1.8(°C)).

Clearly, there are inconsistencies in the data, most notably toward the end of each relaxation test, that make the master-curve determination problematic. The value of *m* in Equation 9-2 is assumed to be a function of time (through Equation 9-3) to allow the master-curves to be non-linear on the log-log plot, but the amount of curvature built into the model by the value of *a* in Equation 9-3 is somewhat subjective. In addition, it is necessary to place unequal weighting on different parts of each relaxation experiment when performing the time-temperature shifting, and this weighting also is somewhat subjective. The net effect is that the master-curves necessarily are subject to some degree of uncertainty. Additional experience with this method and independent verification with other experiments (dynamic modulus, for example) is necessary in order to achieve more confidence in the mixture visco-elastic properties.

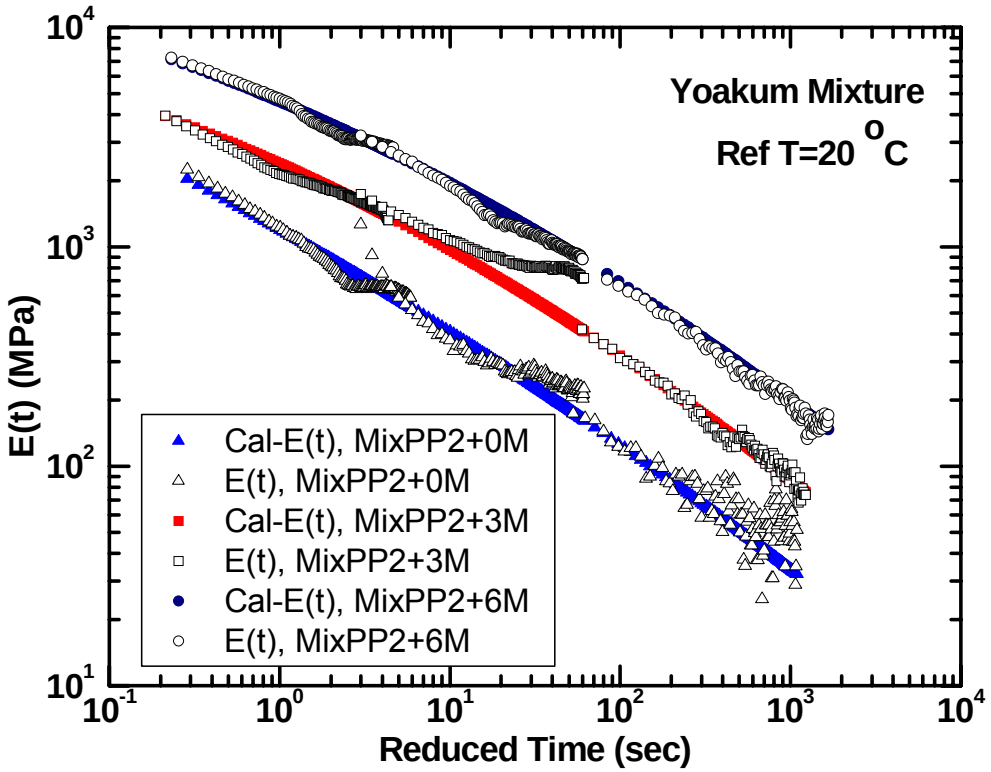

Figure 9-12. Master-Curves of Yoakum Mixture for *E(t)* (°F = 32 + 1.8(°C)).

.

Note that the data for the PP2 and PP2 plus 3 months aging levels were obtained on the same mixture specimens for both the Bryan and Yoakum mixtures. The PP2 plus 6 months data for each mixture were from a different specimen, one used for the CMSE data analysis. Six-month data on the 0 and 3 month specimens will be obtained as part of this project to complete the 0, 3, and 6 month series on a single specimen.

The objective of obtaining a set of data at different aging levels from the same mixture specimen is to study the effect of binder aging alone on mixture stiffness and visco-elastic behavior. If different specimens are studied, then the whole host of mixture variables (aggregate gradation, VMA, VFA, binder content, and aggregate alignment configuration) is brought in to play, and greater variability in the aging data would result.

Clearly, oxidative aging stiffens the tensile RM of the mixture significantly, consistent with stiffening of the neat binder with aging. Also noted is that the Bryan mixture is stiffer than the Yoakum mixture at comparable levels of aging and test condition.

From these tensile RM master-curves, dynamic shear moduli master-curves, also at a reference temperature of 20 °C (68 °F), were calculated as defined by Equations 9-4 through 9-8. The results are given in Figure 9-13 (G', G'') for the Bryan mixtures and in Figure 9-14 (G', G'') for the Yoakum mixtures.

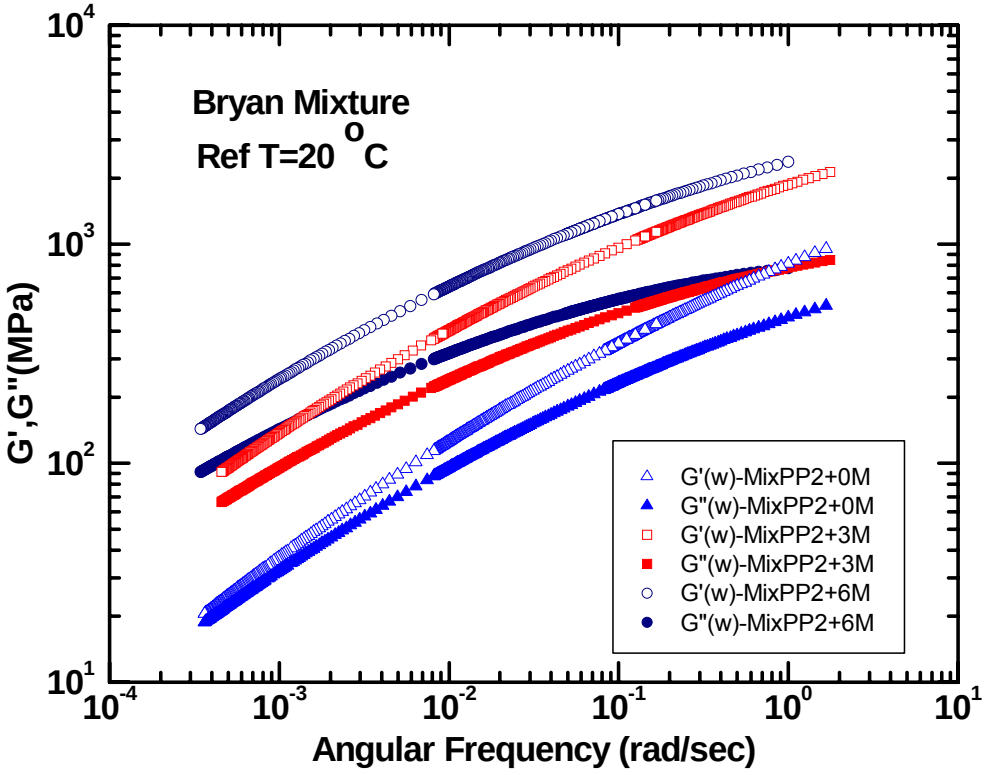

Figure 9-13. Master-Curves of Bryan Mixture for $G'(\omega), G''(\omega)$ (°F = 32 + 1.8(°C)).

Again, stiffening of the mixture with oxidative aging is evident as G', G'', and G^* all increase, and the crossover frequency (frequency at which $G' = G''$) moves to a lower frequency. The effects of 60 °C (140 °F) aging for 0, 3, and 6 months beyond PP2 conditioning are evident in Figures 9-11 and 9-12.

In addition, Figure 9-15 compares the complex dynamic shear moduli (G^*) of the Bryan and Yoakum mixtures. Note that G^* increases with aging for both mixtures, and the Bryan mixture is stiffer than the Yoakum mixture, which is most evident at the lower frequencies.

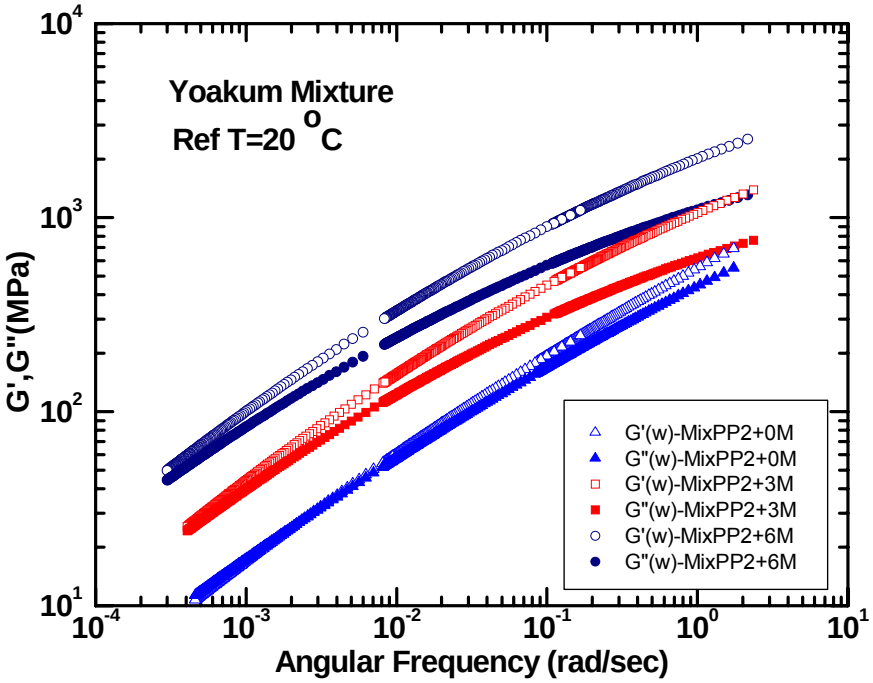

Figure 9-14. Master-Curves of Yoakum Mixture for $G'(\omega)$, $G''(\omega)$ (°F = 32 + 1.8(°C)).

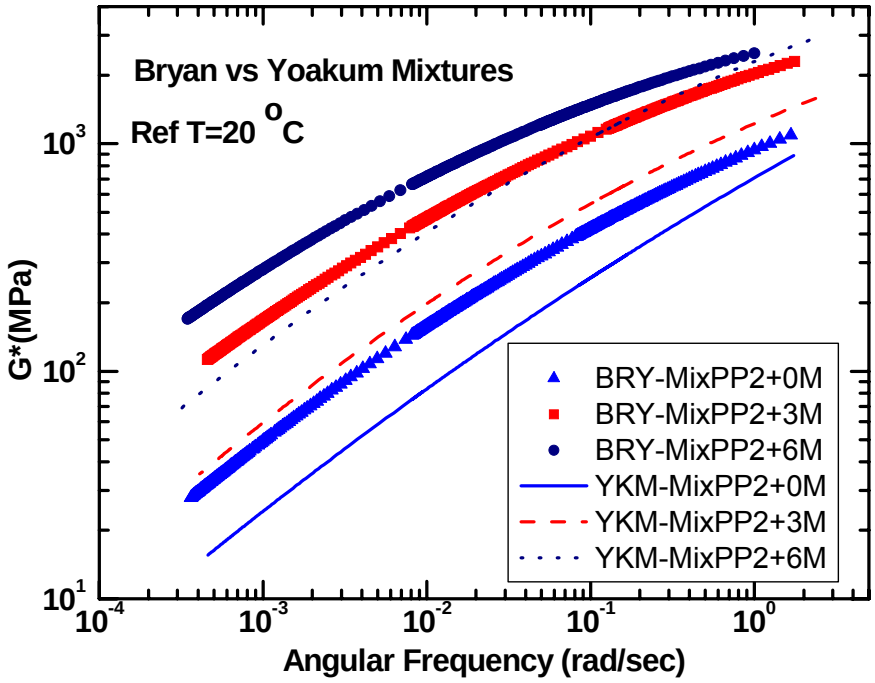

Figure 9-15. Master-Curve Comparisons between Bryan and Yoakum Mixtures for *G*(ω)* (°F = 32 + 1.8(°C)).

Similar to the DSR map for the recovered binders, a visco-elastic property aging map can be constructed from the mixture visco-elastic master-curves. As described previously, values from the 20 °C (68 °F) reference master-curves at 0.002 rad/s were used to plot G' versus η'/G', and the results are shown in Figures 9-16 (Bryan) and 9-17 (Yoakum). Remember that the PP2+6 months data are from different HMAC mixture specimens than the PP2+0 and PP2+3 months data.

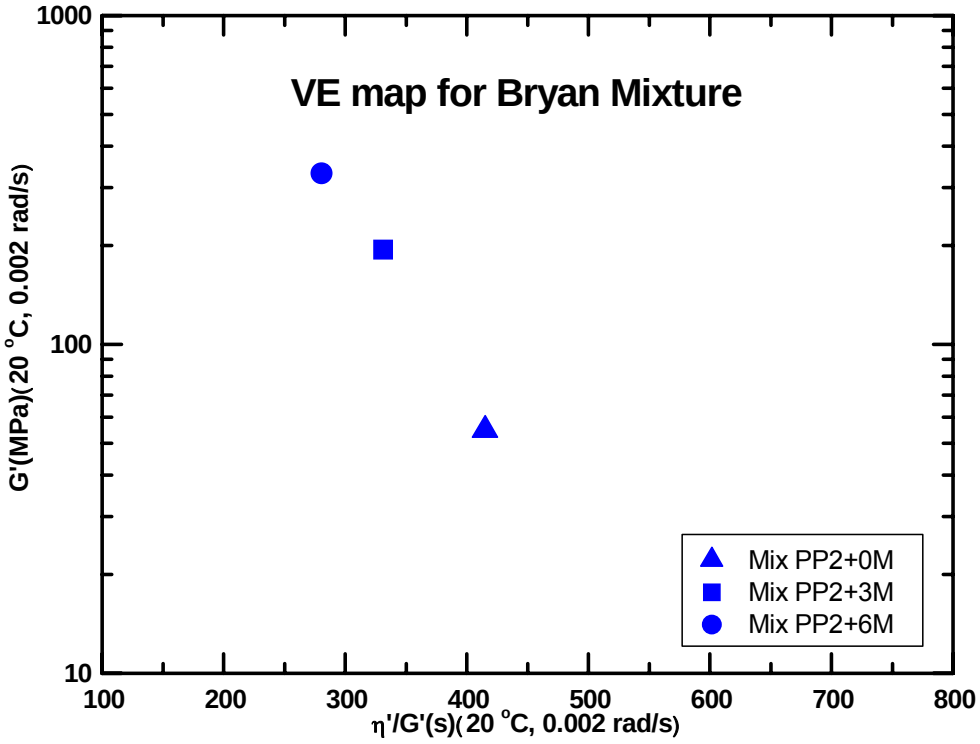

Figure 9-16. VE Function of Bryan Mixture (°F = 32 + 1.8(°C)).

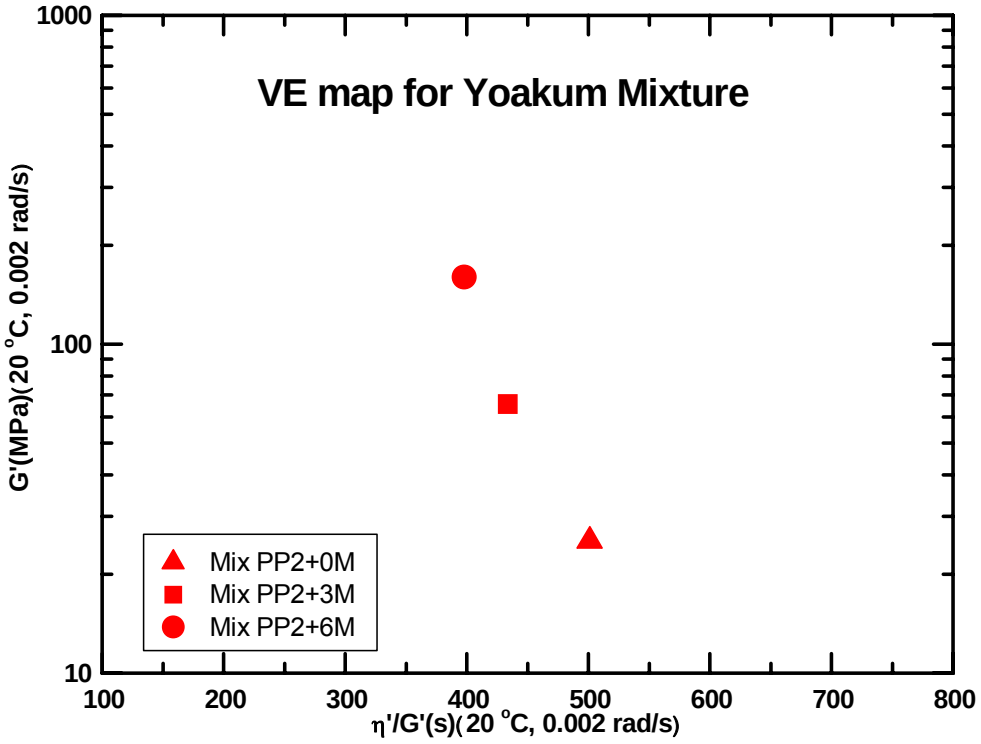

Figure 9-17. VE Function of Yoakum Mixture (°F = 32 + 1.8(°C)).

Binder-Mixture Comparisons

The mixture trends are obvious and very similar to the recovered binder DSR map. With aging, the mixture moves to the left and upward due to binder stiffening. The good correlation between the mixture and binder maps is shown in Figure 9-18, where the VE function ($G'/(\eta'/G')$) is plotted against the DSR function. Interestingly, the slopes of the Bryan and Yoakum plots are virtually identical, and differences are manifested primarily in an offset (magnitude) of the two sets of data.

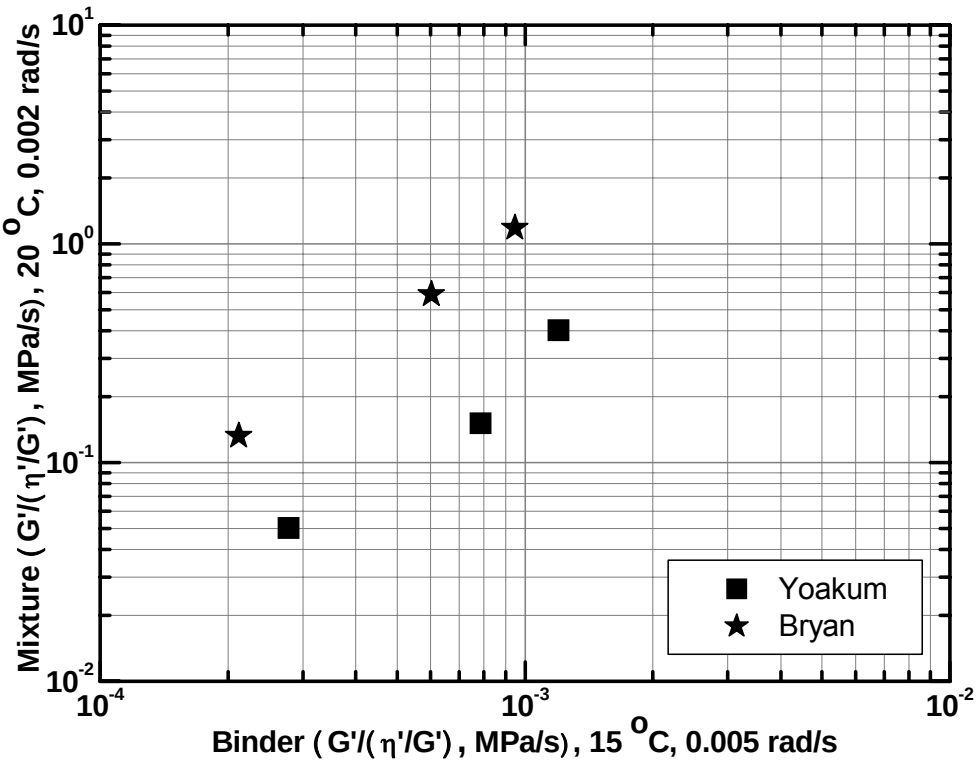

Figure 9-18. VE Function vs. DSR Function (°F = 32 + 1.8(°C)).

SUMMARY

In this project, two HMAC mixtures were tested to obtain mixture visco-elastic properties at three conditions (0, 3, and 6 months) of binder aging. Nondestructive tensile RM tests were used to produce mixture dynamic shear storage and loss moduli master-curves. Binders recovered from aged mixtures were used to determine corresponding master-curves for the binder. From these binder-mixture aging experiments, the following results were obtained:

- Mixtures stiffen significantly in response to binder oxidative aging. Mixture stiffening was reflected in both the tensile relaxation modulus and the dynamic shear moduli.

- A mixture visco-elastic property map of G' versus η'/G' at the three levels of mixture aging (PP2, PP2+3 months, PP2+6 months) provided a useful means of tracking mixture stiffening with binder oxidative aging. This mixture VE map is analogous to the binder DSR map developed in Project 0-1872 (*52*).
- A mixture VE function, defined as $G'/(\eta'/G')$ at 20 °C (68 °F), 0.002 rad/s correlated linearly with the binder DSR function $G'/(\eta'/G')$ at 15 °C (59 °F), 0.005 rad/s.
- The Bryan (PG64-22) binder is softer than the Yoakum (PG76-22) binder. However, the Bryan mixture is stiffer than the Yoakum mixture, at comparable angular frequency or at comparable binder stiffness.

CHAPTER 10
HMAC MIXTURE RESULTS AND ANALYSIS

This chapter presents the mixture results analyzed at a typical 95 percent reliability level. For simplicity and because HMAC fatigue cracking is generally more prevalent at intermediate pavement service temperatures, most of the laboratory tests were conducted at 20 °C (68 °F). Otherwise, the results were normalized to 20 °C (68 °F).

MIXTURE PROPERTIES FOR PREDICTING N_f

Laboratory test results for mixture properties related to N_f predictions are presented in this section for the three aging conditions (0, 3, and 6 months) for both Bryan and Yoakum mixtures. These results, which include BB, tensile strength, relaxation modulus, DPSE, SE, anisotropy, and dynamic modulus, represent mean values of at least two test specimens.

BB Laboratory Test Results

Table 10-1 is a summary of the BB fatigue test results conducted at two test strain levels (374 and 468 microstrain) at 20 °C (68 °F) and 10 Hz frequency. These results are an average of at least two test specimens per mixture type per aging condition. Detailed results are attached in Appendix C.

Table 10-1. BB Laboratory Test Results.

Aging Condition	Mean *N* Value			
	Bryan @ 374 Test Microstrain	Bryan @ 468 Test Microstrain	Yoakum @ 374 Test Microstrain	Yoakum @ 468 Test Microstrain
0 months	127,000	50,667	223,790	105,350
3 months	80,187	39,833	172,167	86,187
6 months	53,000	27,500	108,200	47,150

In Table 10-1, N (without subscript f) refers to the average number of laboratory load cycles or repetitions to fatigue failure during the BB test. Fatigue failure, as defined in Chapter 4, is the point of 50 percent reduction in the initial HMAC flexural stiffness measured at the 50th load cycle (*2*, *59*). From Table 10-1, while N decreased significantly with aging for both mixtures, the Yoakum mixture sustained higher N values at both strain levels for all aging conditions compared to the Bryan mixture.

The reduction in N, which was approximately 25 and 50 percent after 3 and 6 months aging, respectively, indicates that aging has a very significant effect on the HMAC mixture fatigue resistance. The relatively higher N for the Yoakum mixture was possibly due to the higher binder content (5.6 percent compared to 4.6 percent for the Bryan mixture by weight of aggregate) and the effect of the SBS modifier.

N_f-ε_t Empirical Relationships

Figures 10-1 (a) and (b) show plots of the average N versus test ε_t on a log-log scale. Based on these figures, empirical fatigue relationships of the power format shown in Table 10-2 were derived and used to estimate lab N_f. These empirical fatigue equations and material constants (k_i) in Table 10-2 were derived by fitting power regression trend lines through the N data points in Figure s 10-1 (a) and (b), and were also checked using least squares line regression analysis. Each N data point in Figure 10-1 is a mean value of three replicate measurements.

Table 10-2. Mixture Empirical Fatigue Relationships.

Aging Condition	Mixture	Equation	Materials Constants	
			k_1	k_2
0 months	Bryan	$N_f = 1\times10^{-9}(\varepsilon_t)^{-4.0984}$	1×10^{-9}	4.0984
	Yoakum	$N_f = 7\times10^{-7}(\varepsilon_t)^{-3.3603}$	7×10^{-7}	3.3603
3 months	Bryan	$N_f = 2\times10^{-6}(\varepsilon_t)^{-3.1205}$	2×10^{-6}	3.1205
	Yoakum	$N_f = 5\times10^{-6}(\varepsilon_t)^{-3.0861}$	5×10^{-6}	3.0861
6 months	Bryan	$N_f = 5\times10^{-6}(\varepsilon_t)^{-2.9263}$	5×10^{-6}	2.9263
	Yoakum	$N_f = 2\times10^{-8}(\varepsilon_t)^{-3.7047}$	2×10^{-8}	3.7047

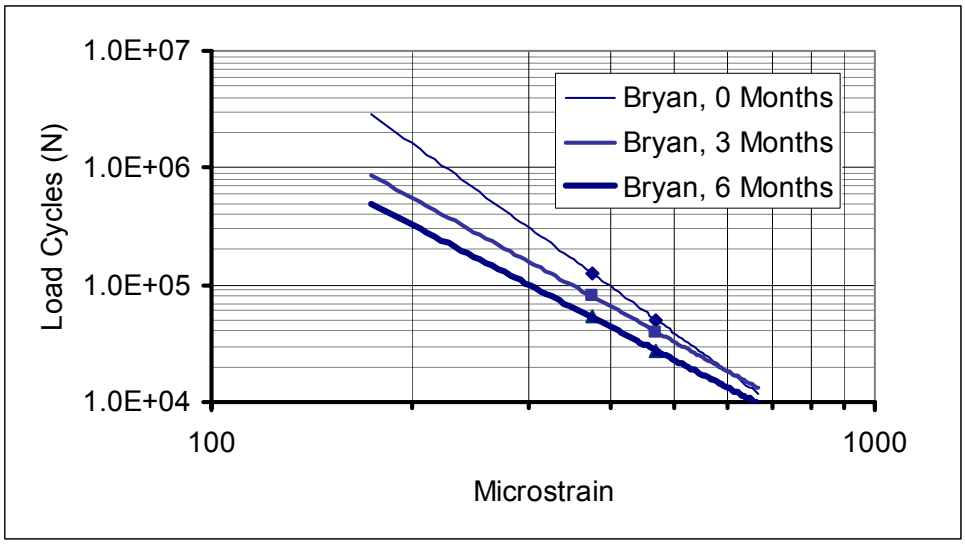

Figure 10-1(a). *N* vs. ε_t at 20 °C (68 °F) (Bryan Mixture).

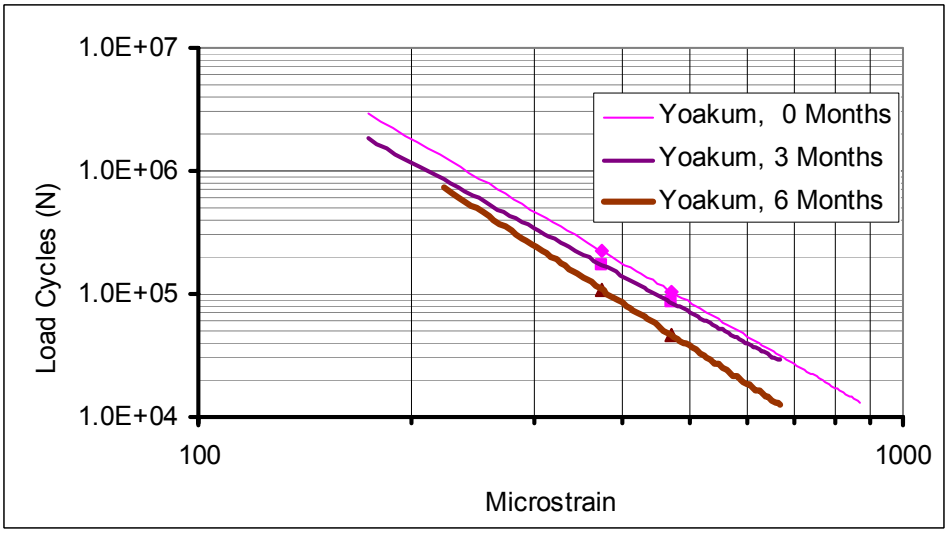

Figure 10-1(b). *N* vs. ε_t at 20 °C (68 °F) (Yoakum Mixture).

Note that the fatigue results in Figure 10-1 were based on two test strain levels for each mixture per aging condition. For better N_f predictions and statistical analysis, more data points (collected at more than two test strain levels) are recommended. Generally, more testing at different strain levels would lead to a better fatigue relationship, but bearing in mind that BB testing is quite a lengthy test. However, each data point in Figure 10-1 is a mean value of three replicate measurements of different HMAC beam specimens.

Tensile Strength (σ_t)

Table 10-3 is a summary of the average σ_t results measured at 20 °C (68 °F). Figures 10-2(a) through 10-2(c) are examples of plots of tensile stress and strain at break as a function of aging condition for each mixture.

Table 10-3. Mixture Tensile Strength.

Aging Condition	Mixture	Mean σ_t @ Break (psi)	Mean Tensile Strain (ε_f) @ Break
0 months	Bryan	105	1245×10^{-6}
	Yoakum	123	3483×10^{-6}
3 months	Bryan	112	689×10^{-6}
	Yoakum	152	2342×10^{-6}
6 months	Bryan	157	401×10^{-6}
	Yoakum	184	851×10^{-6}

Table 10-3 indicates that as the HMAC ages, it becomes more brittle, thus breaking under tensile loading at a lower strain level (Figure 10-2). For both mixtures, the failure strain (ε_f) at break decreased significantly on the order of at least 30 percent per mixture type. The research team attributed this phenomenon to an increase in mixture brittleness due to binder oxidative aging.

In terms of mixture comparison, the σ_t and ε_f values for the Yoakum mixture were higher than that of the Bryan mixture at all aging conditions, indicating that for the test conditions considered in this project:

- the Yoakum mixture was more ductile than the Bryan mixture, and
- the Yoakum mixture had a better resistance to tensile stress than the Bryan mixture.

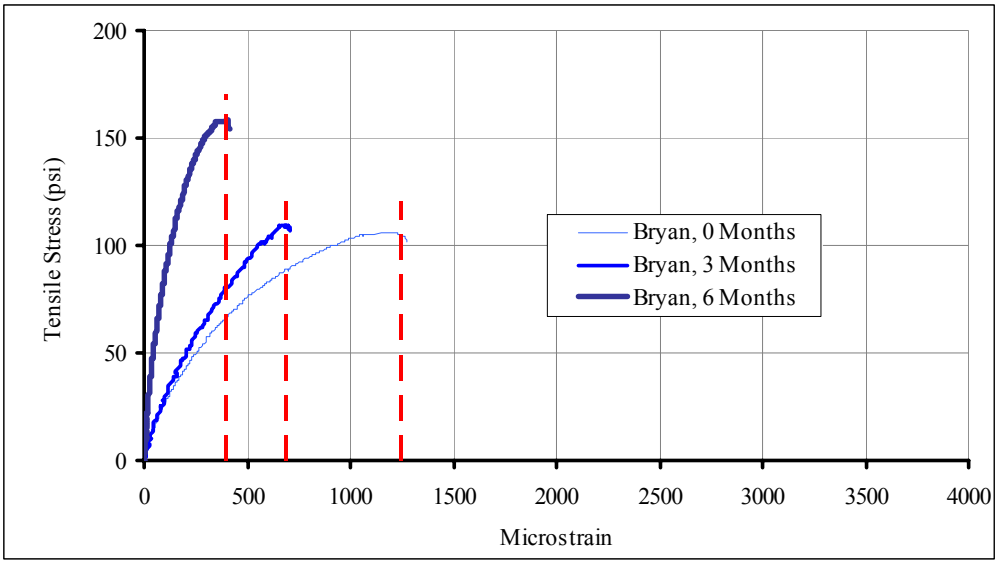

Figure 10-2(a). Mixture Tensile Stress at 20 °C (68 °F) (Bryan Mixture).

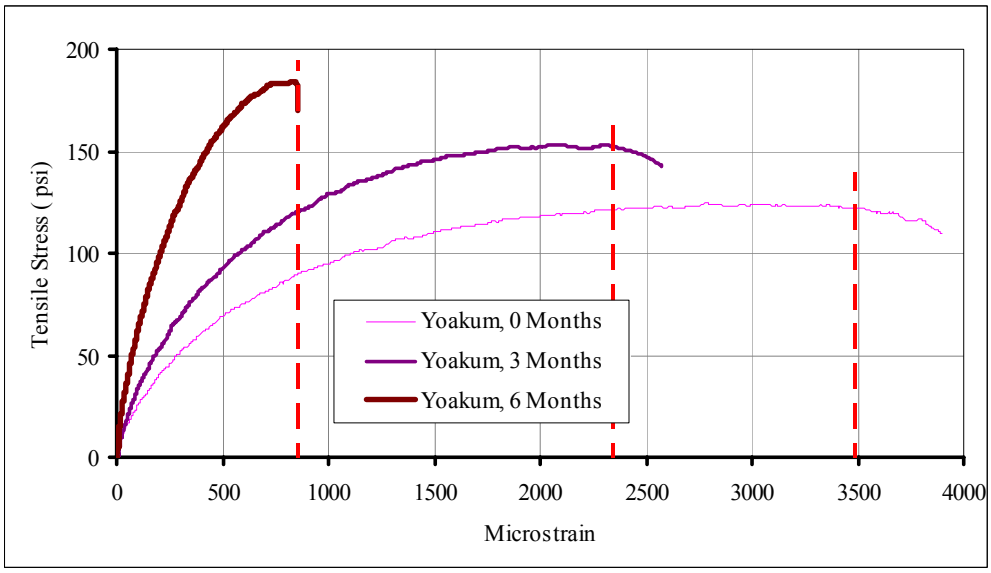

Figure 10-2(b). Mixture Tensile Stress at 20 °C (68 °F) (Yoakum Mixture).

Figure 10-2(c) is a plot of the ε_f values as a function of aging condition. The figure shows the expected decreasing trend of the ε_f values at 20 °C (68 °F) as a function of binder oxidative aging due to increasing mixture brittleness. The increased ductility of the Yoakum mixture is apparent and is indicated by the comparatively higher ε_f values at all aging conditions, which are almost double the Bryan mixture ε_f values.

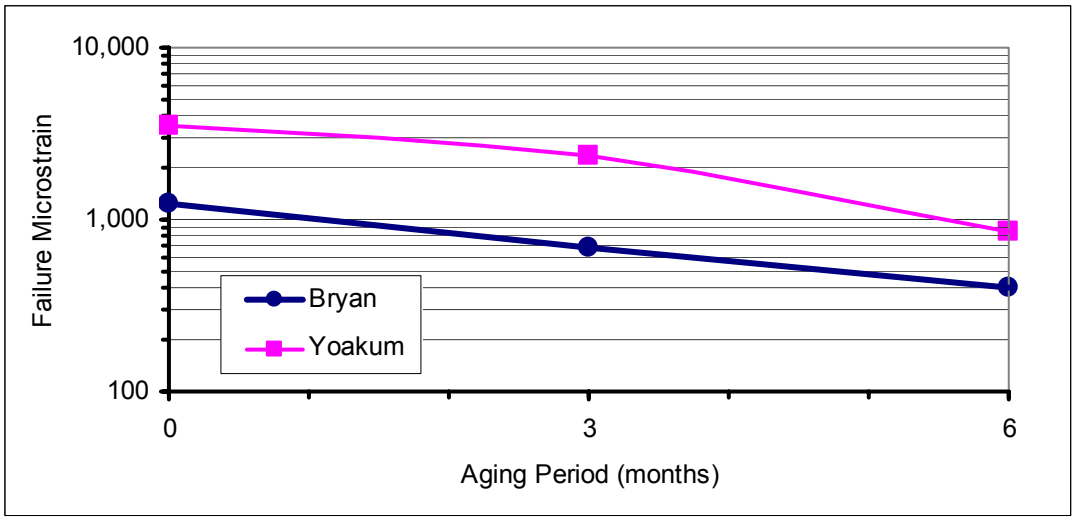

Figure 10-2(c). Mixture Failure Tensile Strain (ε_f) at Break at 20 °C (68 °F).

Relaxation Modulus Master-Curves

The RM test results in terms of the E_1 and m values are summarized in Table 10-4, and some examples are presented graphically in Figure 10-3 on a log-log scale. As expected, E_1 increased with aging due to HMAC hardening and stiffening effects from oxidation of the binder. This stiffening effect, however, also causes the material property parameter m, which describes the rate at which the mixture relaxes the applied stress, to decrease. For visco-elastic materials like HMAC, the higher the m value, the higher the ability of the mixture to relax the stress and the greater the resistance to fracture damage.

Table 10-4. Mixture Relaxation Modulus (Tension) Test Data.

Aging Condition	Average E_1 (psi)		Average m	
	Bryan	Yoakum	Bryan	Yoakum
0 months	208,100	178,785	0.3997	0.5116
3 months	675,600	389,325	0.3774	0.4513
6 months	1,010,215	633,505	0.2945	0.4273

Note that the *E(t)* values in Figures 10-3(a) and (b) are plotted in metric units (where 1 MPa ≅ 145 psi). This was done in order to allow for easy comparison with the binder-HMAC mixture master-curves discussed in Chapter 9 (which includes binder test results). Note that metric units are typically used for binder test results, which is consistent with the PG specification used by TxDOT for binders.

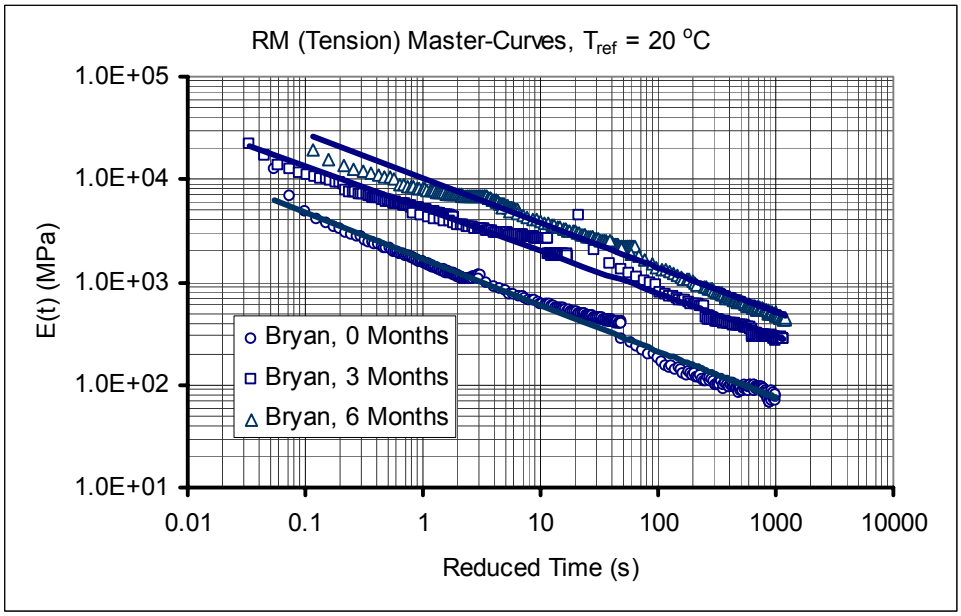

Figure 10-3(a). RM (Tension) Master-Curve at 20 °C (68 °F) (Bryan Mixture).

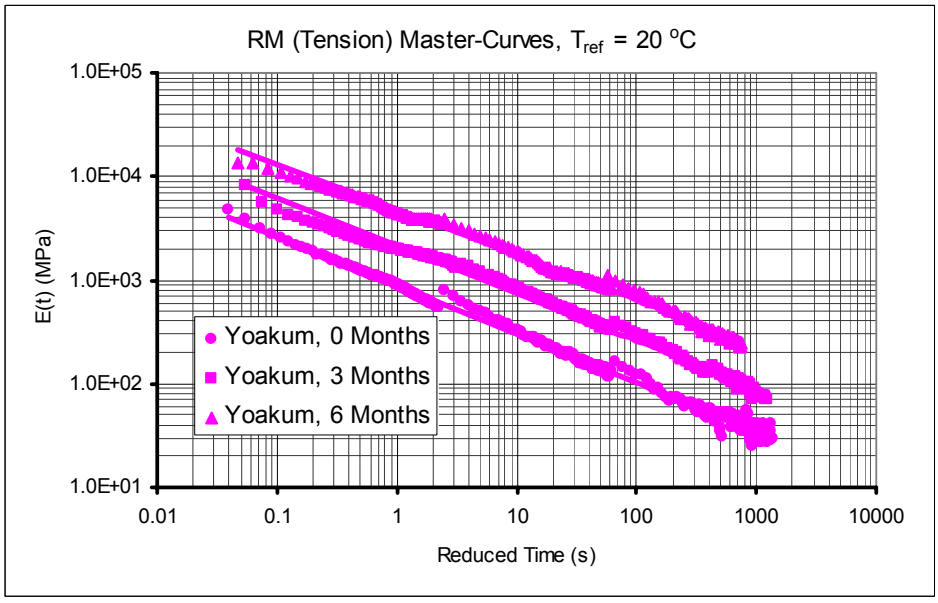

Figure 10-3(b). RM (Tension) Master-Curve at 20 °C (68 °F) (Yoakum Mixture).

From Table 10-4 and Figure 10-3, it is clear that the Bryan mixture, although designed with a softer PG 64-22 binder, was relatively stiffer than the Yoakum mixture. This difference in the stiffness is particularly more pronounced with aging, indicating that the Bryan mixture was probably more susceptible to stiffness age-hardening compared to the Yoakum mixture. While the Yoakum mixture exhibited comparatively lower E_1 values, it exhibited higher m values at all aging conditions. This result indicates that the Yoakum mixture had a relatively better potential to relax the stress than the Bryan mixture.

Note also that for all aging conditions, the E_1 values in compression were higher than the values in tension and vice versa for the m values. This is an expected material response behavior due to the generally higher compactive effort in the vertical direction and confirms the anisotropic nature of HMAC.

RM Temperature Shift Factors, a_T

The a_T values plotted in Figure 10-4 were computed when generating the RM master-curves at a reference temperature of 20 °C (68 °F) using the Arrehnius time-temperature superposition model via spreadsheet SSE regression optimization analysis (*84*). The almost overlapping graphs in Figure 10-4 indicate that the a_T values are not very sensitive to HMAC aging. These values, however, exhibit a linear relationship with temperature. Several researchers, including Christensien et al. (*109*) have reported similar findings.

When comparing Figures 10-4(a) and 10-4(b), the a_T values seem to be material (mixture) dependent, as evidenced in Equations 10-1 and 10-2:

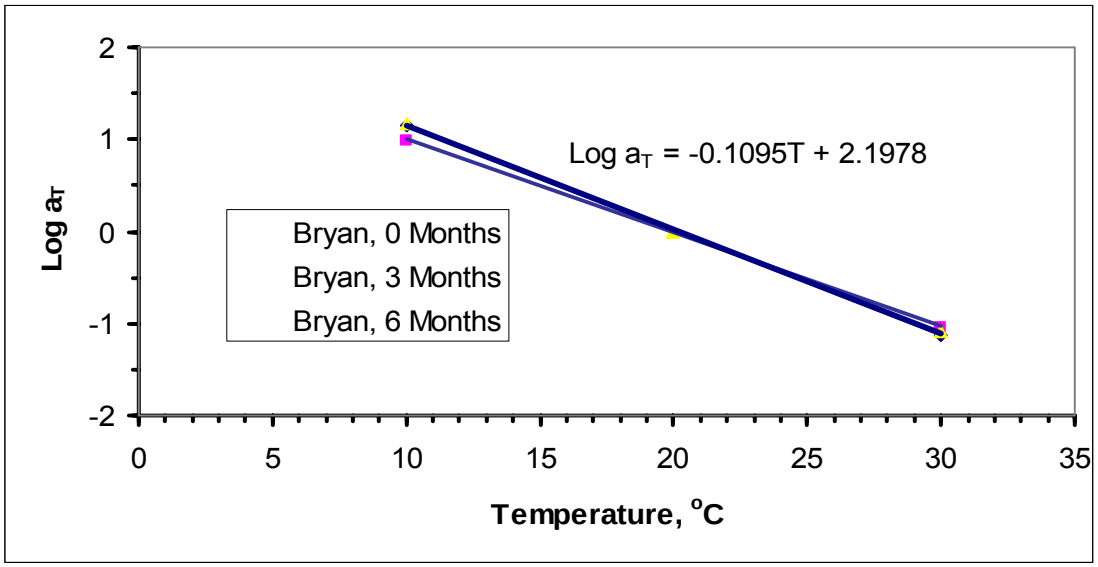

Figure 10-4(a). Temperature Shift Factors, a_T at $T_{Ref=20\ ℃}$ (Bryan Mixture) (°F = 32 + 1.8(°C)).

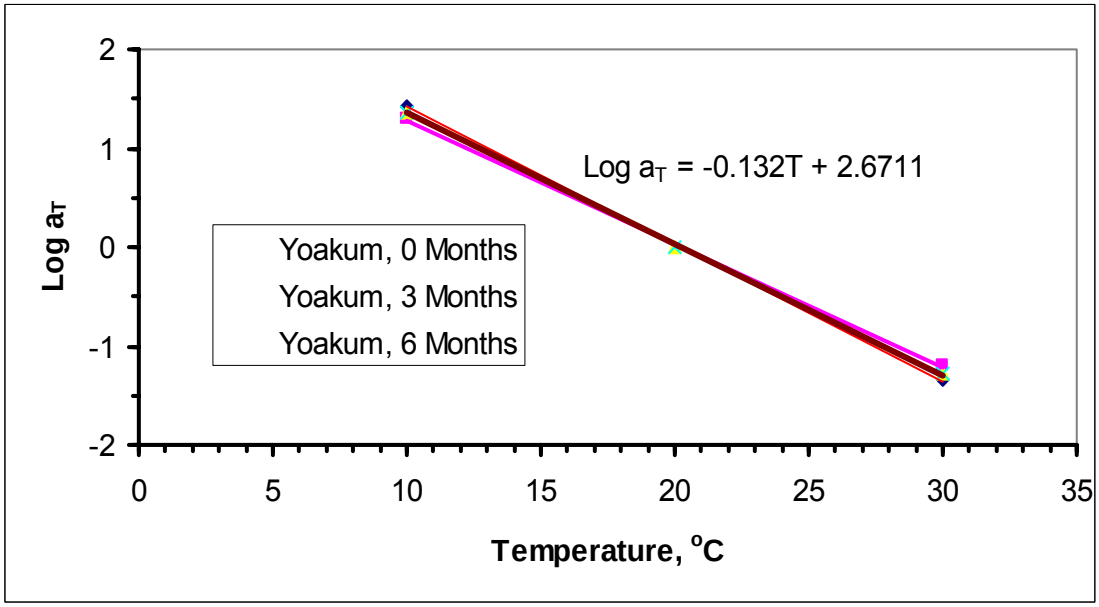

Figure 10-4(b). Temperature Shift Factors, a_T at $T_{Ref=20\ ℃}$ (Yoakum Mixture) (°F = 32 + 1.8(°C)).

- Bryan mixture

$$Log(a_T) = -0.1095T + 2.1978,\ R^2 = 0.998 \qquad \text{(Equation 10-1)}$$

- Yoakum mixture

$$Log(a_T) = -0.132T + 2.6711,\ R^2 = 0.996 \qquad \text{(Equation 10-2)}$$

where:

a_T = Temperature shift factor

T = Temperature of interest (°C)

Dissipated Pseudo Strain Energy and Fracture Damage

Figure 10-5 is a plot of the rate (denoted as constant *b*) of HMAC mixture fracture damage accumulation as a function of the aging condition for each mixture. This constant *b* was calculated as the slope of the plot of DPSE versus log *N* during RDT testing for each mixture type and aging condition, with the test data normalized to 20 °C (68 °F). This parameter *b* is an indicator of the rate of fracture damage accumulation under RDT testing.

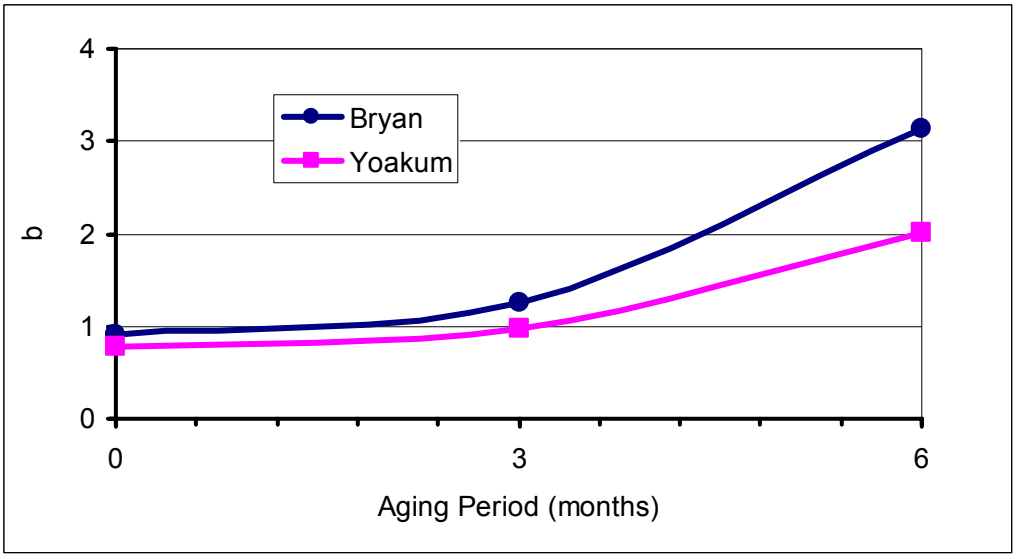

Figure 10-5. Mixture DPSE at 20 °C (68 °F): Constant *b* vs. Aging Condition.

The increasing trend of the *b* value in Figure 10-5 for both mixtures is indicative that the rate of fracture damage accumulation increased with aging. The relatively higher *b* values and greater rate of change (slope of the graphs in Figure 10-5) of the *b* value with aging indicates that the Bryan mixture was accumulating fracture damage at a much faster rate. This observation is evidence that the Bryan mixture was perhaps more susceptible to fracture damage under RDT testing than the Yoakum mixture.

Surface Energy

The average measured SE results in terms of ΔG_f and ΔG_h at 20 °C (68 °F) are shown in Figure 10-6 as a function of aging condition. These SE results shown in Figure 10-6 represent the mixture adhesive bond strengths under dry conditions in the absence of water at an ambient temperature of about 20 °C (68 °F). A minimum of two samples were tested per aging condition.

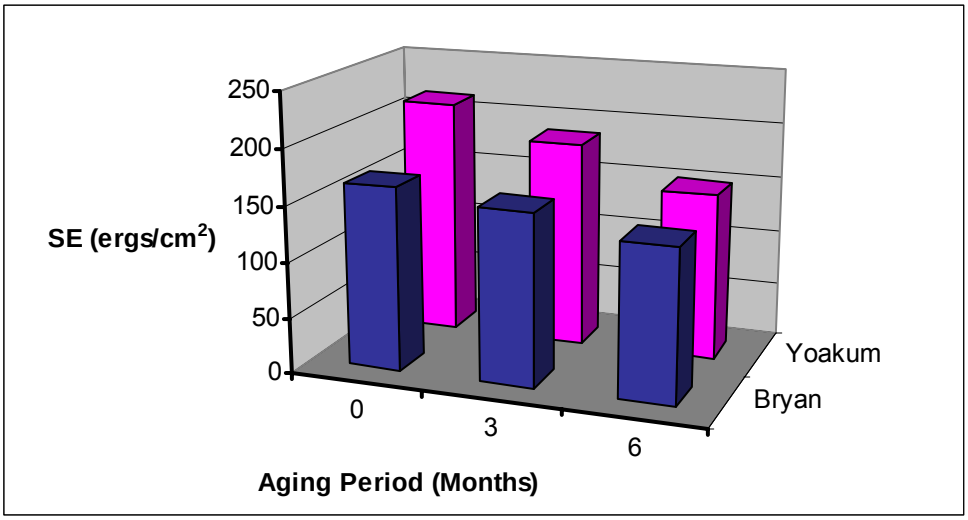

Figure 10-6(a). Mixture Fracture Energy (ΔG_f), ergs/cm^2 (adhesive, dry conditions).

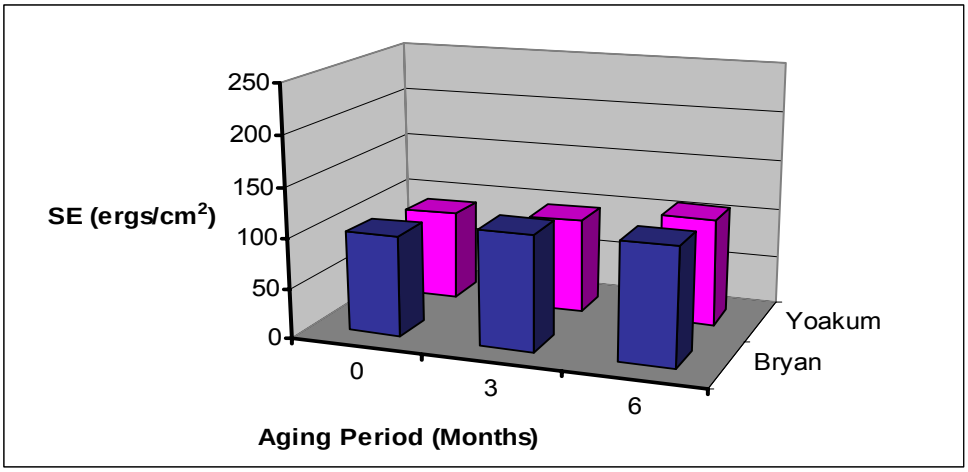

Figure 10-6(b). Mixture Healing Energy (ΔG_h), ergs/cm^2 (adhesive, dry conditions).

Based on simple energy theory concepts, the higher the ΔG_f value, the greater the resistance to fracture damage, and the lower the ΔG_h value, the greater the potential to self heal. With these relationships, the Yoakum mixture has a better adhesive bond strength to resist fracture damage and a stronger potential to self heal, as indicated by the relatively higher fracture and lower healing energies, respectively, compared to the Bryan mixture.

From the SE results in Figure 10-6, the effect on SF_h and Paris' Law fracture coefficient A were determined as shown in Table 10-5. Table 10-5 shows that aging has a significant effect on these parameters (A increased while SF_h decreased with aging). Generally, a lower value of A and higher value of SF_h are indicative of greater resistance to fracture and ability to heal, respectively.

Table 10-5. Paris' Law Fracture Coefficient A and SF_h Value.

Parameter	Mixture	Aging Condition		
		0 Months	3 Months	6 Months
A	Bryan	6.27×10^{-8}	16.00×10^{-8}	23.43×10^{-8}
	Yoakum	5.31×10^{-8}	14.01×10^{-8}	20.64×10^{-8}
SF_h	Bryan	6.73	4.74	3.07
	Yoakum	7.26	4.76	3.81

For the test conditions considered in this project, these limited SE results indicate that:

- ΔG_f decreases and ΔG_h increases with aging.
- Binder oxidative aging reduces HMAC mixture resistance to fracture and ability to self heal. Lytton et al. (*94*) reported similar findings.
- As indicated by the relatively higher ΔG_f and lower ΔG_h values, respectively, the Yoakum mixture had a relatively better resistance to fracture damage and potential to self heal than the Bryan mixture.

In terms of the Yoakum mixture exhibiting relatively better fracture and healing potential properties, the PG 76-22 plus gravel aggregate for the Yoakum mixture as indicated by the SE results exhibits a better adhesive bond strength with the corresponding binder than the component material combination for the Bryan mixture. In other words, the PG 76-22 binder and gravel aggregates were perhaps more compatible in terms of adhesive bond strength than the PG 64-22 and limestone aggregates for the Bryan mixture. Note that SE data are also often used as a measure of material compatibility for HMAC mixture characterization.

The high SBS modified binder content could also have possibly played a role in the relatively better fracture and healing properties of the Yoakum mixture compared to the Bryan mixture. The research team recommends further laboratory HMAC mixture characterization to further explore this issue.

Mixture Anisotropy

Table 10-6 shows the *SFa* results based on mixture AN testing at 20 °C (68 °F). Note that anisotropy arises due to the fact the HMAC mixture properties, such as the elastic modulus, are directionally dependent.

Table 10-6. Mixture Anisotropic Results.

Aging Condition	SF_a	
	Bryan	Yoakum
0 months	1.63	2.10
3 months	1.65	2.08
6 months	2.09	2.40
Average	1.79	2.19

Table 10-8 shows some degree of differences in the SF_a results as a function of mixture type and aging condition. Since anisotropy is predominantly controlled by particle orientation due to compaction, the theoretical assumption is that HMAC mixtures should exhibit similar anisotropic response under all aging conditions. Therefore, the cause of discrepancy could be related to test variability.

Assuming that the SF_a differences are primarily due to test variability and mixture inhomogeneity, the mean SF_a values for the Bryan and Yoakum mixtures can be averaged to be 1.79 and 2.19, respectively, for all aging conditions within an error tolerance of 15 percent (*110*). In terms of the effect of mixture type, some difference in the SF_a values is expected due to the differences in the aggregate gradation that has an effect on the particle orientation during compaction. However, since the 1.79 and 2.19 values do not differ by more than 15 percent, a mean SF_a value of 2.0 is not unreasonable for both the Bryan and Yoakum mixtures for all aging conditions. Aparicio and Oj have reported similar findings (*111*, *112*).

Dynamic Modulus Results

Appendix D includes the mixture |E*| results at 0 months aging condition required for Level 1 fatigue analysis in the M-E Pavement Design Guide for estimating field N_f. And Appendix E is an example of the predicted percent fatigue cracking (in terms of area coverage in the wheelpath) from the M-E Pavement Design Guide software using the HMAC mixture data contained in Appendix D. Note that because the M-E Pavement Design Guide software incorporates Global Aging Model analysis in overall field N_f prediction, the research team considered DM testing of aged mixtures (HMAC specimens) as unnecessary.

HMAC MIXTURE FATIGUE LIVES (N_f)

In this analysis, the research team defined laboratory fatigue life (lab N_f) as the estimated HMAC mixture fatigue resistance without inclusion of any shift factors to simulate field conditions and environmental exposure. Field fatigue life (field N_f) was then calculated as a function of the field shift factors and the HMAC laboratory fatigue life (lab N_f).

Throughout this section and subsequent chapters, the units of fatigue life (lab or field N_f) are defined and expressed in terms of the number of allowable load repetitions to fatigue failure in the laboratory or traffic ESALs in the field. The reference temperature for all the N_f (lab and field) results in this section was 20 °C (68 °F).

ME Lab N_f Results

The predicted mixture lab N_f results from ME analysis described in Chapter 4 for the five pavement structures are attached as Appendix F. These results represent mean values of at least two test specimens. The overall *COV* of Ln N_f considering both mixtures (Bryan and Yoakum) and environmental conditions (WW and DC) ranged between 3.3 percent and 6.8 percent, with a mean Lab N_f value of about 4.60×10^6. Although the *COV* seems to be relatively lower when expressed in terms of Ln N_f, the 95 percent N_f prediction CI margin is very wide, suggesting a high variability and low precision in the predicted N_f results particularly for the Yoakum mixture with the modified binder. For example, for PS#1 and WW environment, the mean lab N_f and 95 percent N_f CI are 4.48×10^6 and 2.12×10^6 to 9.46×10^6 for Bryan mixture and 4.11×10^6 and 0.27×10^6 to 62.99×10^6, respectively. Clearly, there is very high variability associated with the Yoakum mixture for this ME prediction. Inevitably, this result may suggest that the ME approach utilized in this project may not work well with modified binders, and the results need to analyzed and interpreted cautiously.

In terms of mixture lab N_f comparison and the effects of aging, Figure 10-7 shows an example for one pavement structure designated as PS# 1 (Table 3-10) under WW environmental conditions.

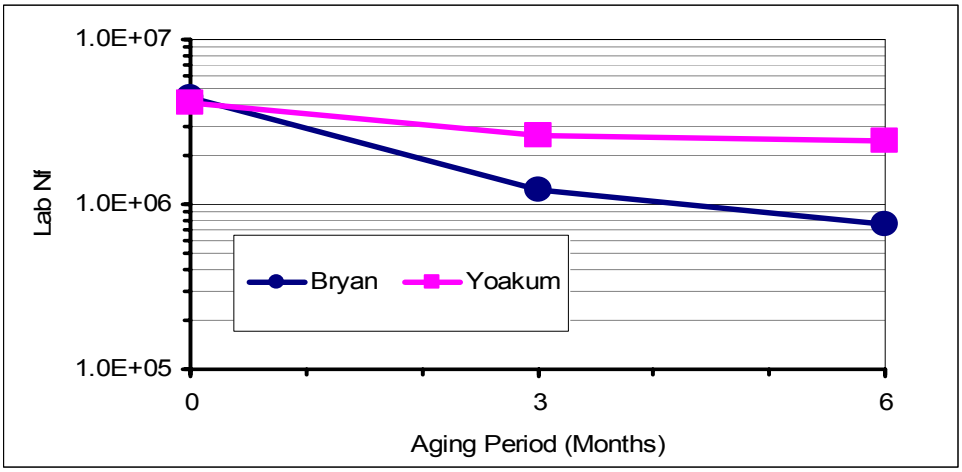

Figure 10-7. Mixture Lab N_f at 20 °C (68 °F) for PS#1, WW Environment (Bryan vs. Yoakum Mixture) – ME Analysis.

For both mixtures, Figure 10-7 shows that N_f decreases with aging, and the Yoakum mixture generally exhibited relatively higher N_f values compared to the Bryan mixture. This trend was observed for all pavement structures in both the WW and DC environmental conditions and is consistent with the prediction from the material property results reported in the preceding sections.

Ln N_f variability in terms of *COV* was comparatively higher for the Yoakum mixture, on the order of about 10 percent more than that of the Bryan mixture. This result is in agreement with Rowe et al.'s suggestion that while the current ME test protocol and analysis procedure may work well for unmodified binders (Bryan mixture), it may not be so with modified binders, and thus the results must be analyzed and interpreted cautiously (*113*).

CMSE Lab N_f Results

Appendix G contains a list of the mixture N_f results consistent with the CMSE analysis procedure described in Chapter 5. Like the ME approach, these results represent mean values of at least two test specimens. In terms of variability, the overall *COV* of Ln N_f ranged between 1.9 and 2.9 percent.

The overall 95 percent lab N_f prediction CI was 0.80×10^6 to 13.12×10^6 with a mean lab N_f value of 6.10×10^6. Considering HMAC mixture inhomogeneity, test variability, and experimental errors, these results are reasonable and indicate better precision compared to the ME approach.

For the given pavement structure (PS# 1, Table 3-7) and environmental conditions (WW), Figure 10-8 indicates that mixture lab N_f decreases with aging and the Yoakum mixture exhibited higher lab N_f values at all aging conditions. Like the ME approach, this trend was observed for all pavement structures in both the WW and DC environmental conditions and was consistent with the measured CMSE mixture material properties.

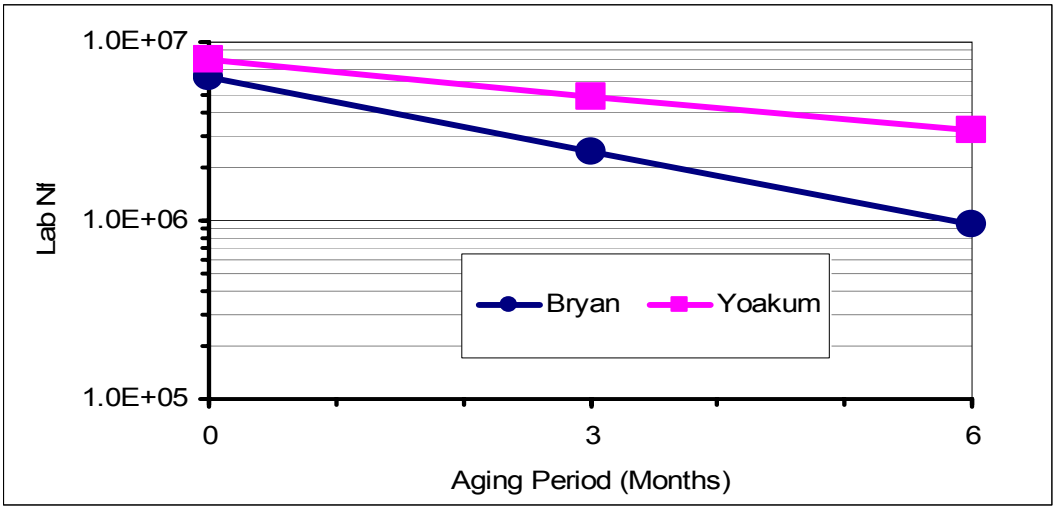

Figure 10-8. Mixture Lab N_f at 20 °C (68 °F) for PS#1, WW Environment (Bryan vs. Yoakum Mixture) – CMSE Analysis.

CM Lab N_f Results

The predicted mixture CM Lab N_f results are tabulated in Appendix J and do not differ significantly from the CMSE results both in terms of the N_f magnitude and variability. Essentially, the mixture N_f results and performance trend were similar to the CMSE results for all pavement structures and environmental conditions for all aging conditions. The mixture N_f, when plotted as a function of aging condition, is shown in Figure 10-9 for PS# 1 under WW environmental conditions.

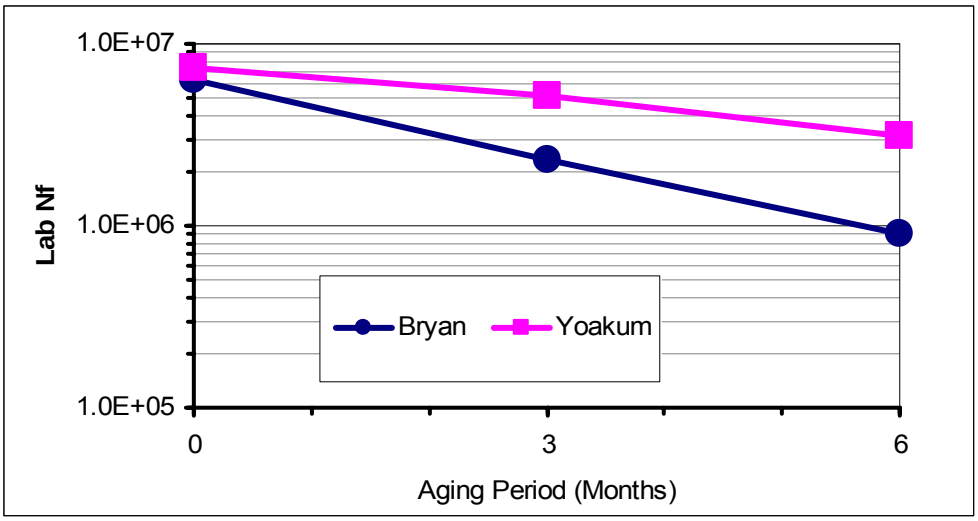

Figure 10-9. Mixture N_f at 20 °C (68 °F) for PS#1, WW Environment (Bryan vs. Yoakum Mixture) – CM Analysis.

Figure 10-9 shows that while the mixture N_f generally decreased with aging, the Yoakum mixture exhibited relatively higher N_f values at all aging conditions. Table 10-7 shows that these CM results are insignificantly different from the CMSE results. Both of these CM and CMSE results (Table 10-7) are for the same pavement structure (PS# 1) under WW environmental conditions.

Table 10-7. CM vs. CMSE Mixture Lab N_f Results for PS#1, WW Environment.

Aging Condition	Mixture	Mixture Lab N_f		Difference
		CMSE	CM	
0 months	Bryan	6.31×10^6	6.29×10^6	-0.32%
	Yoakum	7.88×10^6	7.28×10^6	-7.61%
3 months	Bryan	2.42×10^6	2.31×10^6	-4.55%
	Yoakum	4.95×10^6	5.17×10^6	+4.44%
6 months	Bryan	0.94×10^6	0.91×10^6	-3.19%
	Yoakum	3.23×10^6	3.13×10^6	-3.10%

Overall, this correlation between the CM and CMSE N_f results suggests that the CM approach can be utilized for mixture fatigue analysis in lieu of the CMSE approach, thus minimizing costs in terms of both laboratory testing and data analysis. Note that SE measurements (binder and aggregate) and RM tests in compression are not required in the CM approach. However, this correlation between the CM and CMSE results was expected because the CM empirical analysis models were modified and calibrated to the CMSE approach as discussed in Chapter 5. Consequently, more independent HMAC mixtures need to be characterized for fatigue resistance to validate this CM-CMSE correlation.

Mixture Field N_f Results – ME, CMSE, and CM Analyses

Figure 10-10 is an example of a plot of the field N_f results as a function of aging condition for PS#1 under WW environmental conditions based on the ME, CMSE, and CM analyses. Detailed field N_f results are contained in Appendix I. Note that field N_f is simply a product of field shift factors (SF_i) and the estimated lab N_f as described in Chapters 4 through 7. For this analysis, 0 months aging at 60 °C (140 °F) was considered equivalent to 0 years, 3 months to 6 years, and 6 months to 12 years, respectively, in terms of HMAC pavement age (*52*). Consequently, field N_f is plotted as a function of pavement age, as shown in Figure 10-10.

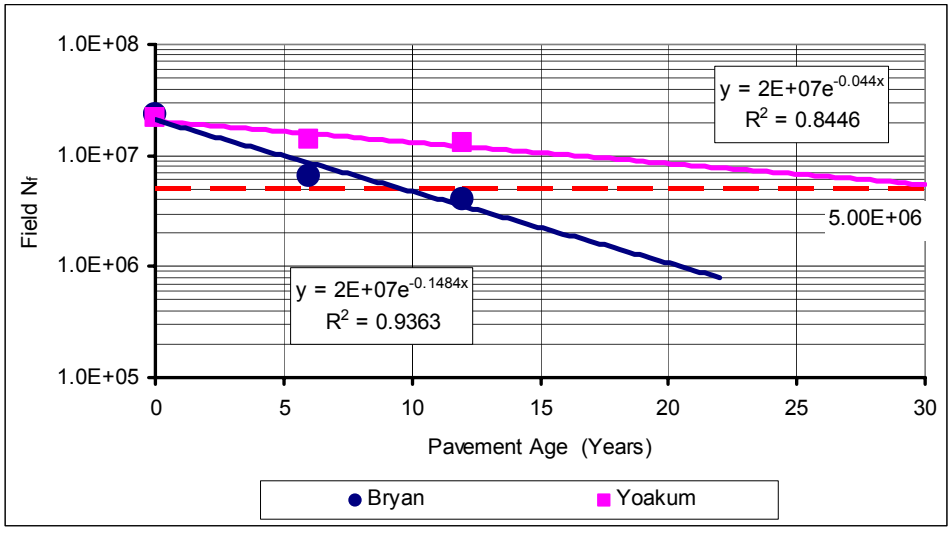

Figure 10-10(a). Field N_f for PS#1, WW Environment – ME Analysis.

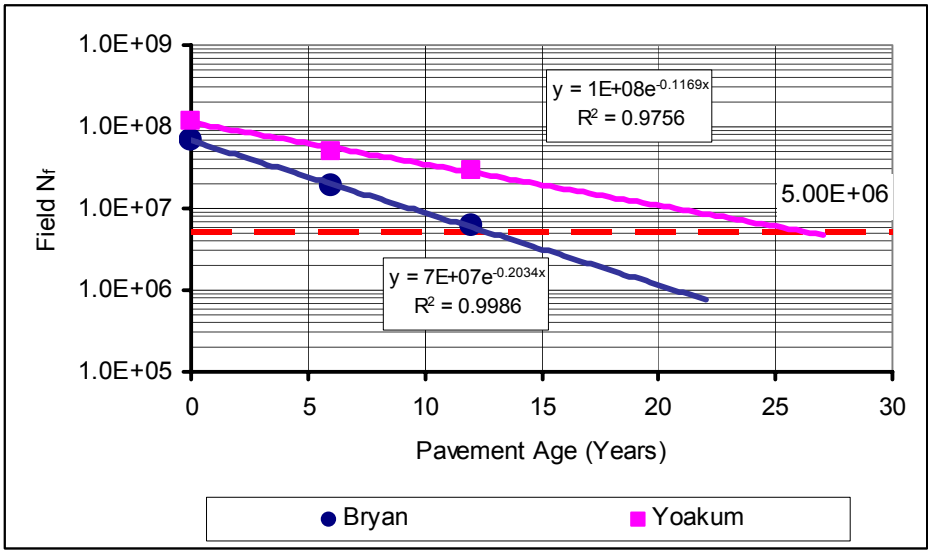

Figure 10-10(b). Field N_f for PS#1, WW Environment – CMSE Analysis.

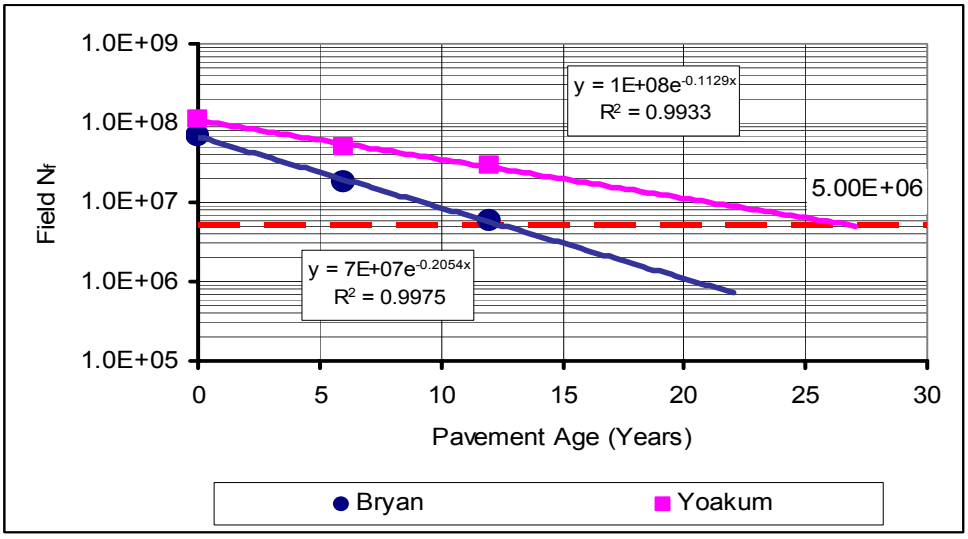

Figure 10-10(c). Field N_f for PS#1, WW Environment – CM Analysis.

Like for the lab N_f, these results indicate a decreasing trend for both mixtures with aging, and the Yoakum mixture exhibits a high field N_f magnitude at all aging conditions. In fact, Figure 10-10, indicates an exponentially declining N_f trend with aging for both mixtures, and the rate of N_f decay is mixture dependent based on the slopes of the exponential trend lines fitted through the N_f data points. Based on the 5×10^6 design traffic ESALs over a 20 year service life at 95 percent reliability level, all fatigue analysis approaches indicate inadequate and adequate theoretical fatigue performance for the Bryan and Yoakum mixture, respectively.

Mixture Field N_f Results – The M-E Pavement Design Guide Analysis

The mixture field N_f results from the M-E Pavement Design Guide software analysis are presented in Appendix I as mean values of at least two test specimens. Unlike the ME and CMSE/CM approaches, these results represent field N_f values that incorporate laboratory-to-field shift factors and effects of aging over a 20 year design period. Essentially, these field N_f results represent the number of traffic ESALs that the HMAC pavement structure can carry over a 20 year design life prior to 50 percent fatigue cracking in the wheelpath. Figure 10-11 is an example of the mixture field N_f results from the M-E Pavement Design Guide software analysis.

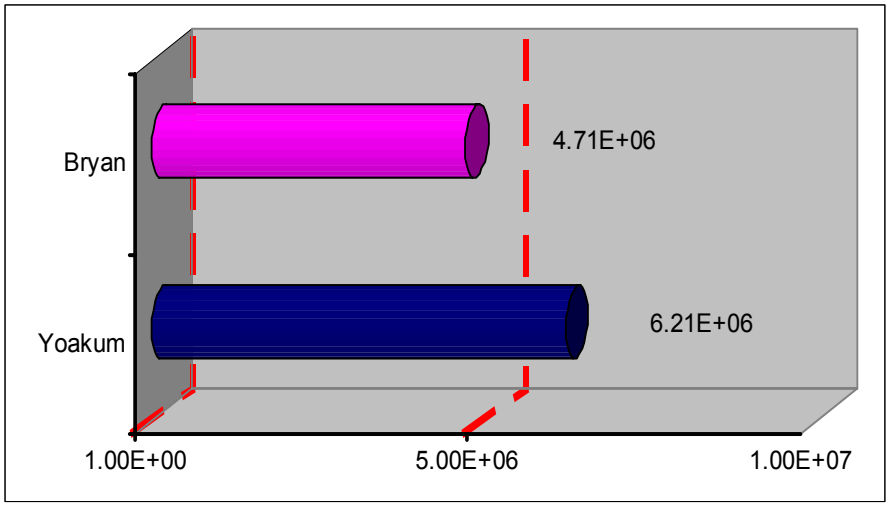

Figure 10-11. Field N_f for PS#1, WW Environment – M-E Design Guide Analysis.

The comparatively higher field N_f values of the Yoakum mixture for PS# 1 under the WW environment shown in Figure 10-11 are consistent with the predictions made by the other fatigue analysis approaches. Considering a 20-year design service life with traffic design ESALs of 5.0×10^6, Figure 10-11 shows that only the Yoakum mixture passes the 50 percent wheelpath cracking failure criterion at 95 percent reliability level. Among other factors, the research team attributed the comparatively better performance of the Yoakum mixture in terms of higher field N_f values to the higher binder content in the mixture. Note that binder content is a direct input parameter in the M-E Pavement Design Guide software, and therefore, field N_f can be tied directly to this parameter.

DEVELOPMENT OF A CMSE-CM SHIFT FACTOR DUE TO AGING

As part of this project's secondary objective, an attempt was made to develop a shift factor (SF_{ag}) that accounts for binder oxidative aging when predicting mixture field N_f using the CMSE and CM approaches. This section discusses the SF_{ag} development based on the binder dynamic shear rheometer tests that were conducted by CMAC. The CMSE and CM field N_f predictions using the developed SF_{ag} and field N_f at 0 months are also provided.

Theoretical Basis and Assumptions

In this analysis, the SF_{ag} was solely based on neat binder shear properties and the following assumptions, where neat binder refers to binder not mixed with aggregate but that directly aged in thin films:

- SF_{ag} was considered as a multiplicative factor that tends to reduce N_f, and therefore, its magnitude was postulated to range between 0 and 1 ($0 < SF_{ag} \leq 1$). A numerical SF_{ag} value of 1 represents unaged conditions or no consideration of aging effects in N_f analysis.
- SF_{ag} was only considered as a function of the neat binder properties in terms of the DSR function (DSR_f) and oxidative aging period (time). The hypothesis is that only the binder in the HMAC mixture ages, and therefore, it is not unreasonable to determine SF_{ag} solely based on binder properties. The idea is that researchers and/or end-users would only measure unaged and aged binder properties without having to measure aged mixture properties and thereafter estimate SF_{ag} and ultimately predict aged mixture field N_f from unaged mixture field N_f.
- The DSR_f was utilized on the hypothesis that this function provides a better representation of the binder shear properties in terms of ductility and durability, properties that are considered critical to fatigue performance for aged HMAC field pavements (*52*). The DSR function's correlation with ductility, durability, and HMAC pavement age is discussed in Chapter 8 of this report.

- The binder oxidative aging conditions as conducted by CMAC were consistent with the stirred air flow test and pressure aging vessel (PAV*) procedures to simulate both short-term aging that occurs during the hot-mixing process and construction operations and long-term aging during service (*97*). These laboratory aging conditions were SAFT + PAV* 0 hrs, SAFT + PAV* 16 hrs, and SAFT + PAV* 32 hrs, respectively, and simulate approximately up to 6 years of Texas field HMAC aging exposure (*52*,*97*).
- In contrast to SAFT + PAV* laboratory aging of binders, field aging is a relatively complex process involving fluctuating environmental conditions and a general decreasing AV content due to traffic compaction. These factors were not directly taken into account by the SF_{ag} developed in this study. It must also be emphasized that the effect of aging on HMAC mixture fatigue resistance is considered as a three stage process involving binder oxidation, binder hardening, and mixture field N_f decay. Additionally, mixture design parameters such as binder content and polymer modification probably also play a significant role in these three processes.

SF_{ag} Formulation and the Binder DSR Master-Curves

In this project, the SF_{ag} was formulated as a function of the DSR data from the binder DSR master-curve, as shown by Equation 10-5.

$$SF_{ag} = u\left[\chi(t)\right]^{w} \quad \text{(Equation 10-5)}$$

$$\chi(t) = \left(\frac{m'@t_i}{m'@t_0}\right)\left(\frac{DSR_{f(1)}@t_0}{DSR_{f(1)}@t_i}\right) \quad \text{(Equation 10-6)}$$

$$DSR_f = \left[G'/(\eta'/G')\right] \quad \text{(Equation 10-7)}$$

$$DSR_f(\varpi) = DSR_{f(1)}(\varpi)^{m'} \quad \text{(Equation 10-8)}$$

where:

SF_{ag} = Shift factor due to binder oxidative aging

$\chi(t)$ = Material property ratio that relates the aged to the unaged binder shear properties as a function of time

u, w = Material regression constants

m' = Slope of the binder $DSR_f(\omega)$ master-curve at a reference temperature of 20 °C (68 °F)

ϖ = Reduced angular frequency (rad/s)

$DSR_{f(1)}$ = $\left[G'/(\eta'/G')\right]$ at 1 rad/s (Pa·s)

G' = Elastic dynamic shear modulus (MPa)

η' = Dynamic viscosity (Pa·s)

Figure 10-12 is a plot of the binder DSR master-curves on a log-log scale in the form of a power function expressed by Equation 10-8. These binder DSR master-curves were generated from DSR test data that were measured at three test temperatures of 20, 40, and 60 °C (68, 104, and 140 °F), respectively within an angular frequency of 0.1 to 100 rad/sec. For analysis simplicity, SAFT+PAV* 0 hr was assumed to be equivalent to 1 year Texas field HMAC exposure, SAFT+PAV* 16 hrs to 2 years, and SAFT+PAV* 32 hrs to 6 years, respectively (*52*). The SF_{ag} at 0 years field HMAC exposure was arbitrary assigned a numerical SF_{ag} value of 1.0 on the premise that no significant aging occurs during this period. Based on the data from Figure 10-12 and using Equation 10-5 (with $u \cong w \cong 1$), SF_{ag} values were estimated as a function of pavement age, as shown in Table 10-8.

Table 10-8. CMSE-CM SF_{ag} Values.

Pavement Age (Years)	SF_{ag}	
	PG 64-22 (Bryan)	PG 76-22 (Yoakum)
0	1.000	1.000
1	0.854	0.783
2	0.330	0.303
6	0.160	0.221
12	0.073	0.109
18	0.049	0.081
20	0.045	0.070

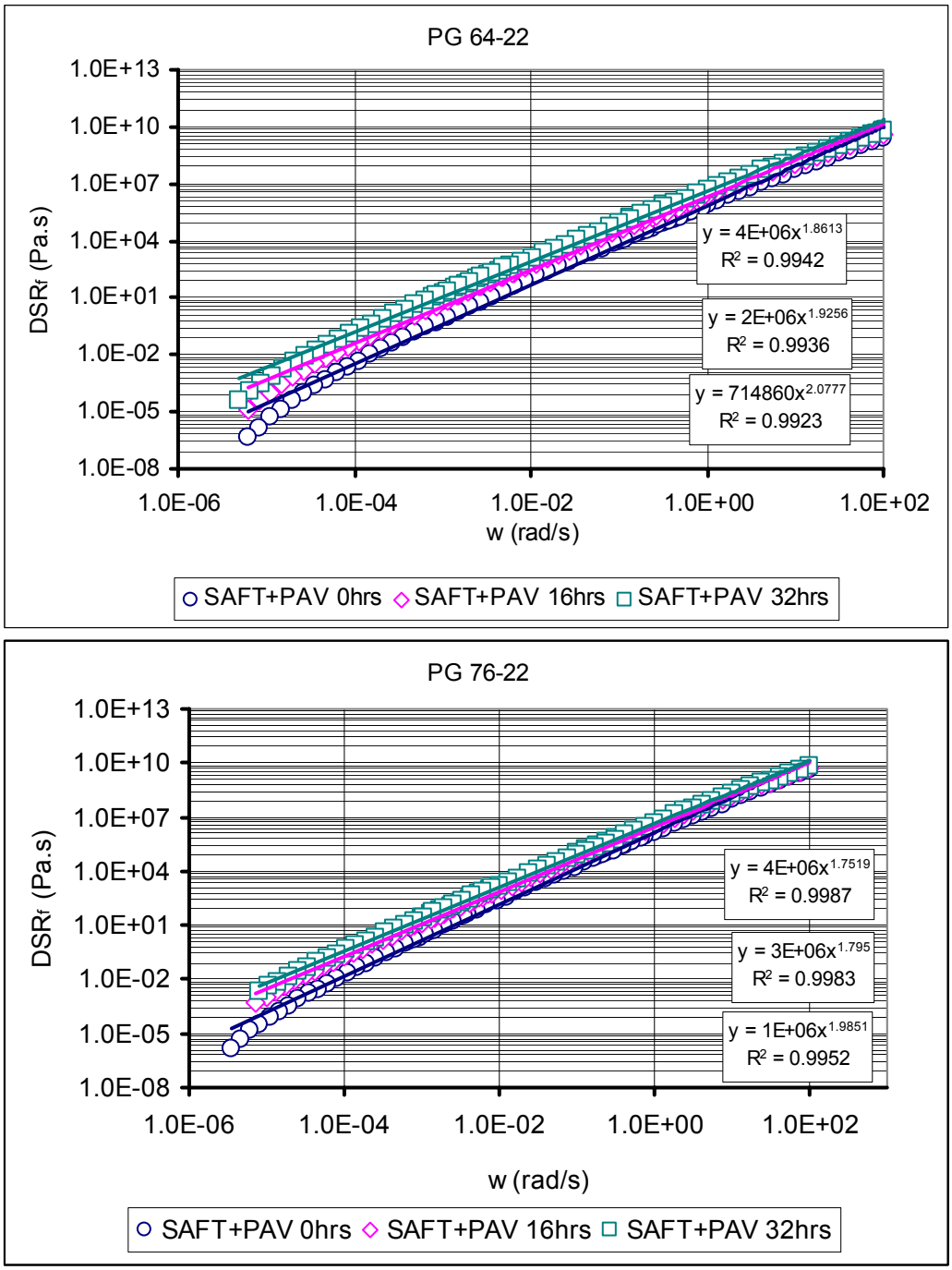

Figure 10-12. Binder $DSR_f(\omega)$ Master-Curves at 20 °C (68 °F).

Note that SF_{ag} values beyond 6 years field HMAC exposure were determined based on the SAFT+PAV* 0 hrs, SAFT+PAV* 16 hrs, and SAFT+PAV* 32 hrs data. Additional laboratory aging conditions are recommended, i.e., SAFT+PAV* 64hrs that may be realistically close to a 20 year field HMAC exposure, which is consistent with typical HMAC pavement design periods.

CMSE-CM Field N_f Prediction Using SF_{ag}

Using the SF_{ag} data in Table 10-8 and the field N_f at 0 years field HMAC exposure, the field N_f at any pavement age can be estimated using the following relationship:

$$Field\ N_{f(t_i)} = SF_{ag(t_i)} \times Field\ N_{f(t_0)} \qquad \text{(Equation 10-9)}$$

Table 10-9 provides an example of the estimated field N_f at year 20 for PS#1 and the WW environment. Predictions for other PSs and the DC environment are contained in Appendix I.

Table 10-9. Example of Field N_f Predictions at Year 20 (PS#1, WW Environment).

Approach	Mixture	Field N_f Value @ Year 20
CMSE	Bryan	3.11×10^6
	Yoakum	8.40×10^6
CM	Bryan	3.10×10^6
	Yoakum	7.77×10^6
Design traffic ESALs over 20 year design period at 95 percent reliability level: 5.00×10^6		

From Table 10-9, the field N_f estimate by the two approaches do not differ significantly. In fact, both approaches indicate inadequate and adequate theoretical fatigue performance for Bryan and Yoakum mixtures, respectively, based on a 5.00×10^6 design traffic ESAL over a 20-year design period at 95 percent reliability level. For this pavement structure (PS#1), these results are comparable to the predictions by the M-E Pavement Design Guide of 4.71×10^6 and 6.21×10^6 for the Bryan and Yoakum mixtures, respectively. For the ME approach, the predictions are approximately 1.03×10^6 and 8.30×10^6 for the Bryan and Yoakum mixture, respectively, based on extrapolations and the exponential relationships in Figure 10-10(a).

SUMMARY

In this chapter, the HMAC mixture results were presented and the following summarizes the key findings (based on the test conditions considered in the project).

BB Testing

- The number of laboratory load cycles to failure denoted as N (without subscript f) decreased with binder oxidative aging.
- The Yoakum mixture performed better in terms of the number of N to failure during BB testing at 20 °C (68 °F).

Tensile Stress

- Due to more brittle behavior with binder oxidative aging, the mixture tensile failure strain (ε_f) at break under tensile loading at 20 °C (68 °F) decreased significantly with aging.
- While the tensile stress at break (σ_t) did not vary significantly as a function of aging and was within the expected test variability, the Yoakum mixture exhibited more ductility at all aging conditions compared to the Bryan mixture.
- With aging, the failure mode under tensile loading for each mixture changed from ductile to brittle, indicating a decrease in mixture ductility with aging.

Relaxation Modulus

- While the mixture elastic relaxation modulus (E_1) increased with binder oxidative aging due to stiffening effects, the RM results indicated that the Yoakum mixture had a better potential to relax stress than the Bryan mixture based on a larger m value. However, as expected, the ability to relax the stress (m value) generally decreased with aging for both mixtures.

- Although designed with a relatively softer PG 64-22 binder, the relaxation modulus (E_1) of the Bryan mixture was relatively higher than that of the Yoakum mixture designed with a stiffer SBS modified PG 76-22 binder, particularly after aging. These results are suggestive that for the test conditions considered in this project, the Bryan mixture was perhaps more susceptible to stiffness age-hardening due to binder oxidative aging.
- The logarithm of the temperature shift factor (Log a_T) determined when generating the RM master-curves exhibited a linear relationship with temperature, but this parameter was insensitive to binder oxidative aging conditions. By contrast, Log a_T exhibited some degree of sensitivity to HMAC mixture type.

DPSE and SE Results

- The DPSE results indicated that the Bryan mixture was more susceptible to fracture damage than the Yoakum mixture, and the rate of fracture damage accumulation generally increased with aging.
- The SE results indicated better adhesive bond strength for the Yoakum mixture relative to the Bryan mixture, and mixture resistance to fracture and potential to heal as measured in terms of SE magnitude generally decreased with aging.

Mixture Anisotropy

- Within a ±15 percent error tolerance, mixture anisotropy (SF_a) was observed to be insignificantly affected by binder oxidative aging and did not vary substantially as a function of mixture type. Consequently, a mean SF_a value of 2.0 was proposed for both the Bryan and Yoakum mixtures for all aging conditions.

Mixture N_f

- When comparing the two mixtures for the test conditions considered in this project:
  - The Yoakum mixture exhibited better fatigue resistance than the Bryan mixture in terms of the magnitude of both lab and field N_f.
  - The Yoakum mixture was more resistant to fracture damage, had a better potential to heal, and was less susceptible to aging compared to the Bryan mixture.
- An attempt was made to develop shift factors due to aging (SF_{ag}) based on the binder DSR function for the CMSE and CM approaches. While the SF_{ag} methodology utilized produced reasonable results, validation of these concepts is still required through testing of additional binders and HMAC mixtures, possibly with longer laboratory aging periods that realistically simulate current HMAC pavement design practices. The further development of representative SF_{ag}, particularly as a function of time, with more research will inevitably allow for realistic N_f predictions at any desired pavement age. Furthermore, there is a need to incorporate mixture volumetric properties such as AV and binder content in the SF_{ag} model. These volumetric properties are hypothesized to play a significant role in the aging phenomenon of HMAC mixtures due to binder oxidation.

CHAPTER 11
DISCUSSION AND SYNTHESIS OF RESULTS

This chapter compares and discusses the mixture field N_f results and variability including the effects of other input variables, and binder oxidative aging. BM characterization and another proposed methodology for the aging shift factor (SF_{aging}) analysis for the CMSE approach are also discussed.

COMPARISON OF MIXTURE FIELD N_f

Generally, all fatigue analysis approaches predicted higher N_f (both lab and field) values for the Yoakum mixture under all aging and environmental conditions for all pavement structures. Mixture property results discussed in Chapter 10 also indicated that the Yoakum mixture had better fatigue resistant properties than the Bryan mixture and was therefore expected to perform better in terms of N_f (lab or field) magnitude under the test conditions considered in this project. Figure 11-1 is an example of the mixture field N_f for WW environmental conditions for PS# 1.

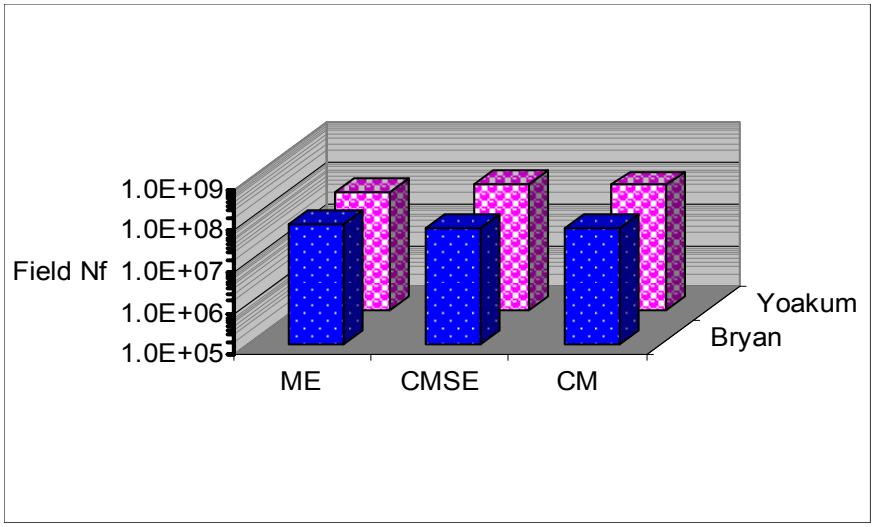

Figure 11-1(a). Mixture Field N_f (0 Months, PS#1, WW Environment).

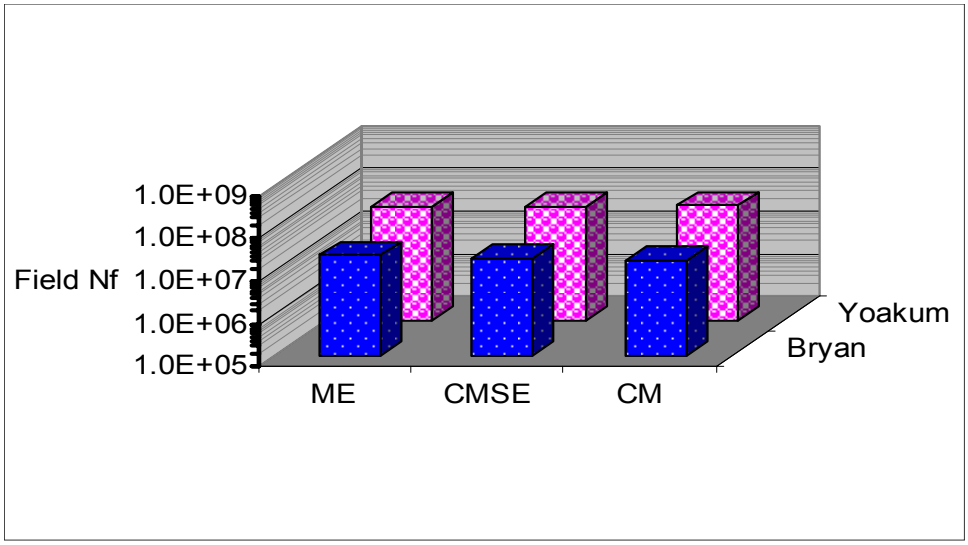

Figure 11-1(b). Mixture Field N_f (3 Months, PS#1, WW Environment).

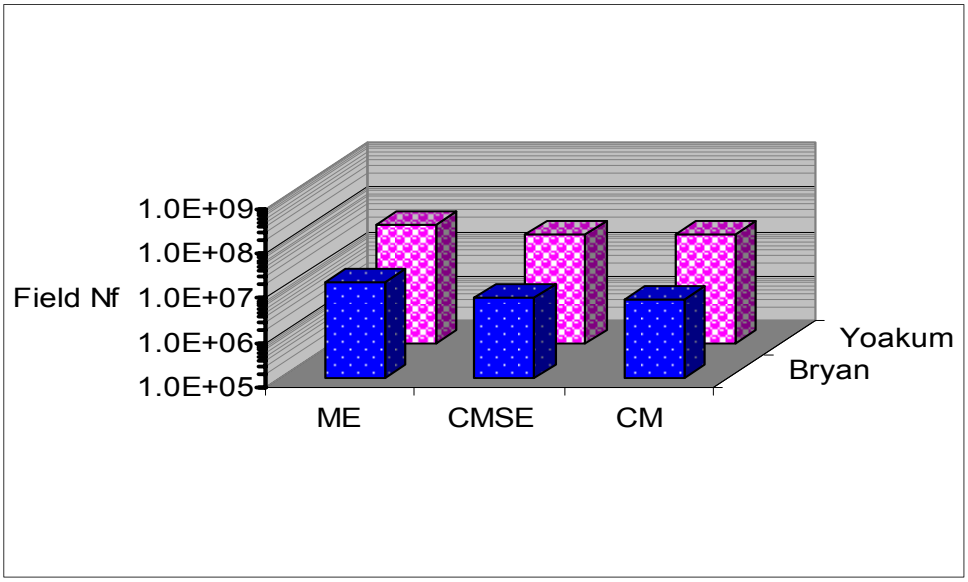

Figure 11-1(c). Mixture Field N_f (6 Months, PS#1, WW Environment).

Figure 11-1(a) represents field N_f values that were measured at 0 months with no aging effects being considered. The 3 and 6 months field N_f results for the ME, CMSE, and CM approaches in Figures 11-1(b) and (c) represent approximately 3 to 6 years of field aging (*52*).

Figures 11-1(a), (b), and (c) show better fatigue resistance for the Yoakum mixture in terms of field N_f magnitude. Note that the difference (Figure 11-1) in the field *Nf* values between the two mixtures gets more significant as aging progresses, indicating that the Bryan mixture's fatigue life was decaying much faster than that of the Yoakum mixture. This result is consistent with the material property results reported in Chapter 10.

The M-E Pavement Design Guide results represent field N_f values at year 20 and incorporates laboratory-to-field shift factors and effects of aging through the GAM over the entire 20 year design period and were not included in Figures 11-1(a), (b), and (c). These M-E Pavement Design Guide results are included in Figure 11-1(d), which is an example of the mixture field N_f prediction comparison based on a 20-year design life and 95 percent reliability level for PS# 1 under the WW environment.

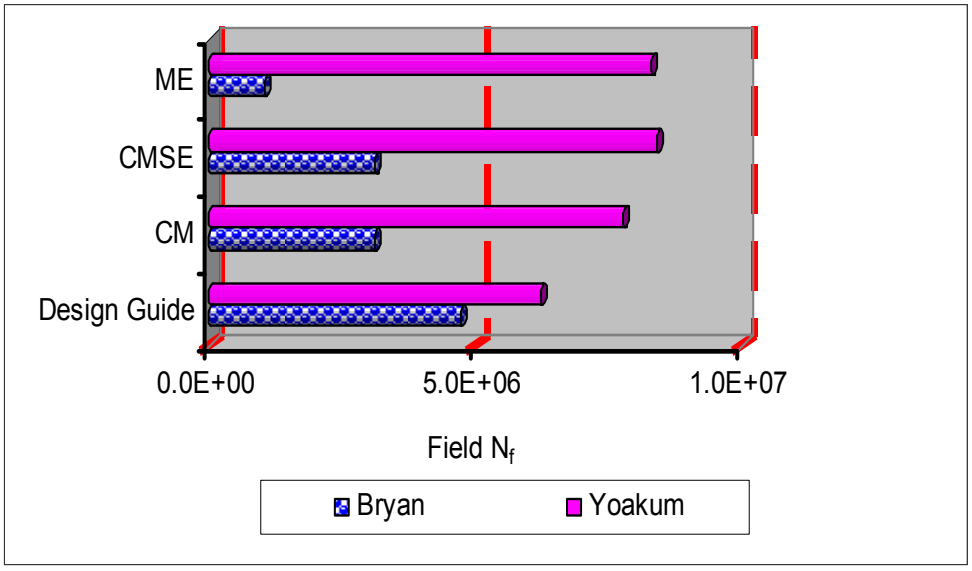

Figure 11-1(d). Mixture Field N_f Comparison (PS#1, WW Environment)

For all the fatigue analysis approaches, Figure 11-1(d) shows better fatigue resistance for the Yoakum mixture in terms of field N_f magnitude compared to the Bryan mixture. Based on the 5×10^6 design traffic ESALs and 20 years service life at 95 percent design reliability level for this pavement structure and the environmental conditions under consideration, all the fatigue analysis approaches (although with different failure criteria) indicate inadequate and adequate theoretical fatigue performance for the Bryan and Yoakum mixtures, respectively.

Considering that the Yoakum mixture was designed with a relatively stiffer SBS modified PG 76-22 binder, this relatively better fatigue performance in terms of field N_f results was theoretically unexpected. In fact, the theoretical expectation was that the Yoakum mixture's fatigue performance in terms of field N_f magnitude would be worse compared to the Bryan mixture. However, the research team attributed this response behavior to the following factors:

- Compared to the Bryan mixture, the Yoakum mixture had relatively higher binder content (5.6 percent versus 4.6 percent by weight of aggregate).
- Contrary to theoretical expectations based solely on stiffness alone, the SBS modifier probably improved the Yoakum mixture's fatigue resistance as well as reduced its susceptibility to binder oxidative aging.
- The Yoakum mixture incorporated a 1 percent hydrated lime in the mixture design. Although lime is often added to improve mixture resistance to moisture damage, this lime perhaps increased the mixture's resistance to both fatigue damage and aging. Wisneski et al. made similar observations that lime tended to improve the performance of recycled asphalt (*114*).
- SE results in Chapter 10 indicated a better fracture resistance and stronger potential to heal for the Yoakum mixture than for the Bryan mixture. Based on these SE results, it can be theorized that the PG 76-22 binder-gravel aggregate has an increased bond strength compared to that of the PG 64-22 binder-limestone aggregate combination. Note that one of the SE measurements' objectives is often to asses the affinity and bond (cohesive and/or adhesive) strength of binders and aggregates. Theoretically, a comparatively better bond strength compatibility between the binder and aggregate (in this case for the Yoakum mixture) is generally expected to exhibit superior performance.
- Tensile strength and RM results in Chapter 10 indicated that the Yoakum mixture was more ductile and less susceptible to stiffness age-hardening compared to the Bryan mixture, properties which probably contributed to its higher field N_f values. Additionally, the Yoakum mixture exhibited better potential to relax the stress, as indicated by higher m values, compared to the Bryan mixture.

Although theoretically possible, the research team considers that it may be inappropriate and/or rather complex to make a direct comparison between these two mixtures because their mix-design characteristics (binder content, aggregate type and gradation) and materials (the aggregates) were different. Therefore, because of the many existing variable parameters, the comparison of these two HMAC mixtures may be inconclusive.

Overall, these results, however, suggests that binder stiffness or initial mixture stiffness alone may not be used as the sole determinant or measure of HMAC mixture fatigue resistance or field fatigue performance. A mixture designed with a stiffer binder may not necessarily imply that it will perform poorly in fatigue compared to a mixture designed with a softer binder. The entire mix-design matrix and spectrum of material properties need to be evaluated, particularly in performance comparison studies of this nature. Equally to be considered is the pavement structure, the environmental conditions, and the mixture sensitivity to aging in terms of binder oxidation and stiffness age-hardening rate and probably even the binder's potential to heal.

MIXTURE VARIABILITY

As observed in Chapter 10, there was generally a high variability in the Yoakum mixture results, both in terms of mixture properties and field N_f results (*COV* of Ln N_f). Compared to the Bryan mixture, the Yoakum mixture consists of a stiffer SBS modified PG 76-22 binder that is relatively harder to work with when mixing, compacting, and sawing/coring. Table 11-1 shows an example of the mixture AV variability.

Table 11-1. Example of HMAC Specimen AV Variability.

Specimen	Mixture	Target AV	Average AV	Stdev	*COV*
Cylindrical	Bryan	7±0.5%	7.23%	0.20	2.81%
	Yoakum	7±0.5%	7.10%	0.35	5.94%
Beam	Bryan	7±0.5%	7.18%	0.29	4.04%
	Yoakum	7±0.5%	6.98%	0.55	7.87%

Table 11-1 represents the average AV content of 10 random sample specimens per specimen type per mixture type. Although the *COV* values are reasonably acceptable, Table 11-1 clearly shows the high variability in the AV content for the Yoakum mixture. Modified binders are generally more difficult to work with, and consequently, it is more difficult to control the AV content, which was ultimately reflected in the high variability of the final results. For this Yoakum mixture, the other compounding factor may have been the higher binder content. Not only was the PG 76-22 binder stiffer and difficult to work with, its content in the mixture was also higher relative to the PG 64-22 of the Bryan mixture.

From Table 11-1, it is also worthwhile to note the relatively high variability in the AV for the beam specimens. In this project, it was generally more difficult to control the AV for the beam specimens during compaction due to the nature of their shape and the kneading compaction method. This high variability in the AV content was also reflected in the final ME lab N_f results discussed in Chapter 10 and the field N_f results shown in Table 11-2. The cylindrical specimens, on the other hand, are compact and easy to handle, and the gyratory compaction method allows for better control of the AV content.

Mixture field N_f results generally indicated higher variability with the Yoakum mixture and for the ME approach for all PSs, environmental, and aging conditions. Table 11-2 gives a summary example of the mixture field N_f statistical analysis in terms of the *COV* of Ln N_f and the 95 percent CI for PS#1 and WW environment based on a 20-year design period.

Table 11-2. Example of Mixture Field N_f Variability (PS#1, WW Environment).

Approach	**Mixture**	**Field N_f**		
		Mean Value	***COV* of Ln N_f**	**95% CI**
ME	Bryan	1.03×10^6	6.87%	$0.49 – 2.17 \times 10^6$
	Yoakum	8.30×10^6	9.85%	$5.41 – 16.74 \times 10^6$
CMSE	Bryan	3.11×10^6	2.81%	$3.08 – 3.21 \times 10^6$
	Yoakum	8.40×10^6	3.92%	$6.95 – 9.82 \times 10^6$
CM	Bryan	3.10×10^6	2.93%	$2.98 – 4.47 \times 10^6$
	Yoakum	7.77×10^6	3.98%	$6.12 – 8.08 \times 10^6$
M-E Design Guide	Bryan	4.71×10^6	-------	$1.93 – 9.74 \times 10^6$
	Yoakum	6.21×10^6	-------	$2.04 – 15.34 \times 10^6$
Design traffic ESALs over 20 year design period at 95 percent reliability level: 5.00×10^6				

From Table 11-2, it is evident that variability in terms of *COV* of *Ln* N_f and 95 percent CI is relatively higher for the Yoakum mixture. These *COV* values seem low because they are expressed in terms of logarithmic response, which provides a better statistical analysis in terms of an assumed normal distribution. However, they nonetheless provide a comparative basis for the approaches. Note that no *COV* of *Ln* N_f values are reported for the M-E Pavement Design Guide in Table 11-2. This is due to the nature of the back-calculation analysis of field N_f at 50 percent cracking using percentage cracking output values from the M-E Pavement Design Guide software. The N_f backcalculation analysis does not allow for a realistic determination of representative *COV*s. Although three specimens were used for each mixture, the output is just one single field N_f value.

From Table 11-2, it is clearly evident that the ME exhibited the highest statistical variability, both in terms of the *COV* values and 95 percent CI range (particularly for the Yoakum mixture with the modified binder). The CMSE, in contrast, exhibited the least statistical variability as measured in terms of the *COV* values of *Ln* N_f and 95 percent CI range.

EFFECTS OF OTHER INPUT VARIABLES ON MIXTURE FIELD N_f

Among other variables, mixture fatigue performance is dependent on the pavement structure and environment. The effect of these variables on mixture field N_f and fatigue performance assuming similar traffic loading conditions are discussed in this section.

Pavement Structure

HMAC mixture field N_f prediction and fatigue performance is a function of the strain (tensile or shear) as the failure load-response parameter. For any given pavement structure (assuming similar traffic loading and environmental conditions), the critical maximum design strain is computed as a function of the number of structural layers, layer thicknesses, and the E_i and ν values of the respective layers. Figure 11-2 is an example of the effect of pavement structure on the mixture field N_f under WW environmental conditions based on a 20 year design period for the Bryan mixture. Structural details of the pavement structures (PS# 1, PS# 4, and PS# 5) shown in Figure 11-2 are summarized in Table 3-7.

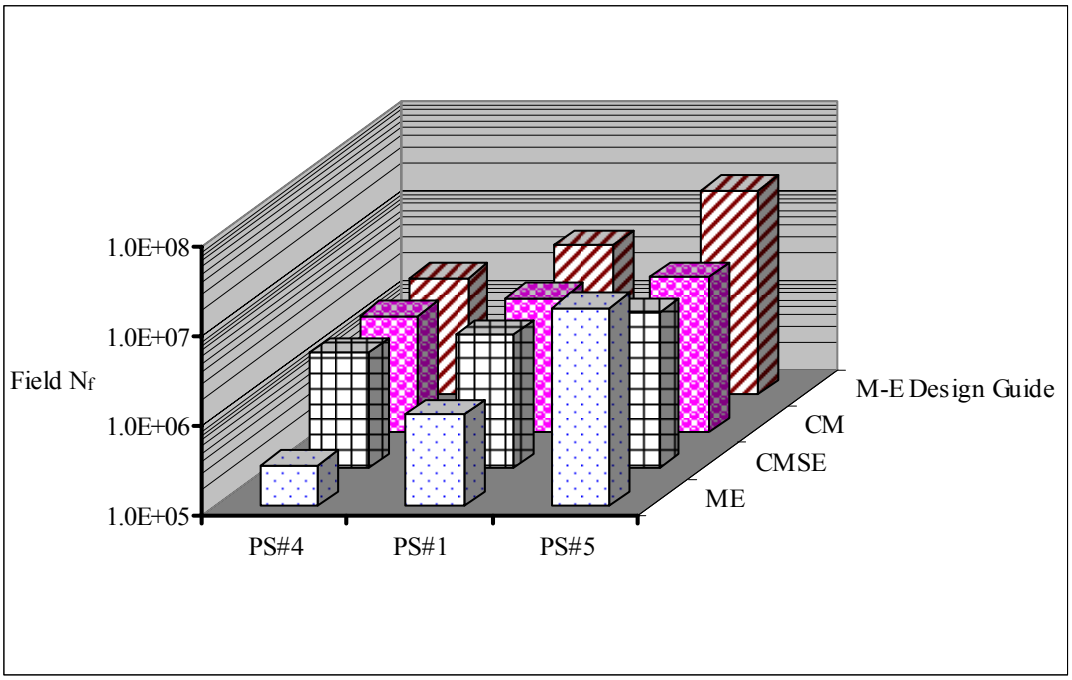

Figure 11-2. Effect of Pavement Structure on Mixture Field N_f (Bryan Mixture, WW Environment).

In terms of fatigue analysis, the optimum combination of the number of layers, layer thicknesses, and E_i values that gives the lowest critical maximum design strain will result in higher field N_f value and better fatigue performance in the field. Because fatigue cracking initiates due to horizontal tensile and/or shear strains in the HMAC layer that exceed the capacity of the HMAC, pavement structures with higher values of the critical maximum design strain will generally be more susceptible to fatigue cracking than those with lower values.

PS# 5 in Figure 11-2 has the least critical maximum design strain (Table 3-7) and therefore highest field N_f values for all the fatigue analysis approaches. According to Table 3-7, PS# 1 and 5 are three-layered pavement structures (including the subgrade), while PS# 4 is four-layered. However, the relatively 4 inch thick HMAC layer in PS# 5 is resting on a stiff cemented base that provides support for the loading and produces lower strains in the top HMAC layer, and subsequently higher field N_f values.

Ultimately, these results demonstrate the inseparable nature of pavement structural design and HMAC mix-design for fatigue resistance. HMAC mixture fatigue resistance cannot be modeled explicitly without consideration of a representative field pavement structure.

Environmental Conditions

As discussed in Chapters 2 and 3, environmental conditions have a significant effect on the pavement material properties in terms of the E_i values. These E_i values, in turn, have an effect on the design strain that ultimately has an effect on N_f. Figure 11-3 shows the effect of environmental conditions for PS# 1 based on the M-E Pavement Design Guide analysis that incorporates a very comprehensive climatic analysis model.

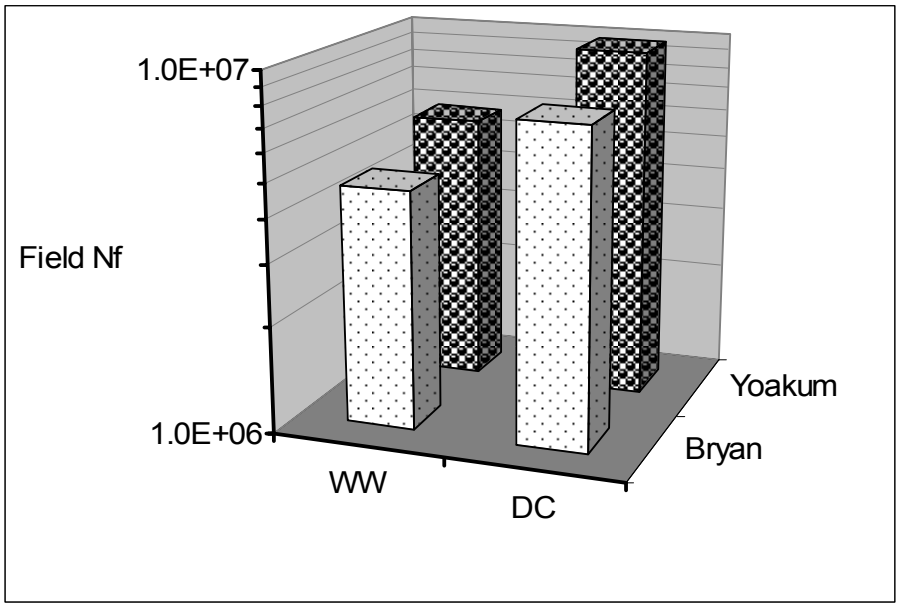

Figure 11-3. Effect of Environmental Conditions on Mixture Field N_f (PS#1).

From Figure 11-3, both mixtures exhibited relatively higher field N_f values in the DC environment. The lower field N_f values in the WW environment are possibly due to the wetting effect (presence of moisture) that had a significant effect on the E_i values of the unbound pavement layers, including the subgrade. Note that the presence of moisture within and/or underneath a PS is to reduce the E_i value that ultimately results in a higher ε_t value in the HMAC layer.

Overall, these results indicate that HMAC mixture fatigue resistance is pavement structure and environmental location dependent. The results signify the importance of adequately interfacing HMAC mix-design and fatigue characterization with pavement structural design and analysis to achieve adequate field fatigue performance.

BINDER TEST RESULTS AND EFFECTS OF AGING

Two binders, an unmodified PG 64-22 and a polymer-modified PG 76-22, were used in this project. Neat binders and binders recovered from laboratory mixtures, at several levels of aging, were evaluated. Neat binders were aged in a HMAC simulation, the stirred air-flow test, to give one level of aging. Then these binders were further aged in the 60 °C (140 °F) environmental room in thin films (approximately 1 mm [0.039 inches] thick) for 3 and 6 months to obtain a second and third aging level (SAFT+3M and SAFT+6M). For recovered binders, aging states were obtained by aging two asphalt-aggregate mixtures (designated Bryan and Yoakum). The mixtures were prepared using the PP2 short-term aging protocol and then compacted; this method produced one aging level (PP2+0M). The second and third levels were obtained by aging the compacted laboratory mixture in the environmental room for 3 and 6 months beyond PP2 conditioning (PP2+3M and PP2+6M). Note that the "0 months," "3 months," and "6 months" refer to environmental room aging *beyond* PP2 aging so that 0 months aging still has a significant level of aging beyond SAFT aging.

The binders in the compacted mixtures were extracted and recovered according to the procedure outlined in Chapter 8. SEC was used to check whether the solvent residues exist in the binder. SEC chromatograms for recovered binders from Bryan mixtures are shown in Figure 11-4 and show that the recovered binders did not have solvent residue, which, if present, would significantly affect the rheological properties. They also show that the asphaltene peak, centered at about 23 minutes of retention time, increased with aging, a common result.

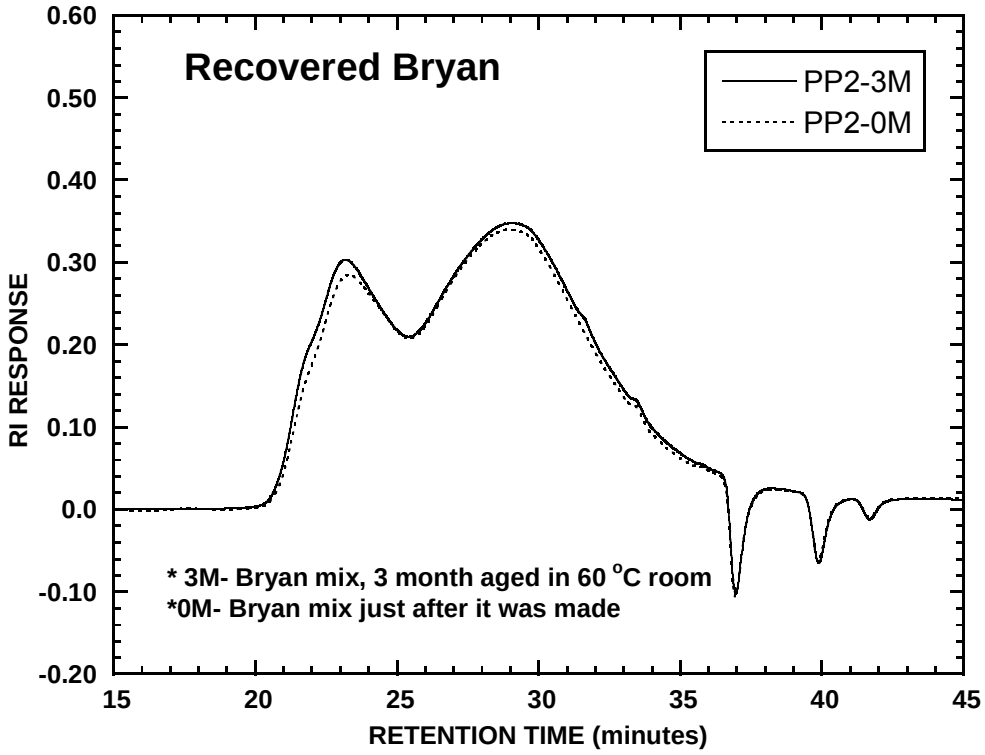

Figure 11-4. SEC Chromatogram for Recovered Binders from Bryan Mixtures (°F = 32 + 1.8 (°C)).

The aged binders were characterized by DSR and FTIR measurements. Aging increases carbonyl area (oxygen content), viscosity, and the elastic modulus, but decreases the ductility. Figures 11-5 and 11-6 are a plot of the CA and zero shear viscosity, respectively, for the Bryan binder (PG 64-22).

Figure 11-5 shows that CA increases with aging time for neat and recovered binders from Bryan mixtures. SAFT aging leaves the binder within the initial jump (higher aging rate) region, whereas PP2 aging is more severe and produces a binder that is past this region. Thus, the three PP2 data points show a uniform aging rate where as the SAFT points show a higher rate (slope) between 0 and 3 months than between 3 and 6 months.

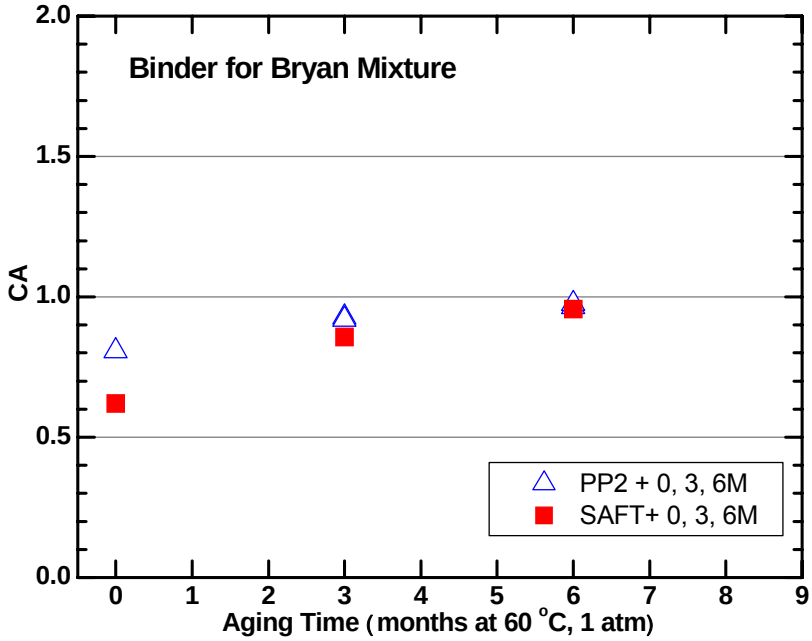

Figure 11-5. CA Rate of Bryan Binder (PG 64-22) (F = 32 + 1.8(C)).

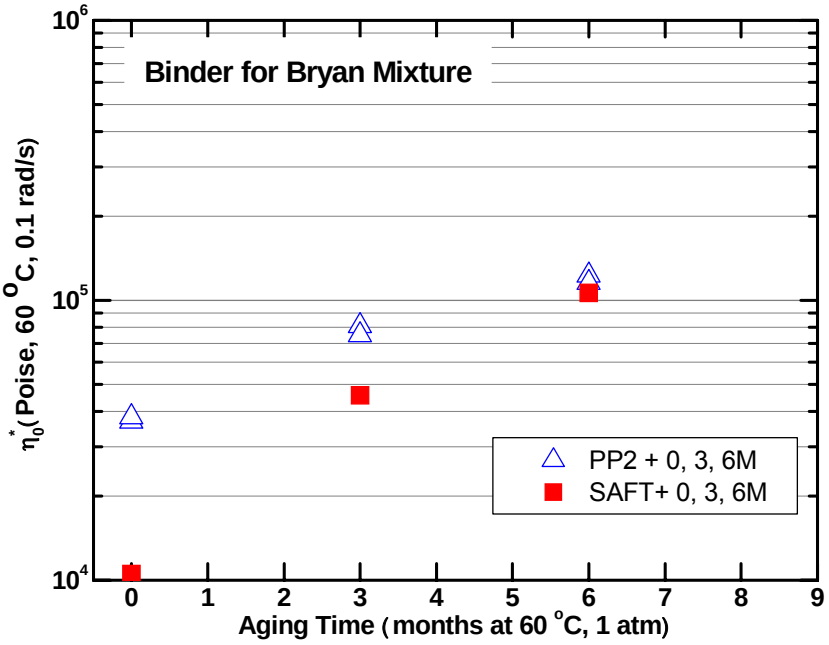

Figure 11-6. Zero Shear Viscosity Hardening Rate of Bryan Binder (PG 64-22) (F = 32 + 1.8(C)).

The zero shear viscosity of the Bryan binder also increases with aging time, and PP2 aged binder seems to have passed the initial jump period in Figure 11-6, as the data for all three aging times show the same hardening rate. The DSR function (G'/(η'/G')) for the Bryan binder, shown in Figure 11-7, versus the CA, also increases with aging. The DSR function is plotted on a logarithmic scale against the CA, which represents the amount of aging. Thus, aging time is removed as a factor, and PP2-aged binder and SAFT-aged binder show the some relation between CA and DSR function.

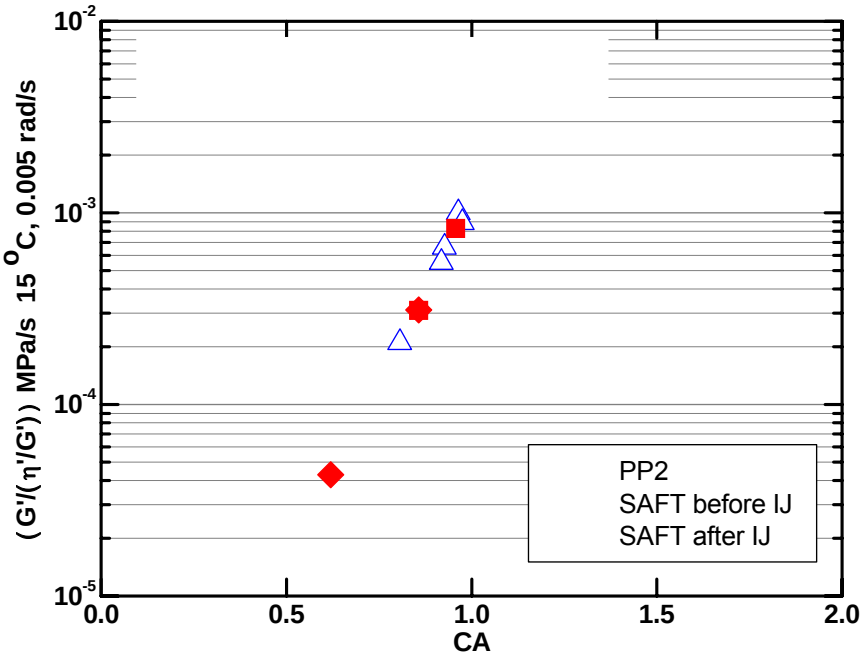

Figure 11-7. DSR Function vs. Carbonyl Area of Bryan Binder (PG 64-22) (°F = 32 + 1.8(°C)).

The Yoakum binder is a polymer modified binder, PG76-22, for which the zero shear viscosity is not appropriate for characterizing hardening rate (polymer-modified binders typically do not exhibit a zero shear viscosity). Instead, the DSR function (at a defined temperature and frequency) hardening rate is used to represent changes of binder physical properties with aging in Figure 11-8.

The DSR function of the Yoakum binder increases with aging time, and the PP2 aging process (PP2 + 0M) aged the Yoakum binder more than the SAFT process (SAFT + 0M). However, after 3 and 6 months additional aging in the 60 °C (140 °F) room, the neat thin-film aged Yoakum binder was somewhat harder than the mixture aged binder.

The thin film binder catches up with the mixture binder partly because, after SAFT, it is still in the higher aging-rate initial jump period, but also because binder aging in thin film has more access to oxygen than binder in compacted mixtures. In the case of the Bryan binder (Figures 11-5 and 11-6), it appears that the same process is occurring, but the neat binder takes longer to catch up to the mixture-aged binder. Increase of the CA for the Yoakum binder is shown in Figure 11-9.

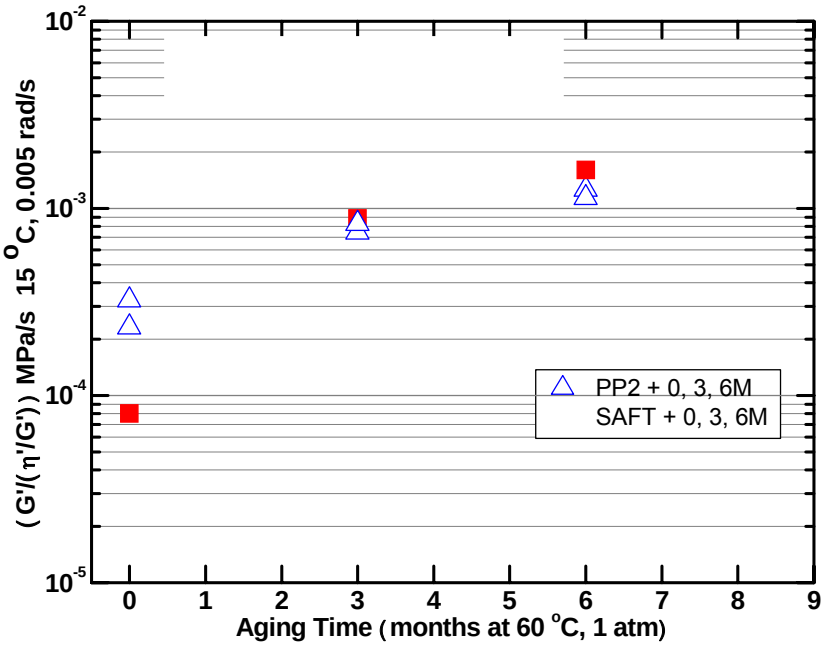

Figure 11-8. DSR Function Hardening Rate of Yoakum Binder (PG 76-22)

(°F = 32 + 1.8(°C)).

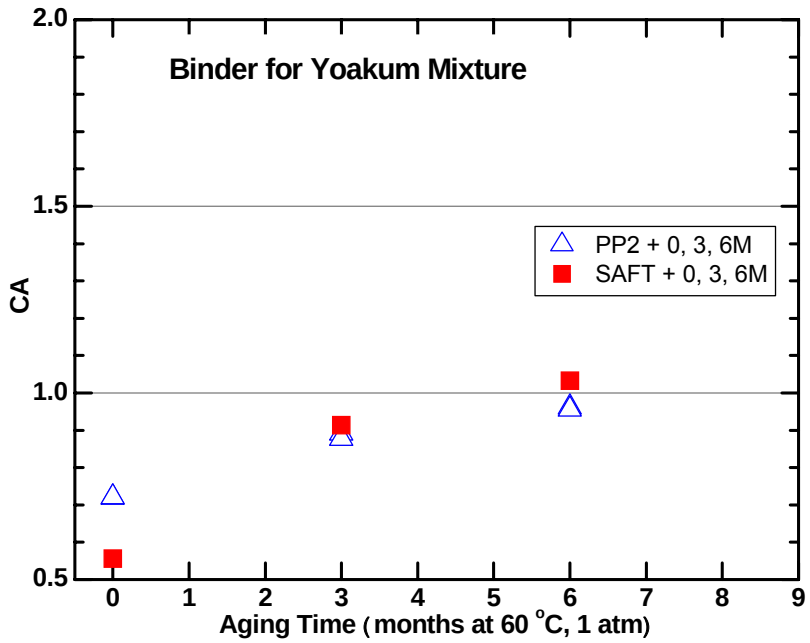

Figure 11-9. CA Rate of Yoakum Binder (PG 76-22)

(°F = 32 + 1.8(°C)).

Figure 11-10 shows the increase in DSR function with CA for the Yoakum binder. Again, both neat binder and mixture aged binder show the relation, suggesting the same aging mechanism is followed in both cases.

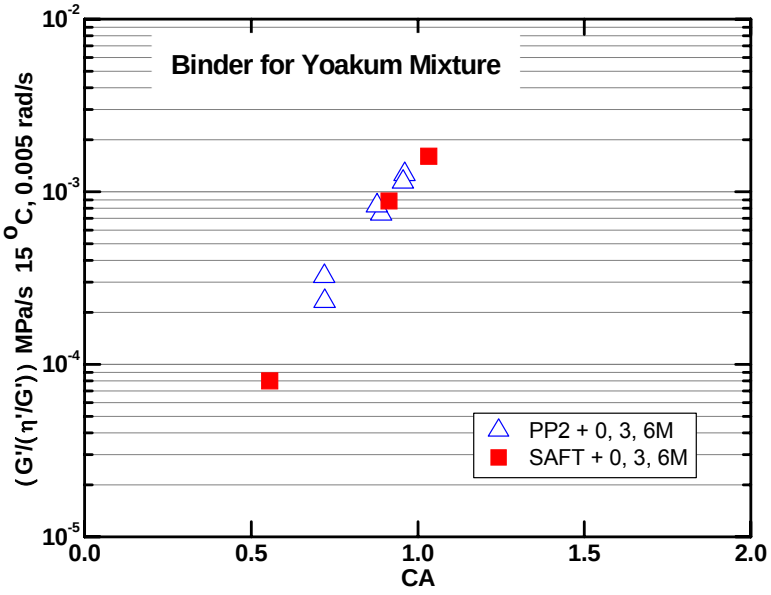

Figure 11-10. DSR Function vs. CA for Yoakum Binder (PG 76-22) (°F = 32 + 1.8(°C)).

BINDER-MIXTURE CHARACTERIZATION AND AN AGING SHIFT FACTOR

In Chapter 10, the effect of binder oxidative aging on mixture fatigue life was presented. The decrease in fatigue life with aging is striking, and significant differences in the rate of decline were noted between the Bryan and Yoakum mixtures. The reasons for these differences are, as yet, unknown. The discussion in this section elaborates on the possible impact of this decline in fatigue life on a pavement's service life. The question addressed is, "What shift factor should be applied to a pavement's service life due to binder oxidative aging?"

Another approach, different from the SF_{ag} approach discussed in Chapter 10, is presented in this section. The approach, discussed below, utilizes binder DSR functions and attempts to incorporate the significant aspect of traffic loading, and is based on field N_f.

First the following definitions are made:

N_f = Field fatigue life, in ESALs, and

R_L = Pavement loading rate, ESALs/yr.

Then N_f / R_L = Pavement Fatigue Life Expectancy, in years, is a constant over the life of the pavement value of field N_f. If, however, field N_f is a function of time (and declines with binder oxidative aging, e.g.), then this decline must be taken into account when estimating the pavement fatigue life. For a differential time period *dt* during which the field fatigue life is $N_f(t)$, the fraction of a pavement's total available fatigue life consumed during *dt* is calculated as:

$$\text{Fraction of Life Expended During Time } dt = \frac{dt}{N_f(t)/R_L} \qquad \text{(Equation 11-1)}$$

Then, Miner hypothesis (*18, 115*) is used to sum over the pavement's entire life, defined to be the amount of time to reach an integrated fraction equal to unity as follows:

$$\int_0^{t_{end}} \frac{dt}{N_f(t)/R_L} = 1 \qquad \text{(Equation 11-2)}$$

From the experimental data for the decline of field N_f with binder oxidative aging, $N_f(t)$ can be represented by an exponential relation:

$$N_f(t) = N_{f0} e^{-K_1 K_2 t} \qquad \text{(Equation 11-3)}$$

where K_1 is the magnitude of the power law slope that relates the decline of N_f to the increase in the DSR function G'/(η'/G') with aging, and K_2 is the (exponential) rate of increase of the DSR function with aging time in the pavement. Solving this integral for t_{end} gives the following equation:

$$t_{end} = \frac{\ln(K_1 K_2 N_{f0} / R_L + 1)}{K_1 K_2} \qquad \text{(Equation 11-4)}$$

An aging shift factor can be defined as the ratio of the age-shortened fatigue life to the unaged fatigue life expectancy:

$$SF_{aging} = \frac{\text{Age-shortened Life}}{\text{Unaged Life Expectancy}} = \frac{\ln(K_1 K_2 N_{f0} / R_L + 1)}{K_1 K_2 N_{f0} / R_L} \qquad \text{(Equation 11-5)}$$

From this relation, the bigger K_1 and K_2 are in magnitude; the smaller the aging shift factor, the shorter the pavement's fatigue life expectancy. Equation 11-5 also shows that K_1 and K_2 have an identical effect on this shift factor. That is, the impact of aging on the DSR function and the response of the fatigue life to these changes in DSR function produce the same effect on the final aging shift factor.

The decline of mixture fatigue with increasing DSR function is shown for both the Bryan and Yoakum mixtures in Figure 11-11. Values of N_{f0} (here equal to the fatigue life of the PP2-aged compacted mixtures) were reported in Chapter 10, and K_2, the ln (DSR function) hardening rate, is taken from a lab-to-field hardening rate conversion obtained in Project 0-1872 (Table 9-8) (*52*) and applied to the DSR function hardening rate (Figure 11-12). Hardening rates, of course, vary from pavement to pavement and depend principally upon the climate, but also, and perhaps to a lesser degree, on air voids and binder content. Consequently, the value used here gives only a very approximate indication for any specific pavement.

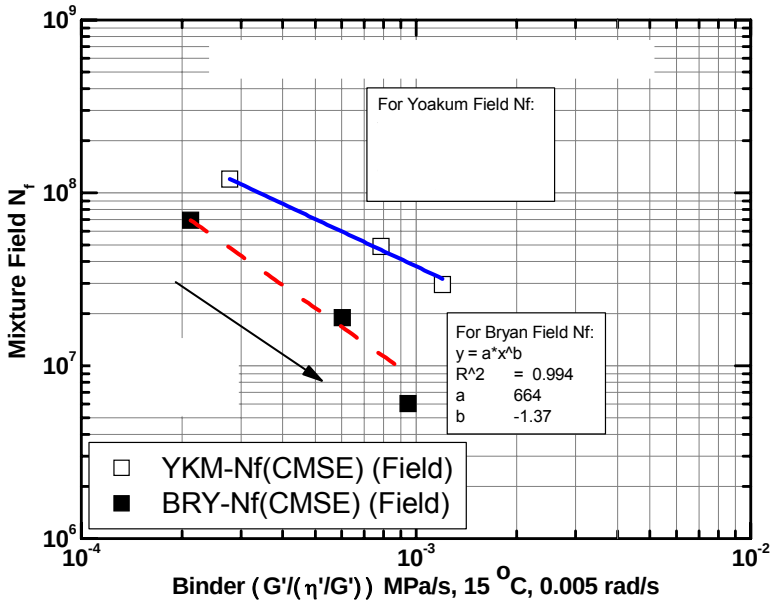

Figure 11-11. Decline of Mixture N_f with Binder DSR Function Hardening (°F = 32 + 1.8(°C)).

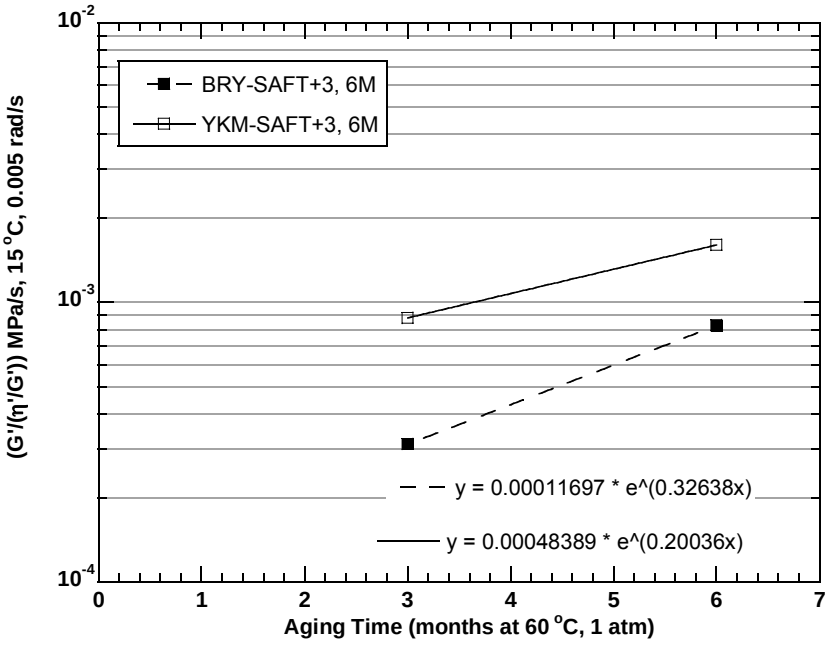

Figure 11-12. DSR Function Hardening Rate of Neat Binder after Initial Jump

(°F = 32 + 1.8(°C)).

Table 11-3 summarizes the parameters and calculations for the two mixtures. A loading rate of 3 million ESALS/yr was arbitrarily selected for these calculations. This number is high, perhaps corresponding to a heavily traveled freeway in a major city. A lower number will give longer fatigue lives. These calculations are intended only to represent a calculation procedure that shows the differences in fatigue life that might be expected between different mixtures, based upon laboratory measurements that take into account binder oxidative aging. More laboratory and field data are needed to verify this approach.

Table 11-3. Summary of Pavement Fatigue Life Parameters.

Mixture	N_{f0} 1 ×10⁶ ESALs	R_L 1 ×10⁶ ESALs/Yr	K_1	K_2	SF_{aging}	Pavement Fatigue Life (Yrs after PP2)
Bryan	69	3	1.37	0.26	0.27	6.2
Yoakum	120	3	0.91	0.16	0.33	13.2

The calculated shift factors are markedly different, and the differences in the estimated pavement fatigue life (after PP2 short-term aging) results for the two mixtures are striking. It should be noted again that the PP2 short-term aging produces a binder in the mixture that is significantly more aged than the SAFT (RTFOT equivalent) aged binder. How PP2 aging compares to the aging of an in-service HMAC pavement is yet unknown. However, based upon SH 21 data, reported in Project 0-1872 (*52*), the PP2 aging may reflect as much as 4 years of HMAC pavement in-service life. If so, the 6 years after PP2 (Bryan mixture) amounts to 10 years HMAC pavement total service life, and the 13 years after PP2 for the Yoakum mixture would correspond to 17 years of HMAC pavement total service life.

The differences in aging shift factors and pavement fatigue lives for the two mixtures are the results of K_1, the rate at which the fatigue life declines with oxidative hardening of the binder and K_2, the binder's hardening rate in the pavement. This is seen dramatically in Figures 11-13 through 11-15.

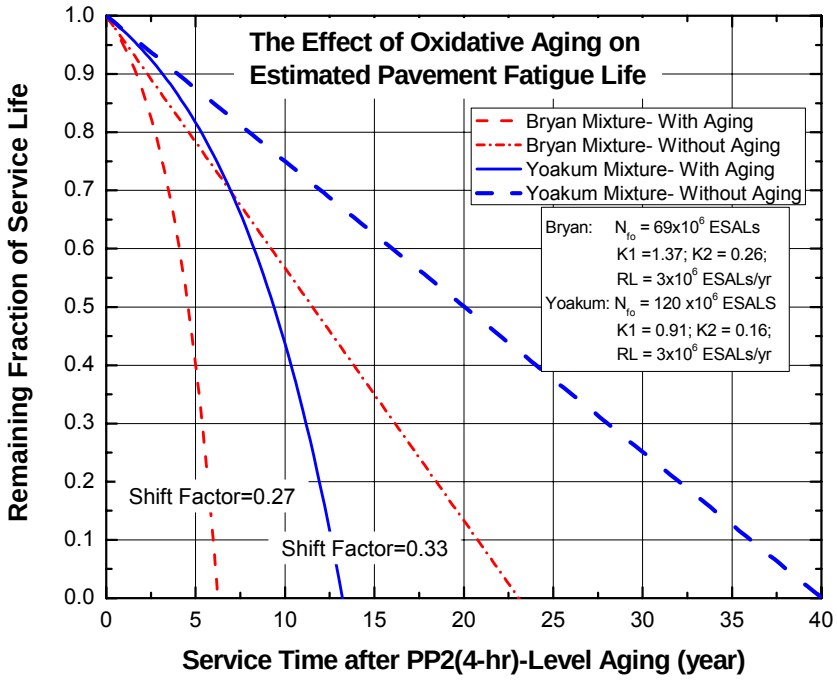

Figure 11-13. Calculated Decline of Remaining Pavement Fatigue Service Life.

Figure 11-13 shows the decline of the remaining fatigue life with service time (after PP2 aging), determined by integrating Equation 11-2 for times shorter than t_{end}. Both the Bryan and Yoakum mixtures are shown, and the straight-line decline assumes that there is no decline in fatigue life with aging. Without aging, the Yoakum mixture has a longer service life than the Bryan mixture due to its initially higher fatigue life (120 versus 69 million ESALs). With binder oxidative aging, the difference remains, and one might reasonably assume this difference is also because of the different initial fatigue lives.

Figure 11-14 shows a hypothetical calculation with the Bryan mixture the same, but the hypothetical case for the Yoakum mixture is the same except that the initial fatigue life is nearly the same as the Bryan mixture (not identical so both straight-line depreciations can be identified). While the initial fatigue lives are the same, the shift factors, and thus the service lives, are significantly different.

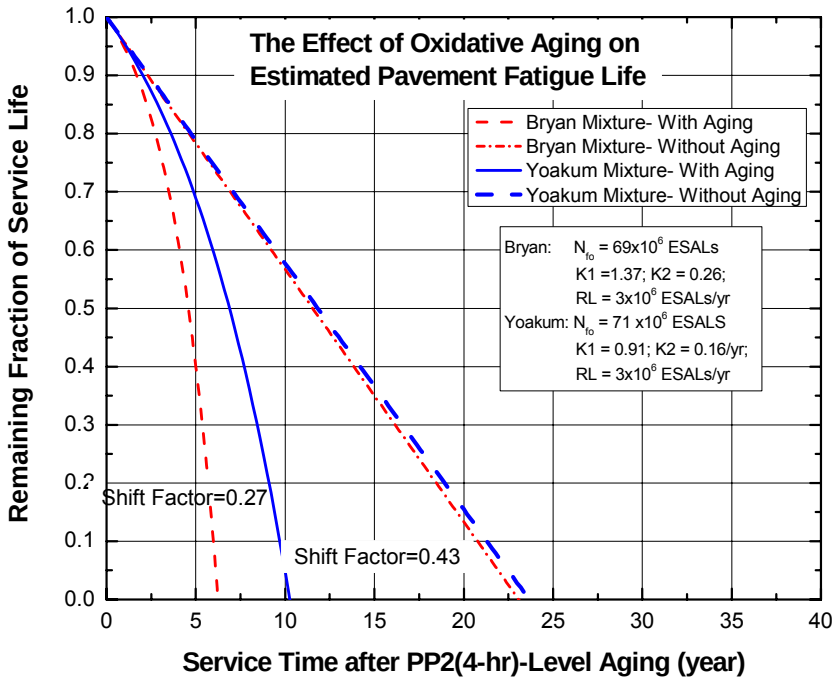

Figure 11-14. Hypothetical Decline of Pavement Fatigue Service Life, Initial Fatigue Lives Equal.

A second hypothetical case (Figure 11-15) changes the values of K_1 and K_2 but leaves the initial fatigue life the same as for the Yoakum mixture. Now, the conclusion is that the initial difference in fatigue life has minimal impact on the service life, but the rate of decline of fatigue life with binder hardening has a very profound impact. This conclusion is tentative as the amount of data is sparse with only two mixtures. Nevertheless, the results are compelling that the effect of binder oxidative aging in mixtures can have an extremely significant impact on the pavement service life in terms of fatigue performance.

Additional comments about pavement aging are appropriate. The above data suggest that when binder aging occurs in the pavement, it can have a very significant impact on pavement service life in terms of fatigue performance. However, it does not address whether or not binders in pavements actually age. At least one report in the literature is used to support the idea that pavements age primarily near the surface and very little more than an inch below the surface (*116*). If this is the case, then the issue of the effect of binder oxidative aging on fatigue may be of little importance.

On the other hand, a recent TxDOT report (*52*) provides considerable pavement recovered binder data that support the notion that binders, in fact, do age in HMAC pavements at depths up to several inches (at least six) and at rates that appear to be minimally abated by depth. If this is the case, then the impact of binder oxidative aging on HMAC pavement fatigue performance is of considerable importance and should be considered when designing HMAC pavements.

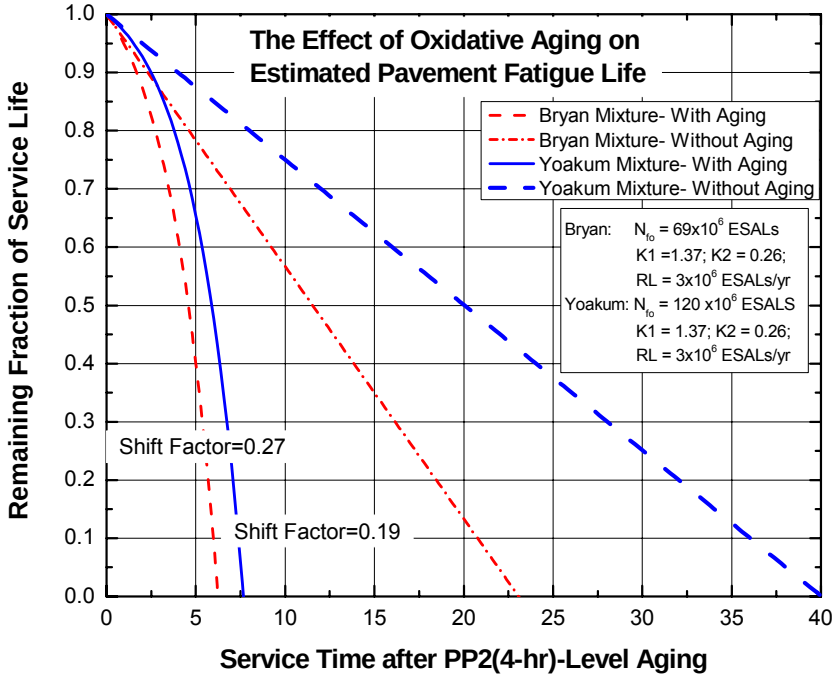

Figure 11-15. Hypothetical Decline of Pavement Fatigue Service Life, K_i Values Equal.

SUMMARY

Key points from a discussion and synthesis of the results are summarized as follows:

- The Yoakum mixture exhibited higher field N_f values compared to the Bryan mixture. This was probably due to the higher SBS modified binder content and the lime in the mixture. By contrast, the Yoakum field N_f results exhibited higher variability in terms of the *COV* of Ln N_f and the 95 percent CI.
- While the Yoakum mixture exhibited better fatigue performance in terms of the field N_f magnitude in all the analysis approaches, the mixture field N_f also depends on the following input variables; pavement structure and environmental conditions.

- While certain HMAC mixtures may perform satisfactorily well in a particular pavement structure and environmental location, it may not be true when these variables (pavement structure and environmental location) are changed.
- For the test protocols and conditions considered in this project, binder test results, when analyzed as a function of oxidative aging, indicated that:
    - Aging increases the carbonyl area (oxygen content), DSR function, viscosity, and elastic modulus.
    - Aging decreases both binder and mixture ductility.
    - CA correlates linearly with the DSR function.
    - AASHTO PP2 4 hrs short-term oven aging has a greater oxidative aging impact on the binder than SAFT aging. This was evident through the absence of the initial jump periods in the CA rates of extracted binders from mixtures subjected to AASHTO PP2 4 hrs short-term oven aging as well as the higher level of aging after the PP2 procedure compared to SAFT aging.
- An approach for developing shift factors due to aging, denoted as SF_{aging} (to differentiate it from the *SFag* approach), was developed that includes both binder hardening due to oxidative aging and decline in fatigue life due to binder hardening. This approach produced an expected pavement fatigue life in years, based upon an assumed ESALs/yr loading rate. The impact on fatigue life of binder hardening due to oxidation was dramatic, and the SF_{aging} results indicated that the Bryan mixture was more susceptible to decline in fatigue life due to aging than was the Yoakum mixture.

CHAPTER 12
COMPARISON AND SELECTION OF THE FATIGUE ANALYSIS APPROACH

This chapter presents the comparative evaluation of the fatigue analysis approaches, including the selection criteria and the selected and recommended fatigue analysis approach.

COMPARATIVE REVIEW OF THE FATIGUE ANALYSIS APPROACHES

Table 12-1 is a summary comparison of the four fatigue analysis approaches in terms of laboratory testing, equipment, input data, data analysis, failure criteria, and variability of the results. Tables 12-1(c) and (d) represent field N_f predictions based on a 20-year design period with aging effects considered. Only Bryan results are given for the corresponding actual field section PS#5. Statistical analysis for these approaches was based on least squares regression and typical spreadsheet descriptive statistics tools discussed in Chapters 4 through 7.

Table 12-1(a). Summary Comparison of the Fatigue Analysis Approaches.

Item	Fatigue Analysis Approach		
	Design Guide	**ME**	**CMSE/CM**
Concept	Mechanistic-empirically based	Mechanistic-empirically based	Continuum micromechanics & fundamental HMAC properties
Laboratory testing	Easy but lengthy temperature conditioning time	Rigorous & lengthy	Numerous but easy to run & less costly (no SE for CM approach)
Testing time	≅ 5 hrs	≅ 30 hrs	≅ 70 hrs (≅ 5 hrs for CM approach)
Equipment cost*	≅ $130,000 (minus the software)	≅ $155,000 (≅ $25,560 for BB device)	≅ $210,000 (≅ $80,000 for SE devices)
Input data	Comprehensive/flexible	Comparatively few	Comprehensive (no SE for CM approach)
COV of input data	≅ 5% - 23%	≅ 5% - 28%	≅ 4% - 12%
Failure criteria	50% cracking in wheelpath	50% reduction in flexural stiffness	7.5 mm microcrack growth & propagation through HMAC layer

Table 12-1(b). Summary Comparison of the Fatigue Analysis Approaches.

Item	Fatigue Analysis Approach		
	Design Guide	**ME**	**CMSE/CM**
Analysis procedure	Comprehensive	Relatively easy & straightforward	Comprehensive & lengthy
Analysis time**	≅ 4.5 hrs	≅ 3 hrs	≅ 6 hrs (≅ 5 hrs for CM)
Mechanistic failure load-response parameter	Maximum critical design tensile strain (ε_t) @ bottom of HMAC layer	Maximum critical design tensile strain (ε_t) @ bottom of HMAC layer	Maximum critical design shear strain (γ) @ edge of loaded tire
Fatigue model	$N_f = \beta_{f1} k_1 (\varepsilon_t)^{-\beta_{f2} k_2} (E)^{-\beta_{f3} k_3}$	$N_f = SF\left[k_1 (\varepsilon_t)^{-k_2}\right]$	$N_f = SF(N_i + N_p)$ $N_p = k_1 (\gamma)^{-k_2}$
Aging effects	Software incorporates a Global Aging model	None (but can possibly use Miner's hypothesis)	Shift factor (SF_{ag}) being developed
Mean field N_f value***	5.46×10^6	4.67×10^6	5.60×10^6
COV of Ln N_f (field)***	----------	≅ 6.87 - 9.85%	≅ 2.81 – 3.98%
95% field N_f CI ***	≅ 1.93 – 15.34×10^6	≅ 0.49 – 16.74×10^6	≅ 2.98 – 8.92×10^6

Note: *Equipment costs were based on July 2004 estimates;
**Analysis time estimates based solely on the researchers' experience with each approach
***Field N_f, *COV* and 95% CI values based on PS# 1 and WW environment only

An example of the analysis used to obtain the field N_f results shown in Tables 12-1 (c) and (d) for the ME, CMSE, and CM approaches in PS# 1 and the WW environment is given in Appendix I. For the M-E Pavement Design Guide, the N_f analysis is software-based. Based on Tables 12-1 (c) and (d), the field N_f varies across pavement structures, particularly for the ME and M-E Pavement Design Guide approaches. This variation is attributed to the predominant sensitivity of these approaches, particularly the ME analysis models, to the critical design tensile strain, ε_t, at the bottom of the HMAC layer, a parameter which is itself largely dependent on the entire pavement structure. For the ME approach, it should also be noted that the field N_f predictions strongly depend on the selected shift factor (*SF*) (Chapter 4).

Table 12-1(c). Summary Comparison of the Fatigue Analysis Approaches.

PS	Mixture	Field N_f (WW Environment)			
		ME	CMSE	CM	Design Guide
1	Bryan	1.03×10^6	3.11×10^6	3.10×10^6	4.71×10^6
	Yoakum	8.30×10^6	8.40×10^6	7.77×10^6	6.21×10^6
2	Bryan	0.26×10^6	2.13×10^6	2.38×10^6	4.05×10^6
	Yoakum	0.97×10^6	6.56×10^6	5.55×10^6	5.75×10^6
3	Bryan	0.25×10^6	2.18×10^6	2.06×10^6	1.93×10^6
	Yoakum	0.98×10^6	6.57×10^6	6.23×10^6	3.41×10^6
4	Bryan	0.28×10^6	1.96×10^6	1.96×10^6	2.02×10^6
	Yoakum	0.99×10^6	4.45×10^6	4.59×10^6	2.97×10^6
5	Bryan	2.16×10^6	5.49×10^6	5.38×10^6	19.29×10^6
	Yoakum	----------	----------	----------	----------

Table 12-1(d). Summary Comparison of the Fatigue Analysis Approaches.

PS	Mixture	Field N_f (DC Environment)			
		ME	CMSE	CM	Design Guide
1	Bryan	1.18×10^6	3.60×10^6	3.59×10^6	5.19×10^6
	Yoakum	9.59×10^6	9.07×10^6	8.46×10^6	8.02×10^6
2	Bryan	0.34×10^6	2.46×10^6	2.74×10^6	5.23×10^6
	Yoakum	1.27×10^6	6.78×10^6	5.80×10^6	7.43×10^6
3	Bryan	0.33×10^6	2.52×10^6	2.39×10^6	4.29×10^6
	Yoakum	1.27×10^6	6.79×10^6	6.51×10^6	5.57×10^6
4	Bryan	0.35×10^6	2.26×10^6	2.27×10^6	3.56×10^6
	Yoakum	1.27×10^6	4.61×10^6	4.79×10^6	5.24×10^6
5	Bryan	2.18×10^6	6.34×10^6	6.21×10^6	22.00×10^6
	Yoakum	----------	----------	----------	----------

Theoretical Concepts

Unlike the mechanistic-empirically based M-E Pavement Design Guide and ME approaches, the CMSE and CM approaches were formulated on the fundamental concepts of continuum micromechanics and energy theory, with fracture and healing as the two primary mechanisms controlling HMAC mixture fatigue damage. The CMSE/CM approaches utilize the fundamental HMAC mixture properties to estimate lab and/or field N_f.

Input Data

The input data for the CMSE and CM approaches and associated laboratory tests are comprehensive, which is necessary to sufficiently and adequately predict field N_f by considering all relevant factors that affect HMAC fatigue performance. The CMSE and CM approaches incorporate various material properties such as modulus, tensile strength, fracture, healing, and anisotropy, which is not the case with the ME approach.

The input data for the M-E Pavement Design Guide is also comprehensive but can be flexible depending on the level of analysis selected. Level 1 requires comprehensive input data in terms of traffic, environment, and material properties, with HMAC mixture properties characterized in terms of the |E*| values.

Laboratory Testing

The BB test for the ME approach is comparatively complex and time consuming. Note also that the laboratory BB equipment is limited to only third-point loading HMAC beam fatigue testing in a flexural mode. The linear kneading compactor may also be limited to rectangular beam shaped specimens, while most of the current Superpave HMAC mixture characterization tests use gyratory compacted cylindrical specimens.

The CMSE laboratory tests may be numerous, but they are relatively simple to run and less time consuming (provided specimens are well aligned along the axis of loading during testing). With the exception of SE measurements, the average test time for CMSE testing was at most 5 hrs. Additionally, CMSE cylindrical specimens are relatively easy to fabricate and handle. In the case of the CM approach, SE measurements (both for binder and aggregate) and RM tests in compression are not required, thus making the CM approach even more advantageous in terms of laboratory testing and subsequent data analysis.

However, with the CMSE uniaxial testing of the HMAC mixtures, it is imperative that the cylindrical specimens are properly aligned along the axis of loading (tensile or compressive) to prevent the induction of undesirable moments that can lead to erroneous results.

DM testing for Level 1 fatigue analysis of the M-E Pavement Design Guide is relative easy and simple to run but very time consuming in terms of temperature conditioning time for the specimens. Since a complete DM test for a single cylindrical specimen is often conducted at five temperatures, the minimum total conditioning time in this project was 10 hrs, i.e., a minimum of 2 hrs for each test temperature.

BB testing with the ME approach utilizes kneading compacted beam shaped specimens that are comparatively difficult to fabricate, time consuming to make, and require delicate handling and storage. Improper handling and/or storage can easily induce residual stresses within the specimen that can have a negative impact on the results.

Also, the beam shape of the specimens and the linear compaction procedure makes it difficult to adequately control the AV content to the target level. For instance, the *COV* of the AV content for the beam specimens in this project ranged between 4 to 8 percent. While this *COV* range may be acceptable, it was nonetheless higher than the approximately 3 to 6 percent *COV* for the cylindrical specimens utilized in the M-E Pavement Design Guide and CMSE/CM approaches. All these factors ultimately contribute to the relatively high variability in both the input data and final field N_f results for the ME approach.

Failure Criteria

The M-E Pavement Design Guide failure criterion is based on a percentage cracking in the wheelpath. In this project, the research team used 50 percent as the threshold value consistent with the TxDOT tolerable limits (*61*). However, the research team feels that this percent cracking does not correlate well with the actual fatigue damage accumulation (i.e., crack growth through the HMAC layer) or crack severity in an in situ HMAC pavement structure. For instance, a severely cracked HMAC pavement structure with only 10 percent crack area coverage may be considered adequate according to this criterion. Whereas a 60 percent cracked pavement section with cracks only initiating (beginning) will be considered inadequate according to this criterion. Therefore, there may be a need to review this failure criterion.

In the case of the ME approach, the correlation between fatigue crack area and severity on an in situ pavement structure and/or crack length through the HMAC layer thickness and 50 percent flexural stiffness reduction is not clear. As pointed out by Ghuzlan et al. (*116*), 50 percent initial stiffness reduction for constant strain BB testing is an arbitrary failure criterion that does not correlate well to the actual damage accumulation in the HMAC material. These researchers instead proposed the use of energy concepts. Rowe et al.'s study also suggests that while this 50 percent stiffness reduction may work well for unmodified binders, it may not be applicable for modified binders, and thus, results must be analyzed and interpreted cautiously (*113*). Note that the Yoakum mixture with the modified binder generally exhibited higher Ln N_f (both lab and field) variability in this project.

In addition, the ME assumption of bottom-up crack failure mode due to horizontal ε_t as utilized in this project may not always be true particularly for thick, stiff or thin, flexible HMAC pavement structures. This also applies to the M-E Pavement Design Guide approach. For the CMSE approach, the failure criterion needs to be further reviewed to establish the adequacy of assuming one microcrack (7.5 mm) initiating and propagating through the HMAC layer thickness as representative of the fatigue cracking process in the entire HMAC pavement structure. The current CMSE version is based on the generalized hypothesis that the growth of one crack is representative of the field HAMC pavement crack size distribution. Consequently, more data are thus required to validate this hypothesis.

Both the ME and the M-E Pavement Design Guide utilize tensile strain as the failure load-response parameter and exhibit considerable sensitivity to this parameter (*3*, *4*, *59*). Though still subject to review, recent research including the preliminary observation of this project has shown that because of the anisotropic nature of HMAC, this may not always be true, particularly for thick stiff HMAC pavement structures. Therefore, the use of ε_t at the bottom of the HMAC layer may provide an under- or over-estimation of the mixture N_f, particularly for pavement structures where ε_t at the bottom of the HMAC layer is not critical to fatigue performance. Based on this theory, it appears that the ME approach may be applicable only to pavement structures where ε_t at the bottom of the HMAC layer is critical to fatigue performance. Otherwise the approach tended to over predict N_f, particularly for pavement structures with ε_t less than 100 microstrain in this project. Various researchers, including Nishizwa et al.(*34*), have also reported infinite N_f at low strain levels less than 200 microstrain with the ME approach.

Data Analysis

In terms of analysis, the CMSE and CM approaches are comparatively complex and lengthy because of the comprehensive input data requirements. Inevitably, this type of analysis is necessary to adequately model the HMAC mixture fatigue resistance by analyzing and directly incorporating all the influencing factors. However, these numerical calculations can easily be simplified if a simple spreadsheet analysis program is developed for the computations, as was the case in this project. Alternatively, a CMSE/CM fatigue analysis software can be developed to simplify and reduce the time needed for these calculations.

Nonetheless, a comprehensive sensitivity analysis of the CMSE/CM fatigue analysis procedure is recommended to simplify the calculations by eliminating/reducing less critical and/or redundant variables. While the CMSE/CM analysis procedure produced reasonable results in this project, it should be noted that this is a relatively new fatigue analysis procedure and may therefore still be subject to review and modifications in continuing research work during the validation phase.

For the ME approach, the simplified AASHTO TP8-94 analysis procedure utilized in this project was relatively easy and straightforward, probably because of the relatively fewer input data required (*59*). For the M-E Pavement Design Guide, the fatigue analysis process is software based but utilizes the ME concepts (*3, 4*).

While the ME laboratory-to-field shift factors (*SF*) may be environmentally specific and require calibration to local conditions, the CMSE/CM calibration constants were developed based on a wider environmental spectrum covering the USA (*45*), thus making the CMSE approach more flexible. By contrast, the M-E Pavement Design Guide incorporates a comprehensive climatic model that computes the shift factors based on a specific environmental location (*3, 4*). The M-E Pavement Design Guide Level 1 fatigue analysis actually computes these calibration constants based on actual climatic (current or past) data from local weather stations. In this context, the M-E Pavement Design Guide may therefore be considered as being more accurate and realistic in terms of simulating field environmental conditions compared to the other fatigue analysis approaches. The M-E Pavement Design Guide software also encompasses a comprehensive traffic analysis model that more closely simulates field traffic loading conditions than the ME and CMSE/CM approaches (*3, 4*).

Furthermore, the M-E Pavement Design Guide software incorporates a default empirically-based Global Aging Model that takes into account the effects of aging in HMAC mixture fatigue analysis (*3, 4*). By contrast, the ME and the current CMSE/CM approaches do not directly incorporate the effects of aging in the analysis. In the case of the CMSE approach, attempts are being made to develop shift factors due to aging (Chapters 10 and 11) in the ongoing research and will possibly be incorporated in the final CMSE version. For the ME approach, Miner's hypothesis (*18*) can be utilized to develop and incorporate the effects of aging in field N_f prediction, but this was beyond the scope of this study.

Additionally, the M-E Pavement Design Guide software has an added advantage of simultaneously predicting other HMAC pavement distresses besides fatigue cracking. These include thermal cracking, rutting, and pavement roughness expressed in terms of the international roughness index (IRI). The CMSE approach on the other hand, has the potential to simultaneously model HMAC moisture sensitivity through the use of surface energy data under wet conditions (*46*, *47*, *68*, *71*). In this project, however, dry conditions were assumed with no consideration of moisture sensitivity analysis for the HMAC mixtures.

Results and Variability

Although the computed mixture field N_f results presented in Chapters 10 and 11 were comparable, the CMSE and CM approaches exhibited relatively low variability in terms of the *COV* of Ln N_f compared to both the ME and the M-E Pavement Design Guide approaches. As highlighted in Chapter 11 (Table 11-2), the ME approach exhibited the highest statistical variability both in terms of the *COV* of Ln N_f and 95 percent field N_f CI. Furthermore, the ME field N_f predictions are significantly dependent on the selected *SF* value (Chapter 4), which will obviously lead to different results if a different *SF* value is selected. Note that this *SF* value for the ME approach was not measured in this project (Chapter 4).

Although this lower statistical variability may also indicate that the CMSE/CM test repeatability was better than the BB and DM tests, more comprehensive statistical analyses for the CMSE/CM approaches are required, including more laboratory HMAC mixture fatigue characterization and field validation.

Costs – Time Requirements for Laboratory Testing and Data Analysis

The cost comparisons in this project were evaluated in terms of billable time requirements for laboratory testing (specimen fabrication, machine set up, and actual test running time) and data analysis. These typical time estimates based on at least four HMAC specimens for the ME and CMSE/CM approaches and at least two HMAC specimens for the M-E Pavement Design Guide to obtain at least a single value of field N_f are shown in Table 12-1.

Detailed time requirements are attached as Appendix J. Note that these time estimates were purely based on the work contained in this project, but actual time requirements for laboratory testing and data analysis may generally vary from one person to another and from machine to machine or computer to computer (e.g., in the case of the M-E Pavement Design Guide).

In Table 12-1, laboratory testing time does not include aggregate pre-heating, binder liquefying, short-term oven aging, heating for compaction, cooling after compaction, and temperature conditioning time of the specimens prior to testing, because time for these processes was considered equal in each approach and may often not be billable. Based on the billable time requirements in Table 12-1, the M-E Pavement Design Guide was ranked as the cheapest (shortest billable time requirement) followed by the CM approach.

Generally, the ME approach required more time for specimen fabrication, machine setup, and actual testing but less time for data analysis primarily due to the simplified AASHTO TP8-94 analysis procedure selected and the fewer input data requirements *(59)*.

For the CMSE approach, SE values for binders and aggregates are required as input data. Though the current test protocol for aggregates might require a test time of about 30 to 60 hrs per aggregate, various alternate and time-efficient SE measurement methods are being investigated in an ongoing research project *(77)*. Despite the lengthy test time, however, SE measurements are only performed once for any binder or aggregate type from a particular source (as long as there are no major compositional changes). The SE data can then be utilized for numerous analysis applications including fatigue, permanent deformation, and moisture sensitivity modeling in HMAC pavements. Thus, SE measurements are actually efficient considering their repeated and widespread use for binder and aggregate materials that may be utilized in different mixture designs for different projects.

Costs – Equipment

In terms of equipment cost, the CMSE was ranked as the most expensive approach with an approximate total cost of $210,000 (with about $80,000 being for the SE equipment) followed by the ME approach, based on current equipment costs. Although the SE equipment appears costly, its versatility in terms of data measurements for HMAC mixture fatigue, permanent deformation, and moisture sensitivity analysis may actually offset the high initial cost. This is especially significant for numerous concurrent projects.

The equipment costs for the M-E Pavement Design Guide (≅ $130,000) and the CM (≅ $210,000 - $80,000 = $130,000) approaches are similar. However, the cost of the M-E Pavement Design Guide software, which is not included in Table 12-1, may raise the M-E Pavement Design Guide total cost to a value higher than that of the CM approach.

The ME equipment cost is lower than that of the CMSE, but it exceeds the M-E Pavement Design Guide and the CM approaches by approximately $25,560 based on the current price of the BB device (Table 12-1) (*118*). The limited use of the BB device for flexural fatigue testing only also indirectly makes the ME approach more costly.

SELECTION OF FATIGUE ANALYSIS APPROACH

Table 12-2 summarizes the advantages and disadvantages of each fatigue analysis approach as observed in this project. Table 12-3 is a summary rating based on a comprehensive value engineering assessment including laboratory test results, statistical analysis, and relative comparison of each analysis procedure. The assessment and rating criteria, including a TxDOT evaluation survey questionnaire to rate the assessment factors according to their degree of significance, are discussed in this section. A detailed rating analysis is attached as Appendix K.

Table 12-2. Summary Comparison of the Fatigue Analysis Approaches.

Approach	Advantage	Disadvantage
CMSE	• Utilizes fundamental HMAC mixture properties to estimate N_f • Exhibits greater flexibility & potential to incorporate material properties that are critical to HMAC mixture fatigue performance • Utilizes shear strain as failure load-response parameter • Utilizes cylindrical specimens that are easy to fabricate & handle • Requires numerous tests that are easy & relatively less costly to run • Relates fatigue failure to damage accumulation within HMAC material • Procedures N_f results that exhibits lower statistical variability • Produces fatigue performance results as a function of microcrack growth through HMAC layer thickness • Utilizes calibration constants that were developed nationwide • Incorporates aging, healing, & anisotropic effects in N_f analysis • Laboratory tests and resultant data are versatile in their application	• Validity & applicability • More mixture characterization • Test protocols & analysis procedure subject to review • Lab testing – specimen alignment • Adequacy of failure criteria • Statistical analysis criteria needs more review • SE testing is lengthy & costly
CM	• Same as CMSE but with no SE tests & reduced analysis	
M-E Pavement Design Guide	• Ideal for pavement structures where tensile strain is critical to fatigue performance • Incorporates global aging model • Predicts distress as a function of pavement age • Incorporates comprehensive traffic and climatic analysis models • Utilizes cylindrical specimens that are easy to fabricate & handle • Tests are easy and less costly • Failure criteria is based 50 % cracking in wheelpath • Versatility – other tests & analyses	• Empirically based • Global aging model may not be good for modified binders • No direct incorporation of healing nor anisotropy • Failure criteria does not clearly relate to damage & severity • Only bottom-up cracking failure mode was considered in this study.
ME	• Ideal for pavement structures where tensile strain is critical to fatigue performance • Requires local calibration to field conditions • Failure criteria is based on 50% stiffness reduction	• Empirically based • Beam specimen are difficult to fabricate and handle • Laboratory testing is lengthy • No direct incorporation of aging, anisotropy, & healing effects in analysis • High variability in results • Not applicable to pavement structures where tensile strain critical to fatigue performance • Test equipment is limited to BB testing only.

TxDOT Evaluation Survey Questionnaire

An evaluation survey questionnaire was conducted with TxDOT personnel to ascertain the degree of significance of the various factors to be used in evaluating and rating the four fatigue analysis approaches consistent with the TxDOT HMAC mixture fatigue characterization and pavement structural design for fatigue resistance. These factors include laboratory testing, material properties, input data variability, analysis, field N_f results, and associated costs. Appendix K is an example of the evaluation survey questionnaire and shows the sub-factors associated with each factor. For each factor and sub-factor, the rating score was from 1 to 10, with 10 representing the most significant factor/sub-factor and 1 being the least significant.

Figure 12-1 summarizes these rating results in a decreasing order of significance for both the factors and sub-factors. Based on these rating scores, the averaged weighting scores out of a total score of 100 percent were determined and are shown in parentheses in Figure 12-1. According to these rating results, mixture field N_f results in terms of variability and tie to field performance is the most significant factor to consider when selecting and recommending an appropriate fatigue analysis approach to TxDOT. This factor has a weighting score of 22 percent. Material properties were considered the least significant factor with a total weighting score of 14 percent. Within the factor "material properties," mixture volumetrics (binder content and AV) and modulus/stiffness were considered the most significant sub-factors with an equal weighting score of 17 percent, while anisotropy was the least significant (9 percent). It is also worthwhile to note that the factors "analysis" and "laboratory testing" have the same degree of importance (with an equal weighting score of 15 percent).

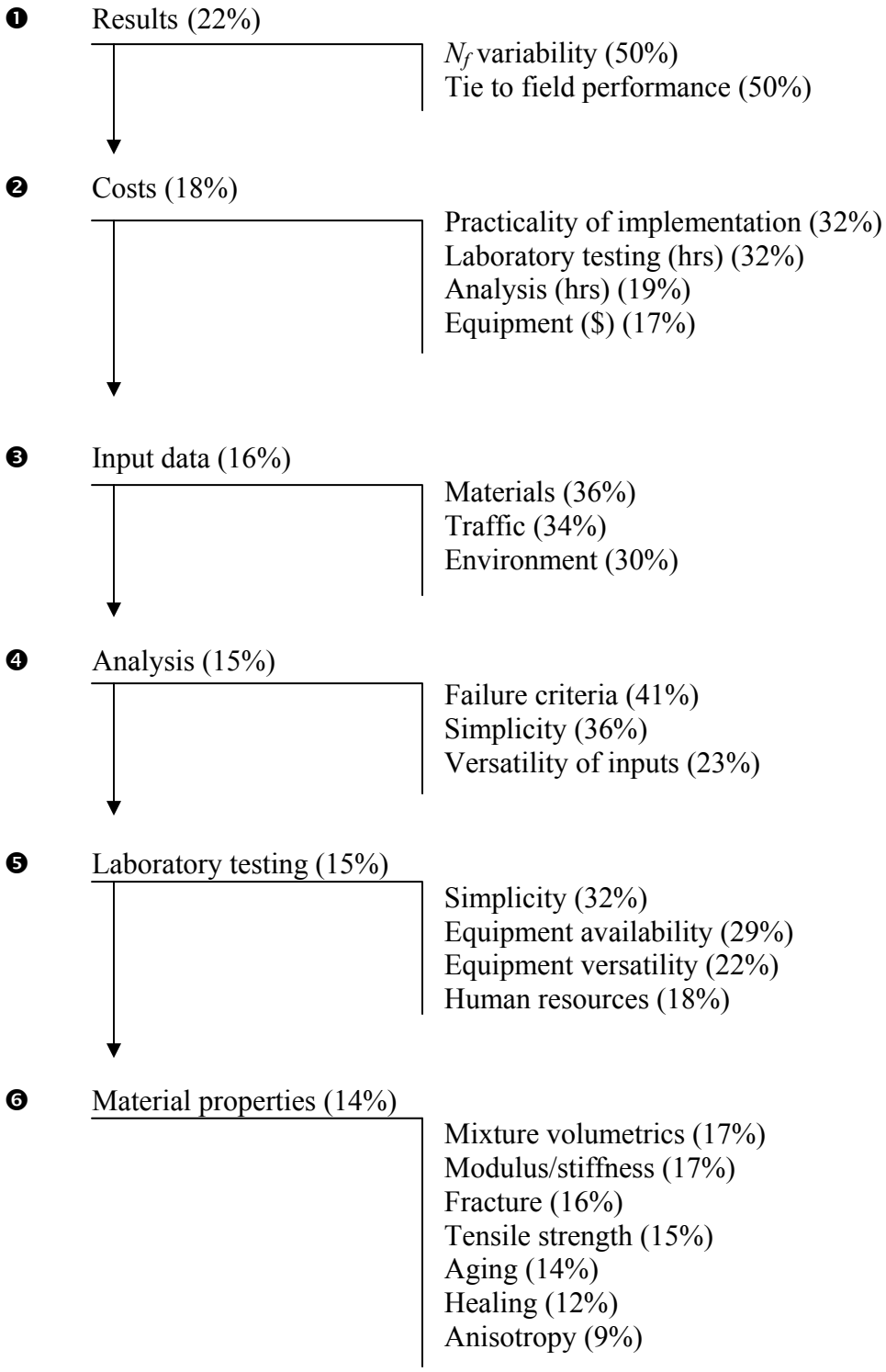

Figure 12-1. Assessment Factors/Sub-factors and Associated Weighting Scores.

Assessment and Rating Criteria of the Fatigue Analysis Approaches

Using Tables 12-1 and 12-2, the research team assigned scores (out of 10) to each sub-factor, as shown in Appendix L. For this analysis, the scores (with a range of 0 to 10) for each sub-factor, e.g., those associated with the factor "results," were defined as follows:

- Variability: 10/10 ≅ low, 5/10 ≅ low to high, and 0/10 ≅ high variability.

- Tie to field performance: 10/10 ≅ high, 5/10 ≅ low to high, and 0/10 ≅ low degree of or poor tie to field performance.

Using Figure 12-1, the weighted scores for each factor for each approach were summed up as shown in Appendix L. Table 12-3 provides an evaluation summary of the scores and ratings of the fatigue analysis approaches.

Table 12-3. Weighted Scores and Rating of the Fatigue Analysis Approaches.

Category	Weight	Evaluation Score			
		Guide	ME	CMSE	CM
Results	*22%*	11%	9%	14%	13%
Cost	*18%*	12%	10%	12%	13%
Input data variability	*16%*	12%	8%	10%	10%
Analysis	*15%*	9%	9%	11%	10%
Laboratory testing	*15%*	12%	6%	12%	12%
Incorporation of material properties	*14%*	10%	8%	13%	12%
Total	*100%*	66%	50%	**72%**	70%

Table 12-3 shows the weighting scores associated with each factor and the actual score assigned for each approach. "Results," for instance, has a total weighted score of 22 percent. For this factor, the CMSE approach scored the highest score (14 percent) and would be ranked first based on this factor. In terms of laboratory testing, while all the other approaches have the same ranking based on equal scores (12 percent), the ME approach would be ranked last with a score of 6 percent out of a weighted total of 15 percent. In terms of the overall scores (out of a total of 100 percent), the order of ranking is CMSE (72 percent), CM (70 percent), M-E Pavement Design Guide (66 percent), and ME (50 percent).

The Selected Fatigue Analysis Approach – The CMSE Approach

Based on this value engineering assessment, as shown in Table 12-3, and considering the test conditions in this project, the CMSE fatigue analysis approach with the highest score (75 percent) is recommended for predicting HMAC mixture fatigue life. With the possibility of establishing a SE database in the future from various ongoing TxDOT projects, the CMSE approach will become a reality both in terms of further validation and practical implementation. Furthermore, a sensitivity analysis with more HMAC mixture characterization to streamline the CMSE procedure will make the approach simple and practical to implement.

Based on the score ranking, the CM is recommended as the second alternative approach in lieu of the CMSE approach to be utilized particularly in the absence of SE data. Note, however, that the CM analysis models were modified in this project based on the CMSE results. Consequently, more independent HMAC mixtures need to be characterized for fatigue resistance to validate this correlation between the CMSE and the CM approaches. With further validation through additional HMAC mixture characterization, CM is a potentially promising fatigue analysis approach to be recommended over CMSE possibly at the end of this project.

Although the CMSE fatigue analysis approach is recommended in this project, it should be noted that any fatigue design approach can produce desired results provided it is well calibrated to the environmental and traffic loading conditions of interest and that all relevant factors affecting performance are appropriately taken into consideration.

Incorporation of Aging Effects in Field N_f Prediction

With further research and more binder and HMAC mixture fatigue characterization, a shift factor due to aging (SF_{ag} or SF_{aging}) will possibly be incorporated in the CMSE fatigue analysis model, as illustrated in Chapters 10 and 11. While some aging shift factors were developed in this project (SF_{ag} in Chapter 10 and SF_{aging} in Chapter 11), validation of these concepts is still required through testing of additional binders and HMAC mixtures. In contrast to the simplicity adopted in these concepts, HMAC aging should possibly be modeled as a function of three processes: binder oxidation, binder hardening, and field N_f reduction.

Additionally, the SF_{ag} (or SF_{aging}) should be able to account for mix-design characteristics, traffic loading, and environmental conditions. As pointed out in Chapter 10, field HMAC aging is a relatively complex process involving fluctuating traffic loading and environmental conditions. Note, however, that traffic (in terms of design ESALs) and environmental effects (in terms of temperature) are also taken into account by the SF_h (Chapter 5) in this CMSE approach. In addition, the rate of aging or response to binder oxidation and hardening and subsequent reduction in fatigue resistance may differ from mixture to mixture depending on the material type and mix-design characteristics. Most importantly, the SF_{ag} (or SF_{aging}) must be derived as a function of time so that N_f at any pavement age can be predicted. Once these SF_{ag} have been developed and validated for a group of similar HMAC mixtures, laboratory testing of aged HMAC mixtures may be unnecessary.

Recommendations on a Surrogate Fatigue Test and Analysis Protocol

The fatigue analysis approaches discussed in this report and the selected CMSE approach incorporate stress-strain analysis that depends on both pavement structure and environmental location. This is because stress and/or strain are required as an input parameter in these analyses. Unlike other distresses, such as rutting or permanent deformation, fatigue cracking in the HMAC layer depends on the entire pavement structure and its response to both traffic loading and the environment. Consequently, a surrogate fatigue test and analysis protocol that is independent of the pavement structure and environment cannot be recommended based on the fatigue analysis approaches and results presented in this report. However, investigation of surrogate fatigue test

protocols based on CMSE testing for use in mix design and HMAC mixture screening without prediction of N_f is reported in Research Report 0-4468-3.

In the absence of a fatigue analysis model that is independent of stress and/or strain as input parameters, the research team proposes establishing a database of a range of design stress and/or strain levels for typical TxDOT HMAC pavement structures and the Texas environment. Establishment of such a database to be used in conjunction with these fatigue analysis approaches will facilitate an easier and quicker way of characterizing the fatigue resistance of HMAC mixtures using some of the tests described in this report as surrogate tests. This will also eliminate the need to conduct an extensive stress-strain analysis every time a HMAC mixture is to be characterized for fatigue resistance.

SUMMARY

Key points from a comparison and selection of the fatigue analysis approaches are summarized as follows:

- The four fatigue analysis approaches (ME, CMSE, CM, and M-E Pavement Design Guide) were comparatively analyzed in terms of the following factors: theoretical concepts, input data, laboratory testing, failure criteria, data analysis, results and variability, and associated costs.
- Selection of the fatigue analysis approach was based on field N_f results, costs, input data variability, analysis, laboratory testing, and incorporation of material properties consistent with the TxDOT level of significance of each parameter. Based on this value engineering assessment criteria and considering the test conditions in this project, the CMSE fatigue analysis approach was selected and recommended for predicting HMAC mixture field N_f.
- Although the CMSE fatigue analysis approach was selected in this project, any fatigue analysis approach can produce desired results provided it is well calibrated to the environmental and traffic loading conditions of interest and that all relevant factors affecting fatigue performance are appropriately taken into account.

CHAPTER 13
CONCLUSIONS, RECOMMENDATIONS, AND FUTURE WORK

From the data presented and analyzed in this interim report, the following conclusions, recommendations, and future work plans are presented.

CONCLUSIONS

The selected fatigue analysis approach, a comparison of mixture field N_f, the effects of binder oxidative aging and other input variables, binder and binder-mixture results are summarized in this section.

Selected Fatigue Analysis Approach – CMSE

(1) Based on a value engineering assessment including laboratory testing, input data, statistical analysis, costs, and the analysis procedure of each approach, the CMSE fatigue analysis approach is recommended for predicting HMAC mixture fatigue life.

(2) In comparison to other approaches that were evaluated and for the test conditions considered in this project, the CMSE approach exhibited better mixture field N_f prediction capability:
- It utilizes fundamental mixture properties to estimate field N_f, and incorporates the continuum micromechanics-energy theories of fracture and healing in the fatigue analysis of HMAC mixtures.
- It exhibits greater flexibility and the potential to account for most of the fundamental HMAC material properties that affect HMAC pavement fatigue performance. These properties include fracture, binder aging effects, healing, visco-elasticity, anisotropy, crack initiation, and crack propagation.

- With the exception of SE measurements, the CMSE laboratory tests are less costly both in terms of billable time requirements and equipment. Laboratory testing for this approach utilizes gyratory compacted specimens that are relatively easy to fabricate and handle compared to beam specimens for the ME approach.
- The failure criterion of a 7.5 mm (0.3 inches) microcrack initiation, growth, and propagation through the HMAC layer thickness closely correlates with actual fracture damage accumulation in an in situ HMAC pavement structure compared to the failure criteria of the other approaches, the M-E Pavement Design Guide and the ME approach.
- The CMSE mixture results exhibited lower variability in terms of the *COV* of Ln N_f.
- Has the potential to simultaneously model HMAC moisture sensitivity through the use of surface energy data under wet conditions.

(3) Although the SE measurements for the CMSE analysis are lengthy in terms of test time, the tests are performed only once for any binder or aggregate type from a particular source (as long as there are no major compositional changes). The SE data can then be utilized for numerous analysis applications including fatigue, permanent deformation, and moisture sensitivity modeling in HMAC pavements. Thus, SE measurements are actually efficient considering their repeated and widespread use for binder and aggregate materials that may be utilized in different mixture designs in different projects.

(4) In the absence of SE data, the CM approach can be utilized in lieu of the CMSE approach. The fundamental concepts, failure criteria, and analysis procedure are basically similar, except for the following:

- SE laboratory measurements (both for binders and aggregates) and RM tests in compression are not required in the CM approach.
- SE input data for both the binder and aggregate are not required in the CM approach. Instead, the CM approach utilizes empirical relationships that were calibrated to the CMSE approach to compute SF_h and Paris' Law fracture coefficients that are dependent on RM (compression) and SE data in the CMSE approach.

Comparison of Mixture Field N_f

(1) The Yoakum mixture exhibited better fatigue resistance in terms of the field N_f values for all aging and environmental conditions and for all pavement structures considered in this project compared to the Bryan mixture. This finding was observed in all the fatigue analysis approaches. Also, the Yoakum mixture exhibited less susceptibility to aging compared to the Bryan mixture. The research team hypothesizes that the Yoakum mixture's improved fatigue performance may be due to the following factors:
   - The higher binder content for the Yoakum mixture (5.6 percent by weight of aggregate) probably increased its fatigue resistance compared to the Bryan mixture, which was a 4.6 percent binder content by weight of aggregate.
   - The effect of the SBS modifier and the 1 percent hydrated lime in the mixture could have possibly decreased the Yoakum mixture's susceptibility to oxidative hardening. In their study, Wisneski et al. made similar observations that hydrated lime tended to improve the performance of recycled asphalt (*114*). However, this phenomenon is yet to be explored in greater depth.
   - The binder-aggregate bond strength, as exhibited by the SE results, indicated a relatively better bond compatibility for the Yoakum mixture (PG 76-22 plus gravel aggregate) than for the Bryan mixture (PG 64-22 plus limestone aggregate).

(2) For the field N_f results, the Yoakum mixture exhibited higher variability in terms of the *COV* of Ln N_f and 95 percent CI range.

Effects of Binder Oxidative Aging and Other Variables

(1) Binder aging reduces HMAC mixture resistance to fracture and ability to heal. Generally, all mixtures exhibited a declining field N_f with aging.

(2) Both binders and mixtures stiffen with aging, and these changes quantitatively correlated with each other.

(3) HMAC mixture field N_f performance depends on both pavement structure and environmental conditions.

(4) The computed temperature shift factors (a_T) for the HMAC mixtures based on time-temperature superposition principles using the Arrhenius model exhibited a linear relationship with temperature. While these a_T showed some sensitivity to mixture type, they were by and large insensitive to binder oxidative aging effects.

Binder-Mixture Characterization

(1) Mixtures stiffen significantly in response to binder oxidative aging.
(2) For a given mixture specimen, mixture stiffening correlates directly to binder stiffening.
(3) The change in mixture stiffness for different mixtures relates differently to binder stiffness. The Bryan mixture has a softer binder but a stiffer mixture compared to the Yoakum mixture.
(4) Mixture fatigue life declines significantly when the binder stiffens due to oxidative aging. The amount of decline for a given amount of binder stiffening can vary significantly from one mixture to the next.
(5) The decline in fatigue life with binder hardening appears to have a dramatic effect on pavement service life. Thus, differences between mixtures and the impact of binder aging on fatigue life can have a very significant impact on pavement life-cycle cost.
(6) From the binder-mixture relationships, aging shift factors (SF_{ag}) based on the binder visco-elastic properties were developed for each mixture type, and a relationship was developed between binder properties and mixture field N_f values. With more HMAC fatigue characterization, development of a single set of SF_{ag} coefficients for a different group of similar mixtures will inevitably allow for prediction of N_f at any pavement age without the need to test aged mixtures.

RECOMMENDATIONS

From the findings of this project, the following recommendations were made.

(1) More HMAC mixture laboratory fatigue characterization is recommended to:
- provide confidence and validation in the selected CMSE approach. The CMSE laboratory test protocol, failure criteria, and analysis procedure should be reviewed and if needed, modified accordingly. For instance, the 7.5 mm (0.3 inches) microcrack threshold should be reviewed to establish its adequacy as representative of the fatigue cracking process in the entire HMAC pavement structure. The current CMSE version is based on the generalized hypothesis that the growth of one crack is representative of the field pavement crack size distribution.
- populate the field N_f database of commonly used TxDOT rut resistant mixtures.
- provide additional data so as to adequately model and incorporate the effects of binder oxidative aging.

(2) A numerical analysis software for the CMSE (and CM) fatigue analysis approach(es) should be developed based on the analysis procedure described in this report. Such a program will among others lead to the following benefits:
- simplify and reduce the time required for the CMSE/CM fatigue analysis process.
- minimize human associated errors resulting from manual calculations.
- facilitate a faster methodology of conducting a sensitivity analysis on the CMSE/CM approach so as to reduce/eliminate redundant variables in CMSE/CM analysis models.
- facilitate a quicker and convenient way to validate and, if need be, modify the CMSE/CM approach based on more laboratory HMAC mixture characterization.

(3) Because of the apparent importance of fatigue decline with oxidative binder stiffening, more work is needed to understand this phenomenon and the essential features of mixture design that impact this decline. This effect is believed to be as much a mixture as a binder property and, if so, can only be established and understood through additional, carefully designed combined mixture-binder studies.

(4) For CMSE uniaxial laboratory testing, it is strongly recommended that the specimens must always be properly aligned along the central axis of loading to minimize the induction of undesirable moments that can lead to erroneous results.

CLOSURE

The CMSE/CM approaches described in this interim report are relatively new analysis procedures for fatigue characterization of HMAC mixtures and therefore still may be subject to review and/or modifications. These approaches predict N_f and recognize the dependence of fatigue cracking on the entire pavement structure when subjected to traffic loading. Investigation of surrogate fatigue test protocols based on CMSE testing for use in mix design and HMAC mixture screening is reported in Research Report 0-4468-3.

CURRENT AND FUTURE FY05 WORK

In the modified project, the research team plans to expand on the materials characterized in this interim report. This laboratory characterization of more HMAC mixtures will increase the TxDOT field N_f database, validate and provide more confidence in the selected CMSE/CM approach and, if need be, provide guidance on any necessary modifications. The third year will also provide more data for understanding the important phenomenon of binder oxidative aging and its influence on HMAC mixture fatigue resistance as well as developing shift factors to account for binder oxidative aging when estimating mixture field N_f.

Based on the limited timeframe and budget for the third year, mixture design for the FY05 mixtures will be limited to Superpave mixes only, with gravel as the only aggregate to be used. PG 64-22 and PG 76-22 binders will be used with two modifiers (SBS and tire rubber (TR)). In line with the prime objective and title of the overall project, the emphasis of the third year work plan is to characterize more rut resistant mixtures and compare the subsequent findings to the Yoakum mixture as well as to further investigate the effect of binder oxidative aging on the mixture fatigue resistance. Consequently, the focus of the modified project will be on modified binders, which provide rut resistant mixtures.

Two binder content levels, optimum and optimum plus 0.5 percent, consistent with TxDOT recommendations, will be utilized to investigate the effect of binder content on the fatigue resistance of the rut resistant mixtures. In terms of aging conditions, only two (0 and 6 months at 60 °C [140 °F]) will be addressed to supplement the 0, 3, and 6 months aging conditions.

Table 13-1 summarizes the possible FY05 mixtures based on a comprehensive factorial experimental design that can estimate all the main factors (binder type-modifier type (BTMT), binder content (BC), and aging) considered in the third year and the two-way interactions (BC*aging, BTMT*aging, and BTMT*BC).

Table 13-1. Example of a Factorial Experimental Design for FY05.

Run/Mixture	Binder Type-Modifier Type	Binder Content	Aging Condition (Months)
1	*PG 76-22_SBS*	*Optimum*	0
2	PG 76-22_TR	Optimum	0
3	PG 76-22_SBS	Optimum + 0.5%	0
4	PG 76-22_TR	Optimum + 0.5%	0
5	PG 64-22	Optimum	0
6	PG 64-22	Optimum + 0.5%	0
7	*PG 76-22_SBS*	*Optimum*	6
8	PG 76-22_TR	Optimum	6
9	PG 76-22_SBS	Optimum + 0.5%	6
10	PG 64-22	Optimum	6
11	PG 64-22	Optimum + 0.5%	6
12	PG 76-22_TR	Optimum + 0.5%	6

Note that the mixtures in *Italics* (Runs # 1 and 7) in Table 13-1 are the rut resistant mixtures already characterized in Phase I and presented in this interim report. At the end of the project in the third year modification, the following will be addressed:

- validation and provision of more confidence in the selected and recommended CMSE approach through utilization of more HMAC mixtures,

- a database of mixture field N_f results based on the CMSE approach,
- a better understanding and quantification of the binder-mixture relationships and effects of binder oxidative aging,
- development of a shift factor due to aging to be incorporated in the CMSE approach,
- investigation of the effects of binder content and modification on mixture field N_f and aging,
- development of a fatigue design check criteria for the CMSE fatigue analysis approach, and
- investigation of the possibility of establishing a surrogate fatigue test protocol based on CMSE testing (TS, RM, or RDT) for use only in mix design and HMAC mixture screening without prediction of N_f

REFERENCES

1. Deacon, J. A., J. S. Coplantz, A. A. Tayebali, and C. L. Monismith, "Temperature Considerations in Asphalt-Aggregate Mixture Analysis and Design," *Transportation Research Record* 1454, pp. 97-112 (1994).

2. Tayebali, A.A., J.A Deacon, J.S. Coplantz, J.T. Harvey, and C. L., Monismith, Fatigue Response of Asphalt Aggregate Mixes. SHRP A-003 (1992).

3. Superpave Models Team, *Simple Performance Test: Test Results and Recommendations Interim Task C Report*, NCHRP 9-19 Superpave Support and Performance Models Management, Project Deliverable Subtask C.3, Arizona State University: College of Engineering and Applied Sciences, Department of Civil and Environmental Engineering (2000).

4. Witczak, M., *Chapter 2: Material Characterization*, Draft NCHRP 1-37A Report, Arizona State University: College of Engineering and Applied Sciences, Department of Civil and Environmental Engineering (2001).

5. Kim, Y. R., H-J Lee, and D. N. Little, "Fatigue Characterization of Asphalt Concrete Using Viscoelasticity and Continuum Damage Theory," *Journal of the Association of Asphalt Paving Technologists*, Vol. 66, pp. 520-569 (1997).

6. Kim, Y. R., H-J Lee, Y. Kim, and D. N. Little, "Mechanistic Evaluation of Fatigue Damage Growth and Healing of Asphalt Concrete: Laboratory and Field Experiments," *Proceedings of the 8th International Conference on Asphalt Pavements*, Seattle, Washington, August 10-14, pp. 1089-1107 (1997).

7. Epps, A. L., J. T. Harvey, and C. L. Monismith, "Performance Characteristics of Mixes Containing Asphalt Cements and Crumb Rubber Modified Binders," presented at the Symposium on Asphalt, Number One Thermoplastic Polymer as part of the 217th American Chemical Society Meeting, Anaheim, California, March 23 (1999).

8. Harvey, J., T. Hoover, W. Nokes, N. F. Coetzee, and F. Rust, "CalTrans Accelerated Pavement Test (CAL/APT) Program – Test Results: 1994-1997," *Journal of the Association of Asphalt Paving Technologists*, Vol. 67, pp. 644-689 (1998).

9. Rowe, G. M., and S. F. Brown, "Validation of the Fatigue Performance of Asphalt Mixtures with Small Scale Wheel Tracking Experiments," *Journal of the Association of Asphalt Paving Technologists*, Vol. 66, pp. 31-73 (1997).

10. Rowe, G. M., and S. F. Brown, "Fatigue Life Prediction Using Visco-Elastic Analysis," *Proceedings of the 8th International Conference on Asphalt Pavements*, Seattle, Washington, August 10-14, pp. 1109-1122 (1997).

11. Matthews, J., C. L. Monismith, and J. Craus, "Investigation of Laboratory Fatigue Testing Procedures for Asphalt Aggregate Mixtures," *Journal of Transportation Engineering*, Vol. 119, July/August, pp. 634-654 (1993).

12. Walubita, L.F., F. Hugo, and A. Epps, "Indirect Tensile Fatigue Performance of Asphalt Concrete after MMLS3 Mk3 Trafficking Under Different Environmental Conditions," *Journal of the South African Institute of Civil Engineering* (2001).

13. Walubita, L., F. Hugo, and A. Epps, *Performance of Rehabilitated Lightweight Aggregate Asphalt Concrete Pavements Under Wet and Heated Model Mobile Load Simulator Trafficking: A Comparative Study with the TxMLS*, Center for Transportation Research Report #1814-3, Austin, Texas: The University of Texas at Austin (2000).

14. van de Ven, M., A. d. F. Smit, and R. Krans, "Possibilities of a Semi-Circular Bending Test," *Proceedings of the 8th International Conference on Asphalt Pavements*, Seattle, Washington, August 10-14, pp. 939-950 (1997).

15. Monismith, C. L., J. A. Deacon, and J. T. Harvey, *WesTrack: Performance Models for Permanent Deformation and Fatigue*, University of California, Berkeley: Pavement Research Center, Institute of Transportation Studies (2000).

16. Tsai, B. W., J. T. Harvey, and C. L. Monismith, "WesTrack Fatigue Performance Prediction Using Miner's Law," presented at the 81st Annual Meeting of the Transportation Research Board, Washington, D.C., January 13-17 (2002).

17. Ali, H. A., and S. D. Tayabji, "Evaluation of Mechanistic-Empirical Performance Prediction Models for Flexible Pavements," *Transportation Research Record* 1629, pp. 169-180 (1998).

18. Miner, M.A. Cumulative Damage in Fatigue, Transactions of ASME, Vol. 67, pp A159-A164 (1945)

19. Tasi, B.W., J.T. Harvey, and C.C.L Monismith, "Calibration of Pavement Fatigue Performance Using Recursive Miner's Law," 2nd International Conference on Accelerated Pavement Testing, Minnesota (2004).

20. Castell, M. A., and P. Pintado, "Sensitivity Analysis for Estimation of Pavement Fatigue Life," *Journal of Transportation Engineering*, Vol. 125, No. 2, pp. 114-122 (1999).

21. Bonnaure, F., A. Gravois, and J. Udron, "A New Method for Predicting the Fatigue Life of Bituminous Mixes," *Proceedings of the Association of Asphalt Paving Technologists*, Vol. 49, pp. 499-524 (1980).

22. Witczak, M., and T. Pellinen, "Use of Stiffness of Hot-Mix Asphalt as a Simple Performance Test," presented at the 81st Annual Meeting of the Transportation Research Board, Washington, D.C., January 13-17 (2002).

23. Ioannides, A. M., "Fracture Mechanics in Pavement Engineering: The Specimen-Size Effect," *Transportation Research Record* 1568, pp. 10-16 (1997).

24. Molenaar, A. A. A., and T. O. Medani, "Rational Testing Methods for Performance Based Specifications," *Proceedings of the 1st International World of Asphalt Pavements Conference*, Sydney, Australia, February 20-24, CD-ROM (2000).

25. Hopman, P., and R. Nilsson, "COMPASS: To Design Functional Mixes," *Proceedings of the 1st International World of Asphalt Pavements Conference*, Sydney, Australia, February 20-24, CD-ROM (2000).

26. Schapery, R. A., "Correspondence Principles and a Generalized J-Integral for Large Deformation and Fracture Analysis of Viscoelastic Media." *International Journal of Fracture*, Vol. 25, pp. 195-223 (1984).

27. Mamlouk, M. S., and P. P. Khanal, "Bimodular Analysis of Asphalt Pavements," *Proceedings of the 8th International Conference on Asphalt Pavements*, Seattle, Washington, August 10-14, pp. 707-723 (1997).

28. Zhang, T., and L. Raad, "Numerical Methodology in Fatigue Analysis: Applications," *Journal of Transportation Engineering*, Vol. 127, No. 1, pp. 59-66 (2001).

29. Jacobs, M. M. J., P. C. Hopman, and A. A. A. Molenaar, "Application of Fracture Mechanics Principles to Analyze Cracking in Asphalt Concrete," *Journal of the Association of Asphalt Paving Technologists*, Vol. 65, pp. 1-39 (1996).

30. Simons, J. W., and L. Seaman, "Finite-Element Analysis of Fatigue Lifetime in Pavements," Transportation Research Record No. 1709, pp. 36-42 (2000).

31. Mobasher, B., M. Mamlouk, and H-M Lin, "Evaluation of Crack Propagation Properties of Asphalt Mixtures," *Journal of Transportation Engineering*, Vol. 123, No. 5, pp. 405-413 (1997).

32. Kim, Y. R., H-J Lee, and D. N. Little, "Fatigue Characterization of Asphalt Concrete Using Viscoelasticity and Continuum Damage Theory," *Journal of the Association of Asphalt Paving Technologists*, Vol. 66, pp. 520-569 (1997).

33. Kim, Y. R., H-J Lee, Y. Kim, and D. N. Little, "Mechanistic Evaluation of Fatigue Damage Growth and Healing of Asphalt Concrete: Laboratory and Field Experiments," *Proceedings of the 8th International Conference on Asphalt Pavements*, Seattle, Washington, August 10-14, pp. 1089-1107 (1997).

34. Nishizawa, T., S. Shimeno, and M. Sekiguchi, "Fatigue Analysis of Asphalt Pavements with Thick Asphalt Mixture Layer," *Proceedings of the 8th International Conference on Asphalt Pavements*, Seattle, Washington, August 10-14, pp. 969-976 (1997).

35. Daniel, J. S., and Y. R. Kim, "Development of a Simplified Fatigue Test and Analysis Procedure Using a Viscoelastic, Continuum Damage Model," to be presented at the Annual Meeting of the Association of Asphalt Paving Technologists, March 18-20 (2002).

36. Wen, H., and Y. R. Kim, "A Simple Performance Test for Fatigue Cracking of Asphalt Concrete Based on Viscoelastic Analysis of Indirect Tensile Testing and Its Validation Using WesTrack Asphalt Mixtures," presented at the 81st Annual Meeting of the Transportation Research Board, Washington, D.C., January 13-17 (2002).

37. AASHTO, *AASHTO Provisional Standards*, Interim Edition, Washington, D.C.: American Association of State Highway and Transportation Officials (2000).

38. Uzan, J., "Asphalt Concrete Characterization for Pavement Performance Prediction," *Journal of the Association of Asphalt Paving Technologists*, Vol. 65, pp. 573-607 (1996).

39. Lee, N. K., G. R. Morrison, and S. A. M. Hesp, "Low Temperature Fracture of Polyethylene-Modified Asphalt Binders and Asphalt Concrete Mixes," *Journal of the Association of Asphalt Paving Technologists*, Vol. 64, pp. 534-574 (1995).

40. Zhou, J., and R. Y. Liang, "Fatigue Model of Asphalt Concrete," *Proceedings of the 11th Conference on Engineering Mechanics*, Fort Lauderdale, Florida, May 19-22, pp. 563-567 (1996).

41. Liang, R. Y., and J. Zhou, "Prediction of Fatigue Life of Asphalt Concrete Beams," *International Journal of Fatigue*, Vol. 19, No. 2, pp. 117-124 (1997).

42. Uzan, J., "Evaluation of Fatigue Cracking," Transportation Research Record 1570, pp. 89-95 (1997).

43. Little, D., R. Lytton, D. Williams, C. W. Chen, Y. R. Kim, and H. J. Lee, *Fundamental Properties of Asphalts and Modified Asphalts: Task K – Microdamage Healing in Asphalt and Asphalt Concrete, Final Report, Volume I: Microdamage and Microdamage Healing – Project Summary Report*, Washington, D.C.: Federal Highway Administration (1998).

44. Little, D., R. Lytton, Z. Si, D. Xin, and Y. R. Kim, *Crack Phenomenology: Formation and Healing - Task K Findings, Interim Report*, Texas Transportation Institute, College Station, Texas (2000).

45. Lytton, R. L., J. Uzan, E. G. Fernando, R. Roque, D. Hiltunen, and S. Stoffels, *Development and Validation of Performance Prediction Models and Specifications for Asphalt Binders and Paving Mixes*, SHRP-A-357, Washington, D.C.: Strategic Highway Research Program, National Research Council (1993).

46. Hefer, A. W. "Adhesion in Bitumen-Aggregate Systems and Quantification of the Effects of Water on the Adhesion Bond." PhD Dissertation, Texas A&M University, College Station, Texas (2004).

47. CastelloBlanco, A., "Probabilistic Analysis of Air Void Structure and Its Relationship to Permeability and Moisture Damage of Hot-Mix Asphalt." Masters Thesis, Texas A&M University, College Station, Texas (2004).

48. Knorr, D. B., Jr., R. R. Davison, and C. J. Glover, "The Effect of Various Aging Techniques on Asphalt Low-Temperature Properties," presented at the 81st Annual Meeting of the Transportation Research Board, Washington, D.C., January 13-17 (2002).

49. Doyle, P. C., "Cracking Characteristics of Asphalt Cement," *Proceedings of the Association of Asphalt Paving Technologists*, Vol. 27, pp. 581-597 (1958).

50. Halstead, W. J., *Relation of Asphalt Chemistry to Physical Properties and Specifications*, FHWA/VA-84/85, Virginia Department of Highways and Transportation (1984).

51. Ruan, Y., R. R. Davison, and C. J. Glover, "An Investigation of Asphalt Durability: Relationships between Ductility and Rheological Properties for Unmodified Asphalts," accepted for publication, *Petroleum Science and Technology* (2002).

52. Glover, C.J., R.R. Davison, C.H. Domke, Y. Ruan, P. Juristyarini, D.B. Knorr, and H.S. Jung.,Development of a New Method for Assessing Asphalt Binder Durability with Field Validation. Technical Research Report FHWA/TX-03/1872-2 (2003).

53. Texas Department of Transportation (TxDOT), *Standard Specifications for Construction and Maintenance of Highways, Streets, and Bridges*, Texas (1995).

54. Texas Department of Transportation (TxDOT), Bryan District Laboratory. HMACP Mixture Design Used on US 290 and SH 47: Unpublished Internal Laboratory Test Report. Bryan, Texas (2002).

55. AASHTO PP6-94, Standard Practice for Grading or Verifying the Performance Grade of an Asphalt Binder (1996).

56. AASHTO TP5-98, Standard Test Method for Determining the Rheological Properties of Asphalt Binder Using a Dynamic Shear Rheometer (DSR) (1998).

57. *Pocket Facts*. TxDOT Test Specification Manuals. (http://manuals.dot.state.tx.us) Accessed May (2003).

58. AASHTO Designation: PP2. Standard Practice for Short and Long Term Aging of Hot Mix Asphalt, *AASHTO Provisional Standards*, Washington, D.C June Edition (1994).

59. AASHTO TP8-94, Standard Test Method for Determining the Fatigue Life of Compacted Hot-Mix Asphalt (HMA) Subjected to Repeated Flexural Bending (1996).

60. Tom, F. *Flexible Pavement Database.* Texas Transportation Institute. Ongoing Research Project 187-06, College Station, Texas (2004).

61. TxDOT, "Condition of Texas Pavements. Pavement Management Information System (PMIS) Annual Report, FY 2001 – 2003," TxDOT, Construction Division, Materials and Pavement Section, April (2003).

62. Ahlborn G., "ELSYM5, Computer Program for Determining Stresses and Deformations in Five Layer Elastic System." University of California, Berkeley (1969).

63. Park, D. W., "Characterization of Permanent Deformation in Asphalt Concrete Using a Laboratory Prediction Method and an Elastic-Viscoplastic Model." Ph. D. Dissertation, Texas A&M University, College Station, Texas (2004).

64. Huang, Y.H. "Pavement Analysis and Design." Prentice Hall, New Jersey (1993)

65. ABAQUS, *ABAQUS Users Manual.* Hibbit, Karlsson and Sorenson, Inc., Pawtucket, R.I., (1996).

66. Asphalt Institute, AI Research, Determination of Threshold Strain Level for Infinite Fatigue Life in Asphalt Mixtures. Interim Report for the Asphalt Alliance (2002).

67. Jianlong, Z., and L. Francken, "A Research on the Dissipated Energy Density of Bituminous Mixtures and Overlay," *Proceedings of the XIIIth World Meeting of the International Road Federation*, Toronto, Canada, June 16-20 (1997).

68. Si, Z., "Characterization of Microdamage and Healing of Asphalt Concrete Mixtures." Ph.D. Dissertation, Texas A&M University, College Station, Texas (2001).

69. Lytton, R.L., "Characterizing Asphalt Pavements for Performance," *Transportation Research Record* 1723, pp. 5-16 (2000).

70. Good, R. J., and C. J. Van Oss, "The Modern Theory of Contact Angles and the Hydrogen Bond Components of Surface Energies, *Modern Approaches to Wettability*, M. E. Schrader and G. Loeb, eds., New York: Plenum Press (1992).

71. Cheng, D., "Surface Free Energy of Asphalt-Aggregate System and Performance Analysis of Asphalt Concrete based on Surface Free Energy." Ph.D. Dissertation, Texas A&M University, College Station, Texas (2002).

72. Arramon, Y. P., M.M. Mehrabadi, D.W. Martin, and S.C. Cowin., "A Multidimensional Anisotropic Strength Criterion based on Kelvin Modes." *International Journal of Solids and Structures*, Vol. 37, pp. 2915-2935 (2000).

73. Tashman, L., E. Masad, H. Zbib, D. Little, and K. Kaloush., "Microstructural Viscoplastic Continuum Model for Asphalt Concrete." *Journal of Engineering Mechanics, ASCE* (2003).

74. Adu-Osei, A., "Characterization of Unbound Granular Base" Ph.D. Dissertation, Texas A&M University, College Station, Texas (2000).

75. Kim. S.H., D.N. Little, E. Masad, and R.L. Lytton., "Determination of Anisotropic Moduli Considering Aggregate Particle Shape and Gradation in Unbound Granular Layer" *Paper Presented at the 83rd Annual Meeting of the TRB*, Washington D.C. (2004).

76. Maugis, D., *Contact, Adhesion and Rupture of Elastic Solids.* Springer, New York, pp. 3-12 (1999).

77. Little, N.D., A. Bhasin, R. L Lytton, and A. Hefer., *Interim Report on Using Surface Energy Measurements to Select Materials for Asphalt Pavements*, NCHRP 9-37, Washington, D.C.: National Cooperative Highway Research Program, Transportation Research Board, National Research Council (2003).

78. Khanal, P.P., and M. Manlouk., "Tensile versus Compressive Moduli of Asphalt Concrete" TRB, Transportation Research Record No. 1482, Washington D.C., pp. 144-150 (1995).

79. Lytton, R.L., "*CVEN 689, Special Topics in Micromechanics of Civil Engineering" Graduate Civil Engineering Course offered in Fall 2001*, Texas A& M University, College Station, Texas (2001).

80. Tseng, K. H., and R. L. Lytton., "Fatigue Damage Properties of Asphaltic Concrete Pavements." *Transportation Research Record No. 1022*, TRB, National Research Council, Washington, D.C., 52-59 (1990).

81. Al- Qadi, I.L., and W.N. Nassar, "Fatigue Shift Factors to Predict HMA Performance", *The International Journal of Pavement Engineering*, Vol. 4(2), pp. 69-76, June (2003).

82. Blab, R., and J. Litzka, "Measurements of the Lateral Distribution of Heavy Vehicles and its Effects on the Design of Road Pavements", *Proceedings of the International Symposium on Heavy Vehicle Weights and Dimensions*, Ontario, Canada, pp. 389-395 (1995).

83. Lytton, R. L., *Personal Communication*, Texas Transportation Institute (TTI), College Station, Texas (2004).

84. Francken, L. and C. Clauwaert, "Characterization and Structural Assessment of Bound Materials for Flexible Road Structures," Proceedings 6th International Conference on the Structural Design of Asphalt Pavements, Ann Arbor, 1987; University of Michigan, pp. 130-144, Ann Arbor, Michigan (1988).

85. Daniel, J. S., and Y. R. Kim, "Development of a Simplified Fatigue Test and Analysis Procedure Using a Viscoelastic, Continuum Damage Model," to be presented at the *Annual Meeting of the Association of Asphalt Paving Technologists*, March 18-20 (2002).

86. Wen, H., and Y. R. Kim, "A Simple Performance Test for Fatigue Cracking of Asphalt Concrete Based on Viscoelastic Analysis of Indirect Tensile Testing and Its Validation Using WesTrack Asphalt Mixtures," presented at the 81st Annual Meeting of the Transportation Research Board, Washington, D.C., January 13-17 (2002).

87. *Pocket Facts*. Traverse Area Determination: Double Meridian Distance Method http://www.tpub.com/content/engineering/14070/css/14070_136.htm Accessed April (2004).

88. Marek, C.R., and M. Herrin, "Tensile Behavior and Failure Characteristics of Asphalt Cements in Thin Films," *Proceedings of the Association of Asphalt Paving Technologists*, Atlanta, Georgia, February 26-28, Vol. 37, pp. 386-421 (1968).

89. AASHTO, (2004*). Pocket Facts.* AASHTO 2002 Pavement Design Guide. http://www.2002designguide.com/ http://www.trb.org/mepdg/ Accessed June (2005).

90. Mirza, M.W. and M.W. Witczak, "Development of a Global Aging System Short and Long Term Aging of Asphalt Cements," *Journal of the Association of Asphalt Paving Technologists,* Vol. 64, pp. 393-430 (1995).

91. AASHTO Designation: TP 62-03. Standard Method of Test for Determining Dynamic Modulus of Hot Mix Asphalt Concrete Mixtures (2001).

92. Pellinen, T.K., and M.W. Witczak, "Stress Dependent Master Curve Construction for Dynamic (Complex) Modulus," *Annual Meeting of the Association of Asphalt Paving Technologists*, Colorado, March (2002).

93. Liu, M., et al. *The Kinetics of Carbonyl Formation in Asphalt.* Aiche Journal, Vol. 42, pp. 1069-1076 (1996).

94. Welborn, J.Y., *Physical Properties as Related to Asphalt Durability: State of the Art.* Transportation Research Record No. 999, pp. 31-36 (1984).

95. Kandhal, P.S., and W.C. Koehler, *Significant Studies on Asphalt Durability: Pennsylvania Experience.* Transportation Research Record No. 999, pp. 41-50 (1984).

96. Ruan, Y., R.R. Davison, and C.J. Glover, *An Investigation of Asphalt Durability: Relationships between Ductility and Rheological Properties for Unmodified Asphalts.* Petroleum Science and Technology, pp. 231-254 (2003).

97. Vassiliev, N.Y., R.R. Davison, and C.J. Glover, *Development of a Stirred Airflow Test Procedure for Short-Term Aging of Asphaltic Materials.* Bituminous Binders, pp. 25-32 (2002).

98. Vassiliev, N.Y., et al., *Air Blowing of Supercritical Asphalt Fractions.* Industrial & Engineering Chemistry Research, pp. 1773-1780 (2001).

99. Stegeman, J.R., et al., *Compositional and Physical Properties of Asphalt Fractions Obtained by Supercritical and Solvent Extraction.* Fuel Science & Technology International, pp. 767-794 (1992).

100. Davison, R.R., et al., *Size Exclusion Chromatography of Asphalts.* Chromatographic Science Series, pp. 211-247 (1995).

101. ASTM D 113 – 86. "Standard Test Method for Ductility of Bituminous Materials," Annual Book of ASTM Standards, 04.03, ASTM, Easton, Maryland, 23 (1994)

102. Jemison, H.B., et al., *Application and Use of the ATR, FTIR Method to Asphalt Aging Studies.* Preprints - American Chemical Society, Division of Petroleum Chemistry, pp. 490-495 (1990).

103. Liu, M., et al., *Oxygen Uptake as Correlated to Carbonyl Growth in Aged Asphalts and Asphalt Corbett Fractions.* Industrial & Engineering Chemistry Research, pp. 466-467 (1998).

104. Ferry, J. D. Viscoelastic Properties of Polymers, Wiley, New York (1980).

105. Williams, D.J., Polymer science and engineering. Prentice-Hall International Series in the Physical and Chemical Engineering Sciences, Prentice-Hall, New Jersey (1971).

106. Huang, Y.H., Pavement Analysis and Design. Prentice Hall, New Jersey (1993).

107. Kandhal, P.S., *Low-Temperature Ductility in Relation to Pavement Performance*. In ASTM STP 628: Low-Temperature Properties of Bituminous Materials and Compacted Bituminous Paving Mixtures, C.R. Marek (Ed.), American Society for Testing and Materials, PP. 95-106 (1977).

108. Schapery, R.A., A Theory of Crack Growth in Viscoelastic Media, Technical Report No. 2, Mechanics & Materials Research Center, Texas A&M University, College Station, Texas (1973).

109. Christensen, R.M., and D.A. Anderson, 'Interpretation of Dynamic Mechanical Test Data for Paving Grade Asphalt Cements." *Journal of the Association of Asphalt Paving Technologists*, Vol. 61, pp. 67-98 (1992).

110. Medani, T.O., Huurman, M., and A.A.A. Molenaar, "On the Computation of Master Curves for Bituminous Mixes." EuroBitumen (2004).

111. Aparicio Ramos, S I., "Study of the Asphalt Pavement Damage through Non-Destructive Testing on Overweight Truck Routes," Masters Thesis, Texas A&M University, College Station, Texas (2003).

112. Oh, Jeong-Ho, "Field Monitoring and Modeling of Pavement Response and Service Life Consumption Due to Overweight Truck Traffic," PhD Dissertation, Texas A&M University, College Station, Texas (2004).

113. Rowe, G.M., and M. G. Bouldin, "Improved Techniques to Evaluate the Fatigue Resistance of Asphaltic Mixtures". 2nd Euroaphalt and Eurobitumen Congress, Book 1, pp. 754-763, Barcelona, Spain, September (2000).

114. Wisneski, M.L., J.M. Chaffin, R.R. Davison, J.A. Bullin, and C.J. Glover, Use of Lime in Recycling Asphalt. Transportation Research Board No. 1535, pp. 117-123 (1996).

115. Juvinall, R.C., and K.M. Marshek, Fundamentals of Machine Component Design. John Wiley & Sons (2000).

116. Coons, R.F., and P.H. Wright, *An Investigation of the Hardening of Asphalt Recovered from Pavements of Various Ages*. *Journal of the Association of Asphalt Paving Technologists*, pp. 510-528 (1968).

117. Ghuzlan, K., and S. Carpenter, "Energy-Derived, Damage-Based Failure Criterion for Fatigue Testing," Transportation Research Board, Vol. 1723, National Academy Press, Washington D.C. (2000).

118. James Cox & Sons, Inc., *2004 Price List*, Model CS7600 4-pt Bending Fixture, Colfax, California (2004).

APPENDICES

APPENDIX A: EVALUATION FIELD SURVEY QUESTIONAIRE (FOR GOVERNMENT AGENCIES AND THE INDUSTRY)

TxDOT PROJECT 0-4468 FATIGUE RESISTANT MIXES AND DESIGN METHODOLOGY SURVEY

This survey is conducted as part of the Texas Department of Transportation (TxDOT) research Project No. 0-4468, Evaluation of the Fatigue Resistance of Rut Resistant Mixes, under the supervision of Gregory Cleveland (512-506-5830). The primary goal of this project is to develop and recommend the process for incorporating fatigue analysis and testing into TxDOT's pavement design and mixture design process. TxDOT already has the means to screen out mixtures that are susceptible to rutting; mixtures with stiffer binders greatly decrease the risk of premature failure due to rutting. However, there are concerns that some of the mixtures that are highly resistant to rutting may be more prone to fatigue failure. To identify, document, and compare several materials, mixtures, and pavement structure types in terms of fatigue resistance, we are sending out this survey to several government agencies and industry representatives in order to create a complete knowledge database.

We would appreciate your participation. If there are any questions concerning this survey or this project, please contact Dr. Amy Epps Martin (979-862-1750) of the Texas Transportation Institute. Once again we appreciate your time and assistance.

Agency Name: _____ **Contact Name:** _____

Phone: (____ ___) - _____ - _____ **Fax:** (_____) - _____ - _____

---

1. Do you utilize any methodology or approach to design and/or check for fatigue resistance?

   YES _____ *please proceed to question 2*. **NO** _____ *please stop*.

2. What mix design methodology(ies) or approach(es) do you follow?_____

3. List literature references you have found useful to approach fatigue resistance designs.

   _____

4. List the laboratory tests, and corresponding standards, performed as part of the fatigue resistance approach(es) you use.

   _____

5. What type(s) of aggregate(s) and binder(s) grades do you use for fatigue resistant mixes?

Aggregate Type	Binder Grade

6. What pavement structure(s) do you commonly use for fatigue resistant pavement design?

Layer	Thickness	Elastic Modulus

7. What type and amount of resources (time, persons, equipment, etc.) do you require to perform a fatigue resistant mix and pavement design?

Thank you for your time and effort in completing this survey. The results will aid us to identify, document, and compare several materials, mixtures, and pavement structure types in terms of fatigue resistance.

APPENDIX A (CONTINUED): SUMMARY RESULTS OF EVALUATION FIELD SURVEY QUESTIONNAIRE

(FROM GOVERNMENT AGENCIES AND THE INDUSTRY)

TxDOT PROJECT 0-4468: FATIGUE RESISTANT MIXES AND DESIGN METHODOLOGY SURVEY

Table A1. Summary of Respondent Questionnaire Survey Details.

No.	Agency	Contact	Fatigue Methodology	Laboratory Tests	Materials		Pavement Structures			Resources	Standards/ References
					Aggregate	Binder	Layer	Thickness	Modulus		
1	Advanced Asphalt Technologies, LLC	D W. Christensen 814-278 1991	Continuum damage analysis (NCHRP 9-25 and 9-31)	Uniaxial fatigue testing	9.5 – 12 mm, dense gradation	-	-	-	-	-16 hrs -Compactor, ovens, molds, saw, coring rig, MTS system	AAPT papers on Continuum Damage modeling & analysis
2	Abatech	G.Rowe 215 – 215 258	Superpave	Bending beam and SHRP IDT	-	-	-	-	-	≥ $40,000	Various paper publications
3	Louisiana DOTD	C.Abadie 225-767 9109	Superpave	Modified T-283, Moisture sensitivity & retained ITS	Various	PG 76-22 Modified	-	-	Use SN criteria, i.e. 0.44 to 0.48 for HMAC	No special design procedure for fatigue	Superpave
4	North Carolina State University	Y.R. Kim 619-515 7758	Visco-elastic continuum damage model	Uniaxial tension & indirect tension	Granite	PG 64-22	-	-	-	MTS & graduate students	-
5	Minnesota DOT	S. Dai 651-779 5218	Superpave & MnPave	No fatigue tests	-	-	Mechanistic-empirically based			One researcher	Superpave
6	UCB, Berkeley	M.O. Bejarano 510-231-5746	Caltrans & Asphalt Institute	Bending beam, AASHTO TP-8	Crushed stone, dense graded	AR 4000 AR 8000	AC	150 mm	1000 to 8 000 MPa	-2-3 wks -4 people -bending beam device (Cox & Sons)	-NCHRP 39 -Various publications

APPENDIX B : HMAC ANISOTROPIC ADJUSTMENT FACTORS

Table B1. Example of Determination of Anisotropic Adjustment Factors (a_i).

Test#	HMAC Elastic Modulus (MPa) Under Unconfined Conditions		HAMC Elastic Modulus (MPa) Under Confined Conditions		$a_x = E_{x(c)}/E_{x(u)}$	$a_z = 1/(E_{z(c)}/E_{x(u)})$
	$E_{x(u)}$	$E_{z(u)}$	$E_{x(c)}$	$E_{z(c)}$		
1	1789	3399	1940	4450	1.08	0.76
2	1569	2980	1785	3927	1.14	0.76
3	1678	3188	1963	4320	1.17	0.74
4	1589	3219	1900	4180	1.20	0.77
5	1498	2846	1760	3972	1.17	0.71
Mean	1625	3127	1870	4170	1.15	0.75
Stdev	112	216	92	223	0.04	0.02
COV	6.90%	6.91%	4.91%	5.35%	3.76%	2.96%

APPENDIX B (CONTINUED):
THE UNIVERSAL SORPTION DEVICE

Table B2. Summary of the Testing and Analysis Procedure for Determining the Surface Energy of Aggregates Using the USD Method.

Step	Action
1	The aggregate sample is prepared from the fraction passing the No.4 (4.75mm) sieve, retained on the No.8 (2.36mm) sieve. • Wet sieve approximately 150 g of each type of aggregate. • Wash the samples again using distilled water and dry in a 120 °C (248 °F) oven for at least 8 hrs. • Move the samples into a vacuum desiccator at about 1 torr and 120 °C (248 °F) for at least 24 hrs to de-gas. • Wash the aggregate sample holder with distilled water and acetone and then dry in a 120°C (248 °F) oven for 1 hr.
2	Place the weighed aggregate in the container and proceed with chamber conditioning: • Connect the temperature control circulator with the high-pressure steel chamber. • Activate and calibrate the Magnetic Suspension Balance. • Use the vacuum pump to evacuate the chamber to below 1 torr for one day while it is heated up to 60 °C (140 °F). • Reduce and maintain the chamber temperature at 25°C (77 °F) under the vacuum of below 1 torr for 8 hrs.
3	Proceed with testing using the selected solvents: n-hexane (apolar), methyl-propyl-ketone (mono-polar) and water (bipolar): • Initiate the computer program to control testing and control data capturing and enter 8 to 10 predetermined pressure steps based on the saturation vapor pressure of the solvents used. The following two steps are then controlled automatically and is included for completeness of process description. • Solvent vapor is injected into the system until the first predetermined value is reached by using the macro-adjustment valve. After the steady-state adsorption mass is reached and measured by the system, the pressure is changed to the next setting point. • Last step is repeated while the computer records the absorbed mass and vapor pressure until the saturated vapor pressure of solvent is reached.
4	Use the specific amount of solvent adsorbed on the surface of the adsorbent and vapor pressure at the surface of the asphalt or aggregate to do surface energy calculations: • Calculate the specific surface area of the aggregate using the BET equation. • Calculate the spreading pressure at saturation vapor pressure for each solvent using Gibbs adsorption equation. • Calculate the three unknown components of surface energy utilizing the equilibrium spreading pressure of adsorbed vapor on the solid surface and known surface energies of the a polar, mono-polar, and bipolar solvents.
5	Using SE results from step 4, calculate the total surface energy of the aggregate.

APPENDIX C: BENDING BEAM LABORATORY TEST DATA FOR THE MECHANISTIC EMPIRICAL APPROACH

Table C1. ME Mixture *N* Data for 0, 3, and 6 Months Aging Conditions.

Rows	Micro Strain	Nf Lab Bryan-0M	Nf Lab Bryan-3M	Nf Lab Yoakum-0M	Nf Lab Yoakum-3M	Nf Lab Yoakum-6M
1	374	131000	71400	246580	170000	76600
2	374	120000	90600	201000	191000	138000
3	374	130000	78560	.	155500	110000
4	468	55000	47000	95200	68200	40450
5	468	51000	32000	115500	90000	46000
6	468	46000	40500	.	100300	55000
7	157	.	.	.	.	.
8	278.96	.	.	.	.	.
9	273.21	.	.	.	.	.
10	289.47	.	.	.	.	.
11 (US290)	98.97	.	.	.	.	.

Table C2. Example of ME Log-Transformation of Table B1 Data.

Rows	Log Micro Strain	Log Nf Lab Bryan-0M	Log Nf Lab Bryan-3M	Log Nf Lab Yoakum-0M	Log Nf Lab Yoakum-3M	Log Nf Lab Yoakum-6M
1	5.92	11.78	11.18	12.42	12.04	11.25
2	5.92	11.70	11.41	12.21	12.16	11.84
3	5.92	11.78	11.27	.	11.95	11.61
4	6.15	10.92	10.76	11.46	11.13	10.61
5	6.15	10.84	10.37	11.66	11.41	10.74
6	6.15	10.74	10.61	.	11.52	10.92
7	5.06	.	.	.	.	.
8	5.63	.	.	.	.	.
9	5.61	.	.	.	.	.
10	5.67	.	.	.	.	.
11 (US290)	4.59	.	.	.	.	.

APPENDIX C (CONTINUED): BB LABORATORY TEST DATA

Table C3. Example of ME 95 Percent Prediction Interval Estimates of Log N_f (Bryan Mixture).

Rows	Log Micro Strain	Predicted Log Nf Bryan-0M (Yhat_B0)	Lower 95% prediction interval for Yhat_B0	Upper 95% prediction interval for Yhat_B0	Predicted Log Nf Bryan-3M (Yhat_B3)	Lower 95% prediction interval for Yhat_B3	Upper 95% prediction interval for Yhat_B3
1	5.92	11.75	11.52	11.98	11.29	10.77	11.80
2	5.92	11.75	11.52	11.98	11.29	10.77	11.80
3	5.92	11.75	11.52	11.98	11.29	10.77	11.80
4	6.15	10.83	10.60	11.06	10.58	10.06	11.10
5	6.15	10.83	10.60	11.06	10.58	10.06	11.10
6	6.15	10.83	10.60	11.06	10.58	10.06	11.10
7	*5.06*	*15.32*	*14.57*	*16.06*	*14.02*	*12.36*	*15.69*
8	*5.63*	*12.96*	*12.59*	*13.32*	*12.21*	*11.39*	*13.03*
9	*5.61*	*13.04*	*12.66*	*13.42*	*12.28*	*11.43*	*13.12*
10	*5.67*	*12.80*	*12.46*	*13.15*	*12.10*	*11.32*	*12.87*
11 (US290)	*4.59*	*17.21*	*16.14*	*18.28*	*15.48*	*13.08*	*17.88*

Table C4. Example of ME 95 Percent Prediction Interval Estimates of Log N_f (Yoakum Mixture).

Rows	Log Micro Strain	Predicted Log Nf Yoakum-0M (Yhat_Y0)	Lower 95% prediction interval for Yhat_Y0	Upper 95% prediction interval for Yhat_Y0	Predicted Log Nf Yoakum-3M (Yhat_Y3)	Lower 95% prediction interval for Yhat_Y3	Upper 95% prediction interval for Yhat_Y3
1	5.92	12.31	11.57	13.05	12.05	11.54	12.56
2	5.92	12.31	11.57	13.05	12.05	11.54	12.56
3	5.92	12.31	11.57	13.05	12.05	11.54	12.56
4	6.15	11.56	10.82	12.30	11.35	10.84	11.86
5	6.15	11.56	10.82	12.30	11.35	10.84	11.86
6	6.15	11.56	10.82	12.30	11.35	10.84	11.86
7	*5.06*	*15.23*	*12.50*	*17.96*	*14.77*	*13.13*	*16.41*
8	*5.63*	*13.30*	*12.01*	*14.58*	*12.97*	*12.17*	*13.77*
9	*5.61*	*13.37*	*12.03*	*14.70*	*13.04*	*12.20*	*13.87*
10	*5.67*	*13.17*	*11.97*	*14.38*	*12.85*	*12.10*	*13.61*

APPENDIX D: DYNAMIC MODULUS LABORATORY TEST DATA FOR THE M-E PAVEMENT DESIGN GUIDE

Table D1. Summary of DM Values for Bryan Mixture: Basic TxDOT Type C Mixture [PG 64-22 + Limestone].

Specimen # BDM0001, AV =6.56 Percent

Temperature		Dynamic Modulus, psi					
°C	°F	0.1 Hz	0.5 Hz	1.0 Hz	5.0 Hz	10 Hz	25 Hz
-10	14	2,833,936	3,359,219	3,512,016	3,959,646	4,093,719	4,340,675
4.4	40	1,362,920	1,742,570	1,922,417	2,313,526	2,529,980	2,753,048
21.1	70	471,605	680,590	808,919	1,125,797	1,300,089	1,599,810
37.8	100	152,623	247,913	297,864	490,257	622,778	878,987
54.4	130	68,023	92,476	106,168	175,264	230,189	366,307

Specimen # BDM0002, AV =7.50 Percent

Temperature		Dynamic Modulus, psi					
°C	°F	0.1 Hz	0.5 Hz	1.0 Hz	5.0 Hz	10 Hz	25 Hz
-10	14	2,120,104	2,497,956	2,645,111	3,008,257	3,159,546	3,359,538
4.4	40	1,109,930	1,483,373	1,657,332	2,085,121	2,303,968	2,614,421
21.1	70	418,492	630,972	753,195	1,080,343	1,276,608	1,604,175
37.8	100	172,696	266,202	311,860	531,505	659,501	948,953
54.4	130	52,025	74,158	84,804	138,163	188,041	283,114

Specimen # BDM0003, AV =6.90 Percent

Temperature		Dynamic Modulus, psi					
°C	°F	0.1 Hz	0.5 Hz	1.0 Hz	5.0 Hz	10 Hz	25 Hz
-10	14	2,316,644	2,778,531	2,950,198	3,420,947	3,601,258	3,895,873
4.4	40	1,269,660	1,634,343	1,813,320	2,221,456	2,431,326	2,738,008
21.1	70	445,048	655,781	781,057	1,103,070	1,288,348	1,601,993
37.8	100	125,313	193,466	226,085	369,658	478,044	645,244
54.4	130	72,983	95,478	104,862	165,952	215,831	338,576

Binder Content = 4.6 percent by weight of aggregate
VMA = 14 percent at maximum density

APPENDIX D (CONTINUED): DM LABORATORY TEST DATA

Table D2. Summary of DM Values for Yoakum Mixture: Rut Resistant 12.5 mm Superpave Mixture [PG 76-22 + Gravel].

Specimen # YDM0001, AV =6.80 Percent

Temperature		Dynamic Modulus, psi					
°C	°F	0.1 Hz	0.5 Hz	1.0 Hz	5.0 Hz	10 Hz	25 Hz
-10	14	1,823,472	2,389,410	2,612,666	3,241,115	3,485,344	3,899,108
4.4	40	1,124,434	1,558,590	1,759,177	2,291,190	2,525,325	2,890,051
21.1	70	269,944	504,934	638,616	1,011,870	1,223,640	1,607,120
37.8	100	71,852	124,239	152,333	283,839	388,353	641,603
54.4	130	32,996	46,862	52,547	95,116	135,030	251,495

Specimen # YDM0002, AV =6.90 Percent

Temperature		Dynamic Modulus, psi					
°C	°F	0.1 Hz	0.5 Hz	1.0 Hz	5.0 Hz	10 Hz	25 Hz
-10	14	1,102, 693	1,520,779	1,742,483	2,348,088	2,615,828	2,924,933
4.4	40	1,062,343	1,513,991	1,693,229	2,166,255	2,380,446	2,607,213
21.1	70	294,499	513,564	657,877	1,082,518	1,325,065	1,634,097
37.8	100	72,852	119,526	148,635	281,170	383,001	619,616
54.4	130	50,502	63,033	69,038	133,174	187,041	327,597

Specimen # YDM0003, AV =7.30 Percent

Temperature		Dynamic Modulus, psi					
°C	°F	0.1 Hz	0.5 Hz	1.0 Hz	5.0 Hz	10 Hz	25 Hz
-10	14	1,131,831	1,576,792	1,770,302	2,275,236	2,518,580	2,810,991
4.4	40	710,395	1,028,477	1,187,351	1,600,694	1,763,615	2,005,712
21.1	70	177,758	325,262	419,899	695,877	863,178	1,057,511
37.8	100	45,933	71,214	88,633	156,858	216,353	342,956
54.4	130	29,530	38,116	41,060	64,324	84,238	127,865

Binder Content = 5.6 percent by weight of aggregate
VMA = 15.9 percent at maximum density

APPENDIX E: EXAMPLE OF PERCENTAGE CRACKING ANALYSIS FROM THE M-E PAVEMENT DESIGN GUIDE SOFTWARE

Table E1. Example of the M-E Pavement Design Guide Software Analysis for Bryan Mixture based on a 20-Year Design Life (WW Environment).

Pavement Structure	HMAC Specimen	Traffic ESALs (Millions)	Percent Cracking in Wheelpath (Output from Software)
PS1	BDM0001	2.50	26.80
	BDM0002	2.50	38.3
	BDM0003	2.50	31.80
	BDM0001	5.00	45.60
	BDM0002	5.00	59.90
	BDM0003	5.00	51.60
PS2	BDM0001	2.50	21.9
	BDM0002	2.50	36.80
	BDM0003	2.50	28.60
	BDM0001	5.00	53.90
	BDM0002	5.00	71.50
	BDM0003	5.00	63.20
PS3	BDM0001	1.25	29.90
	BDM0002	1.25	40.10
	BDM0003	1.25	36.60
	BDM0001	2.50	61
	BDM0002	2.50	70.00
	BDM0003	2.50	67.20
	BDM0001	5.00	78.10
	BDM0002	5.00	89.80
	BDM0003	5.00	87.40
PS4	BDM0001	1.25	26.60
	BDM0002	1.25	43.80
	BDM0003	1.25	32.30
	BDM0001	2.50	58
	BDM0002	2.50	70.10
	BDM0003	2.50	64.30
	BDM0001	5.00	85.50
	BDM0002	5.00	96.25
	BDM0003	5.00	88.30
PS5	BDM0001	2.50	7.85
	BDM0002	2.50	13.51
	BDM0003	2.50	9.02
	BDM0001	5.00	15
	BDM0002	5.00	20.40
	BDM0003	5.00	18.10
	BDM0001	25	55.10
	BDM0002	25	70.40
	BDM0003	25	63.89

APPENDIX E (CONTINUED): EXAMPLE OF PERCENTAGE CRACKING ANALYSIS FROM THE M-E PAVEMENT DESIGN GUIDE SOFTWARE

Table E2. Example of the M-E Pavement Design Guide Software Analysis for Bryan Mixture based on a 20-Year Design Life (DC Environment).

Pavement Structure	HMAC Specimen	Traffic ESALs (Millions)	Percent Cracking in Wheelpath (Output from Software)
PS2	BDM0001	2.50	18.40
	BDM0002	2.50	31.60
	BDM0003	2.50	23.70
	BDM0001	5.00	40.00
	BDM0002	5.00	53.90
	BDM0003	5.00	49.70
PS3	BDM0001	2.50	18.40
	BDM0002	2.50	27.90
	BDM0003	2.50	32.60
	BDM0001	5.00	48.50
	BDM0002	5.00	72.10
	BDM0003	5.00	57.6
PS4	BDM0001	2.50	30.50
	BDM0002	2.50	48.80
	BDM0003	2.50	36.50
	BDM0001	5.00	62.80
	BDM0002	5.00	73.00
	BDM0003	5.00	60.40

APPENDIX F: ME MIXTURE LAB N_f RESULTS
Mixture Lab N_f Prediction: ME Approach = 50 Percent Reduction in Flexural Stiffness

Table F1. Example of ME Lab N_f for Bryan Mixture for Wet-Warm (WW) Environment.

Pavement Structure (PS#)	0 Months			3 Months			6 Months		
	Lab N_f	95% Lab N_f Prediction Interval		Lab N_f	95% Lab N_f Prediction Interval		Lab N_f	95% Lab N_f Prediction Interval	
		Lower	Upper		Upper	Lower		Lower	Upper
1	4,483,670	2,124,669	9,461,849	1,232,934	232,469	6,539,046	755,762	13,829	31,095,112
2	423,048	293,301	610,190	201,184	88,761	456,001	123,017	19,976	757,585
3	460,826	315,567	672,950	214,843	92,205	500,598	130,707	19,828	861,609
4	363,435	257,421	513,108	179,035	82,856	386,855	110,460	20,190	604,323
5	29,828,466	10,197,087	87,254,077	5,284,069	480,383	58,123,166	2,512,795	9,467	66,694,421

Table F2. Example of ME Lab N_f for Yoakum Mixture for Wet-Warm (WW) Environment.

Pavement Structure (PS#)	0 Months			3 Months			6 Months		
	Lab N_f	95% Lab N_f Prediction Interval		Lab N_f	95% Lab N_f Prediction Interval		Lab N_f	95% Lab N_f Prediction Interval	
		Lower	Upper		Upper	Lower		Lower	Upper
1	4,105,724	267,604	62,992,098	2,592,589	502,685	13,371,222	2,420,257	208,917	28,038,084
2	595,841	164,629	2,156,527	429,285	192,011	959,764	303,309	91,221	1,008,496
3	639,003	168,256	2,426,800	458,188	199,448	1,052,585	327,014	94,442	1,132,320
4	526,257	158,105	1,751,663	382,383	179,264	815,650	265,371	85,614	822,545

APPENDIX F (CONTINUED): ME MIXTURE LAB N_f RESULTS
Mixture LAB N_f Prediction: ME Approach = 50 Percent Reduction in Flexural Stiffness

Table F3. Example of Variance Estimates for Predicted Log ME Lan N_f (Bryan Mixture, WW Conditions).

Micro Strain	Log (Micro Strain)	Var(Log(Log Nf))_Bryan-0M	Var(Log(Lab N_f)))_Bryan-3M
157	5.06	0.27^2	0.60^2
278.96	5.63	0.13^2	0.29^2
273.21	5.61	0.14^2	0.30^2
289.47	5.67	0.12^2	0.28^2
98.97	4.59	0.39^2	0.86^2

Table F4. Example of Variance Estimates for Predicted Log ME N_f (Yoakum Mixture, WW Conditions).

Micro Strain	Log (Micro Strain)	Var(Log(Lab Nf)))_Yaokum-0M	Var(Log(Log Nf)))_Yaokum-3M	Var(Log(Log Nf)))_Yaokum-6M
157	5.06	0.63^2	0.59^2	0.88^2
278.96	5.63	0.30^2	0.29^2	0.43^2
273.21	5.61	0.31^2	0.30^2	0.45^2
289.47	5.67	0.28^2	0.27^2	0.41^2
98.97	4.59	-	-	-

APPENDIX G: CMSE MIXTURE LAB N_f RESULTS
Mixture Lab N_f Prediction: CMSE Approach = 7.5 mm Crack Growth & Propagation through HMAC Layer

Table G1. Example of Bryan Mixture for Wet-Warm (WW) Environment.

PS#	0 Months			3 Months			6 Months		
	Lab N_f	95% Lab N_f Prediction Interval		Lab N_f	95% Lab N_f Prediction Interval		Lab N_f	95% Lab N_f Prediction Interval	
		Lower	Upper		Upper	Lower		Lower	Upper
1	6,310,031	5,891,450	7,896,612	2,419,856	2,175,875	3,181,037	940,447	820,866	1,258,028
2	4,310,723	4,008,142	4,613,304	2,311,781	1,809,200	2,814,362	1,001,560	798,979	1,204,141
3	4,425,803	4,120,250	4,728,412	2,428,810	1,926,329	2,931,491	1,211,403	1,008,822	1,413,984
4	3,960,542	3,955,200	4,005,620	2,189,413	1,686,832	2,691,994	1,309,518	1,106,937	1,512,099
5	11,123,548	9,820,967	13, 118,456	8,600,514	7,397,933	9,803,095	5,081,720	4,279,139	5,884,301

Table G2. Example of Yoakum Mixture for Wet-Warm (WW) Environment.

PS#	0 Months			3 Months			6 Months		
	Lab N_f	95% Lab N_f Prediction Interval		Lab N_f	95% Lab N_f Prediction Interval		Lab N_f	95% Lab N_f Prediction Interval	
		Lower	Upper		Upper	Lower		Lower	Upper
1	7,879,929	6,315,948	8,921,110	4,954,378	3,733,797	5,334,959	3,229,895	2,179,244	3,980,406
2	5,893,480	4,590,899	7,196,061	3,057,842	2,257,261	3,858,423	2,115,169	1,214,568	3,015,750
3	5,899,598	4,597,017	7,202,179	3,118,460	2,317,879	3,919,041	2,009,481	1,108,900	2,910,062
4	4,001,831	3,979,250	4,041,412	3,057,181	2,156,600	3,957,762	1,980,815	1,080,234	2,881,396

APPENDIX H: CM MIXTURE LAB N_f RESULTS
Mixture Lab N_f Prediction: CM Approach = 7.5 mm Crack Growth & Propagation through HMAC Layer

Table H1. Example of Bryan Mixture for Wet-Warm (WW) Environment.

PS#	0 Months			3 Months			6 Months		
	Lab N_f	95% Lab N_f Prediction Interval		Lab N_f	95% Lab N_f Prediction Interval		Lab N_f	95% Lab N_f Prediction Interval	
		Lower	Upper		Upper	Lower		Lower	Upper
1	6,290,861	5,825,280	7,626,442	2,313,584	1,651,003	3,452,165	914 ,861	612,480	1,413,442
2	4,811,422	3,910,841	5,712,003	2,011,781	2,011,781	2,912,362	989,795	589,214	1,390,376
3	4,181,312	3,980,731	4,381,893	2,611,912	2,611,912	3,512,493	1,009,215	808,634	1,209,796
4	3,980,182	3,959,601	4,000,763	2,204,315	2,204,315	3,104,896	995,850	895,264	1,096,431
5	10,891,433	9,690,852	12,092,014	8,401,515	8,401,515	9,902,096	4,890,253	3,889,672	5,890,834

Table H2. Example of Yoakum Mixture for Wet-Warm (WW) Environment.

PS#	0 Months			3 Months			6 Months		
	Lab N_f	95% Lab N_f Prediction Interval		Lab N_f	95% Lab N_f Prediction Interval		Lab N_f	95% Lab N_f Prediction Interval	
		Lower	Upper		Upper	Lower		Lower	Upper
1	7,281,594	6,121,013	7,922,175	5,169,851	3,960,670	5,761,832	3,132,561	2,633,980	3,335,142
2	4,989,845	4,089,264	5,890,420	3,000,221	2,699,640	3,300,802	2,542,506	2,161,925	2,923,087
3	5,600,125	5,0995,544	6,100,706	2,986,420	2,689,839	3,287,001	1,998,652	1,718,071	2,279,233
4	4,121,458	4,000,877	4,224,039	3,116,108	2,765,527	3,466,689	1,500,824	1,260,243	1,741,405

APPENDIX I: MIXTURE FIELD N_f RESULTS

ME Approach = 50 Percent Reduction in Flexural Stiffness

Table I1. Example of ME Field N_f (Field $N_f = SF \times$ Lab N_f): Bryan Mixture, WW Environment.

Pavement Structure (PS#)	0 Months			3 Months			6 Months		
	Field N_f	95% Field N_f Prediction Interval		Field N_f	95% Field N_f Prediction Interval		Field N_f	95% Field N_f Prediction Interval	
		Lower	Upper		Upper	Lower		Lower	Upper
1	8.519E+07	4.037E+07	1.798E+08	2.343E+07	4.417E+06	1.242E+08	1.436E+07	2.628E+05	5.908E+08
2	8.038E+06	5.573E+06	1.159E+07	3.822E+06	1.686E+06	8.664E+06	2.337E+06	3.795E+05	1.439E+07
3	8.756E+06	5.996E+06	1.279E+07	4.082E+06	1.752E+06	9.511E+06	2.483E+06	3.767E+05	1.637E+07
4	6.905E+06	4.891E+06	9.749E+06	3.402E+06	1.574E+06	7.350E+06	2.099E+06	3.836E+05	1.148E+07
5	5.667E+08	1.937E+08	1.658E+09	1.004E+08	9.127E+06	1.104E+09	4.774E+07	1.799E+05	1.267E+09

Table I2. Example of ME Field N_f (Field $N_f = SF \times$ Lab N_f): Yoakum Mixture, WW Environment.

Pavement Structure (PS#)	0 Months			3 Months			6 Months		
	Field N_f	95% Field N_f Prediction Interval		Field N_f	95% Field N_f Prediction Interval		Field N_f	95% Field N_f Prediction Interval	
		Lower	Upper		Upper	Lower		Lower	Upper
1	7.801E+07	5.084E+06	1.197E+09	4.926E+07	9.551E+06	2.541E+08	4.598E+07	3.969E+06	5.327E+08
2	1.132E+07	3.128E+06	4.097E+07	8.156E+06	3.648E+06	1.824E+07	5.763E+06	1.733E+06	1.916E+07
3	1.214E+07	3.197E+06	4.611E+07	8.706E+06	3.790E+06	2.000E+07	6.213E+06	1.794E+06	2.151E+07
4	9.999E+06	3.004E+06	3.328E+07	7.265E+06	3.406E+06	1.550E+07	5.042E+06	1.627E+06	1.563E+07

APPENDIX I (CONTINUED): MIXTURE FIELD N_f RESULTS

CMSE Approach = 7.5 mm Crack Growth and Propagation through HMAC Layer

Table I3. Example of CMSE Field N_f (Field N_f = [SF_a × SF_h] × Lab N_f): Bryan Mixture, WW Environment.

Pavement Structure (PS#)	0 Months			3 Months			6 Months		
	Field N_f	95% Field N_f Prediction Interval		Field N_f	95% Field N_f Prediction Interval		Field N_f	95% Field N_f Prediction Interval	
		Lower	Upper		Upper	Lower		Lower	Upper
1	6.922E+07	6.463E+07	8.663E+07	1.893E+07	1.702E+07	2.488E+07	6.034E+06	5.267E+06	8.072E+06
2	4.729E+07	4.397E+07	5.061E+07	1.808E+07	1.415E+07	2.201E+07	6.426E+06	5.126E+06	7.726E+06
3	4.855E+07	4.520E+07	5.187E+07	1.900E+07	1.507E+07	2.293E+07	7.773E+06	6.473E+06	9.073E+06
4	4.345E+07	4.339E+07	4.394E+07	1.712E+07	1.319E+07	2.105E+07	8.402E+06	7.102E+06	9.702E+06
5	1.220E+08	1.077E+08	1.439E+08	6.726E+07	5.786E+07	7.667E+07	3.261E+07	2.746E+07	3.776E+07

Table I4. Example of CMSE Field N_f (Field N_f = [SF_a × SF_h] × Lab N_f): Yoakum Mixture, WW Environment.

Pavement Structure (PS#)	0 Months			3 Months			6 Months		
	Field N_f	95% Field N_f Prediction Interval		Field N_f	95% Field N_f Prediction Interval		Field N_f	95% Field N_f Prediction Interval	
		Lower	Upper		Upper	Lower		Lower	Upper
1	1.201E+08	9.629E+07	1.360E+08	4.905E+07	3.697E+07	5.282E+07	2.953E+07	1.993E+07	3.640E+07
2	8.985E+07	6.999E+07	1.097E+08	3.028E+07	2.235E+07	3.820E+07	1.934E+07	1.111E+07	2.758E+07
3	8.995E+07	7.009E+07	1.098E+08	3.088E+07	2.295E+07	3.880E+07	1.837E+07	1.014E+07	2.661E+07
4	6.101E+07	6.067E+07	6.162E+07	3.027E+07	2.135E+07	3.919E+07	1.811E+07	9.878E+06	2.635E+07

APPENDIX I (CONTINUED): MIXTURE FIELD N_f RESULTS

CM Approach = 7.5 mm Crack Growth and Propagation through HMAC Layer

Table I5. Example of CM Field N_f (Field N_f = [SF_a × SF_h] × Lab N_f): Bryan Mixture, WW Environment.

Pavement Structure (PS#)	0 Months			3 Months			6 Months		
	Field N_f	95% Field N_f Prediction Interval		Field N_f	95% Field N_f Prediction Interval		Field N_f	95% Field N_f Prediction Interval	
		Lower	Upper		Upper	Lower		Lower	Upper
1	6.901E+07	6.390E+07	8.366E+07	1.809E+07	1.291E+07	2.700E+07	5.870E+06	3.930E+06	9.069E+06
2	5.278E+07	4.290E+07	6.266E+07	1.573E+07	1.573E+07	2.278E+07	6.351E+06	3.781E+06	8.921E+06
3	4.587E+07	4.367E+07	4.807E+07	2.043E+07	2.043E+07	2.747E+07	6.475E+06	5.188E+06	7.762E+06
4	4.366E+07	4.344E+07	4.389E+07	1.724E+07	1.724E+07	2.428E+07	6.390E+06	5.744E+06	7.035E+06
5	1.195E+08	1.063E+08	1.326E+08	6.571E+07	6.571E+07	7.744E+07	3.138E+07	2.496E+07	3.780E+07

Table I6. Example of CM Field N_f (Field N_f = [SF_a × SF_h] × Lab N_f): Yoakum Mixture, WW Environment.

Pavement Structure (PS#)	0 Months			3 Months			6 Months		
	Field N_f	95% Field N_f Prediction Interval		Field N_f	95% Field N_f Prediction Interval		Field N_f	95% Field N_f Prediction Interval	
		Lower	Upper		Upper	Lower		Lower	Upper
1	1.110E+08	9.332E+07	1.208E+08	5.119E+07	3.921E+07	5.705E+07	2.864E+07	2.409E+07	3.050E+07
2	7.608E+07	6.234E+07	8.981E+07	2.970E+07	2.673E+07	3.268E+07	2.325E+07	1.977E+07	2.673E+07
3	8.538E+07	7.775E+08	9.301E+07	2.957E+07	2.663E+07	3.254E+07	1.828E+07	1.571E+07	2.084E+07
4	6.284E+07	6.100E+07	6.440E+07	3.085E+07	2.738E+07	3.432E+07	1.372E+07	1.152E+07	1.592E+07

APPENDIX I (CONTINUED): MIXTURE FIELD N_f RESULTS

The M-E Pavement Design Guide = 50 Percent Cracking in Wheelpath

Table I7. Example of 0 Months Results with Global Aging Model Analysis based on a 20-Year Design Life (WW Environment).

PS#	Bryan Mixture			Yoakum Mixture		
	Field N_f	95% Field N_f Prediction Interval		Field N_f Lower	95% Field N_f Prediction Interval	
		Lower	Upper		Lower	Upper
1	4.705E+06	1.927E+06	9.737E+06	6.210E+06	2.037E+06	1.534E+07
2	4.047E+06	1.996E+06	6.354E+06	5.750E+06	2.348E+06	1.054E+07
3	1.932E+06	0.000E+00	3.737E+06	3.410E+06	1.345E+05	7.771E+06
4	2.018E+06	2.802E+05	3.563E+06	2.970E+06	3.491E+05	6.000E+06
5	1.929E+07	1.420E+07	2.483E+07	-	-	-

Table I8. Example of 0 Months Results with Global Aging Model Analysis based on a 20-Year Design Life (DC Environment).

PS#	Bryan Mixture		
	Field N_f	95% Field N_f Prediction Interval	
		Lower	Upper
2	5.229E+06	2.948E+06	9.924E+06
3	4.290E+06	1.646E+06	7.836E+06
4	3.563E+06	2.639E+05	6.530E+06

APPENDIX I (CONTINUED): MIXTURE FIELD N_f RESULTS

Example of CMSE and CM Field N_f Prediction at Year 20 (PS# 1, WW Environment)

Table I9. Example of CMSE Field N_f Prediction at Year 20 (PS# 1, WW Environment)

HMAC Mixture	SF_{ag} @	SF_a	SF_h	$[N_i + N_p]$	$N_f = [SF_{ag}] \times [SF_a \times SF_h] \times [N_i + N_p]$
Bryan	0.045	1.63	6.73	6.31E+06	3.11E+06
Yoakum	0.070	2.10	7.26	7.88E+06	8.40E+06

Table I10. Example of CM Field N_f Prediction at Year 20 (PS# 1, WW Environment)

HMAC Mixture	SF_{ag} @	SF_a	SF_h	$[N_i + N_p]$	$N_f = [SF_{ag}] \times [SF_a \times SF_h] \times [N_i + N_p]$
Bryan	0.045	1.63	6.73	6.29E+06	3.10E+06
Yoakum	0.070	2.10	7.26	7.28E+06	7.77E+06

APPENDIX I (CONTINUED): MIXTURE FIELD N_f RESULTS

Example of ME Field N_f Prediction at Year 20 (PS# 1, WW Environment)

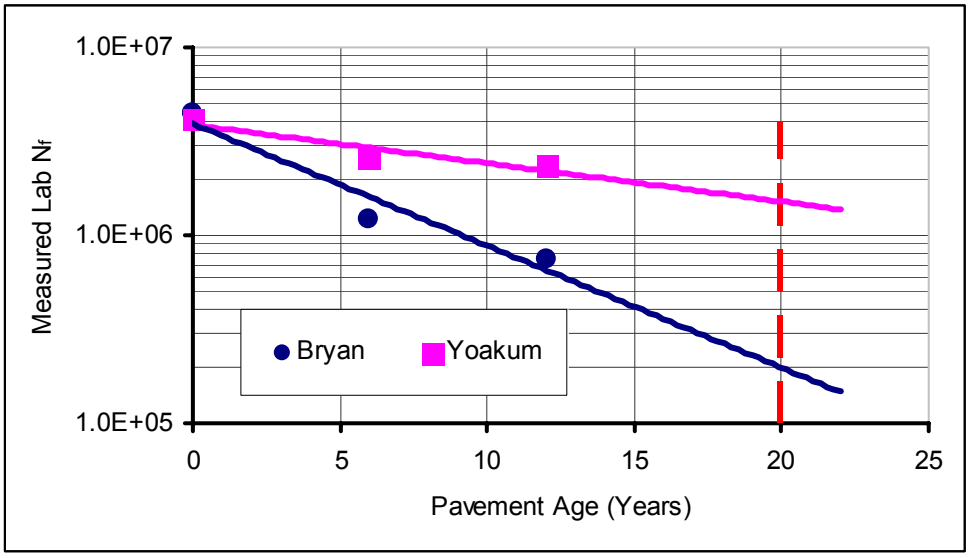

Figure I1. Example of Lab N_f Trend with Pavement Age (0 months ≅ 0 years, 3 months ≅ 6 years, and 6 months ≅12 years).

Approximate Lab N_f values at year 20 based on extrapolations in Figure I1 are approximately:

Bryan mixture: Lab N_f = 0.20 E+06

Yoakum mixture: Lab N_f = 1.56 E+06

Using the following ME equation (Chapter 4) with SF = 19, M = 3.57, and TCF = 1, the field N_f values at year 20 are approximately predicted as follows:

$$FieldN_f = \frac{SF\left[k_i(\varepsilon_t)^{-k_2}\right]}{M \times TCF} = \frac{SF \times Lab\ N_f}{M \times TCF}$$

Bryan mixture: Field N_f ≅ 19* 0.20E+06/(3.57*1) ≅ 1.03 E+06

Yoakum mixture: Field N_f ≅19*1.56E+06/(3.57*1) ≅ 8.30 E+06

APPENDIX J: RESOURCE REQUIREMENTS

Table J1. Approximate Time (hrs) Requirement to Produce at Least One Mixture N_f Result.

Task	2002 Guide	ME	CMSE	CM
Specimen fabrication	43.75 hrs	45.5 hrs	43.75 hrs	43.75 hrs
Specimen temperature conditioning	20 hrs	4 hrs	15 hrs	11 hrs
Lab testing (including set-up)	5 hrs	30 hrs	70 hrs	5 hrs
Data analysis	4.5 hrs	3 hrs	6 hrs	5 hrs
Total	72.25 hrs	82.5 hrs	134.75 hrs	64.75 hrs

Note: For the CMSE approach, about 65 hrs lab testing is for surface energy measurements. SE values for asphalts and aggregates are required as CMSE input. Though the current SE test protocol for aggregates might require a test time of about 30 to 60 hrs per aggregate, various alternate and time efficient SE measurement methods are being investigated in other ongoing research projects. Despite the lengthy test time, SE measurements are only performed once for any asphalt or aggregate type from a particular source (as long as there are no major compositional changes). The SE data can then be utilized for numerous analysis applications including fatigue, permanent deformation, and moisture sensitivity modeling in HMAC pavements. Thus, SE measurements are actually efficient considering their repeated and widespread use for asphalt and aggregate materials that may be utilized in different mixture designs.

Table J2. Typical Equipment Requirements.

Task	2002 Guide	ME	CMSE	CM
Binder-Aggregate Mixing	Electric mixer	Electric mixer	Electric mixer	Electric mixer
Compacting	SGC	Linear kneading	SGC	SGC
Testing	MTS LVDTs Control unit	MTS LVDT Control unit *BB device*	MTS LVDTs Control unit *Whilmey Plate* *USD device*	MTS LVDTs Control unit
Data acquisition	Automated computer system	Automated computer system	Automated computer system	Automated computer system
Temperature control unit	Thermocouples	Thermocouples	Thermocouples	Thermocouples
Other test accessories			Attachment plates	Attachment plates
Data analysis	2002 Software	Excel/manual	Excel/manual	Excel/manual

APPENDIX J (CONTINUED): RESOURCE REQUIREMENTS

Table J3. Approximate Time (hrs) Requirements for a Single Specimen Fabrication.

#	Task	ME (Beam Specimen)	CMSE, CM, & M-E Pavement Design Guide (Cylindrical Specimen)
1	Aggregate batching	0.5 hrs	0.5 hrs
2	Aggregate pre-heating (minimum ≅ 4 hrs)	12 hrs (overnight)	12 hrs (overnight)
3	Binder liquefying (heating)	0.5 hrs	0.5 hrs
4	Binder aggregate mixing	0.25 hrs	0.25 hrs
5	PP2 Short-Term Oven Aging @ 135 °C (275 °F)	4 hrs	4 hrs
6	Heating for compaction	0.5 hrs	0.5 hrs
7	Compaction	0.25	0.25 hrs
8	Specimen cooling	12 hrs (overnight)	12 hrs (overnight)
9	Sawing & coring (with water)	2 hrs	0.5 hrs
10	Drying after sawing/coring	12 hrs (overnight)	12 hrs (overnight)
11	AV measurements	0.75 hrs	0.25 hrs
12	Cleaning up	1 hrs	1 hrs
Total		45.75 hrs	43.75 hrs

APPENDIX K: TxDOT EVALUATION SURVEY QUESTIONNAIRE

Evaluation & Weighting of Factors for the Selection of Appropriate Fatigue Analysis Approach.

Factor	**Rating: 1-10 (1 = least important) (10 = most important)**	**Sub-factor**	**Rating: 1 – 10 (1 = least important) (10 = most important)**
Laboratory testing		Simplicity	
		Equipment availability	
		Equipment versatility	
		Human resources	
Input variability		Traffic	
		Materials	
		Environment (temperature & moisture)	
Incorporation of material properties in analysis		Mixture volumetrics	
		Modulus/stiffness	
		Tensile strength	
		Aging	
		Healing	
		Fracture	
		Anisotropy	
Analysis		Simplicity	
		Versatility of inputs	
		Definition of failure criteria	
Results		N_f variability	
		Tie to field validation	
Cost		Lab testing (hrs)	
		Equipment ($)	
		Analysis (hrs) -Lab data reduction -N_f computation	
		Practicality of implementation	

APPENDIX L: RATING CRITERIA OF THE FATIGUE ANALYSIS APPROACHES

CATEGORY	WEIGHT (1)	ITEM	WEIGHT (2)	ME		CMSE		CM		2002 GUIDE		COMMENT
				SCORE	EVALUATION	SCORE	EVALUATION	SCORE	EVALUATION	SCORE	EVALUATION	
Results	*22%*	N_f variability	*50%*	3/10	3.30%	8/10	8.80%	7/10	7.70%	5/10	5.50%	**CMSE**
		Tie to field validation	*50%*	5/10	5.50%	5/10	5.50%	5/10	5.50%	5/10	5.50%	
			100%	**40%**	**9%**	**65%**	**14%**	**60%**	**13**	**50%**	**11%**	
Cost	*18%*	Practicality	*32%*	6/10	3.46%	6/10	3.5%	6/10	3.5%	6/10	3.5%	**CM**
		Testing (hrs)	*32%*	4/10	2.30%	7/10	4%	8/10	4.6%	7/10	4%	
		Analysis (hrs)	*19%*	8/10	2.74%	6/10	2.05%	6/10	2.05%	6/10	2.05%	
		Equipment ($)	*17%*	6/10	1.84%	8.5/10	2.6%	8/10	2.45%	8/10	2.45%	
			100%	**57%**	**10%**	**65%**	**12%**	**70%**	**13%**	**67%**	**12%**	
Input variability	*16%*	Materials	*36%*	5/10	3%	8/10	5%	8/10	5%	6/10	3%	**2002 GUIDE**
		Traffic	*34%*	5/10	3%	5/10	3%	5/10	3%	9/10	5%	
		Environment	*29%*	5/10	2%	5/10	2%	5/10	2%	8/10	4%	
			100%	**50%**	**8%**	**60%**	**10%**	**60%**	**10%**	**75%**	**12%**	
Analysis	*15%*	Failure criteria	*41%*	5/10	3%	8/10	5%	7/10	4%	5/10	3.1%	**CMSE**
		Simplicity	*36%*	8.5/10	5%	5/10	3%	6/10	3%	6/10	3.2%	
		Versatility of inputs	*23%*	4/10	1%	10	3%	8/10	3%	7/10	2.4%	
			100%	**60%**	**9%**	**74%**	**11%**	**69%**	**10%**	**58%**	**9%**	
Lab testing	*15%*	Simplicity	*32%*	5/10	2.4%	8/10	3.84%	9/10	4.3%	9/10	4.32%	**CMSE**
		Equipment availability	*29%*	3/10	1.3%	7/10	3.05%	7/10	3.0%	7/10	3.05%	
		Equipment versatility	*22%*	2/10	0.7%	10/10	3.30%	8/10	2.3%	8/10	2.64%	
		Human resources	*18%*	5/10	1.4%	8/10	2.16%	8/10	2.2%	8/10	2.16%	
			100%	**38%**	**6%**	**82%**	**12%**	**81%**	**12%**	**81%**	**12%**	
Incorporation of Material Properties	*14%*	Mixture volumetrics	*17%*	6/10	1.4%	9/10	2.1%	9/10	2.1%	10/10	2.4%	**CMSE**
		Modulus/stiffness	*17%*	8/10	1.9%	9/10	2.1%	9/10	2.1%	10/10	2.4%	
		Fracture	*16%*	5/10	1.1%	10/10	2.2%	8/10	1.8%	5/10	1.1%	
		Tensile strength	*15%*	5/10	1.1%	10/10	2.1%	1/100	2.1%	5/10	1.1%	
		Aging	*14%*	5/10	1.0%	9/10	1.8%	9/10	1.8%	8.5/10	1.8%	
		Healing	*12%*	5/10	0.8%	9/10	1.5%	7.5/10	1.3%	5/10	0.8%	
		Anisotropy	*9%*	5/10	0.6%	9/10	1.1%	9/10	1.1%	5/10	0.6%	
			100%	**57%**	**8%**	**93%**	**13%**	**88%**	**12%**	**73%**	**10%**	
Total	***100%***				**50%**		**72%**		**70%**		**66%**	**CMSE**

Example of Score and Evaluation Calculations:
Evaluation = [Score × Weight (1) × Weight (2)], Score sub-total = ∑[Score ×Weight (2)], and Total scores = ∑[Evaluation]